# DEBRIS FLOWS IN THE SOUTHERN COAST MOUNTAINS, BRITISH COLUMBIA: DYNAMIC BEHAVIOUR AND PHYSICAL PROPERTIES

by

ROBERT PETER JORDAN

B.Sc., The University of British Columbia, 1972
M.Sc., The University of British Columbia, 1978

A THESIS SUBMITTED IN PARTIAL FULFILLMENT OF
THE REQUIREMENTS FOR THE DEGREE OF
DOCTOR OF PHILOSOPHY

in

THE FACULTY OF GRADUATE STUDIES

(Department of Geography)

We accept this thesis as conforming
to the required standard

THE UNIVERSITY OF BRITISH COLUMBIA

October 1994

In presenting this thesis in partial fulfilment of the requirements for an advanced degree at the University of British Columbia, I agree that the Library shall make it freely available for reference and study. I further agree that permission for extensive copying of this thesis for scholarly purposes may be granted by the head of my department or by his or her representatives. It is understood that copying or publication of this thesis for financial gain shall not be allowed without my written permission.

(Signature)

Department of Geography

The University of British Columbia
Vancouver, Canada

Date October 31, 1994

DE-6 (2/88)

## ABSTRACT

Debris flows in the southern Coast Mountains exhibit different dynamic and sedimentologic characteristics, depending on the lithology of their source areas. Fine-textured debris flows originating in the Quaternary volcanic complexes are much more mobile than those originating in the coarse-textured plutonic rocks which form most of this mountain range. Mobility can be described as the velocity of flow, the distance of travel of debris flows, and the slope required to sustain flow. The objectives of this study are to examine the effect of different sediment composition on the mobility of debris flows, and to determine which rheologic models are most applicable for modeling debris flows in these geologic environments.

About 25 debris flow events in or adjacent to the southern Coast Mountains were examined, ranging in volume from $10^2$ $m^3$ to over $10^7$ $m^3$. Field methods included sampling of grain-size distribution, measurement of the deposit and channel dimensions, and observation of the stratigraphy of debris flow fans. Shear strength, permeability, and consolidation tests were performed on samples of reconstituted debris, representative of typical fine-textured and coarse-textured debris flows. These samples were also used to model debris flows in a flume.

The coarse-textured, plutonic-source, debris flows typically had a distinct, inversely-graded, clast-supported, surface layer of cobbles and boulders. Their deposits tended to be irregular in thickness, with lobes and levées of coarse material. The fine-textured, volcanic-source, debris flows had no such surface layer, and their deposits were generally uniform in thickness and surface morphology. These observations, and corroborating evidence from the flume results, suggest that fine-textured debris flows behave according to the Bingham flow model, while coarse-textured debris flows can be better described by a granular, or dilatant, flow model. A clay content of about 4% in the matrix (sub-4 mm material) is a useful measure to distinguish the two populations. Several debris flow events of intermediate behaviour and sediment composition were also examined. The permeability of the debris, and hence its rate of consolidation, is an important factor controlling mobility. The volume of debris flow events was found to be the most significant factor controlling runout distance.

## TABLE OF CONTENTS

## LIST OF TABLES

## LIST OF FIGURES

## LIST OF SYMBOLS

| | |
|---|---|
| b | major axis of an ellipse, or half-width of a channel (m) |
| B | channel width (m) |
| Bi | Bingham number |
| c | cohesion (total stress model) (Pa) |
| c' | cohesion (effective stress model) (Pa) |
| $c_s$ | sediment concentration by weight |
| C | term used in derivation of runout model ($s^{-1}$) |
| $c_v$ | coefficient of consolidation ($m^2/s$) |
| $c_v$ | volume concentration of grains or sediment |
| $C_v$ | coefficient of variation |
| d | minor axis of an ellipse, or depth of a channel (m) |
| D | diameter of a grain (mm) |
| e | void ratio |
| F | Bingham flow factor for laminar flow in a channel |
| Fr | Froude number |
| g | acceleration of gravity (9.8 $m/s^2$) |
| G | a dimensionless number used by Bagnold (1954) |
| $G_s$ | specific gravity |
| h | depth below a surface (m) |
| $\Delta h$ | difference in elevation, in superelevation and runup equations |
| H | thickness or depth of flow (m) |
| k | Bingham yield strength (Pa) |
| K | hydraulic conductivity (m/s) |
| K | shape factor for laminar flow in a channel |
| m | mass (kg) |
| $M_z$ | graphic mean (grain-size distribution) (phi) |
| n | exponent in stress - strain rate relation, or "flow behaviour index" |
| N | "Bagnold number", a dimensionless number used by Bagnold (1954) |
| P | dispersive pressure in Bagnold model (Pa) |
| q | discharge per unit area (m/s) |
| r | correlation coefficient |
| r | distance along a radius (m) |
| R | radius (m) |
| $R_0$ | radius of plug in Bingham flow model (m) |
| $r_c$ | radius of curvature in superelevation equation |
| Re | Reynolds number |
| s | sample standard deviation |
| S | channel slope ($\sin\theta$) |
| $S_f$ | friction slope |
| t | time (s) |
| $T_0$ | thickness of plug in Bingham flow model (m) |
| u | pore water pressure (Pa) |
| u | velocity (m/s) |
| U | mean velocity (m/s) |
| V | volume ($m^3$) |

| | |
|---|---|
| $w$ | water content (dry weight basis) |
| $w_L$ | liquid limit |
| $w_P$ | plastic limit |
| $x$ | a Cartesian axis; longitudinal distance, parallel to the channel axis (m) |
| $x_L$ | runout distance of a debris flow (m) |
| $y$ | a Cartesian axis; horizontal distance, perpendicular to the channel axis |
| $z$ | a Cartesian axis; elevation above a datum or perpendicular to the channel axis (m) |
| $\alpha$ | dynamic friction angle (degrees) |
| $\beta$ | width:depth ratio of a channel |
| $\gamma$ | unit weight ($N/m^3$) |
| $\phi$ | phi, logarithmic unit of Wentworth grain-size scale |
| $\phi$ | angle of internal friction (total stress model) (degrees) |
| $\phi'$ | angle of internal friction (effective stress model) (degrees) |
| $\lambda$ | linear concentration in Bagnold model |
| $\lambda$ | ratio used in model scaling |
| $\mu$ | viscosity or flow resistance |
| $\mu_B$ | Bingham viscosity (Pa.s) |
| $\mu_G$ | granular flow resistance ($Pa.s^2$) |
| $\mu_N$ | Newtonian viscosity (Pa.s) |
| $\theta$ | channel slope (degrees) |
| $\rho_f$ | density of fluid ($kg/m^3$) |
| $\rho_s$ | density of solid ($kg/m^3$) |
| $\sigma'$ | effective stress (Pa) |
| $\sigma_I$ | inclusive graphic standard deviation (grain-size distribution) (phi) |
| $\sigma_n$ | normal stress (Pa) |
| $\tau$ | shear stress (Pa) |

## ACKNOWLEDGEMENT

I wish to thank my supervisor, Michael Bovis, as well as the other members of my research committee, Olav Slaymaker, Michael Church, and Oldrich Hungr, for their intellectual support and patience throughout this study. The support of the Killam Trusts (UBC), which provided financial assistance with a scholarship, is gratefully acknowledged. Research funds were provided from an NSERC grant to M. Bovis. Pierre Friele, Michelle Weston, Gordon Clarke, Alan Paige, and Kevin McKechnie provided assistance in the field and the laboratory. Golder Associates Ltd. kindly provided the use of their laboratory for shear strength testing. Steve Evans of the Geological Survey of Canada made a helicopter available for field work on several occasions. I would also like to acknowledge the contributions of Frank Baumann, Steve Evans, Cathie Hickson, Tom Pierson, and Kelin Whipple, with whom I had stimulating field trips which added to my understanding of geologic processes in the study area. I am grateful to an anonymous reviewer, who provided comments to a paper (yet unpublished) based on this research, which were helpful in completing this thesis. Jim Decker and Arvin Stark of C.R.B. Logging Ltd. were very cooperative during my field work in an active logging area, and were also helpful in communicating their local knowledge of the study area.

# CHAPTER 1. INTRODUCTION

## 1.1 STATEMENT OF PROBLEM AND OBJECTIVES

Debris flow is the rapid movement of a mass of saturated, poorly sorted, mineral and organic debris, which behaves as a single-phase slurry as it flows down a steep channel or hillslope. Costa (1984) gives two definitions: "a gravity-induced mass movement intermediate between landsliding and waterflooding, with mechanical characteristics different from either of these processes" (after Johnson, 1970), and "a form of rapid mass movement of a body of granular solids, air, and water" (after Varnes, 1978). Debris flow is a common mass-movement process in steep channels in the mountains of western Canada, and presents a significant hazard in many mountain valleys. Examples from western Canada are described by VanDine (1985) and by Jackson *et al.* (1989).

The dynamic behaviour of debris flows is of interest for assessment of hazards on alluvial fans and in steep channels, for investigation of sediment contributions to rivers, and for design of engineering structures to withstand debris flows. The term "dynamic", in the context of this study, refers to the behaviour of debris flows in motion. Relevant measures of dynamic behaviour include the velocity of flow, the runout or distance of travel on a fan or in a valley, and the slope required to sustain flow. These factors collectively determine debris flow "mobility".

In the past 10 to 15 years, there have been significant advances in North America towards understanding debris flow dynamics. These advances have been motivated by two concerns: the need to protect highways and residential areas from debris flow hazard, in such areas as Howe Sound and the Coquihalla Highway in British Columbia (Hungr *et al.*, 1984, 1987; VanDine, 1985), and the need to understand the hazard presented by large debris flows in valleys below volcanoes, which was made clear by the 1980 eruption of Mount St. Helens (Pierson, 1985; Scott, 1988; Scott, 1989). Considerable experimental and theoretical work has been done in Japan (Okuda *et al.*, 1980; Chen, 1987; Takahashi, 1991), where debris flows present a more serious hazard to settlements and transportation facilities than in North America.

Although several rheologic models have been proposed to explain the dynamic behaviour of debris flows (for reviews see Pierson and Costa, 1987; Chen, 1987), no single model adequately describes the diverse behaviour exhibited by natural debris flows, which include a wide range of materials, initiating mechanisms, and scales. A model for debris flow movement should be able to explain the following properties which are common to many debris flows:

- the apparently laminar flow of most of the debris flow slurry;
- the existence of a rigid "plug" at the surface of some moving debris flows;
- the concentration of large clasts at the surface and at the front of debris flows;
- the formation of levées and of lobate deposits with steep snouts;
- the formation of inversely graded deposits, often with very large boulders supported by finer debris.

Early studies usually concluded that debris flows behave in one typical manner, which could be described by one particular rheologic model. For example, Johnson (1970) concluded that debris flow is viscous, and can be described by the Bingham model, while according to Takahashi (1978), debris flow is inertial, and can be described by a granular flow model. However, the properties of debris flows differ considerably from one study area to another, and they include a wide range of geologic materials, scales, channel morphologies, and initiating mechanisms.

In southwestern British Columbia, most work has focused on coarse-textured debris flows, mostly derived from relatively competent plutonic or metamorphic rocks, since these are the dominant lithologies in most areas where engineering work has been done. The material in these debris flows commonly originates from rockfall or other colluvial processes in or adjacent to steep channels, and may include a significant proportion of woody debris; such debris flows are often referred to as "debris torrents" (Swanston and Swanson, 1976), although this term is not well defined and varies in local meaning. More recently, it has been recognized that large, highly mobile debris flows originating in fine-textured, incompetent volcanic rocks of the Garibaldi Group may present an important geologic hazard, and that these debris flows exhibit

different dynamic properties than the more familiar coarse-textured "debris torrents" (Eisbacher, 1983; Jordan, 1987a).

The objectives of the present study are to examine the effect of different lithologies on the mobility of debris flows in southwestern British Columbia, and to determine which, if any, of the rheologic models that have been proposed for debris flows, are applicable in these geologic environments. Related objectives include investigating the presently available methods for estimating debris flow velocity and runout distance, in terms of their applicability to the range of debris flows present in the study area, and investigating the geotechnical properties which control the rheologic and dynamic properties of debris flows. This study will not address debris flow initiation in any detail, but will focus on debris flow movement in channels, and debris flow deposition.

The main study area is the portion of the Coast Mountains drained by Squamish and upper Lillooet Rivers. A number of debris flow sites have been selected which are representative of the principal lithologies of the region: the Coast Crystalline Complex and the Garibaldi Volcanic Belt. Most of the sites examined are in the Lillooet River and Meager Creek basins upstream from Pemberton. In addition, several debris flow sites were examined in other parts of the southern Coast Mountains and adjacent areas.

The general approach taken in this study is one of field investigation of recent debris flow deposits representative of the two main lithologic groups in the study area, followed by laboratory testing of sampled debris to investigate geotechnical properties of the material. Several debris flow sites in the main study area were selected for detailed study, based on the presence of well-preserved deposits, evidence of frequent occurrence of debris flow events, accessibility, and how well they represented the range of magnitudes and lithologies typical of the study area. A larger number of additional sites was examined in less detail; these included all the known debris flow locations in the study area which it was feasible to visit, as well as sites outside the study area which could provide information on the aspects of flow behaviour being studied. Field methods included sampling of debris for textural and other laboratory analyses, examination of stratigraphic sections, low-level air photography of fans and channels, detailed

mapping of fans and channels, and attempts to sample debris flows in motion or soon after deposition. Laboratory procedures included textural analysis, measurement of geotechnical properties such as permeability, consistency limits, shear strength parameters, and consolidation behaviour, and modeling of miniature debris flows in a flume.

These methods are intended to allow testing of several hypotheses which might describe the influence of debris properties on the mobility of debris flows. These hypotheses state that mobility is controlled by one or more of the following factors:

- the content of fines (clay and silt) in the debris, which would be expected to influence the shear strength and permeability of the debris;
- the abundance and size distribution of large clasts in the debris;
- the water content (or sediment concentration) of the debris;
- the undrained strength parameters of the debris, and the rate of dissipation of excess pore water pressure in the debris;
- the rheologic model which describes the material involved in a particular debris flow;
- the magnitude (or total volume) of the debris flow event.

This study concentrates on debris flows that are large enough to present a significant geologic hazard in valley bottoms, which in this area is a volume of about 10,000 $m^3$ or greater. A major limitation of a field study of debris flow dynamics is that one is extremely unlikely to witness an event; however, by making observations of deposit sedimentology and morphology, and flow dimensions in channels, a reasonable amount of data on the dynamics of recent debris flows can be obtained.

## 1.2 DEBRIS FLOWS AND RELATED SLOPE AND CHANNEL PROCESSES

Most publications on mass movement phenomena use, or at least refer to, the classification developed by Varnes (1978, revised from the original 1958 version). Varnes' classification is based on the type of material (bedrock, debris, and earth) and the type of movement (including amongst others, falls, slides, and flows). Varnes classifies both debris flows and debris avalanches as forms of rapid flow of saturated or near-saturated debris, with debris avalanches distinguished on the basis of higher velocity. Debris slides are translational

movements in which the debris is not completely disaggregated, and are slower moving than debris flows. There is a continuous gradation between debris flows and debris slides; thus, under Varnes' classification, debris flows can include mass movements which are relatively slow. Varnes defines "debris" as material containing 20 to 80% clasts larger than 2 mm; material with less than 20% clasts larger than 2 mm is defined as "earth". Varnes defines mudflow as a category of debris flow containing greater than 50% sand, silt, and clay. Mass movement terms, including "debris flow", are used as both nouns and verbs.

Swanston and Swanson (1976) give a classification of mass movement phenomena in forested environments. They do not identify debris flows as a distinct category, but use it only as a subclass of debris avalanches, according to Varnes' definition above. The events which are described as debris flows in this study would fall into Swanston and Swanson's category of "debris torrents" (see following section).

In humid, temperate environments, there is a continuous gradation through debris slides, debris avalanches, debris flows, and streamflow, in order of increasing water content. VanDine (1985) presents a classification of rapid mass movement phenomena which recognizes this gradation. He uses the term "debris flow" only for events which occur on planar hillsides, and uses "debris torrent" for debris flows which are confined in channels.

The gradation between debris flow and streamflow is discussed in some detail by Pierson and Costa (1987) and by Costa (1988). The distinguishing property of debris flow is that it has a sufficiently high sediment concentration to have significant shear strength, either due to Bingham yield strength or to interactions between large clasts, such that it can carry coarse stones in suspension, and form steep fronts and levées upon deposition. In debris flows, sediment entrainment is irreversible, and solids and water flow together as a single-phase slurry (Costa, 1988). Hyperconcentrated streamflow and debris floods, which are transitional phenomena between debris flow and streamflow, are described in Chapters 5 and 9.

The distinction between debris flows and debris avalanches is (after Pierson and Costa, 1987) that the degree of saturation in debris flows is sufficiently high that excess pore pressures can develop, and thus debris flows are capable of flowing as slurries under their own weight.

Debris avalanches are sufficiently unsaturated that excess pore pressures do not develop in most of the debris volume, and therefore mobility is largely controlled by friction or collisions between grains under drained conditions (although a saturated or liquefied layer at the base of some debris avalanches may contribute to mobility). The practical consequence of this is that debris flows can travel much greater distances on gentler slopes than debris avalanches of similar volume and sediment composition. This distinction has not been clearly made in most earlier references, nor in many recent publications concerning mass movement in British Columbia and adjacent areas. Many of the mass movement events described by Buchanan and Savigny (1990) as debris avalanches, and by Fannin and Rollerson (1993) as debris flows, are in fact the same: events which begin as debris avalanches, and are transformed to debris flows as they move downslope or downstream. It is widely recognized that many mass movement events begin as debris slides or avalanches, and progress to debris flows upon becoming confined in stream channels or gullies and mixing with water (Swanston and Swanson, 1976; Eisbacher and Clague, 1984; Bovis and Dagg, 1988; Fannin and Rollerson, 1993).

In this study, the following terminology is used to describe debris flows and related phenomena:

- Debris avalanche: the rapid, downslope movement of a mostly unsaturated, disaggregated mass of debris. (Some debris avalanches may be transitional to debris flows.)
- Debris flow: the rapid flow of a mixture of debris and water which is sufficiently saturated that the entire weight of debris can be borne by pore water pressure, and which has a sufficiently high sediment concentration that it behaves as a single-phase slurry, in which fluid and large clasts do not separate upon deposition. Debris flow can occur either confined in channels, or unconfined on open slopes.
- Hyperconcentrated streamflow: flow of water which contains a sufficiently high concentration of fine sediment (sand, silt, and clay) that turbulence is significantly damped, but which does not have a sufficiently high yield strength to carry large clasts in suspension (see Pierson and Costa, 1987).

- Debris flood: streamflow which transports very large quantities of coarse sediment, but in which the fluid and sediment move as discrete phases which separate upon deposition (see Chapter 9).
- Streamflow: the term "streamflow" refers to the flow of water in channels, with a relatively minor amount of sediment transported in suspension or as bedload. (Pierson and Costa, 1987, use the term "normal streamflow". Costa, 1988, uses the term "water flood" to describe high streamflow discharges, which contain less than 40% sediment by weight.)

In using these terms, an attempt is made to be consistent both with the classifications referred to above, and with the writer's experience in southwestern British Columbia. The term "debris" is used according to Varnes' definition. All the events observed in this study had a sufficiently high content of coarse material to be classed as debris flows, not mudflows or earthflows. The word "landslide" is used by many authors as an imprecise, general term to describe a variety of mass movement processes and deposits. It is used in this context in the present study.

In addition to the mass movement phenomena discussed above, there are several other categories of mass movement which could be considered transitional to debris flows. In the study area, there are a number of debris flows which originated from rockfall or rock avalanches. If the material initially involved in rock failure consists mainly of bedrock fragments, then it would be classed as a rock avalanche (or fall or slide), not a debris avalanche, but it is not unusual for rock avalanche deposits to be disaggregated and crushed to the point of having a very high proportion of sand and fines. Therefore, there may be events transitional between debris flows and rockfalls or rock avalanches, although no such events have been documented in this study. Events may also occur which are transitional between debris flows and snow avalanches. At the other extreme of texture, mudflows can be transitional with earthflows or other failures of fine-textured material. For example, the sensitive clay landslides of eastern Canada (Mitchell and Markell, 1974) are slumps which evolve to rapid mudflows, but they are not true debris flows because they contain very little coarse sediment.

## 1.3 DEBRIS FLOWS IN THE REGIONAL CONTEXT OF SOUTHWESTERN BRITISH COLUMBIA

Debris flow has long been recognized as a common phenomenon in semi-arid and arctic/alpine regions (Blackwelder, 1928; Rapp, 1960), but it is relatively recently that debris flow has been recognized as an important geomorphic process in humid, temperate regions (Swanston and Swanson, 1976; Miles and Kellerhals, 1981; Costa, 1984; VanDine, 1985). Early descriptions of debris flows used the term "mudflow"; however, most recent publications have adhered to Varnes' definitions of debris flow and mudflow. Much of the earlier work on debris flow processes and geomorphology was done in arid and semi-arid regions (for example, Johnson, 1970), probably because of the lack of obscuring vegetation and the excellent preservation of deposits in these regions. In humid regions such as coastal British Columbia, dense vegetation and active fluvial processes delayed both the recognition and study of debris flows.

In Canada, early descriptions of debris flows were given by Winder (1965) in Alberta, and by Broscoe and Thomson (1969) in Yukon. Owens (1972, 1973) studied debris flows on talus slopes in the Rocky Mountains of Alberta. This was the first thorough study of active debris flow phenomena in Canada. All of these references used the term "alpine mudflow". In the semi-arid southern interior of British Columbia, Ryder (1971) studied early Holocene alluvial fans ("para-glacial" fans) built largely by debris flows shortly following deglaciation. Several descriptions of modern debris flows in British Columbia appeared in unpublished engineering reports before about 1980 (reviewed in VanDine, 1985). In southwestern British Columbia, O'Loughlin (1972) studied debris slides and avalanches in forested terrain in the Howe Sound area, and Russell (1972) identified high rates of sediment movement during floods on small creeks entering Howe Sound. However, the significance of debris flow as a geomorphic process does not appear to have been recognized at this time. The first publication in the scientific literature which described debris flows and recognized their geomorphic importance in the humid, forested environment of southwestern British Columbia was apparently that of Nasmith and Mercer (1979).

In the northwestern United States, the term "debris torrent" was introduced to describe debris flows consisting of non-cohesive mixtures of rock, soil and organic material in steep stream channels in humid, forested environments (Swanston and Swanson, 1976). Since 1980, debris flows of this type have been recognized as frequent occurrences in many steep, low-order channels in southwestern British Columbia (Miles and Kellerhals, 1981; VanDine, 1985; Slaymaker, 1988). Much of the work in this region has focused on debris flows which present a hazard to highways and residential development, especially in the Howe Sound and Fraser Valley areas (Thurber Consultants Ltd., 1983; Evans and Lister, 1984; Hungr *et al.*, 1984, 1987; Bovis and Dagg, 1988). Research attention has also been focused on debris flow processes in forested environments, with respect to the role of logging and forest road development in initiating, and increasing the frequency of, debris avalanches and debris flows (Swanston and Swanson, 1976; Wilford and Schwab, 1981; Benda and Dunne, 1987; Benda and Cundy, 1990; Curran *et al.*, 1990; Buchanan and Savigny, 1990; Fannin and Rollerson, 1993).

Large volcanic-origin debris flows, or lahars, from active or recently active volcanoes have been given considerable attention in the northwestern United States, where they present a significant hazard to populated areas (Crandell, 1971; Crandell *et al.*, 1979; Scott, 1989; Scott *et al.*, 1992). Crandell applied the term "lahar" to all debris flows originating on the slopes of a volcano, whether or not they are associated with volcanic eruptions. However, most recent studies have restricted the term to debris flows which are initiated, directly or indirectly, by a volcanic eruption (*e.g.* Scott, 1988). The latter usage of the term is adhered to in this study. Research on lahars was given a great impetus by the 1980 eruption of Mount St. Helens, which was followed by a number of studies (for example, those of Wigmosta, 1983; Fairchild, 1985; Pierson, 1985; Pierson and Scott, 1985; Major and Voight, 1986; Pierson, 1986; and Scott, 1988). In British Columbia, several large landslides have been described in the Quaternary volcanic complexes (Mathews, 1958; Mokievsky-Zubok, 1977; Moore and Mathews, 1978; Clague and Souther, 1982), and it has been noted that large landslides are relatively more frequent in the volcanic complexes than in other geologic environments (Eisbacher and Clague, 1984; Evans, 1984). Some of these landslides produced relatively small, secondary debris flows.

Two large debris flows in the Mount Meager and Mount Garibaldi volcanic complexes were described in somewhat obscure references (Carter, 1932; Jones, 1959). However, despite these observations, and despite the proximity of the volcanoes of southwestern British Columbia to populated areas, the hazard presented by large debris flows in the valleys below the volcanoes has received almost no attention from either the scientific community or from government authorities, at least until very recently (Jordan, 1987a; Thurber Engineering Ltd. and Golder Associates Ltd., 1993).

Several examples of debris flows initiated by outburst floods from ice-dammed or moraine-dammed lakes have been described in British Columbia (Jackson, 1979; Clague *et al.*, 1985; Jordan, 1987b). Some debris flows on Mount Rainier have been attributed to glacial outburst floods (Richardson, 1968; Driedger and Fountain, 1989).

From the above historical outline, it is apparent that a number of types of debris flows occur in different environments and with different initiating mechanisms. These include (in approximate historic order of introduction in the literature):

a) arid-region, rainstorm-generated debris flows ("desert mudflows");

b) debris flows occurring on steep talus slopes, mostly but not exclusively in alpine or arctic regions ("alpine mudflows");

c) volcanic-source debris flows, originating either from volcanic eruptions (lahars), or from mass movement on volcanoes;

d) large landslides which generate secondary debris flows;

e) debris flows which occur during and following deglaciation, originating in freshly exposed morainal material;

f) debris flows originating from outburst floods of ice-dammed or moraine-dammed lakes (this category could also include debris flows from failure of engineering structures);

g) rainstorm-initiated debris flows in steep creek channels in humid, forested environments;

h) debris flows on forested slopes or in small gullies, initiated by shallow debris slides which are often caused by forestry activities.

Debris flows in all of these categories are likely to occur in British Columbia, and some of them are common enough to be the dominant geomorphic and sediment transfer processes in the environments where they occur. Regardless of their origin, debris flows in all these categories behave in a similar manner with respect to their flow in confined channels, deposition on fans or in valley bottoms, and deposits of similar morphology. Although there is considerable variety in the behaviour and deposit morphology of debris flows, this is due primarily to differences of scale and of debris composition, rather than to origin or hydrologic environment. There are some differences in typical debris flow composition and behaviour between British Columbia and most American locations, due mainly to the abundance of morainal deposits and glacially oversteepened slopes, and the lack of residual soils, in British Columbia.

In the present study, most of the debris flows examined belong to categories (c) and (g) above. They include debris flows in Quaternary volcanic complexes, some of which are sufficiently large and mobile to be equivalent to the "lahars" of Crandell (1971), and debris flows in steep creek channels underlain by predominantly plutonic, coarse-textured rock, which tend to be smaller and less mobile. As will be demonstrated, these two populations of flows differ considerably in their behaviour and deposit morphology.

# CHAPTER 2. THEORY

Materials can respond to an applied stress in several fundamentally different ways, including elastic deformation, viscous deformation, and plastic deformation. Some geologic materials deform in response to shear stress according to one of these simple models, but many respond according to more complex models which are combinations of the simple models (Strahler, 1952; Johnson, 1970). For example, an unsaturated soil may behave in a manner similar to a perfect plastic under shear stress, but some fine-textured soils, or those with a higher water content, may deform with components of both plastic and viscous behaviour.

In the case of a fluid, such as water, which deforms as a simple viscous substance, flow can be laminar or turbulent. In laminar flow, resistance is due to internal viscous deformation; in turbulent flow, resistance is due mainly to the roughness of the flow boundaries (Leopold *et al.*, 1964; Massey, 1970).

Debris flows, which consist of a mixture of water and granular solids (and minor amounts of other materials), could conceivably be described by laminar flow, turbulent flow, plastic deformation, or some combination of these models. Evidence from photographic and eyewitness observations of debris flows (Johnson, 1970; Costa, 1984; Pierson, 1986) indicates that flow in the frontal, deepest part of debris flow surges is predominantly laminar. Exceptions to this generalization may include unusually fluid debris events which are more likely sediment-charged dam-break floods, and the relatively fluid afterflow (or hyperconcentrated flow) phases of many debris flows. The prevalence of laminar flow is a fundamental property of debris flow which distinguishes it from streamflow.

## 2.1 BASIC RHEOLOGIC MODELS

Rheologic models which have been applied to debris flows fall into three general categories: the Newtonian or viscous model, the Bingham or viscoplastic model, and the granular flow or dilatant model. All of these models assume laminar flow.

The flow laws for the three models can be given in one-dimensional form as follows (after Johnson, 1970; Takahashi, 1981; Chen, 1987; and many others):

Newtonian model: $$\tau = \mu \frac{du}{dz} \quad (2.1)$$

Bingham model: $$\tau = k + \mu_B \frac{du}{dz} \quad (2.2)$$

Granular flow model: $$\tau = \mu_G \left(\frac{du}{dz}\right)^2 \quad (2.3)$$

where $\tau$ is shear stress, u is velocity, z is elevation above a datum, du/dz is the strain rate, which is equal to the velocity gradient for one-dimensional flow, k is the Bingham yield strength, and $\mu$ is viscosity or an analogous flow resistance coefficient. Elevation, z, is in the direction of maximum velocity gradient, which for one-dimensional, uniform, open-channel flow, is up and perpendicular to the bed. These flow laws are illustrated in Figure 2.1. They can also be expressed in terms of a general laminar flow law (eq. 2.24).

If a material deforms according to eq. 2.1, it is by definition a Newtonian fluid, and $\mu$ is Newtonian viscosity. In the Bingham model, the fluid deforms only after a finite yield strength k is exceeded, whereupon it deforms at the rate determined by the Bingham viscosity $\mu_B$. The Newtonian law is a special case of the Bingham model with k=0. The Bingham model was applied by Johnson (1970) to explain many observed features of debris flows in the southwestern United States.

The dilatant or granular flow model, in which resistance to deformation (apparent viscosity) increases with increasing strain rate, was applied by Bagnold (1954) to dispersions of uniform-sized particles in a fluid. (With dilatant flow, the exponent in eq. 2.3 can be any number greater than 1; however, Bagnold's model uses an exponent of 2.) Bagnold performed experiments which showed that normal and shear stresses in such a dispersion are resisted by dispersive stresses generated by colliding grains. The model has been applied specifically to debris flows by Takahashi (1978, 1981).

Many other flow laws describing non-Newtonian behaviour are possible. They are usually expressed in terms of different exponents and yield strength terms in the general laminar flow law (Fig. 2.1). For example, the flow of glacier ice is often described by a pseudo-plastic model in which an exponent of 1/3 is applied to the strain rate (Paterson, 1981).

## 2.2 APPLICATION OF RHEOLOGIC MODELS TO DEBRIS FLOW

If the depth of flow, or thickness, in a channel is H, z in the equations above can be replaced with H-h, where h is depth below the surface. For one-dimensional steady flow, the shear stress on a plane, parallel to the surface at depth h and with slope θ, is given by

$$\tau = \gamma h \sin\theta \tag{2.4}$$

where γ is unit weight. Eqs. 2.1 to 2.3 can be combined with eq. 2.4 and integrated to give velocity profiles. The velocity profile equations can be integrated again over depth to give formulae for mean velocity, U, as a function of flow depth. Similar integrations can be performed over radius to give formulae for semi-circular channels, by assuming that shear stress is identical at all points of the channel circumference (*i.e.* the velocity profiles are identical along all radii). These formulae for the three models are given below, replacing sin θ with S for simplicity. Definition sketches for the channels are shown in Figure 2.2, and the general form of the velocity profiles is shown in Figure 2.3.

Newtonian model

For Newtonian flow in an infinitely wide channel of depth H, the velocity profile is given by:

$$u_{(h)} = \frac{\gamma S}{2\mu}\left(H^2 - h^2\right) \tag{2.5}$$

and the mean velocity, U, is:

$$U = \frac{\gamma S H^2}{3\mu} \tag{2.6}$$

For a semi-circular channel of radius R, the velocity profile and mean velocity are, where r is radial distance from the centre:

$$u_{(r)} = \frac{\gamma S}{4\mu}\left(R^2 - r^2\right) \tag{2.7}$$

$$U = \frac{\gamma S R^2}{8\mu} \tag{2.8}$$

These formulae (or similar ones) can be found in many fluid mechanics texts (for example, Massey, 1970), where the equivalent of eq. 2.8 is usually developed for flow in pipes. The simple Newtonian model, while it does not explain some commonly observed features of debris

flows such as apparently rigid plugs and segregation of coarse clasts, is useful in that it provides a simple, single-parameter index of debris flow mobility (Hungr, 1981). Since the apparent Newtonian viscosity can be easily calculated from eqs. 2.6 and 2.8, given observations or estimates of mean velocity and debris density, many investigators have calculated apparent viscosities for debris flows (reviewed in Costa, 1984). Some of these results are reviewed in Table 2.1.

Bingham or visco-plastic model

The Bingham model combines a plastic yield strength, k, with a viscous resistance term (Bingham viscosity, $\mu_B$). It was applied to debris flow by Johnson (1970) and by Johnson and Rodine (1984), who used it to explain features of debris flow deposits observed on alluvial fans in the southwestern United States. The applicability of the Bingham model to debris flow and other mass movement phenomena had been suggested earlier by Strahler (1952).

In a flowing Bingham substance, shear stresses near the surface, and near the centre for flow in a semi-circular channel, will be less than the yield strength of the substance, and no shear deformation will occur. The result is a "plug" of undeformed material, the dimension of which is a function of the yield strength k. The thickness $T_0$ for an infinitely wide channel, and the radius $R_0$ for a semi-circular channel, are given respectively by:

$$T_0 = \frac{k}{\gamma S} \tag{2.9}$$

$$R_0 = \frac{2k}{\gamma S} \tag{2.10}$$

For a wide channel, the velocity profile and mean velocity are:

$$u_{(h)} = \frac{\gamma S}{2\mu_B}\left[\left(H^2 - h^2\right) - 2T_0(H-h)\right], \quad h \geq T_0 \tag{2.11}$$

$$U = \frac{\gamma S H^2}{3\mu_B}\left[\frac{1}{2}\left(\frac{T_0}{H}\right)^3 - \frac{3}{2}\frac{T_0}{H} + 1\right] \tag{2.12}$$

and for a semi-circular channel:

$$u_{(r)} = \frac{\gamma S}{4\mu_B}\left[\left(R^2 - r^2\right) - 2R_0(R-r)\right], \quad r \geq R_0 \tag{2.13}$$

$$U = \frac{\gamma S H^2}{8\mu_B}\left[\frac{1}{3}\left(\frac{R_0}{R}\right)^4 - \frac{4}{3}\frac{R_0}{R} + 1\right] \qquad (2.14)$$

If k = 0, then eqs. 2.11 to 2.14 reduce to the corresponding equations for a Newtonian fluid; thus, the Newtonian model can be considered a special case of the Bingham model.

The yield strength of static debris can be determined by observing the thickness of debris flow deposits on alluvial fans, from eq. 2.9, or from the size of large boulders supported by fine debris in the deposits (Johnson, 1970; Johnson and Rodine, 1984). The yield strength and Bingham viscosity of moving debris can be determined only if the velocity and dimensions of the moving plug can be measured, something which can be accomplished only under the most favourable conditions. Johnson (1970) measured the velocity profile across a debris flow at Wrightwood, California by photographing moving debris and measuring the streaks caused by sunlight reflecting off stones in the debris (a technique which is feasible only in an arid climate!). Pierson (1986) calculated the Bingham parameters for a small debris flow at Mount St. Helens by using velocity profiles recorded by motion picture photography.

Dilatant or granular flow model

Takahashi (1978) developed a model for debris flow movement based on the dispersive pressure concept of Bagnold (1954). Bagnold performed experiments in which neutrally buoyant, uniform-sized spheres were sheared in an annular apparatus. Under fully inertial conditions, for which viscous effects can be considered negligible, Bagnold found that the dispersive pressure P exerted by shearing grains is proportional to the square of the velocity gradient du/dz and of grain diameter D:

$$P = a\rho_s\lambda^2 D^2\left(\frac{du}{dz}\right)^2 \cos\alpha \qquad (2.15)$$

where a is a constant, $\rho_s$ is grain density, $\lambda$ is "linear concentration" (related to the cube root of volumetric grain concentration), and $\alpha$ is an internal friction angle. This is related to shear stress $\tau$ by

$$\tau = P\tan\alpha \qquad (2.16)$$

This is the same as eq. 2.3, if the terms describing material properties are replaced by $\mu_G$. If these equations are solved, the velocity profile is:

$$u_{(h)} = \frac{2}{3}\left(\frac{\gamma S}{\mu_G}\right)^{1/2}\left(H^{3/2} - h^{3/2}\right) \tag{2.17}$$

and the mean velocity is:

$$U = \frac{2}{5}\left(\frac{\gamma S}{\mu_G}\right)^{1/2} H^{3/2} \tag{2.18}$$

More specifically, Takahashi (1978) gave the velocity profile as

$$u_{(h)} = \frac{2}{3D}\left\{\frac{gS}{a\sin\alpha}\left[c_v + (1-c_v)\frac{\rho_f}{\rho_s}\right]\right\}^{1/2}\left[\left(\frac{c^*}{c_v}\right)^{1/3} - 1\right]\left(H^{3/2} - h^{3/2}\right) \tag{2.19}$$

where $\rho_f$ is interstitial fluid density, $c_v$ is volumetric concentration of grains, $c^*$ is concentration of grains in the static bed, and $\lambda$ in eq. 2.15 is replaced with

$$\lambda = \left[\left(\frac{c^*}{c_v}\right)^{1/3} - 1\right]^{-1} \tag{2.20}$$

Hungr *et al.* (1984) give eq. 2.18 in similar form, using the term $\xi$ in place of $(\gamma/\mu_G)^{1/2}$.

If the derivation of eqs. 2.17 and 2.18 is repeated for a semi-circular channel, these become:

$$u_{(r)} = \frac{1}{3}\left(\frac{2\gamma S}{\mu_G}\right)^{1/2}\left(R^{3/2} - r^{3/2}\right) \tag{2.21}$$

$$U = \frac{1}{7}\left(\frac{2\gamma S}{\mu_G}\right)^{1/2} R^{3/2} \tag{2.22}$$

According to Takahashi (1981), experiments have found that the median grain diameter can be used as the representative diameter D. He has also shown (Takahashi, 1980), by experiment and theoretical analysis, that the concentration of clay likely to exist in the interstitial fluid is too small for the debris to behave as a Bingham substance capable of supporting large particles, or for the debris to exist outside the fully inertial range according to Bagnold's (1954) criteria. He used Bagnold's theory to explain the migration of large particles to the surface of the debris and towards the debris flow snout.

Other models

Johnson and Rodine (1984) extended the simple visco-plastic model to give the more generalized Coulomb-viscous model, in which the Bingham yield strength is replaced by the Coulomb strength parameters:

$$\tau = c + \sigma_n \tan\phi + \mu_c \frac{du}{dz} \qquad (2.23)$$

where c is cohesion, $\sigma_n$ is normal stress, $\phi$ is the apparent angle of internal friction, and $\mu_c$ is viscosity. In this model, the plastic yield strength is due to two components, cohesion of fine-grained material, and friction between coarse clasts. The latter component depends on depth in the debris as well as the frictional properties of the debris. (c and $\phi$ are given in terms of the total stress model, not the effective stress model used in Chapter 6.)

The equations describing velocity profiles and plug thickness are of similar form to those for a Bingham substance, with the addition of $\phi$ (Johnson and Rodine, 1984). No flow in this model would be possible unless the slope is greater than $\phi$. Johnson and Rodine (1984) give a method for calculating c and $\phi$ if both the thickness of a deposit and the maximum size of supported clasts can be observed. When this method was applied by Johnson and Rodine to debris flow deposits, the apparent friction angle $\phi$ was very small, 2° or less, and apparent cohesion c was close to the value of k calculated for the Bingham model. Johnson and Rodine (1984) attributed this result to undrained conditions which prevail in flowing debris. This model, therefore, does not contribute much useful information beyond that given by the Bingham model.

Chen (1987, 1988) presented a generalized visco-plastic model, which can be written (making some changes to Chen's notation, and assuming cos $\phi$ = 1)

$$\tau = c + \sigma_n \tan\phi + \mu\left(\frac{du}{dz}\right)^n \qquad (2.24)$$

where n is a "flow behavior index". It is apparent that all the models described previously are special cases of this model. For the one-dimensional case, Chen obtained general equations for the velocity profile and for mean velocity. The latter can be written:

$$U = \frac{n}{n+1}\left(\frac{\gamma S}{\mu}\right)^{\frac{1}{n}}\left(1-\frac{T_0}{H}\right)^{\frac{n+1}{n}}\left[1-\frac{2}{2n+1}\left(1-\frac{T_0}{H}\right)\right]H^{\frac{n+1}{n}} \qquad (2.25)$$

It can be seen that eqs. 2.6, 2.12, and 2.18 are special cases of this equation, with n=2 for the granular flow model, and n=1 for the Bingham and Newtonian models. Chen also solved his equations to give a velocity profile without assuming that concentration of solids (and therefore unit weight) is constant with depth. This profile, according to Chen, agrees with some Japanese experimental results better than do the previously described models, which assume a uniform grain concentration.

The Coulomb-viscous model and the generalized visco-plastic model use an increasing number of parameters to describe the physical properties of the debris. Eq. 2.24 uses four parameters, compared with one for the simple Newtonian and the granular flow models. This makes it possible to fit the model to almost any set of experimental or field data; however, it makes it almost impossible to calculate parameters for debris flows which have left limited or ambiguous field evidence.

Some Russian investigators have developed empirical formulae for debris flow movement based on the Chezy equation; these are reviewed by Hungr (1981) and by Costa (1984). According to Hungr, this approach is inappropriate, as most debris flow is believed to be laminar. However, Pierson (1980, 1986) has observed turbulent flow in some debris flows, and Pierson and Costa (1987) identify hyperconcentrated streamflow as a flow regime between debris flow and streamflow, in which turbulence is damped by high sediment concentration. A turbulent flow model might be appropriate for such flow, and for the more fluid phase of some debris flows.

Discussion

The three basic rheologic models described above (or two, since the Newtonian model is a special case of the Bingham model) are simple one or two parameter models which can be used to describe the flow of a uniform fluid or dispersion of grains. Several more complex or more inclusive models achieve better description of debris flow by using a greater number of parameters which can be adjusted to fit a particular set of observations. It is difficult, and

probably unjustified, to apply the more complex models to predict actual debris flow behaviour, since there is rarely sufficient information available from field evidence to reliably estimate more than one or two parameters. Hungr *et al.* (1984) found that either of the one-parameter models, with a unique flow resistance value, could adequately describe observed peak velocities for a number of debris flow events in southwestern British Columbia.

All the models described above apply to the main body of a debris flow surge, which forms the bulk of the volume of most events, and controls the behaviour of the surge at the peak flow depth (see Figure 2.8). As discussed in section 2.5 below, it is unlikely that a single rheologic model can be used to describe the behaviour of all parts of a debris flow surge, since debris flow is a highly non-uniform phenomenon in which material properties vary in different parts of the surge. Any of the models described above can be used for mathematical simulation of unsteady, non-uniform flow, but such simulations generally require uniform values of the flow parameters throughout the flow. The models which have been applied to debris flow and other natural phenomena are generally those which lend themselves to analytic solution of flow problems, not necessarily those which provide the best empirical description of the deformation behaviour of the materials involved.

However, application of the above models describing ideal rheologic substances has proven valuable for explaining qualitatively some of the features of debris flows and their deposits which have been observed in the field. Johnson (1970) found that the Bingham model could explain the existence of an approximately rigid plug of material in a moving debris flow, as well as features such as the formation of lateral deposits or levées, deposition of debris in "dead zones" on the channel sides and bottoms, and the tendency of debris flows to erode U-shaped channels. The existence of these U-shaped channels justifies the choice of a semi-circular cross-section as a reasonable one for the analysis of debris flow movement. Takahashi (1981) found that the granular flow model, based on Bagnold's concept of dispersive stress, could explain the migration of coarse clasts to the top and front of the flow, and the transport of very large stones by debris flows.

Takahashi's model has been criticized on several grounds (Hungr, 1981; Iverson and Denlinger, 1987). In particular, it assumes uniform concentration of grains (although according to Iverson and Denlinger, this is not required by the equation of flow), and it tries to explain the behavior of debris which has a variety of grain sizes, although Bagnold's experiments and equations, on which the model is based, used uniform-sized grains. A major problem with Takahashi's model is that it treats debris as two distinct phases, grains and interstitial fluid. The distinction between the two phases is arbitrary, especially in a widely-graded slurry. Iverson and Denlinger (1987) point out that to overcome this difficulty, such a model must deal with the interactions between the two phases, something that would further increase the mathematical complexity of the model. Hungr (1981) mentions that, according to Takahashi's model, steady uniform flow would only be possible on slopes for which $\theta=\phi$ (or $\alpha$); also, Takahashi's analysis is based on completely drained loading of the bed by the debris flow, something that would be possible only for coarse uniform material.

The two categories of model represent two end points of debris flow behaviour, which were termed "viscous" and "inertial" by Bagnold (1954). They may describe two distinct types of debris flow, consisting of different material: viscous (Bingham or Newtonian) flows of relatively fine-textured, cohesive material; and inertial (dilatant or granular) flows of coarse-textured, stony debris with a relatively non-viscous interstitial fluid. Flows of intermediate flow properties must also exist; an intermediate constitutive equation could theoretically be given by eq. 2.24, although such models have not often been applied in practice. As Hungr *et al.* (1984) point out, the Newtonian and dilatant models are not very different rheologically; for modeling flow in channels they give similar results, and therefore intermediate models may not be necessary. It is also possible that the two types of model may apply to different parts of a flow, or that a debris flow could change from one type of flow to another if its water content or sediment composition change during flow.

## 2.3 EFFECT OF CHANNEL SHAPE

For the Newtonian model, Hungr *et al.* (1984) give the equation for mean velocity in the form of

$$U = \frac{\gamma S}{K\mu} H^2 \qquad (2.26)$$

where K is a shape factor which varies from 3 for an infinitely wide rectangular channel, to 8 for a semi-circular channel. Formulae of this form for flow in conduits of various shapes, derived from analytical or numerical solutions, are found in the fluid mechanics literature. A number of them are summarized in Straub *et al.* (1958), who by theory and experiment show that resistance to laminar flow is sensitive to channel shape. Their experiments confirmed the validity of the theoretical shape factors for flow in smooth channels, although in rough channels resistance to flow was found to be slightly greater than that predicted by eq. 2.26. Two channel shapes which are useful for describing debris flow channels are the semi-ellipse and the rectangle.

For a semi-elliptical channel, if the width:depth ratio (twice the ratio of the major and minor axes of the ellipse) is $\beta$, the shape factor can be given by

$$K = \frac{4(\beta^2 + 4)}{\beta^2} \qquad (2.27)$$

Since many natural channel cross-sections approximate a semi-ellipse, this formula provides a practical means for modeling Newtonian flow. For a semi-circular channel, $\beta$=2 and K=8, and for an infinitely wide elliptical channel, K=4.

The shape factors for a rectangular channel are given by a complex formula (Fig. 2.4); for a width:depth ratio of 2, K=7.11, and for an infinitely wide channel, K=3. This formula and those for several other channel shapes are summarized in Fig. 2.4. Most of these formulae are due to Boussinesq (1868). The shape factor for a "trapezoidal" channel given by Straub *et al.* (1958) is incorrect. Fig. 2.4 gives the correct factor, after Synge (1953).

For Bingham flow in an elliptical channel, Johnson and Rodine (1984) give a formula for calculating the yield strength from the width and thickness of a stalled "plug" filling a channel. If $\beta$ is the width:depth ratio and T is plug thickness (or depth), this can be written as

$$k = \frac{T\gamma S}{(1 + 4/\beta^2)} \qquad (2.28)$$

which is similar in form to eq. 2.27. Although Johnson and Rodine apply this formula only to a stalled plug, it seems reasonable to apply it also to a moving plug in an elliptical channel, since it

becomes eq. 2.9 for an infinitely wide channel and eq. 2.10 for a semi-circular channel. Johnson and Rodine (1984) also derived eqs. 2.13 and 2.14 for Bingham flow in a semi-circular channel. Analytic solutions apparently do not exist for Bingham flow in elliptical channels of other dimensions, or for channels of other shapes. Johnson and Rodine stated that the velocity distribution for Bingham flow in a rectangular channel should be similar to that for a semi-circular channel, on the assumption, supported by field observations, that "dead zones" should form in the corners of a rectangular channel, leading to an essentially elliptical flow boundary.

The analysis of Johnson and Rodine (1984) is based on observations of moving debris flows, or of debris flow deposits, to calculate the Bingham yield strength and viscosity. Although many natural debris flow channels can be approximated reasonably by a semi-ellipse, a problem with applying their methods is that it is impossible to directly observe the plug thickness (or for that matter, the depth of flow) in a moving debris flow, and calculations based on observations of width alone are likely to be unreliable because most natural channels depart considerably from the theoretical elliptical shape at the channel edges. In addition, many natural channels have a width:depth ratio greater than 2, so the analytic solutions of Johnson and Rodine for a semi-circular channel do not apply.

Some useful information on the effect of channel shape on the flow of Newtonian and Bingham fluids can be gained by examining the distribution of velocity and shear stress in elliptical and rectangular channels. The formulae for velocity distribution of a Newtonian fluid are shown on Fig. 2.4. The velocity gradient vector at any point is given by

$$\nabla \mathbf{u} = \mathbf{i}\frac{\partial u}{\partial y} + \mathbf{j}\frac{\partial u}{\partial h} \tag{2.29}$$

where **i** and **j** are unit vectors in the y and h directions. For an elliptical channel, the magnitude of the velocity gradient is

$$|\nabla \mathbf{u}| = \frac{\gamma S}{\mu\left(b^2 + d^2\right)}\left(d^4 y^2 + b^4 h^2\right)^{1/2} \tag{2.30}$$

For a rectangular channel, the velocity gradient can be calculated numerically from the velocity field (unless one wishes to differentiate the formula in Fig. 2.4). The shear stress on a surface perpendicular to the velocity gradient vector is, from eq. 2.1,

$$\tau = \mu|\nabla \mathbf{u}| \tag{2.31}$$

As an example, Figure 2.5 shows the distribution of velocity and velocity gradient across elliptical and rectangular channels with a width:depth ratio of 4, and a mean velocity of 1 (arbitrary units), for a Newtonian fluid. Fig. 2.5d shows that, in a rectangular channel, there is a concentration of shear stress at the centre of the channel bottom, and at the top corners, and shear stress approaches zero at the bottom corners. Thus, erosion of the channel boundaries is likely to be concentrated at the bottom centre and at the top corners, and if the channel is erodible it will tend to develop an elliptical shape. If the material is a Bingham fluid, the critical shear stress will probably not be exceeded in the bottom corners, and "dead zones" will form, as suggested by Johnson and Rodine (1984). Deposition in these dead zones will contribute to the tendency for an elliptical cross-section to form. In an elliptical channel (Fig. 2.5b), shear stress is concentrated on the channel bottom; thus, erosion will tend to deepen the channel. In a semi-circular channel, shear stress will be equal at all points of the circumference. Most fluvially dominated channels down which debris flows travel tend to have high width:depth ratios, so wide elliptical cross-sections are common for debris flows. Some channels which are dominated by debris flows rather than fluvial processes have low width:depth ratios and are close to semi-circles (for examples, see Chapter 4). This analysis shows that, in erodible materials, debris flow channels should tend to develop an elliptical, and ultimately a semi-circular, cross-section.

Shape factors for Newtonian flow in elliptical and rectangular channels are graphed on Fig. 2.6, along with an estimated curve for granular flow in elliptical channels. For granular flow, solutions for channel shapes other than semi-circular and wide rectangular are not known to the writer. For these shapes, K is 4.95 and 2.5 respectively, if the equation of flow is written

$$U = \frac{1}{K}\left(\frac{\gamma S}{\mu_G}\right)^{1/2} H^{3/2} \tag{2.32}$$

For practical purposes, an estimated curve for elliptical channels is derived by interpolating between these two end points, and drawing a curve similar to the curve for Newtonian flow. There is no theoretical justification for this procedure; however, an estimated curve is necessary

for application of this model to field data and, given the uncertainty in fitting an ideal shape to an irregularly shaped natural channel, it is probably sufficiently accurate.

For Bingham flow, eqs. 2.12 and 2.14 can be rewritten as

$$U = \frac{\gamma S}{K\mu_B} H^2 F \qquad (2.33)$$

where K is the shape factor as defined above for Newtonian flow, and F is the "Bingham factor", a function of the ratio of plug thickness to flow depth. Figure 2.7 shows this factor plotted for a semi-circular and a wide rectangular channel. The two curves are not very different. Given the great imprecision in estimating plug thickness from field observations, either curve could be used for channels of other shapes. (If greater precision is desired, one could interpolate between them, using $4/\beta^2$ as an interpolation factor.)

There are two objectives of the above development of shape factors and equations of flow:

- to permit calculation of flow parameters from observations of debris flows in motion, or from deposits or channel dimensions observed after debris flow events; and
- to enable mathematical modeling of debris flow in channels of specified dimensions.

The following procedure is proposed for determining parameters in the equations of flow:

- Calculate channel cross-sectional area A.
- Fit the channel as well as possible by either a semi-ellipse or a rectangle with the same area. For an elliptical channel, use the maximum depth H in all formulae. (For an elliptical channel of width B, area is $A = (\pi/4)HB$.)
- Use eq. 2.26, 2.32, or 2.33 for the appropriate flow model. (The shape factor for granular flow is defined here only for an elliptical channel.)

Most of the channels examined in this study could be described better by an elliptical than a rectangular cross-section. This agrees with the observations of Johnson (1970) and Johnson and Rodine (1984). Rectangular cross-sections might apply to wide fluvial floodplains and to some bedrock canyons.

The analysis above, and Figs. 2.4 and 2.6, show that the parameters for laminar flow are highly sensitive to channel shape and width:depth ratio. The procedure described in this section

is probably reasonably accurate for calculating flow parameters in most channels of simple cross-section. However, it would be less accurate for channels with irregular cross-sections, such as a deep inner channel within a wider outer channel (such cross-sections were often observed in this study). For these channels, using an equivalent elliptical cross-section would tend to underestimate K, since a semi-ellipse is the most efficient channel shape for a given width:depth ratio.

## 2.4 CHANNEL BENDS AND OBSTRUCTIONS

In the absence of eyewitness observations, debris flow velocities are often estimated using the superelevation at bends or the runup on obstructions, as defined by mud lines left by debris flows. The superelevation equation is given by Chow (1959), Johnson and Rodine (1984), Costa (1984), Pierson and Scott (1985), and others as

$$U = \left[ \frac{g r_c \Delta h \cos\theta}{B} \right]^{1/2} \tag{2.34}$$

where $r_c$ is the radius of curvature of the centre line of a channel bend, $\Delta h$ is the superelevation between the two sides of the flow, B is the surface width, $\theta$ is the longitudinal channel slope, and g is the gravitational constant.

Hungr *et al.* (1984) believed that this equation overestimates velocity, and included a correction factor of 2.5 in the denominator (which reduces calculated velocities by a factor of 1.58), based on Japanese experiments on granular flow. Chen (1987), however, expressed reservations about the validity of these experiments. The experiments are described by Takahashi (1991); they were performed on flows of relatively low concentrations of sand and fine gravel in water, and may not be representative of typical debris flows.

Wigmosta (1983) analyzed the assumptions involved in the superelevation equation, which include:

- the square of the cross-sectionally-averaged velocity can be substituted for the mean of the squares of the filamental velocities (Chow, 1959);
- the cross-channel slope is constant (it is not, it is more likely to be concave upward); and
- $b \ll r_c$.

Wigmosta found that these assumptions produced compensating errors, with the error (up to 44%) due to the first assumption tending to dominate and produce a small net underestimate of velocity.

The superelevation equation was found to slightly underestimate velocity by Pierson (1985), who measured superelevation at a number of bends on large lahars at Mount St. Helens, and compared the calculated velocities to independently measured average velocities for the lahars. On this basis, Pierson used the superelevation equation in its uncorrected form.

The question of the accuracy of the superelevation equation remains unresolved. In the present study, eq. 2.34 is used uncorrected, on the basis of Wigmosta's (1983) and Pierson's (1985) conclusions, and because the lahars studied by Pierson (1985) are similar in texture and behaviour to several of the large debris flows examined in this study.

The runup or velocity head equation can be applied to debris flows which run up against an obstruction oriented roughly perpendicular to the flow direction:

$$U = (2g\Delta h)^{1/2} \qquad (2.35)$$

where $\Delta h$ is the height of runup. It results from the assumption that all the kinetic energy of a moving object is converted to potential energy (Chow, 1959; Pierson, 1985).

Hungr *et al.* (1984) describe a method for predicting debris flow runout and runup, based on a momentum conservation theory for snow avalanche movement (see section 2.6 below). It is applicable to granular debris dominated by frictional effects, and is sensitive to the value chosen for the dynamic angle of friction. This model predicts runup elevations comparable to, or somewhat greater than, the velocity head equation when both the approach channel and the upstream face of the barrier have slopes gentler than about 20°, but it predicts lower runup on steep barriers. Both this runup model and the velocity head equation have also been applied to rock avalanches (Evans *et al.*, 1989).

Wigmosta (1983) analyzed the runup of flowing debris on trees in the path of the flow, using a combination of empirical measurements and theoretical analysis of laminar viscous flow around a cylinder. He derived the formula

$$U = (1.21g\Delta h)^{1/2} \qquad (2.36)$$

where $\Delta h$ is the elevation difference between the upstream and downstream sides of the tree. He found this to be reasonably accurate (errors less than about 15%) for Reynolds numbers greater than 20.

Debris flow velocities, whether calculated from the methods described above or based on field observations, are subject to large errors, except in the few cases where they have been recorded photographically. Newtonian viscosity and other rheologic parameters are often back-calculated from mean velocity and depth (using eqs. 2.26, 2.33, or their equivalents). These equations contain the square of depth; depth of flow is also often only an approximation, since channels may be of irregular cross-section, or are subject to scour and fill during multiple debris flow events. Thus back-calculated rheologic parameters are likely to be subject to very large errors (in the order of 100%, considering the component errors discussed above), and therefore their calculation by methods other than very simple rheologic models is probably not justified.

## 2.5 TURBULENCE, FLOW REGIMES, AND INSTABILITY

### Flow regime, rheology, and debris properties

The above discussion of models describing debris flow movement assumes that debris flow is laminar. Abundant evidence from eyewitness and photographic observations of moving debris flows shows that this assumption is justified in most cases, and many observations of debris flow deposits show features consistent with laminar flow models (Johnson, 1970; Johnson and Rodine, 1984; Costa, 1984). However, some observations of moving debris flows show that, although flow in the frontal, deepest part of debris flow surges is predominantly laminar, turbulent flow can occur in other parts of debris flow surges (Pierson, 1980, 1986).

A generally accepted model has emerged in which a typical debris flow surge includes a steep front consisting mainly of coarse clasts, followed by the main head portion of the surge, which is the deepest part of the flow and in which flow is laminar. This is followed in turn by a shallower, finer-textured, tail of the flow, in which flow may be turbulent and the water content is higher (Takahashi, 1981; Johnson and Rodine, 1984; Eisbacher and Clague, 1984; Costa, 1984; Pierson, 1986; Pierson and Costa, 1987). These phases of the surge grade into each other (Figure 2.8), and thus the surge forms a continuum in which mean grain size, sediment

concentration, and viscosity decrease from the front (head) of the surge to the tail. This model is applicable to many debris flows of both coarse and fine texture; although the coarse frontal phase may be less well developed, most eyewitness observations and photographs of fine-textured debris flows have described a coarse frontal concentration of stones.

The bouldery front may be deficient in matrix, consisting mainly of cobbles and boulders with open spaces between them. Here, resistance to flow is primarily frictional (Pierson, 1980). The main body of the debris surge which follows consists of a very poorly sorted, saturated, sediment-rich slurry, in which sediment concentration is typically 70-85% by weight (Costa, 1984; Pierson, 1986). Coarse clasts are frequently, but not always, concentrated towards the top of the flow. The tail portion of the flow typically grades into muddy streamflow, or "hyperconcentrated flow", in which sediment concentration is still high enough that turbulence is damped (Pierson and Scott, 1985; Pierson and Costa, 1987).

These flow phases can result in different facies of debris flow deposits. These indicate varying sediment composition and flow dynamics in different parts of the surge, as well as changes in the downstream direction, as described by Scott (1988). The dynamics of the debris flow surge and its phases apparently depend on sediment texture (Pierson and Costa, 1987). If the concentration of large clasts is high, the surge will tend to behave according to a granular flow model, and the bouldery front and concentration of coarse clasts on top will be well developed. Finer textured debris flow surges will tend to behave according to a viscous flow model. If the proportion of cohesive sediment (clay) is high, yield strength will be relatively high. Such debris flows tend to resist mixing with water as they progress downstream; however, non-cohesive debris flows (those low in clay) are likely to entrain additional water as they overtake slower-moving streamflow, becoming lower in viscosity and yield strength as they do so. Many debris flows also entrain gravel and sand from fluvial stream-bed deposits as they move downstream, thus becoming coarser textured. Large non-cohesive lahars (debris flows originating in volcanic material) on Mount St. Helens and Mount Rainier have been observed, or inferred from deposits in the case of older events, to progress from debris flows to hyperconcentrated streamflow as they move downstream (Pierson and Scott, 1985; Scott,

1988), while large cohesive lahars have flowed long distances without significantly changing their sediment composition or flow behaviour (Scott *et al.*, 1992).

A debris flow event often consists of a number of surges in close succession (Johnson and Rodine, 1984; Pierson, 1980, 1986; Costa & Williams, 1984 [video]; and many other descriptions). This may be a result of repeated damming of the stony front of the flow in channel constrictions (Conway, 1907; Sharp and Nobles, 1963; Pierson, 1986), or it may be due to a fundamental instability of the flow (Davies, 1986; see discussion of Froude numbers below).

Although different parts of the flow may be described by quite different rheologic models, the flow behaviour of the surge as a whole can be explained by the deep, sediment-rich, frontal portion, behind which the shallower and more fluid phases are impounded. Thus, it is reasonable to apply a simple, one or two parameter, laminar flow model to the bulk behaviour of debris flow surges. Back-calculation of flow parameters from high mud lines in channels should likewise describe the behaviour of the laminar frontal portion of the surge, since this is the deepest part of the flow. According to Hungr *et al.* (1984), a debris flow surge can be modeled as a simple roll wave (after Chow, 1959). If applicable, this approximation allows the flow at and behind the peak of the surge to be described by the equation of steady, uniform flow, with the speed of the wave front equal to the average flow velocity at the peak.

Laminar and turbulent flow

The distinction between the mechanics of debris flow and debris transport by turbulent streamflow was described (apparently first) by Stini (1910; in German, quoted in English by Eisbacher and Clague, 1984). The distinction is that debris flow behaves as a single-phase phenomenon, which can be modeled as a slurry in which solid particles and liquid move at equal average velocities, while streamflow is a two-phase phenomenon, in which coarse sediment particles are transported by traction at the base of the turbulent, faster-moving liquid.

Various dimensionless parameters, discussed below, are used in fluid mechanics to describe the properties of flow. If physical models are to be constructed for laboratory study, then these parameters can be used to design models so that the properties of flow in the model are similar to those in the "prototype" (or real world). This subject is addressed in Chapter 8.

Also, the dimensionless parameters can be applied to field observations to test assumptions about the flow regime of debris flows of different scales.

The Reynolds number, Re, which is the ratio of inertial to viscous forces, describes whether the flow behaviour of a fluid is laminar or turbulent:

$$Re = \frac{UH\rho_f}{\mu} \qquad (2.37)$$

where H is depth (more commonly given as hydraulic radius) and $\rho_f$ is fluid density. For water, flow is turbulent if Re > 2500, and laminar if Re < 500, with a transition regime at intermediate values (Chow, 1959). For slurries of high sediment concentration, these Reynolds numbers are usually considered to be similar; Davies (1986) gives values of 600 and 1500 for debris flows. Observations of debris flows for which estimates of viscosity and velocity are available generally exhibit Reynolds numbers well within the laminar range (Table 2.1).

Froude number and flow stability

The Froude number

$$Fr = \frac{U}{(gH)^{1/2}} \qquad (2.38)$$

is the ratio between inertial and gravitational forces. A Froude number of 1 distinguishes subcritical from supercritical flow; in the latter, gravity waves cannot be propagated upstream. Pierson (1986) observed "vigourous turbulence" in some debris flows for which Fr > 1; however, there is no theoretical reason why the Froude number should indicate laminar or turbulent flow. It is possible that the disturbed flow surface sometimes observed in the main frontal surge of rapidly moving debris flows (for example, the video of Costa and Williams, 1984) is due to waves caused by channel irregularities in critical or slightly supercritical flow, rather than to actual turbulence.

Debris flows have often been observed to occur as a series of surges. An important question is whether this can be explained by fluid mechanics principles, or if it is due simply to repeated jamming of the debris in channel constrictions. The tendency of some debris flows to occur as a series of closely-spaced pulses or surges was explained by Davies (1986, 1988) as being due to instability of the flow at Froude numbers in excess of a critical value. In some large

debris flows in wide, low-gradient channels, these surges appear remarkably similar to the roll waves often observed in shallow water flow (such waves can also be observed during heavy rainfall on pavement, and with shallow flow through culverts). Henderson (1966) shows that such instability should occur in either laminar or turbulent flow if $Fr > 2$. Mayer (1961) distinguished slug flows, or waves in turbulent flow, from roll waves in laminar flow. The former occur if $Fr > 2$, but the latter can occur at lower Froude numbers. According to Davies (1986), pulsing flow can occur at Froude numbers as low as 0.6 in laminar flow, explaining the waves observed in some large debris flows in China (Li *et al.*, 1983). Savage (1988) showed theoretically that the critical Froude number could be 0.6 or even lower for laminar flow, and that greater cohesion and viscosity would result in a lower critical Froude number. He also states that roll waves have been observed in dry granular flow. Schaerer and Salway (1980) show evidence of similar pulsing flow in a dry snow avalanche. Major and Iverson (1993) report that multiple surges formed in model debris flows in a 95 m long flume, which lends support to the theory that pulsing flow is a fundamental dynamic property of debris flow.

This discussion suggests that, in some cases, a debris flow surge may spontaneously break down into a succession of waves or surges due to hydraulic instability. This has a practical consequence, in that for an event of a given total volume, the peak discharge and velocity would be less if it broke down into a succession of waves, than if it remained as a single surge.

Flow regime, Bingham number, and Bagnold number

The Reynolds Number and the Froude number relate to laminar or turbulent flow regime and to the stability of flow, but they do not provide any information on the flow models (viscous or inertial) which govern the flow of a debris slurry. Enos (1977) refers to experiments on slurry flow in pipes which suggest that the velocity at which flow becomes turbulent is independent of pipe diameter (hence presumably of depth in open channels), but is dependent on the shear strength of the slurry. Therefore the Bingham number

$$Bi = \frac{kH}{\mu_B U} \tag{2.39}$$

which is the ratio of the yield strength to the viscous resistance per unit area, might be a relevant indicator of flow regime. However, no unique value of the Bingham number was found to distinguish laminar from turbulent flow (Enos, 1977).

Bagnold (1954), identified viscous and inertial regimes as a result of his experiments on granular dispersions under shear. He defined two dimensionless parameters which distinguish these regimes. The first of these is analogous to a particle Reynolds number, where D is particle diameter and $\lambda$ is linear grain concentration:

$$G^2 = \frac{\rho_s D^2 \tau}{\mu^2 \lambda} \tag{2.40}$$

The viscous regime is defined by $G < 10$, and the inertial regime by $G > 55$. The other parameter, called by some authors the "Bagnold number" (Lowe, 1976), relates the dispersive stress under inertial and viscous conditions:

$$N = \frac{\lambda^{\frac{1}{2}} \rho_s D^2}{\mu} \frac{du}{dz} \tag{2.41}$$

The viscous regime is defined by $N < 40$, and the inertial regime by $N > 450$. Bagnold found that in the inertial regime, a dilatant rheologic model (eq. 2.3) applied, and in the viscous regime, a linear or viscous model (eq. 2.1) applied. From eqs. 2.40 and 2.41 above, an inertial regime would be favoured by larger particle size, lower viscosity of the interstitial fluid, and greater rates of shear.

(If Bagnold's results are accepted, only one of these two parameters is necessary for the present purpose, which is to distinguish the inertial and viscous flow regimes. Bagnold used a graph of the two parameters to determine the flow behaviour index in each flow regime from his experimental data.)

An inertial regime indicates that a dilatant flow model is more applicable, while a viscous regime favours the Bingham model (or its simplification, the Newtonian model). If representative values of D and $\lambda$ can be defined, then the Bagnold number should define the model which is applicable to a particular debris flow. The Bagnold number has been applied by some authors to justify the use of a viscous model (Davies, 1986; Major and Pierson, 1992), or an inertial model (Takahashi, 1981).

## 2.6 RUNOUT DISTANCE OF DEBRIS FLOWS

The distance of runout of a debris flow on an unconfined fan is a problem of great practical importance. An equation for runout based on momentum conservation was developed by Takahashi and Yoshida (1979; in Japanese, summarized by Hungr *et al.*, 1984, and by Takahashi, 1991). This equation is based on a granular flow model, in which resistance is due to a dynamic internal friction angle $\alpha$. The runout distance $x_L$ is given by

$$x_L = \frac{V^2}{G} \tag{2.42a}$$

$$V = U_0 \cos(\theta_0 - \theta)\left[1 + \frac{gH_0 \cos\theta_0}{2U_0^2}\right] \tag{2.42b}$$

$$G = g(S_f \cos\theta - \sin\theta) \tag{2.42c}$$

$$S_f = \frac{(\rho_s - \rho_f)c_v}{(\rho_s - \rho_f)c_v + \rho_f}\tan\alpha \tag{2.42d}$$

where $\theta$ is the runout slope angle, $S_f$ is the friction slope, $c_v$ is the volume concentration of grains, and $\theta_0$, $U_0$, and $H_0$ are the entry channel slope, velocity, and depth. The equation, the derivation of which is given in Hungr *et al.* (1984), includes terms for the momentum flux and lateral thrust from debris in the upstream channel.

The Takahashi and Yoshida model is dependent on the chosen value of $S_f$. If the fan slope is equal to $S_f$, the runout distance is infinite, and if $\theta > S_f$ then the debris will accelerate. Since colluvial fans have been built by debris flows similar to the ones of interest for modeling, the fan slope is probably very close to the equilibrium slope at which a debris flow will neither accelerate nor decelerate, at least near its apex. This is obviously of some concern for successful application of the runout model for hazard assessment. However, Hungr *et al.* (1984) found that the model compared well with observed runout distances for several coarse-textured debris flows in coastal British Columbia, if a friction slope of tan 10° (corresponding to $\alpha = 30°$) was used.

The approach to modeling runout distance should depend on the rheologic model applied to the debris. In the case of the Newtonian and Bingham models, the above approach is not

applicable, since frictional resistance is assumed to be zero, and all resistance is due to viscous deformation. There are three cases to consider:

1. Granular flow: The frictional model of Takahashi and Yoshida is applicable. As shown by Hungr *et al.* (1984), and as discussed in Chapter 8, a frictional model is applicable to coarse-textured debris flows derived from competent plutonic rocks.

2. Newtonian flow: On any slope, the debris will flow infinitely far and spread to zero thickness, although velocity will become infinitesimally small as it does so. Although the Newtonian model is a reasonable approach for describing many debris flows in relatively deep, confined channels, it is unsuitable for describing runout on fans. The debris will have some Bingham yield strength or frictional strength, which will become significant as the debris thins and spreads out upon losing confinement.

3. Bingham flow: The runout distance of a Bingham fluid is a function of the total volume of the debris flow and the critical plug thickness $T_0$ (eq. 2.9). As the fan gradient decreases, $T_0$ increases; therefore, on a lower gradient fan or wide valley, runout distance (or, more properly, runout area) will be less. On a fan of constant slope, the available debris will spread out to a constant thickness, much as mortar is spread by a trowel. As will be shown in later chapters, there is considerable evidence that the Bingham model is applicable to many fine-textured debris flows derived from weak, clay-rich, geologic materials.

For the Newtonian and Bingham flow models, the velocity of the decelerating debris is of interest because of the high mobility of fine-textured debris flows, and the question remains of whether momentum effects are important in runout. The following derivation analyzes, in a simplified manner, the deceleration of an isolated unit volume of viscous debris. It does not incorporate the equation of continuity, or the momentum imparted by the debris discharging from the channel upstream from the unit volume. It is therefore comparable to the Voellmy (1955) runout equation for frictional debris, not to the Takahashi and Yoshida (1979) model.

Consider a unit volume of debris, flowing as a Newtonian fluid, which discharges from a confined channel with initial velocity $U_0$, onto an unconfined, lower gradient fan of slope $S = \sin \theta$. Assume that, upon reaching the fan apex, the unit volume instantaneously widens and thins to

thickness H, while keeping the same cross-sectional area. At this point, the unit volume still has velocity $U_0$, and has basal area A and mass $m = (\gamma/g)AH$. Fig. 2.9 gives a definition sketch and an example calculation.

The unit volume of debris will decelerate to an equilibrium, or final, velocity $U_f$, given by eq. 2.6. It is assumed that the velocity profile of the debris remains parabolic, similar to that of the equilibrium velocity profile given by eq. 2.5. It is also assumed that H does not change, and that conservation of volume is achieved as the velocity decreases by widening of the debris flow on the unconfined fan. Cross-sectional shape is assumed to be wide rectangular, which is reasonable for unconfined flow. From eqs. 2.1, 2.5, and 2.6, the velocity gradient at the base is given by

$$\frac{du}{dz_{(z=0)}} = \frac{3U}{H} \tag{2.43}$$

and the basal shear stress $\tau$ is therefore

$$\tau = \frac{3\mu U}{H} \tag{2.44}$$

where z is positive upward, U is mean velocity, and H is thickness. The driving force $F_D$, and the resisting force $F_R$, on the unit volume at any time are given by

$$F_D = mgS = \tau_f A = \frac{3\mu A U_f}{H} \tag{2.45}$$

$$F_R = \tau A = \frac{3\mu A U}{H} \tag{2.46}$$

The acceleration, which is negative, is therefore

$$\frac{dU}{dt} = \frac{3\mu A U_f}{mH} - \frac{3\mu A U}{mH} \tag{2.47}$$

To simplify this, we can introduce a term C, which has units of $s^{-1}$, to replace the quantity representing viscous resistance:

$$C = \frac{3\mu A}{mH} \quad \text{or} \quad C = \frac{3\mu g}{\gamma H^2} \tag{2.48}$$

$$\frac{du}{dt} = C(U_f - U) \tag{2.49}$$

The solution to this equation is, for an initial condition of $U=U_0$ at $t=0$

$$\frac{U - U_f}{U_0 - U_f} = e^{-Ct} \tag{2.50}$$

Thus, the velocity declines exponentially, approaching $U_f$. Define U* to be a specific value, for example 0.1, of the dimensionless excess velocity given by the left side of eq. 2.50, and t* to be the time required for the excess velocity to decline to U*. Eq. 2.50 then simplifies to

$$\ln U^* = -Ct^* \tag{2.51}$$

If distance along the fan is x, velocity is defined as U = dx/dt. Therefore, eq. 2.50 becomes

$$\frac{dx}{dt} = (U_0 - U_f)e^{-Ct} + U_f \tag{2.52}$$

The solution to this equation is, if x=0 at t=0,

$$x = \left(\frac{U_0 - U_f}{C}\right)\left(1 - e^{-Ct}\right) + U_f t \tag{2.53}$$

If S and $U_f$ are not zero, the runout distance $x_L$ is infinite, but eq. 2.53 can be used to calculate the distance required for the excess velocity to drop to U*. In the case where S and $U_f$ are zero, eq. 2.53 reduces to, as U approaches zero at t=∞:

$$x_L = \frac{U_0}{C} \tag{2.54}$$

This result was also obtained, using a simpler and less general approach, by Cannon and Savage (1988).

The above calculation applies only to the Newtonian flow model, and requires knowledge of the depth H at which the debris will flow on the unconfined fan. The assumption that H is achieved instantaneously, and remains at that depth, is unjustified, and additional forces, such as thrust from the debris in the channel upstream, are neglected. The purpose of this derivation is not to model runout accurately, but to demonstrate that momentum effects are minor for viscous flows. The calculation in Fig. 2.9, using realistic values for typical debris flows examined in this study, shows that the time and distance required for excess velocity to dissipate are relatively small compared to those calculated by the frictional model. It is therefore reasonable, when viscous debris discharges onto an unconfined fan, to model its flow using eqs. 2.26 or 2.33, neglecting momentum effects at the transition.

If one assumes that H is not reduced on losing confinement, and that width increases only in response to the lowering of velocity, then runout distances are comparable to those calculated from eq. 2.42. However, field observations show that, upon losing confinement, debris flow depth does decrease. This calculation for viscous flow is sensitive to H, the final flow depth, whereas the frictional model (eq. 2.42 or 2.56) is not. Unfortunately, there is no known theoretical way of predicting what H will be, other than perhaps a dynamic wave approach involving a numerical simulation (Chow *et al.*, 1988; Fread, 1991). Also, as H approaches $T_0$, the critical thickness determined by the Bingham yield strength, the approximation of Newtonian flow is no longer valid. The above analytical derivation is not feasible for the Bingham model, due to the additive terms.

If the foregoing derivation (eqs. 2.42 to 2.53) is repeated for a frictional flow model, in which the resisting force is given by

$$F_R = mgS_f \cos\theta \tag{2.55}$$

one obtains the runout equation of Voellmy (1955; in German, referred to by Hungr *et al.*, 1984, and by Hungr and McClung, 1987):

$$x_L = \frac{U_0^2}{2g(S_f \cos\theta - \sin\theta)} \tag{2.56}$$

It is possible to perform a similar analytical derivation for a debris flow with both viscous and frictional resistance, if certain simplifying assumptions are made (Cannon and Savage, 1988). Without such assumptions, it is possible to model the deceleration numerically, and a numerical model may also be able to incorporate the Bingham yield strength (Hungr, 1994).

## 2.7 REVIEW OF PUBLISHED RHEOLOGIC DATA

It is informative to compile published information on rheologic parameters which have been calculated for debris flows, in order to demonstrate the range of values which occur in nature, and to serve as a basis for comparison of the data presented in the following chapters. Table 2.1 presents a summary of selected published information from the English-language literature, for references in which rheologic parameters have been calculated, or which give

sufficient data to calculate them. Similar summary tables have appeared in the literature several times, for example, Costa (1984), and Phillips and Davies (1991).

The approach used in most of these references, and in the present study, is to assume or infer the applicability of a rheologic model, and calculate the rheologic parameters for that model from measurements of velocity and channel flow dimensions. The usual intent is to use the chosen model, and the calculated parameters, to predict or explain the behaviour of other debris flows. For example, Hungr *et al.* (1984) used this approach to design engineering structures for channels subject to debris flows.

The model most widely used in the references listed in Table 2.1 is the Newtonian model, although some sources have calculated parameters for the Bingham model when sufficient data are available. Published calculations of parameters for the dilatant, or granular, model are rare; of the references listed in Table 2.1, only Hungr *et al.* (1984) applied this model. A number of sources in the table present detailed velocity and channel data, but do not apply a rheologic model or calculate parameters. In these cases, the apparent Newtonian viscosity has been calculated using eq. 2.26, making estimates of the shape factor and applicable depth from the data provided. It would be equally feasible to calculate the flow parameter $\mu_G$ for the dilatant model from eq. 2.32.

Some of the velocities reported in the table are from photographic or eyewitness measurement, and some are calculated from superelevation. Several of the latter (references 4 and 5) used a correction factor in the superelevation equation (as discussed in section 2.4 above); these have been recalculated, using eq. 2.34, for consistency with other data in the table and in this study. Several references (1, 7, and 15) incorrectly used eq. 2.6 with a denominator of 2 instead of 3; these viscosities have been corrected. Some of the references report grain size data based on samples which have been truncated at some size, typically 30 to 100 mm but sometimes unreported; therefore the "silt + clay" contents given in the table are not comparable with each other or with other data in this study.

The rheologic parameters in the table, especially the Bingham parameters, show a great variety of values. This is to be expected, given the ranges of event magnitude and debris

composition involved, and the variety of observation and calculation methods used. Where a range of parameters is calculated for one event, either at different sections or at one section at different times, these often vary greatly. This may reflect inaccuracies in observation and calculation methods, inapplicability of the chosen model, or real variability of debris properties within an event.

The range of velocities reported is relatively low, which is somewhat surprising given the wide range of other parameters and debris properties. The lowest values in the table (*e.g.* 15) are for low inter-surge flow or minor surges, and the highest values are for lahars very close to the blast zone of the 1980 Mount St. Helens eruption (2b, 8). If these are excluded, the range of velocities is 2 to 20 m/s, or one order of magnitude, lower than the ranges of viscosity and slope and similar to the range of depths. Since velocity is proportional to the 1.5 or 2 power of depth, depending on the model used, a greater range of velocity would be expected. This suggests a certain conservativeness in debris flow behaviour; the reasons for this will be explored in Chapter 7.

Several large lahars for which velocities were measured at a number of cross-sections (2b, 11, and 13) show a pronounced downstream attenuation of velocity and depth, similar to that shown by dam-break flood waves in rivers (Fairchild, 1985). If apparent Newtonian viscosities are calculated at these sections, these values also decline downstream; *i.e.* calculated viscosity is greater at greater depths of flow. Since the viscosity calculated from eq. 2.26 is proportional to $H^2$, this suggests that the exponent in this model may be too great, and a lower exponent (or flow behaviour index) may apply, such as 1.5 in the dilatant model. However, if the dilatant model is applied, the calculated flow resistance still declines downstream in the Pine Creek lahar (11, the best-documented example). Pierson (1985) obtained a good relation for this lahar by plotting U against $S^{1/2}H^{2/3}$, which is the Manning formula for turbulent flow; however, there is no theoretical justification for using this model to describe debris flow (Hungr *et al.*, 1984).

Most of the events included in the table were described as having high proportions of coarse gravel, and concentrations of cobbles and boulders at the surge fronts. A notable exception is the 1980 North Toutle River lahar (2a). The sample in the table is biased towards

large events ($10^5$ $m^3$ or larger), probably because unusually large events are of more interest as natural hazards, and are therefore more likely to be reported in widely-circulated publications.

## 2.8 CONCLUDING REMARKS

This chapter has reviewed the theoretical development of models of laminar flow which are applicable to debris flow, and developed a simple approach to apply these models to observations of debris flow in channels. The models fall into two categories: viscous, including the Newtonian and Bingham models, and inertial, which includes the dilatant model. Both these categories have been proposed in previous studies as applicable to debris flow. In this study, evidence is presented to show that both may be applicable, each to debris flows of different texture and geologic provenance. Several related topics such as flow regime and runout distance have also been reviewed. The models and methods described here are the basis for the analysis of field data in subsequent chapters.

TABLE 2.1 REVIEW OF PUBLISHED DATA ON DEBRIS FLOW RHEOLOGY

| Reference | Location and Date | Velocity U (m/s) | Depth H (m) | Channel Slope (°) | Apparent Newtonian Viscosity $\mu_N$ (Pa.s) | Yield Strength k (Pa) | Bingham Viscosity $\mu_B$ (Pa.s) | Silt + Clay (%) | Solids concentration by weight (%) | Approximate volume of event ($m^3$) | Remarks | |
|---|---|---|---|---|---|---|---|---|---|---|---|---|
| 1. Curry, 1966 | Mayflower Gulch, CO, 1961 | 2.5 | 1.5 | 15 | 2000 | | | 11 | 91 | 17,000 | A | Velocity determined from motion pictures. |
| 2. Fairchild, 1985; also Wigmosta, 1983 | a. N. Toutle R, WA, 1980<br>b. S. Toutle R, WA, 1980 | 6-12<br>8-33 | 5-18<br>4-30 | 0.3-0.6<br>0.5-2.3 | | 210-260<br>ca. 10 | < 480 | 19-28<br>13-23 | 83 | $1.4x10^8$<br>$1.3x10^7$ | | Silt & clay from Scott, 1988. $\mu_B$ from Wigmosta, 1983. Insufficient data to estimate $\mu_N$. |
| 3. Gallino and Pierson, 1985 | Polallie Cr, OR, 1980 | 12-16 | 3-8 | 3.4-7.1 | 350-2600 | | | 7.5 | 80-87 | ≤ 100,000 | B,D | 5 measured sections. |
| 4. Hungr et al, 1984 | a. M Creek, B.C., 1981<br>b. Charles Cr, B.C., 1983<br>c. Wahleach A, B.C., 1983 | 7<br>7<br>15 | 6<br>5<br>4 | 10<br>14<br>12 | 2600<br>2800-5200<br>1430 | | | 10 | | 20,000<br>20,000<br>55,000 | B,C<br>B,C<br>B,C | Silt & clay from VanDine, 1985.<br>2 measured sections. |
| 5. Jackson et al, 1989 | Cathedral Mtn, B.C., 1984 | 5-9 | 3-5 | 9-23 | 1200-4000 | | | 15 | | 140,000 | B,C | 4 measured sections. |
| 6. Johnson and Rodine, 1984; also Morton and Campbell, 1974 | Wrightwood, CA, 1969 | 1.2<br>0.6-3.8 | 1 | 7 | 500 | 600 | 130<br>40-100 | | 59-86 | 500,000 | | Velocity from photographs. Second line is data given by Morton and Campbell, 1974. |
| 7. Li et al, 1983 | Jiang-Jia Ravine, China, 1966 | 3-13 | up to 4 | 3.5 | 100 | 212 | | 14.5 | 88 | 362,000 | A | Multiple surges; one of many debris flow events observed. |
| 8. Major, 1984 | Mount St Helens, SW side, WA, 1980 | 8-41 | 2-20 | 3-13 | 650-7900 | 790-1940 | 410-7500 | 7 | 84 | 900,000 | | Two lahars; four measurement locations. |
| 9. Niyazov and Degovets, 1975 | Lesser Almatinka R, Kazakhstan, 1973 | 9-11 | 9-10 | 6-10 | 5100-5400 | | | | 79 | $3.4x10^6$ | B,E | |
| 10. Pierson, 1980 | Mount Thomas, N.Z., 1978 | 2-5 | average 1.0 | 6 | 210-810 | 1300-2400 | 19-71 | 10 | 57-84 | 195,000 | | Multiple surges. |
| 11. Pierson, 1985 | Pine Cr, Mount St Helens, WA, 1980 | 9-21 | 6-15 | 1.1-5.3 | 590-7000 | | | 5-17 ? | 84-86 | $1.4x10^7$ | B,D | 12 measured sections. Volume includes another nearby lahar. |
| 12. Pierson, 1986 | Shoestring Glacier, Mount St Helens, WA, 1981-83 | 2-5 | 0.7-2.3 | 7.0-7.6 | 40-280 | ca. 800 | ca. 10 | 11-21 | 77-83 | | B | Several small debris flows observed by automatic camera. |
| 13. Pierson et al, 1990 | Nevado del Ruiz, Columbia, 1985 | 5-17 | 2-20 | 0.6-6.4 | 1500-14,000 | | | 6-10 | | $9x10^7$ | B | 4 large lahars; volume is total. |
| 14. Rodolfo et al, 1989 | Mayon Volcano, Phillipines, 1985 | 4 | 5 ? | 4.5 | 6500 | 4250-5650 | 600 | < 3 ? | 81 | 200,000 | E | |
| 15. Sharp and Nobles, 1953 | Wrightwood, CA, 1941 | 1-3 | 0.8 | 6 | 140-400 | | | 17 | | ≤ 900,000 | A | Many surges over several days. |

Notes:
A. $\mu_N$ recalculated; incorrect formula used in reference.
B. $\mu_N$ calculated from data given in reference.
C. Velocity recalculated from superelevation data given in reference.
D. Silt + clay estimated from cumulative grain-size curves in reference.
E. Solids concentration calculated from reported bulk density, assuming $G_s = 2.65$.

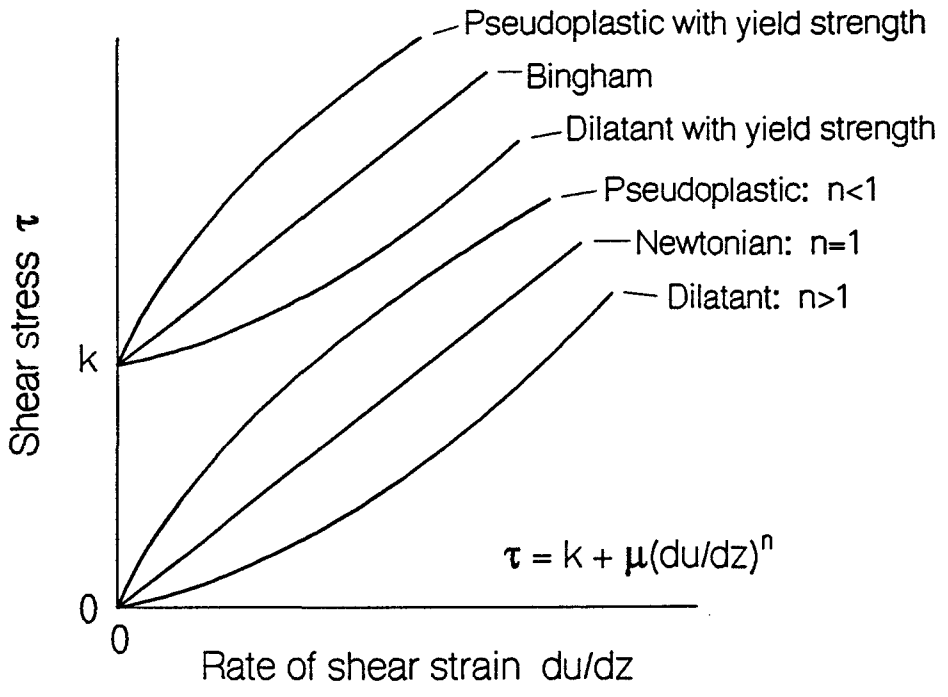


FIGURE 2.1. FLOW CURVES FOR IDEALIZED LIQUID AND PLASTIC MATERIALS.

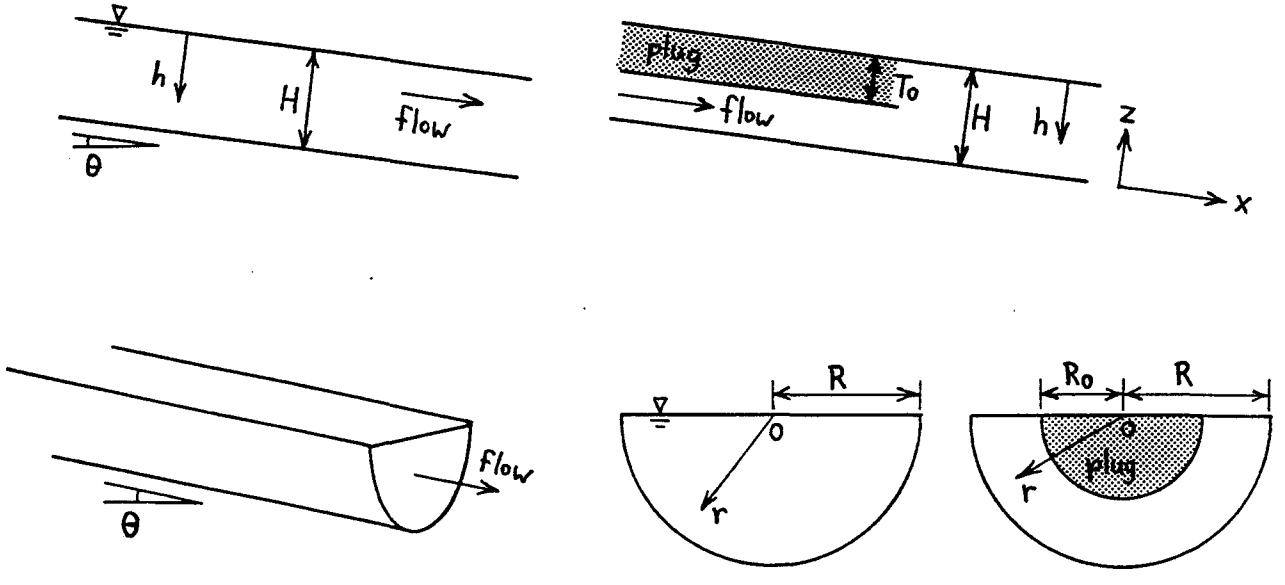


FIGURE 2.2. GEOMETRY OF FLOW IN WIDE AND SEMI-CIRCULAR CHANNELS.

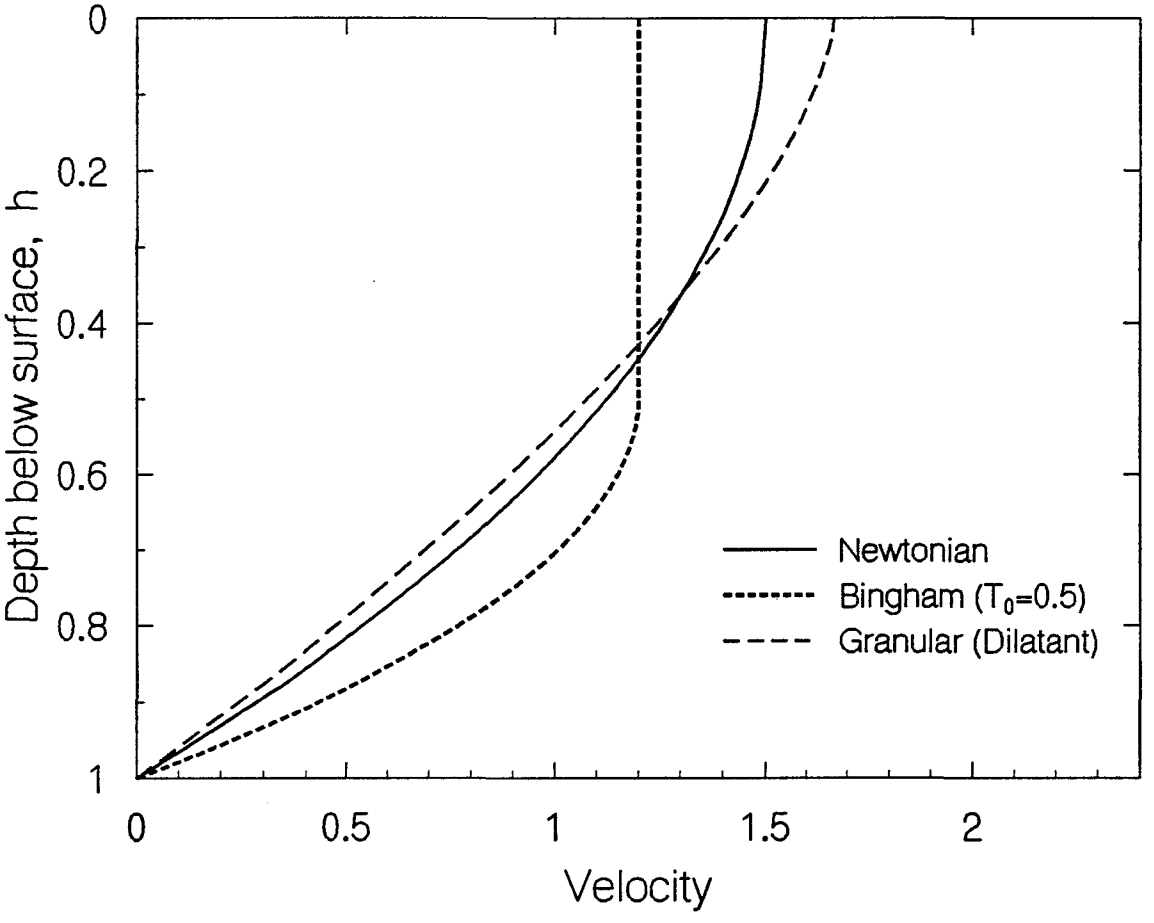


FIGURE 2.3. DIMENSIONLESS VELOCITY PROFILES, WIDE CHANNEL.

Elliptical channel

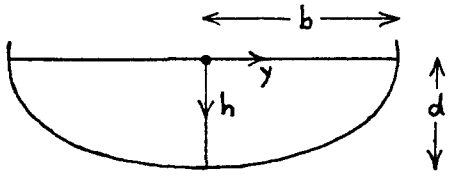


$$u = \frac{\gamma S}{2\mu} \frac{b^2 d^2}{(b^2+d^2)} \left(1 - \frac{y^2}{b^2} - \frac{h^2}{d^2}\right)$$

$$K = \frac{4(b^2+d^2)}{b^2}$$

Rectangular channel

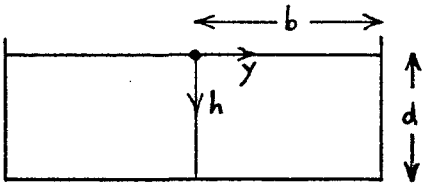


$$u = \frac{\gamma S}{2\mu} d^2 \left[1 - \frac{h^2}{d^2} - \frac{32}{\pi^3} \sum_{n=0}^{\infty} \left( \frac{(-1)^n}{(2n+1)^3} \frac{\cosh\left[\left(\frac{2n+1}{2}\right)\left(\frac{\pi y}{d}\right)\right]}{\cosh\left[\left(\frac{2n+1}{2}\right)\left(\frac{\pi b}{d}\right)\right]} \cos\left[\left(\frac{2n+1}{2}\right)\left(\frac{\pi h}{d}\right)\right] \right)\right]$$

$$K = 3 \left[1 - \frac{192\, d}{\pi^5 b} \sum_{n=0}^{\infty} \left( \frac{1}{(2n+1)^5} \tanh\left[\left(\frac{2n+1}{2}\right)\left(\frac{\pi b}{d}\right)\right] \right)\right]^{-1}$$

Trapezoidal channel with equal 60° sides (semi-hexagon)

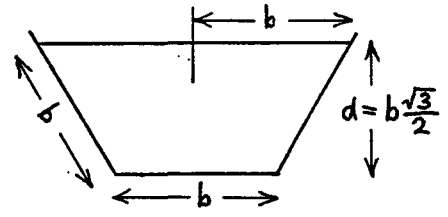


$K \approx 7.5$

120° Triangular channel

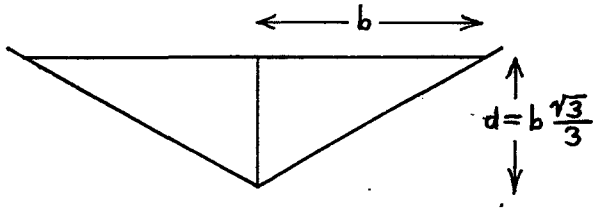


$K \approx 9.4$

90° Triangular channel

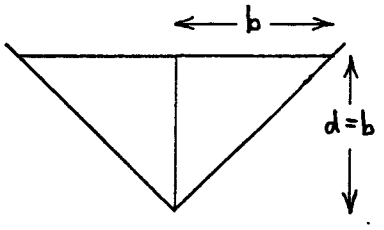


$K \approx 14.2$

FIGURE 2.4. SHAPE FACTORS FOR LAMINAR FLOW IN CHANNELS OF REGULAR GEOMETRIC SHAPE. From Straub et al, 1958. Shape factors are for mean velocity in the form of $U = \gamma S d^2/(K\mu)$. "≈" symbol denotes a numerical approximation.

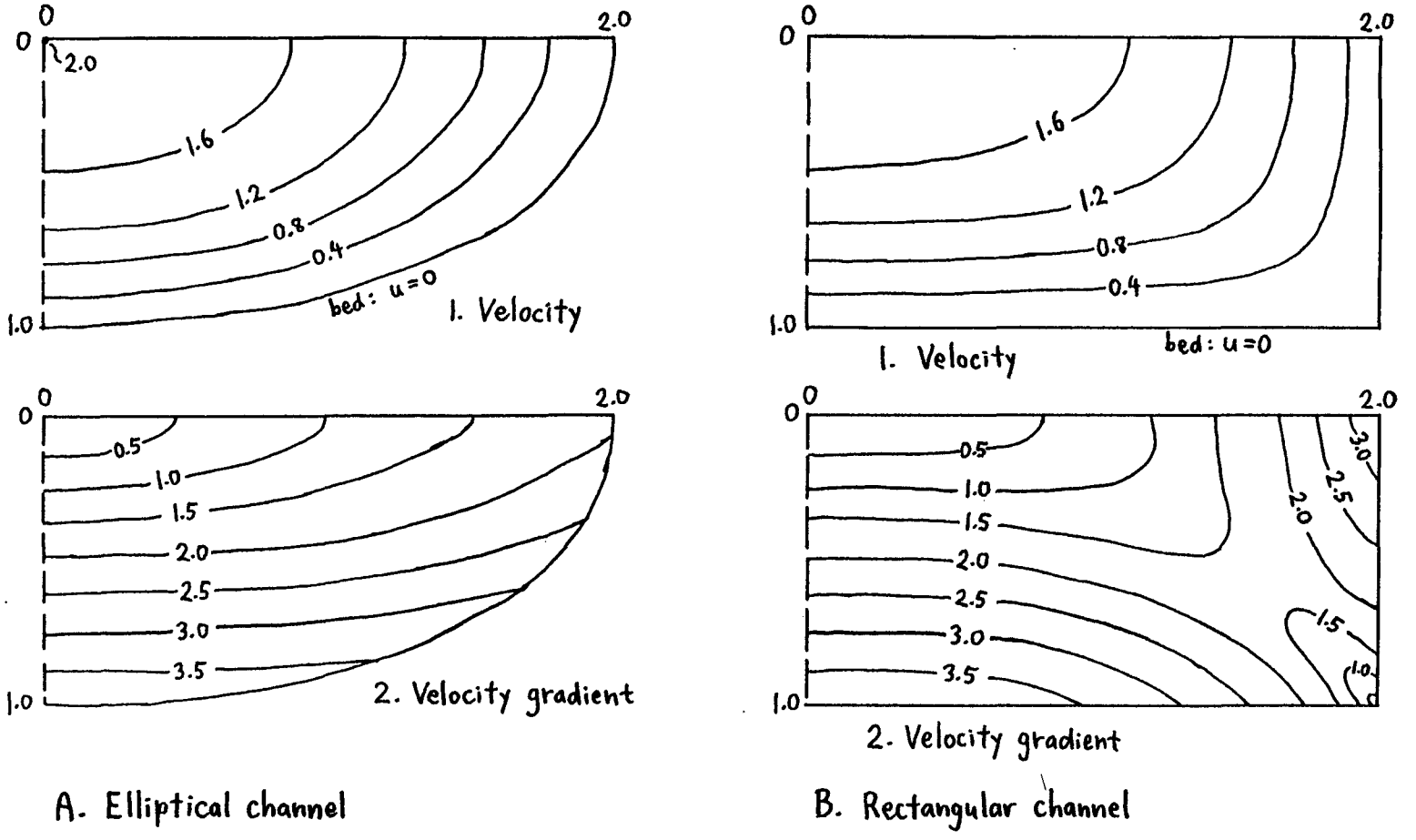


FIGURE 2.5. VELOCITY AND VELOCITY GRADIENT DISTRIBUTIONS FOR LAMINAR FLOW IN ELLIPTICAL AND RECTANGULAR CHANNELS. In each channel, depth d = 1.0, half-width b = 2.0, and mean velocity U = 1.0.

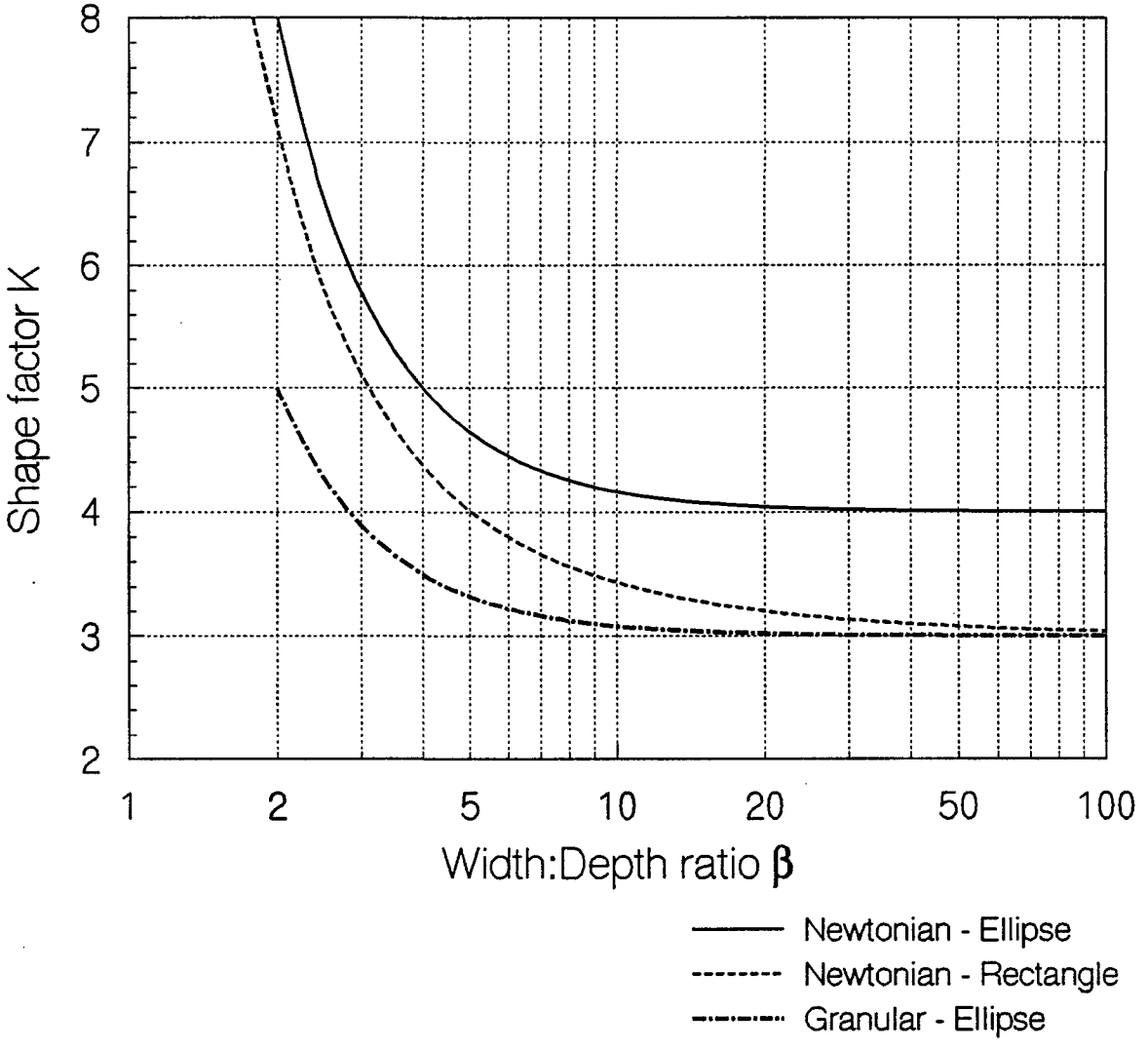


FIGURE 2.6. SHAPE FACTORS FOR ELLIPTICAL AND RECTANGULAR CHANNELS.

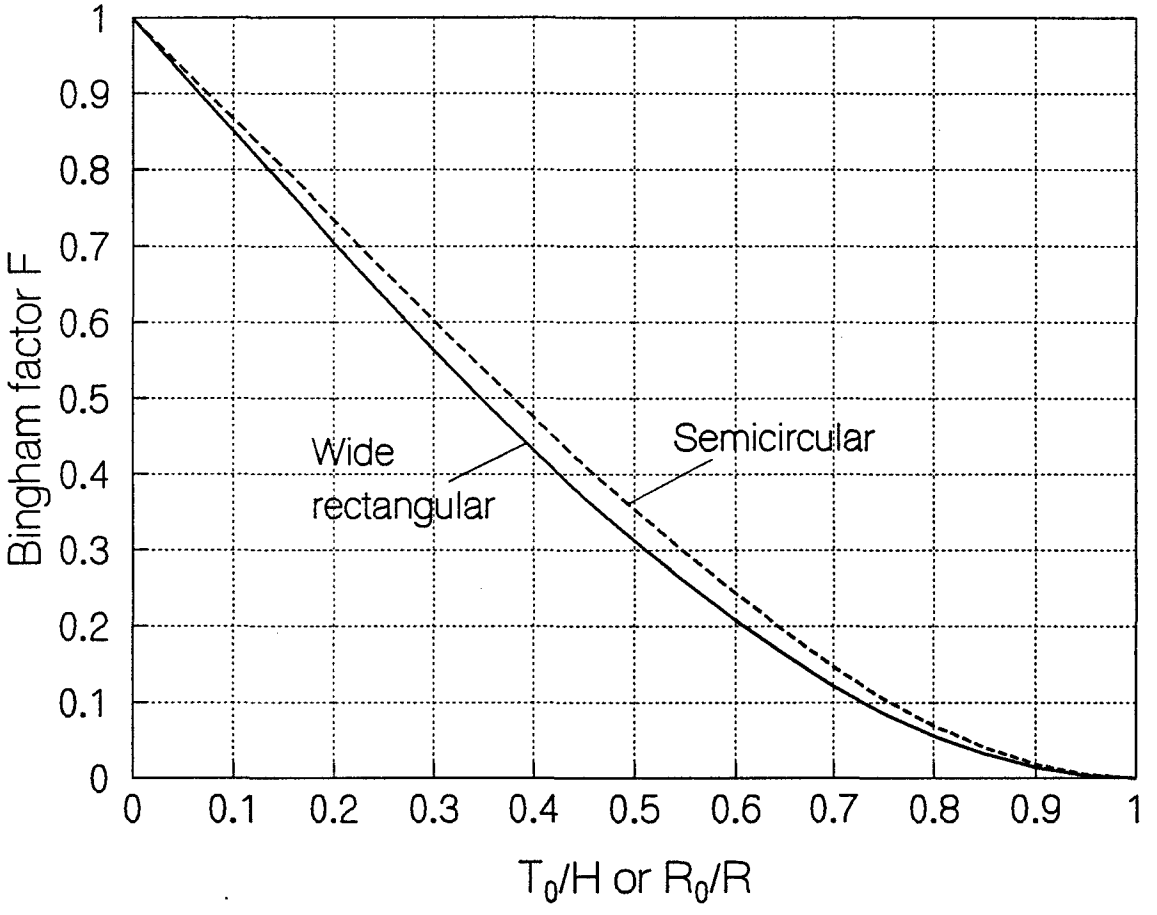


FIGURE 2.7. PLOTS OF "BINGHAM FACTOR" FOR CALCULATING VELOCITY FROM EQ. 2.33.

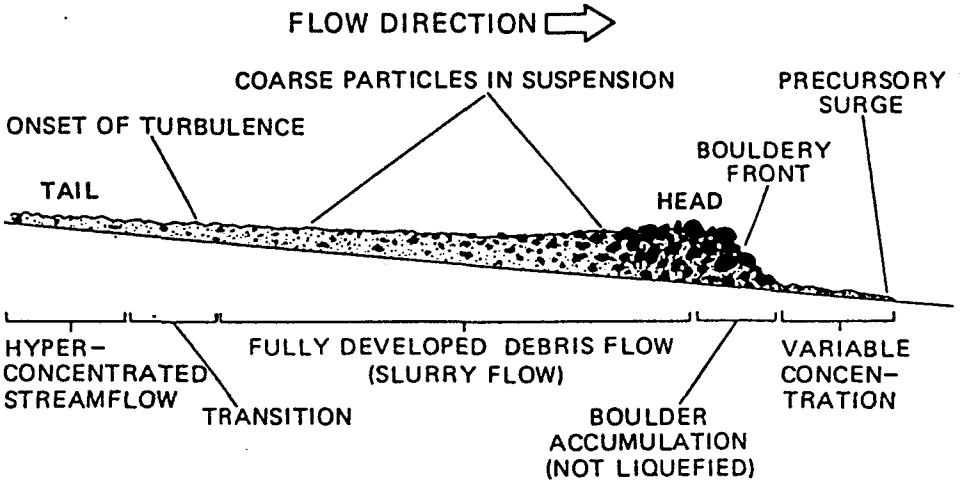


FIGURE 2.8. SCHEMATIC DIAGRAM OF A TYPICAL DEBRIS FLOW SURGE. Vertically exaggerated. From Pierson (1986).

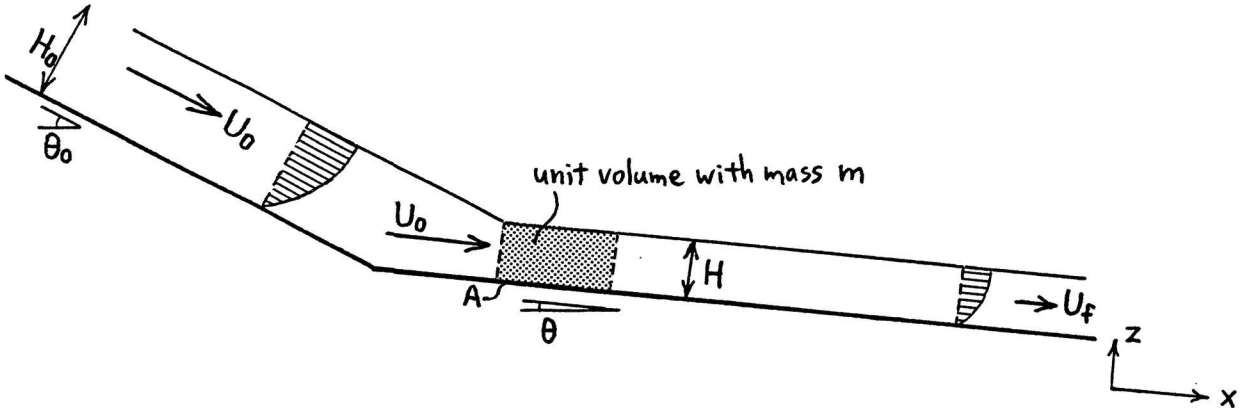


Example: $\gamma = 20$ kN/m$^3$ $H = 1$ m

$\mu = 2000$ Pa.s $\theta = 5°$

$H_0 = 4$ m $K = 3$

$\theta_0 = 15°$

$K = 5$ $\Rightarrow U_f = 0.3$ m/s

$\Rightarrow U_0 = 8.3$ m/s

For $U* = 0.1$, $t* = 0.8$ sec

$x_{(t*)} = 2.7$ m

For a frictional model, using Eq. 2.56 with $S_f = \tan 10°$, $x_L = 40$ m.

FIGURE 2.9. RUNOUT FORMULA FOR VISCOUS DEBRIS: DEFINITION SKETCH AND EXAMPLE.

# CHAPTER 3. THE STUDY AREA

## 3.1 GENERAL DESCRIPTION OF THE STUDY AREA

The study area is defined as the drainages of Squamish and upper Lillooet Rivers, which include about 7000 $km^2$ of the southern Coast Mountains north of Howe Sound. This chapter describes the geology, geomorphology, and hydrology of the study area, with additional detail on the Meager Creek area, where most of the study sites are located. Figure 3.1 shows the location and the generalized geology of the Squamish and upper Lillooet River drainage basins, and adjacent areas of the southern Coast Mountains.

The southern Coast Mountains are part of the Coast Crystalline Complex, which consists predominantly of Mesozoic plutonic rocks, mostly quartz diorite and granodiorite, with inclusions of metamorphic rocks aligned along a northwest structural trend. The Garibaldi Volcanic Belt cuts across the basement rocks on a north-northwest trend (Figure 3.1). It comprises three main volcanic centres of Quaternary age: Mount Garibaldi, Mount Cayley, and the Meager Creek complex, as well as several lesser volcanic fields (Green *et al.*, 1988). The volcanic rocks range in composition from rhyodacite to basalt, with the three stratovolcanoes consisting mainly of dacite, rhyodacite, andesite, and associated pyroclastic deposits.

The physiography of the study area reflects the high relief and the maritime climate of the region, and is dominated by landforms resulting from Pleistocene glaciation (Mathews, 1958). Fiords and deep U-shaped river valleys separate rounded ridges below about 2200 m, and sharp peaks at higher elevations. In the central part of the range, major river valleys such as the Squamish and Lillooet lie between sea level and about 500 m, with the elevations of adjacent peaks typically at 2500 to 2800 m. Present ice cover is extensive; large icefields occupy high elevation areas (above about 2100 m), and feed valley glaciers which are the sources of most rivers.

Annual valley-bottom precipitation in the area ranges from 2250 mm at Squamish to 990 mm near Pemberton, and decreases further towards the semi-arid valleys on the northeast side of the Coast Mountains. Higher elevations receive greater precipitation, most of which falls as

snow. There is a pronounced autumn and winter maximum of precipitation; the highest rainfall intensities and the highest peak discharges on rivers tend to occur from October through January. Figure 3.2 shows the monthly mean temperature and precipitation for Alta Lake (Whistler), which is the climate station most representative of the study area. Figure 3.3 shows the monthly mean hydrograph of Lillooet River, and the daily hydrograph for 1984, which is a typical year except that it includes the second-highest flood on record. This flood was caused by a 3-day rainstorm on October 7-9, 1984, during which many debris flows and extensive river channel changes occurred in the Squamish-Pemberton area (Jordan, 1987b; Hickin and Sichingabula, 1987). The rainstorm was heavy, but not exceptional; estimated return periods at climate stations near the study area were about 5 years for one-day rainfall, and 20 years for 3-day rainfall (Thomas and Stobbe, 1984).

The most important sediment sources to rivers in the study area are glaciers and recently exposed Neoglacial deposits, debris flows in steep creek channels and gullies, and landslides in Quaternary volcanic rocks (Jordan and Slaymaker, 1991). Some of the debris flows have delivered the majority of their debris directly to rivers, while others have deposited the bulk of their debris on fans, where some of it is gradually reworked by fluvial processes. Some of the major landslides have left large deposits filling river valleys, which remain continuing sediment sources for centuries or millennia as the rivers cut into them (Jordan and Slaymaker, 1991).

Although large slope failures have occurred in several parts of the study area underlain by basement rocks (Eisbacher, 1983), large-scale slope instability is much more prevalent in the Quaternary volcanic complexes. The three main volcanic centres have all experienced debris avalanches in the order of $10^8$ $m^3$ or larger during Holocene time (Evans, 1990). The Meager Creek Complex, which has had the most Holocene volcanic activity of the three, is a dissected massif formed of at least 9 volcanic assemblages ranging in age from about 1.9 Ma to 2350 years B.P. (Read, 1990). The Lillooet River valley, on the north side of the complex, is filled with tephra, welded pyroclastic flows, and debris avalanche and debris flow deposits resulting from the most recent eruptive period; their total volume may be in the order of $10^9$ $m^3$. The Meager Creek valley, on its south side, is remote from the site of Holocene eruptions, but is also

deeply filled with debris avalanche and debris flow deposits ranging in age from 4100 years B.P. to the present (Jordan, 1987b; Jordan and Slaymaker, 1991). The valleys below Mount Cayley and Mount Garibaldi contain similar although smaller assemblages of Holocene colluvial deposits (Eisbacher, 1983; Evans, 1990, Evans and Brooks, 1991).

## 3.2 STUDY SITES IN THE MEAGER CREEK VOLCANIC COMPLEX AND LILLOOET RIVER VALLEY

The Meager Creek Volcanic Complex, and the adjacent valleys of Meager Creek and upper Lillooet River, forms the core study area in which most of the study sites are located. This area was chosen because there is a high concentration of debris flow channels and other mass movement features originating in both fine-textured (volcanic) and coarse-textured (plutonic) lithologies, and the frequency of events in some of the debris flow channels has been relatively high. In addition, access to most of the sites of interest is reasonably good.

The geology of the Meager Creek Volcanic Complex has been mapped in detail by Read (1978). The geomorphology and hydrology of the area, and the chronology of debris flows and other mass movement events before 1987, has been described in a previous study by Jordan (1987b). Relevant aspects of this description are included in the sections of Chapter 4 which deal with the individual debris flow basins. Figure 3.4 shows the locations of the study sites in the Meager Creek area, as well as the principal geologic and geomorphic features. Figure 3.5 is an air photo mosaic of the Meager Creek study area.

(On Figure 3.4, place names which do not appear on published topographic maps are shown in quotation marks. In the text below, quotation marks are used only for the first reference to these place names. These unofficial names are in common local usage; most were first applied by loggers or geologists.)

The southern part of the Meager Creek Volcanic Complex, underlying the drainages of Devastation Creek, "Boundary Creek", "No Good Creek", and "Angel Creek" (Map B, Fig. 3.4), consists largely of early Pleistocene dacitic and rhyolitic lava and pyroclastic deposits, which have undergone extensive hydrothermal alteration (Read, 1978). Throughout late Holocene time, there has been extensive landslide and debris flow activity in this area, and a

large proportion of the drainages is covered by unvegetated landslide scars and talus slopes (Fig. 3.5). The landslide deposits and debris flow channels contribute large quantities of sediment to Meager Creek (estimated to be in the order of $10^5$ $m^3a^{-1}$ as a long-term average; Jordan and Slaymaker, 1991). The central and northern parts of the volcanic complex are largely underlain by less altered, mid and late Pleistocene dacitic and andesitic rocks. As these rocks are not as unstable, and because much of the landscape is ice-covered, mass movement activity in these areas is somewhat less prolific at present than in the southern portion. There are extensive landslide and debris flow deposits in the Lillooet River valley on the north side of the massif, as well as a very large debris flow and fluvial fan complex at the outlets of Job and "Affliction" Creeks. However, much of this debris may have been produced as a result of the 2350 years BP eruption, with the notable exception of a large debris flow deposit dated at 900 years BP (see Chapter 4). In the drainage basins of "Canyon Creek", Capricorn Creek, and Affliction Creek, the contact between the basement rocks and the volcanic rocks is at a relatively high elevation of 1500 to 2000 m, and the debris flows produced from these drainages contain a high proportion of basement rock material.

The basement rocks underlying the Meager Creek Volcanic Complex are primarily Mesozoic plutonic rocks, and to a lesser extent, Mesozoic metasedimentary and high-grade metamorphic rocks, and Tertiary volcanic and intrusive rocks. Immediately adjacent to the volcanic complex, landslides and debris flows in the basement rocks are frequent (see Chapter 4). The "Hot Springs Creek" study site is typical of the unstable plutonic rocks bordering the volcanic complex. Elsewhere, however, the basement rocks are relatively competent, and mass movement activity consists primarily of rockfall in structurally-controlled gullies, and debris flows derived largely from this rockfall. Deep, U-shaped valleys bounded by steep bedrock slopes, with thin glacial deposits and active fluvial floodplains and fans in the valley bottoms, dominate the physiography. Glaciers and Neoglacial deposits probably provide most of the sediment supplied to rivers and larger creeks (Jordan and Slaymaker, 1991). The small, steep, rockfall-supplied tributaries of the lower Ryan River and the middle Lillooet River valleys are

study sites which are typical of this environment. Figure 3.6 shows photographs illustrating the typical physiography of the Meager Creek and Lillooet River valleys.

## 3.3 STUDY SITES IN OTHER LOCATIONS

The prime objective of the study is to compare the behaviour of debris flows originating in different geologic provenances, especially the fine-textured volcanic rocks of the Garibaldi Group, and the coarse-textured plutonic rocks of the Coast Crystalline Complex, which are the most widespread rock types in the study area. It is also desirable to investigate other sites with lithologies which show debris flow behaviour intermediate between these extremes. Therefore, some additional study sites were selected in and near the main study area to obtain a larger sample representative of the full range of lithologies. These include a site in an altered dioritic complex near Pemberton; two sites on active debris flow channels draining Mount Cayley and Mount Garibaldi, and two sites in the upper Fraser River valley near Lillooet. This latter area, although just east of the Coast Mountains, was chosen to include debris flows of intermediate texture, derived from sedimentary and metamorphic rocks. The locations of these sites are shown on Figure 3.1. Further details on the debris flow sites are given in Chapter 4.

In physiography, geology, and hydrology, most of the Squamish River drainage is very similar to the Meager Creek and upper Lillooet River areas. The Mount Garibaldi and Mount Cayley Volcanic Complexes do not contain as much highly altered, unstable rock as does the Meager Creek Volcanic Complex; however, there are several sites which are subject to large, highly mobile, debris flows. The geology and physiography of these areas has been described by Mathews (1958) and by Souther (1980).

The two sites near Lillooet are in an area which is quite different in geology and hydrology, being part of the dry Interior Plateau adjacent to the semi-arid Fraser River valley. This area has been described by Ryder (1976) and by Bovis (1985).

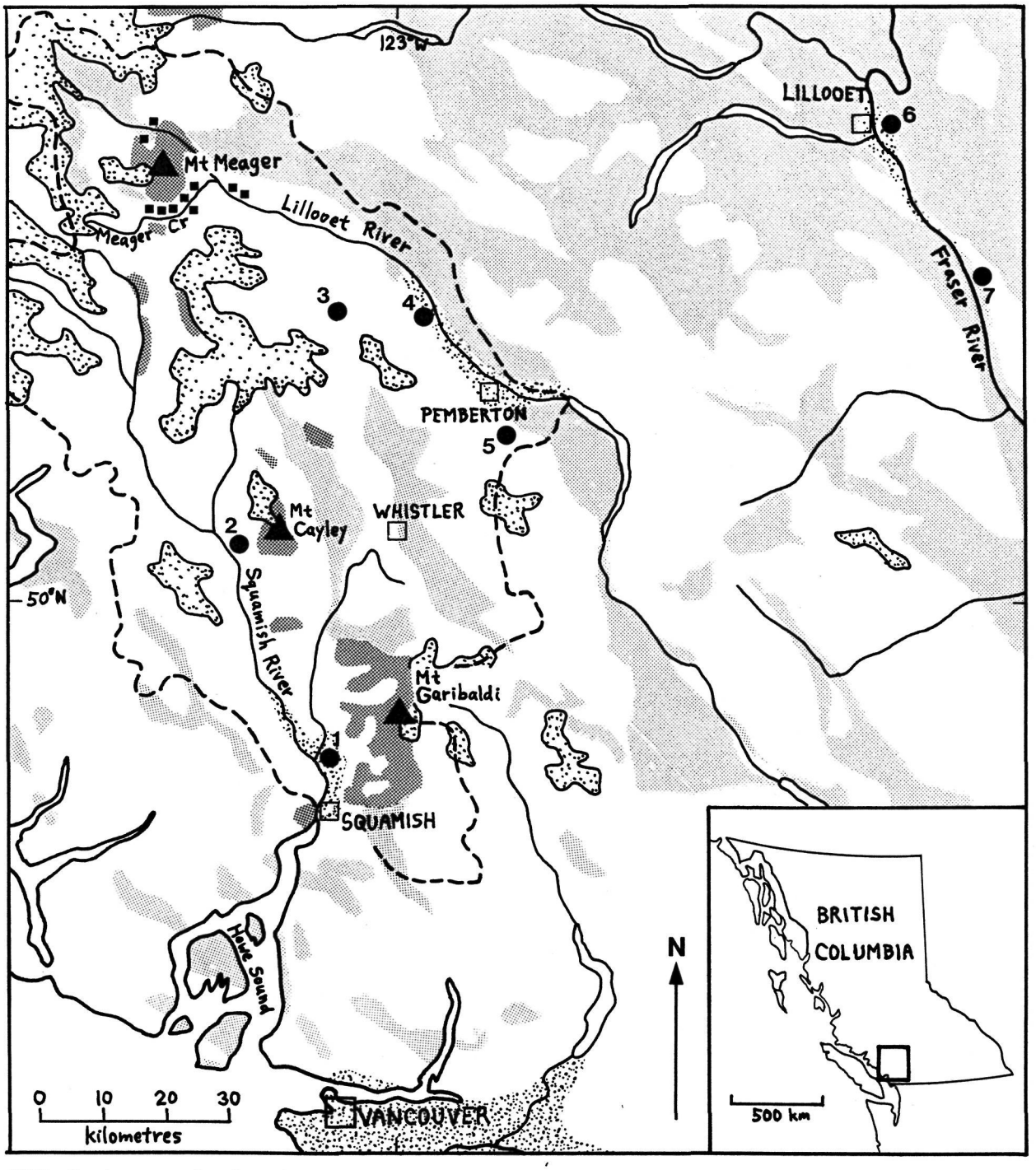


FIGURE 3.1. LOCATION MAP, SHOWING GEOLOGY AND STUDY SITE LOCATIONS.

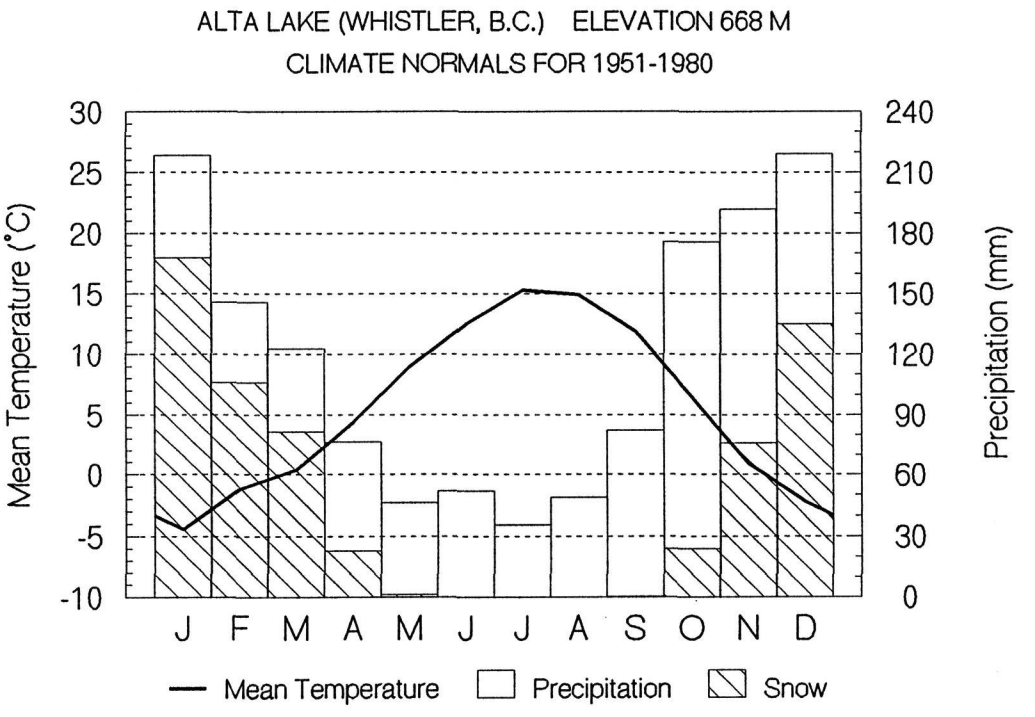


FIGURE 3.2. TEMPERATURE AND PRECIPITATION NORMALS, ALTA LAKE, B.C.

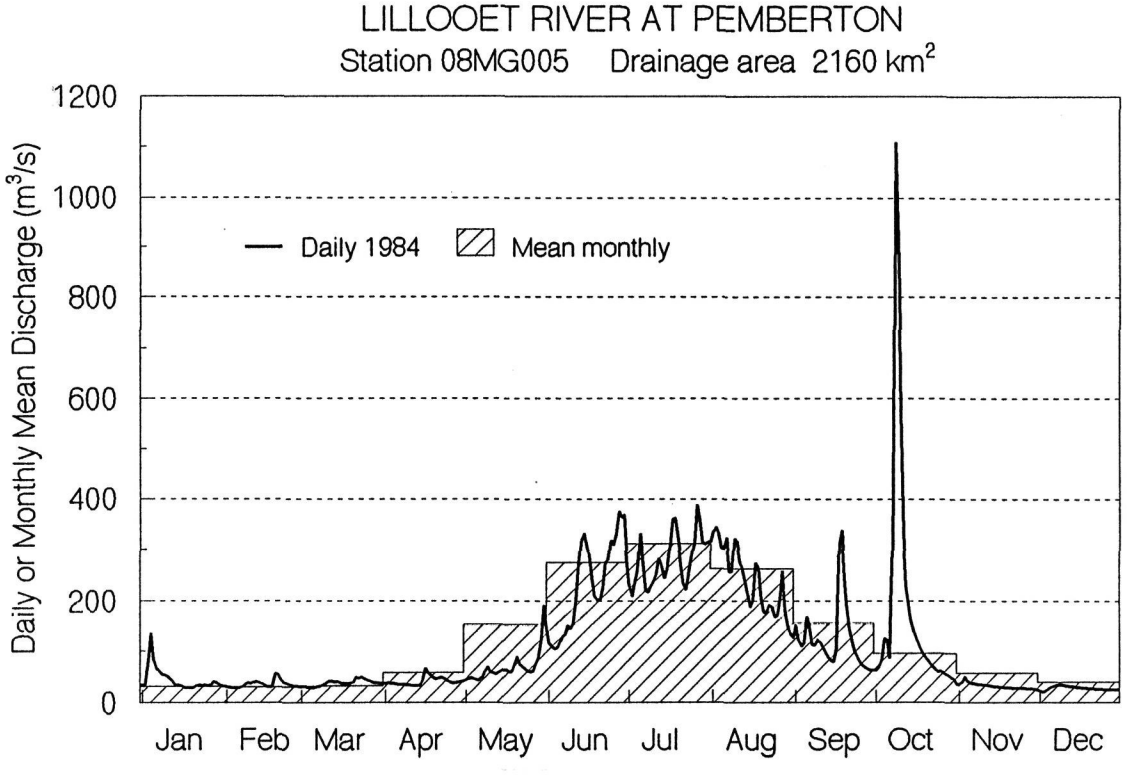


FIGURE 3.3. STREAMFLOW HYDROGRAPHS, LILLOOET RIVER AT PEMBERTON. Mean monthly data are for period 1914-1990.

FIGURE 3.4. MEAGER CREEK VOLCANIC COMPLEX: STUDY SITES AND MASS MOVEMENT FEATURES. A. NORTH MAP SHEET.

(FOR LEGEND, SEE 2ND FOLLOWING PAGE.)

SCALE 1:50,000. PART OF MAP SHEETS 92 J/11, 12.

CONTOURS IN METRES.

0 1 2 3
Kilometres

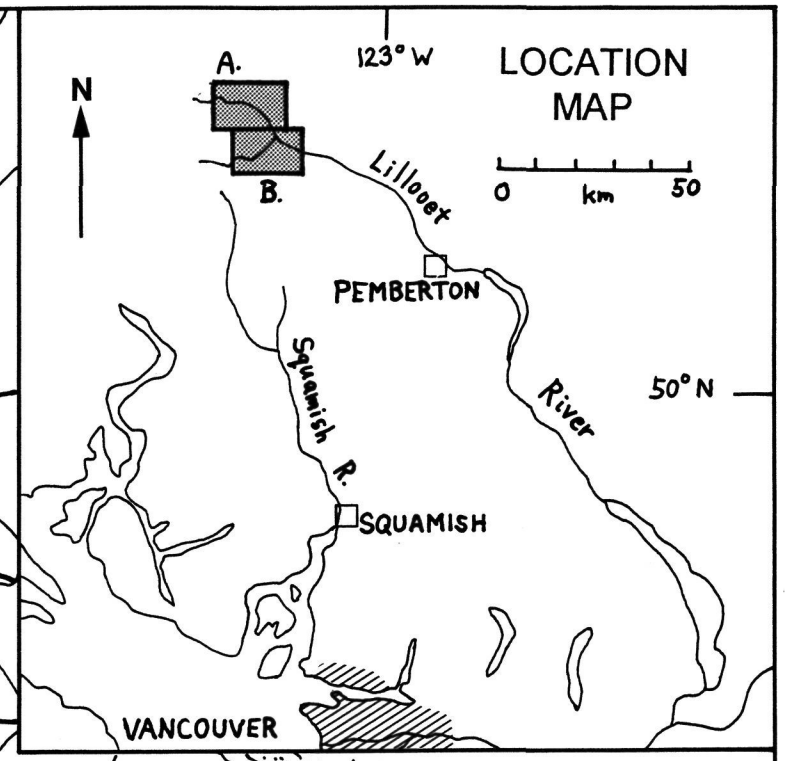

FIGURE 3.4. MEAGER CREEK VOLCANIC COMPLEX: STUDY SITES AND MASS MOVEMENT FEATURES.
B. SOUTH MAP SHEET.
(FOR LEGEND SEE FOLLOWING PAGE.)

SCALE 1:50,000. PART OF MAP SHEETS 92 J/11, 12.

0 1 2 3
Kilometres

CONTOURS IN METRES.

# FIGURE 3.4. LEGEND

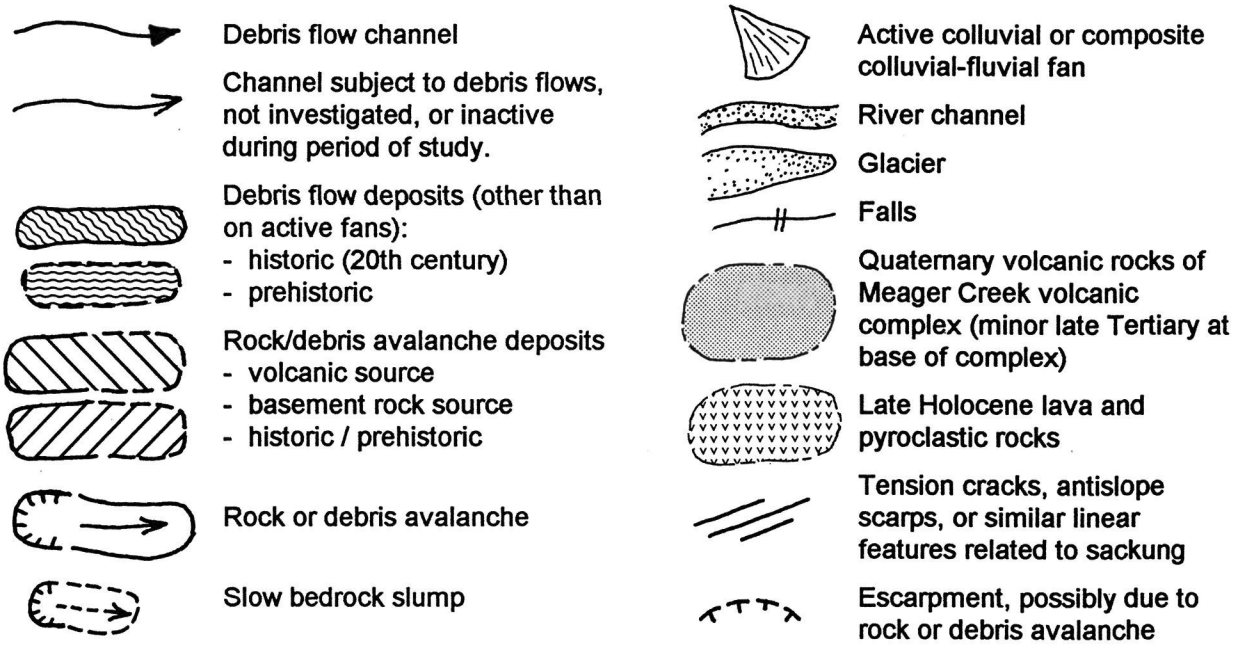


STUDY SITES

1. Boundary Creek debris flows (1987-1989)
2. No Good Creek debris flows (1980-1990)
3. Devastation Creek debris flow deposits (1931)
4. Angel Creek area debris flows (1987-1990)
5. Hot Springs Creek debris flow (1984)
6. Canyon Creek debris flows (1987, 1990)
7. Capricorn Creek debris floods (ca. 1972, 1990)
8. Middle Lillooet River debris flow fans
9. Upper Lillooet River debris flow ($^{14}$C date 900 years B.P.)
10. Affliction Creek debris flow (1984)

OTHER FEATURES

11. Devastation Glacier debris avalanche (1975)
12 Boundary Creek debris fan (undated, more than 200 years old)
13. No Good Creek debris avalanches ($^{14}$C dates 370 - 990 years B.P.)
14. Angel Creek debris avalanche(s) ($^{14}$C date 4100 years B.P.)
15. Hot Springs Creek rock avalanche (undated; underlies unit 14)
16. Meager Creek debris flows (complex of several flows, one $^{14}$C date 3930 years B.P.)
17. Capricorn Creek debris avalanche (undated)
18. Capricorn Creek rock avalanche (ca. 60 or more years old; Croft, 1983)
19. Mount Meager rock avalanche (1986; Evans, 1987a)
20. Plinth Peak debris avalanche (probably due to 2350 years B.P. eruption)
21. Pyroclastic deposits of 2350 years B.P. eruption
22. Lava flow, younger than units 20 and 21
23. Job Creek fan complex (debris flow, fluvial, and other deposits)
24. Debris avalanche (undated)
25. Affliction Creek rock-slope movement site (Bovis, 1990)

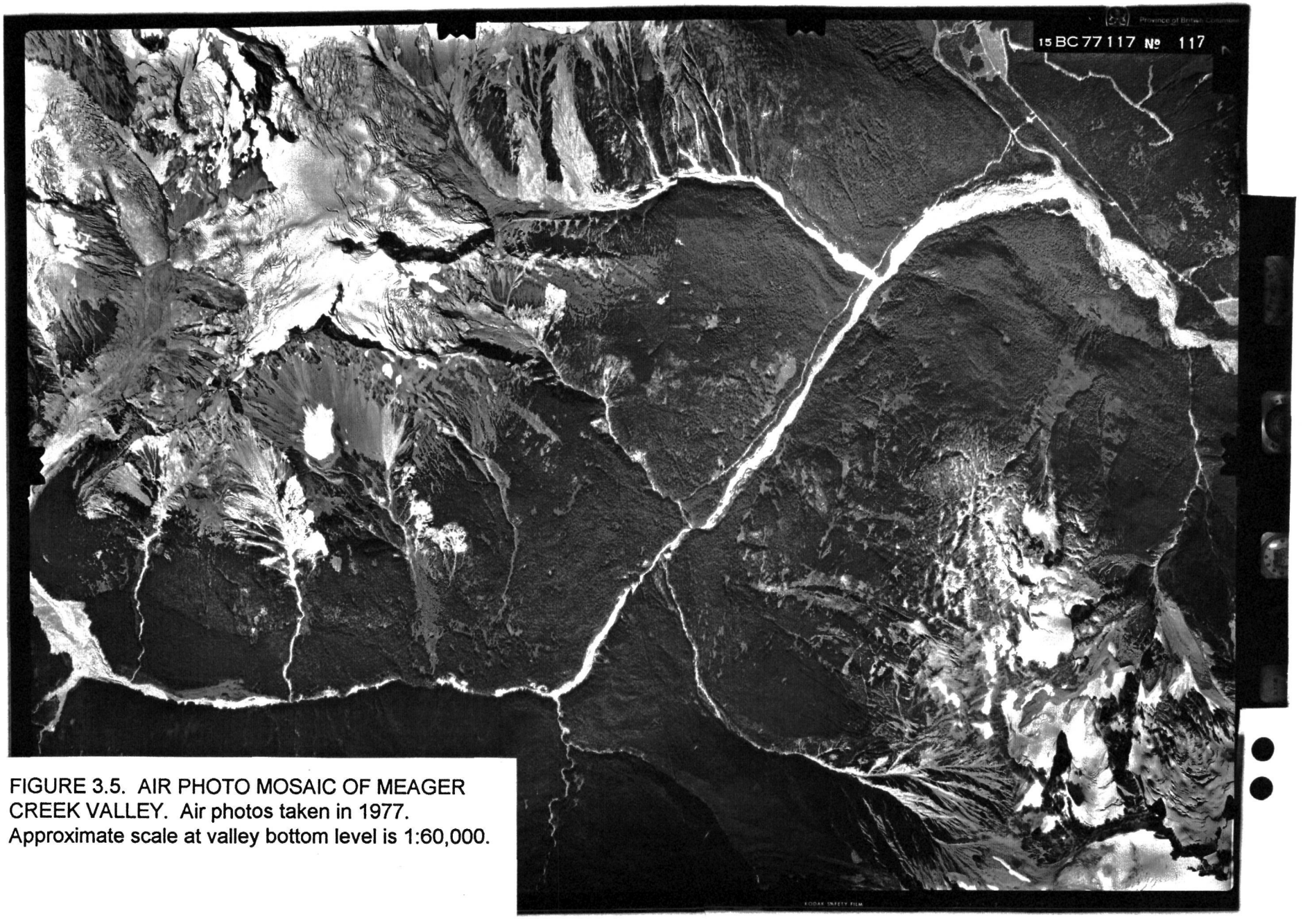


FIGURE 3.5. AIR PHOTO MOSAIC OF MEAGER CREEK VALLEY. Air photos taken in 1977. Approximate scale at valley bottom level is 1:60,000.

A. Confluence of Meager Creek and Lillooet River, looking up Meager Creek valley. Capricorn Creek valley enters in right centre. Photograph was taken in 1976, before logging began.

B. Lillooet River valley above Pemberton, looking upstream to Mount Meager in centre distance.

FIGURE 3.6. PHOTOGRAPHS ILLUSTRATING TYPICAL PHYSIOGRAPHY OF THE STUDY AREA.

# CHAPTER 4. GEOMORPHOLOGY OF DEBRIS FLOW EVENTS AND DEPOSITS

## 4.1 OVERVIEW OF DEBRIS FLOWS IN THE SQUAMISH AND UPPER LILLOOET RIVER DRAINAGES

Debris flow channels are widespread in the study areas and elsewhere in the southern Coast Mountains. Their distribution appears to bear little relation to bedrock geology (VanDine, 1985); they are abundant in both resistant and weak rock types. They are also equally common in the drier northeast part of the range, and in the more maritime central and coastal areas. In an earlier study (Jordan, 1987b), which mapped sediment sources in the drainages of Squamish and Lillooet Rivers, an area of 7000 $km^2$, over 200 debris flow channels were counted which appear to have been recently active, and which are large enough to be identified on 1:50,000 air photos. The most significant factor in their distribution appears to be local relief; debris flow channels were found to be most abundant where the relief from ridge tops to valley bottoms was greater than about 1200 m, with average slopes of about 25° or greater. The record of observation in the Coast Mountains is too short to quantify the frequency of debris flow events in the channels. However, based on the large number of events which occurred during one rainstorm in 1984, on the age of vegetation on fans observed in the field, and on fresh deposits seen on air photos, debris flows in many channels may occur with return periods ranging from several years to several decades (Jordan, 1987b).

Typical volumes of most of the recent debris flows in the study area are in the range of 5000 to 50,000 $m^3$, although numerous smaller ones have probably gone unnoticed. Channels and gullies carrying debris flows typically have drainage areas ranging from 0.1 to 10 $km^2$, and have average gradients between 15° and 35° (Jordan, 1987b). Several unusually large debris flows in the Quaternary volcanic complexes, with volumes up to several million $m^3$, are exceptions to these general observations. Most of the debris flow channels originate above treeline, and the most common sources of debris are rockfall gullies and talus slopes. Steep Neoglacial moraines, small debris slides adjacent to channels, and lake outburst floods are less

common sources. Debris slides on forested or clearcut slopes are not a common source of debris flows in most parts of the study area, unlike some other areas of coastal British Columbia such as Vancouver Island, the Queen Charlotte Islands, and the lower Fraser Valley, where the climate is more maritime and rainfall intensities are higher. Most debris flow events in the study area, as has been observed elsewhere (Swanston and Swanson, 1976; Miles and Kellerhals, 1981; Hungr *et al.*, 1984), have entrained additional colluvial and fluvial material from the channel as they flow, substantially increasing their volume over the size of the initiating event. Most debris flows are initiated during heavy rainfall in the autumn and early winter, although in the less maritime Lillooet River basin, locally intense summer thundershowers are responsible for some debris flows.

Most of the study sites are in or adjacent to the Meager Creek volcanic complex (Fig. 3.4). The steep basins which drain this glacially oversteepened terrain are fed by a prolific supply of debris in the form of rockfall, debris slides, dirty snow avalanches, and small debris flows on talus slopes. Deep-seated, slow failures, some involving basement rocks as well as the overlying volcanics, contribute additional sediment. This unstable geologic environment produces frequent debris flows and occasional debris avalanches, especially on the south side of the massif, where debris flows and debris avalanches which have reached the valley bottom in historic time have ranged in magnitude from about $10^4$ to $10^7$ $m^3$ (Jordan and Slaymaker, 1991). On the north side of the complex, large debris flows have occurred in several drainages, but lack of ground access to the south side of Lillooet River has prevented detailed study.

Several creeks in or adjacent to the volcanic complex, which are underlain by basement rocks, have experienced large rock avalanches in addition to debris flows. Instability and sediment production in the basement rocks appears to be related to deep-seated rock creep, or sackung, which is indicated by linear features such as ridge-top cracks and uphill-facing scarps (Bovis, 1982, 1990). The relation between sackung features and rapid mass movement has been noted in several areas of southwestern British Columbia (Bovis, 1982; Eisbacher, 1983; Savigny, 1990). Deformation and weakening of the basement rocks may be especially prevalent in the Meager Creek area because of emplacement of the volcanic complex.

Large debris flows (in the order of $10^6$ $m^3$ or larger), which may have been initiated from the debris of major slope failures in weak Quaternary pyroclastic rocks, have also occurred in valleys draining Mount Cayley and Mount Garibaldi (Eisbacher, 1983; Jordan, 1987b; Cruden and Lu, 1989; Evans, 1990; Evans and Brooks, 1991).

Debris flows originating in the two lithologic terranes of the study area show very different dynamic behaviour. Debris flows originating in fine-textured pyroclastic rocks are much more mobile than those originating in plutonic rocks. The typical slopes of depositional zones of moderate sized, volcanic-source debris flows ($10^4$ to $10^5$ $m^3$) on alluvial fans is in the range of 3° to 5°, compared to 8° to 12° for flows originating in coarse-textured basement rocks. Some of the larger (more than $10^6$ $m^3$) volcanic-source debris flows have traveled up to 15 km down low-gradient (less than 3°) valley bottoms. For example, the path of the 1931 Devastation Creek event and those of some earlier debris flows are shown on Fig. 4.4. The exceptional mobility of large volcanic-source debris flows has been frequently noted at other volcanoes such as Mount St. Helens and Mount Rainier (Crandell, 1971; Janda *et al.*, 1981; Pierson, 1985; Scott, 1989; Scott *et al.*, 1992), although most of these debris flows (or lahars) have been directly related to volcanic eruptions. The differences in mobility are apparently related to texture, with a high clay content, and a low concentration of cobbles and boulders, favouring more mobile behaviour (Scott, 1988). The actual processes responsible for the differences in mobility are poorly understood, and are the principal focus of this study.

## 4.2 FIELD METHODS

### Site selection

Eight field sites in the study area were selected for detailed study, based on their accessibility, apparent frequency of debris flow activity, and their representation of a range of scales and lithologies. Most of the debris flows examined had occurred within the previous five years; it was necessary that the events be recent enough that the deposits were not eroded or obscured by subsequent events, and that mudlines in the channels could still be recognized. Two very large, much older, debris flows were included in the sample because they had left extensive, well-preserved deposits. All sites, except one, are in the Meager Creek Volcanic Complex. The

exception, in the lower Ryan River valley, was selected because none of the coarse-textured, plutonic-source debris flow channels in the Meager Creek area had bends which would allow estimation of velocity by the superelevation method.

Eleven additional sites were chosen for less detailed study, based on their accessibility, and the desire to obtain a larger sample of debris flow deposits representing a range of debris textures. In one case, Affliction Creek, the site was chosen because the opportunity arose for a helicopter visit to an otherwise inaccessible location in the upper Lillooet River valley. These additional sites were studied in lesser detail because of time constraints; a decision was made that it was better to obtain minimal information for as many additional sites as possible, instead of detailed information from relatively few sites. Table 4.1 gives a summary of the drainage basin morphometry for all the sites.

Field surveys and sampling

Most of the field work in the study was done in 1988 and 1989. A camp was established at Meager Creek, and field work occupied most of the useful (*i.e.* snow-free) field seasons (which in this area extend from June through October). Preliminary field work, including low-level air photography, was done in late summer 1987. Some additional field work was done in July and October 1990, in response to debris flow events which had occurred in late autumn 1989 and in 1990.

For the detailed study sites, most of the field effort involved surveying the deposit areas and the lower channels, and sampling debris flow materials. In addition, the stratigraphy and history of deposits at the study sites, and geomorphic conditions in the starting zones, were examined as the opportunity permitted.

A survey was made of the debris flow deposits at most sites, using a Wild T2 theodolite and an AGA Geodimeter EDM (electronic distance measurement) device. The survey was extended into areas of bush cover or poor lines of sight by traversing with a compass and clinometer, and a tape or hip-chain. One purpose of the surveys was to establish benchmarks and cover the deposits with reference points in case any further debris flows occurred during the study. Two of the surveyed fans were covered by subsequent debris flows and were resurveyed.

The theodolite and EDM were also used to measure channel dimensions and superelevation at suitable locations upstream from the fans. At a few sites, stadia measurements were used when the EDM was unavailable. Theodolite triangulation was used to survey points defining the path of the 1931 Devastation Creek debris flow on the inaccessible south bank of Meager Creek.

The theodolite and EDM produced highly accurate surveys; a 5 km traverse of the upper Meager Creek valley, linking 14 instrument stations, resulted in a closure error of 0.7 m horizontally and 0.1 m vertically. Surveyed points at each debris flow site are precise to within a few millimetres, much less than the imprecision inherent in describing the rough, stony surface of the deposits. Hand surveys with tape and compass typically resulted in closure errors of 1 to 2% horizontally and 0.2 to 0.4% vertically. Closed traverses were made wherever practical; where open traverses were used, errors are probably several times greater. The hand surveys are adequate for estimating deposit areas, channel dimensions, and average slopes, but are not suitable for establishing reference points for repeat surveys.

Low-level vertical air photographs were taken of most of the detailed study sites at the beginning of the study, using a 35-mm camera with a motor drive. It was mounted on a hand-held arm and kept horizontal by observing an attached bubble level, while flying in a helicopter with the rear door removed. The photographs proved very useful for drawing maps of debris flow deposits when combined with ground survey results, but they were subject to errors due to tilt and uneven flight path which made them unsuitable for photogrammetry measurements.

At each detailed study site, samples were taken of the debris deposits to analyze the grain-size distribution. From 2 to 8 samples were taken of each deposit. The sampling strategy varied depending on the extent and state of preservation of each deposit, and the opportunity of finding feasible sample sites. Further details are given in the following sections and in Chapter 5. Samples ranging in size from about 100 to 1000 kg were sieved in the field down to a convenient size (usually 32 mm), and a subsample was taken for lab analysis. At several sites (Boundary 1987, Devastation 1931, Hot Springs 1984, and Ryan 1984), approximately 250 kg of sub-32 mm material was taken to the lab for flume tests and other purposes. Surface stone counts were made on coarse-textured deposits and on the Boundary Creek fan, and at some

sites, stone counts were made along exposed faces to obtain a better sample of the largest size classes.

A major limitation in sampling coarse-textured, plutonic-source debris flow deposits was that the deposits are typically covered with a surface layer of boulders, most of which are too heavy to move by hand. Therefore, samples could only be taken at locations where stream erosion had exposed a section of the deposit. Fine-textured debris deposits could be sampled by digging from the surface, but the holes that could be dug were generally well under 1 m in depth because of the likelihood of encountering immovable boulders.

At most of the minor study sites, surveys were made with a compass and clinometer of the deposits and the lower channels, combined with field sketches. At most sites, a single sample of 200 kg or less was taken, and surface stone counts were taken at some sites. Some sites received only very brief field visits, while others received a day or more of surveying and sampling. Details are given in the following sections.

Measurement errors

In studies of debris flows and similar geologic phenomena, measurement errors are often very large compared with the quantities being measured. Also, sample sizes are small because of the logistical difficulties in collecting data, or because of the rarity of the phenomena. Therefore, it may not be practical to apply standard statistical techniques to test hypotheses. Instead, a more descriptive approach is taken, in which tentative relations inferred from graphical or tabular presentations of data cannot be rigorously tested. However, a quantitative description of errors is still desirable.

In this chapter, the quantities measured are the volume (or magnitude), as well as the area, thickness, and slope of debris flow deposits. Volume "measurement" of a debris flow event is based on deposit area and average thickness, and involves considerable estimation, and sometimes sheer guesswork. Depth at exposures can be easily measured to about ± 10%, as can surface area, subject to correct interpretation of the stratigraphy of the deposit. However, estimating the depth of deposits at locations other than natural exposures requires judgment and guesswork, so errors cannot be readily quantified.

Debris flow volume can cover several orders of magnitude, so it is reasonable to assume that for a population of debris flows, the logarithm of volume is normally distributed, in the absence of other information. In the notes to Table 4.2, the error in volume estimates is expressed as "proportional error", which is defined here as the error in the base 2 logarithm of the quantity. For example, a proportional error of 1 indicates an error of ± 1 base 2 logarithm, which is a range of from 1/2 to 2 times the measured quantity. The term "error" implies a range equivalent to 95% confidence limits, or ± 2 standard deviations.

## 4.3 DETAILED STUDY SITES

This section gives descriptions of the debris flow events and deposits at each detailed study site. Chapter 5 gives further information on the sedimentology of the deposits The channel dimensions and inferred flow behaviour are described in Chapter 7. Table 4.2 summarizes the physical dimensions, lithology, and stratigraphy of the deposits. In this table, and in the descriptions below, the events are grouped in order of geologic provenance, with fine-textured, volcanic-source debris flows first, followed by those of intermediate texture or mixed provenance, and finally by coarse-textured, plutonic-source debris flows.

The data on lithology are based on counts made during field sieving of stones larger than 32 mm. The sample size and distribution amongst size classes vary; the data give an approximate, and probably inaccurate, estimate of the provenance of each debris flow. In general, cobble and boulder size classes have a higher proportion of resistant plutonic rocks. Based on colour, the sand and fines fractions appear to contain a relatively higher proportion of less resistant volcanic rocks. Therefore, the stone counts give results biased toward higher content of basement rocks. The volcanic-source debris flows contain some basement rocks because these rocks crop out at lower elevations in all the channels (Fig. 3.4).

### Boundary Creek

Boundary Creek is one of a pair of steep channels draining the older, hydrothermally altered, southern part of the Meager Creek volcanic complex. This creek and No Good Creek experience frequent debris flows consisting mainly of volcanic-source material. Fig. 4.1 is an air photo, taken in 1986, which shows both channels.

In August, 1987, a debris flow of about 50,000 $m^3$ descended Boundary Creek and filled the floodplain of Meager Creek, which at the confluence is about 100 m wide, diverting Meager Creek to the other side of the valley. (Meager Creek is a sizable river at this point, with a mean annual flood discharge estimated to be in the order of 100 $m^3s^{-1}$.) In the approximately 15 years prior to this event, the channel appeared to have carried only occasional, smaller events, based on the lack of significant deposits at its mouth as seen on air photos. The 1987 debris flow deposit formed a fan with a uniform surface sloping at about 5°. Fig. 4.2 is a map of the deposit. The volume of the fan was calculated by constructing a contour map, and estimating a profile of the underlying floodplain and river channel from surveyed elevations upstream and downstream of the fan. This method gives a minimum volume for the debris flow event, since an unknown volume of debris was carried away by Meager Creek during its emplacement.

The sedimentology of this fan is fairly typical of the clay-rich, fine-textured debris flows from the Mount Meager complex. There is no coarse surface layer, and the fan surface is remarkably smooth and uniform in texture (Figs. 4.3 and 4.5). Where exposed in section, the debris is randomly mixed, with neither inverse nor normal grading. Although coarse clasts are abundant (at least 40% cobbles and boulders), the debris is clearly matrix-supported. There is some systematic textural variation across the fan; a higher proportion of boulders in the apex area suggests that a coarse frontal part of the surge or surges was deposited first, and the main debris flow was followed by a fine afterflow facies which covers the distal parts of the fan. There is no evidence of multiple surges in the deposits, although this does not establish that multiple surges did not occur (Major and Iverson, 1993). This debris flow, like the others which followed, left narrow lateral levées of cobbles and boulders along the channel in some locations.

In September 1988, a second debris flow covered part of the Boundary Creek fan. The debris characteristics were similar to those of the previous event, although coarse clasts were less abundant. The debris formed a smooth sheet of quite uniform thickness, averaging about 0.6 m. The uniform, fine-textured nature of the deposit is shown in Figs. 4.4 and 4.6. A survey of the fan prior to this event makes possible a fairly precise measurement of the debris thickness and the deposit volume, about 5000 $m^3$, although an unknown additional volume of the debris

flowed off the fan and into Meager Creek. In addition, part of the debris flow (about 1500 $m^3$) was impounded behind a logging road bridge and road fill upstream of the fan. Small levées and frontal accumulations of boulders and cobbles in parts of the deposit indicate that this event had a coarse front. The debris flow was sampled four days after the event, at which time the deposit was still in an undrained state in its deeper areas, at or very close to its original water content. The sampled water content was 20% (dry weight basis), measured with respect to the fraction of debris smaller than 32 mm.

The prominent scoop-shaped feature visible on the fan surface in Fig. 4.3 was apparently caused by debris pouring off the edge of the fan into the river, and cutting back into the fan by a process of headward erosion, analogous to the upstream retreat of Niagara Falls as it cuts into its resistant cap-rock. Several similar steps or nick-points caused by the same process were seen in the channel upstream.

A third debris flow occurred in November, 1989, with a deposit volume of about 25,000 $m^3$, and with sediment texture similar to the 1987 event. This event happened during a rainstorm which caused high discharges on Meager Creek and tributary streams; therefore, it is possible that the debris flow volume may have been much greater, since a large portion may have been carried away by flow of the river. The entire fan was covered by deposits, which were about twice as thick on the average as those of the 1988 event. The deposit is more variable in texture and surface features than the two earlier deposits, with several areas of relatively coarse debris; this may indicate that several surges occurred. Roughly 2000 $m^3$ of the debris were derived from a large fill on the logging road upstream (mainly angular quartz diorite boulders), and the debris from the 1988 event which had been impounded behind it. Fluvially reworked material derived from the channel upstream had already covered about half the debris flow fan by the time of the survey. This subsequent fluvial deposit accounts for probably no more than 10% of the total debris volume on the fan.

The volumes and thicknesses of the 1988 and 1989 deposits were calculated by producing computer-generated contour maps of the fan surfaces, based on the theodolite surveys made before and after each event. Each survey included approximately 60 to 100 points. An example

of one of the maps is shown in Fig. 4.7. Each contour surface was then subtracted from the succeeding one, producing a contour map of debris accumulation. Fig. 4.8 shows the two maps produced by this procedure. These maps are hand-drawn to smooth out the considerable "noise" shown on the computer-generated maps.

A flood on Meager Creek, probably in November 1990, removed about half the volume of the Boundary Creek fan, exposing a section through it at its apex. A brief visit was made to the site in June 1992. Although the three different events comprising the fan could be distinguished, there was no stratification, grading, or lateral variations in texture visibly apparent in any of the debris flow deposits (Fig. 4.9).

No Good Creek

Figure 4.10 shows aerial views of the channel and drainage basin of No Good Creek. At least three large debris flows occurred in this channel in the early 1980s, destroying the logging road crossing of the creek in three consecutive years (Jordan, 1987b). The deposits of these events are poorly preserved, since the channel enters Meager Creek where it is confined in a narrow canyon, and almost all the debris entered the river and was transported downstream. At least one of the events briefly dammed Meager Creek to a depth of 8 to 10 m. Small terraces of debris, aligned with the height of the blockage which is visible on the opposing river bank, line the debris flow channel in its lowest 200 m. The slope of these terraces, 4 to 5°, is about the same as the slope of the fan constructed by the Boundary Creek debris flows. The texture, lithology, and stratigraphy (or lack thereof) of the No Good Creek and Boundary Creek debris flows are very similar, which would be expected as they drain adjacent basins of nearly identical geology and physiography.

In the 1987 to 1989 period, several relatively small debris flows occurred, which barely reached the mouth of the channel, and caused about a metre of total aggradation throughout its lowest kilometre. One of these events occurred on the same day (September 6, 1988) as the 1988 event on Boundary Creek described above. Its deposits were sampled and surveyed. Only about 100 $m^3$ were deposited at the mouth of the channel, but most of the debris probably

entered the river and was carried away. A somewhat larger volume of debris was impounded by the large fill of the logging road crossing upstream.

In October 1990, a large debris flow removed all the accumulated material in the channel, and deposited at least 10,000 $m^3$ of debris at its mouth, briefly blocking of Meager Creek to a depth of several metres. The total volume of the event must have been considerably larger, since most of the debris was carried downstream by the river. Figure 4.11 shows the debris flow channel at the logging road crossing in 1987, just after its construction, and shortly after the 1990 debris flow.

In texture and sedimentology, the deposits of the 1988 and 1990 debris flows are very similar to the debris flow deposits of Boundary Creek described above (see Table 5.2).

Devastation Creek

The valley draining Devastation Glacier is well known for a large debris avalanche which caused four fatalities in 1975 (Patton, 1976; Mokievsky-Zubok, 1977; Evans, 1990). An event of similar magnitude in 1931 was described by Carter (1932), who visited the valley and adjacent mountains the following summer. He gave this description:

> The same afternoon a 7780-foot outlier of Pylon Pk. was ascended in order to ascertain the origin of a devastating flood which swept down Meager creek in October, 1931. Traces of its ravages had been evident as we travelled up the creek, and Bert recounted how he had witnessed from his cabin a succession of sudden floods passing down the Lillooet. The river rose many feet in a few minutes, was highly discolored, and bore many newly-uprooted trees. We discovered that a large portion of the volcanic ash and debris forming the flank of the summit on which we now stood had slid onto a glacier below which forms the source of one of the tributaries of Meager creek. The slide had apparently impounded the considerable surface drainage of the glacier, then giving way, had swept down stream. At each sharp bend in the valley great sections of the bank had been washed away and the amount of material deposited throughout the length of Meager valley was enormous. Even the location and nature of the hotsprings had been altered. Remains of the slide still buried the snout of the glacier which we named "Devastation glacier", the peak above being dubbed "The Devastator".

Carter's description, combined with observations of the debris deposits in the valley, indicate that this event was a huge debris flow which may have travelled the full length of Meager Creek valley. The "succession of sudden floods" suggests that there were multiple surges, and that they entered and partially blocked Lillooet River. (The cabin referred to is about 3 km downstream from the mouth of Meager Creek). Alternately, the floods could have been caused by the debris flow blocking the south fork of Meager Creek, which enters 9 km

above the mouth; this would imply a somewhat smaller magnitude for the event. However, there are well-preserved debris flow deposits below this confluence, which suggests that the first explanation is the more likely.

The surface of the 1931 deposit along Devastation Creek (Fig. 4.12) is smooth and regular, unlike the hummocky deposits of the 1975 debris avalanche. The debris is uniformly mixed, unlike the lithogically-zoned debris avalanche deposits, and it is similar in texture to the Boundary Creek and No Good Creek debris flows. An extensive debris terrace from the 1931 event fills part of the wide floodplain of Meager Creek below Boundary Creek, forming a uniform layer at least 3.5 m thick, with an indistinct coarse-textured levée along its left margin. Two similar bouldery ridges are repeated within the terrace, suggesting that the event occurred as multiple surges. Remnants of a similar terrace are found 4 km further downstream. Deposits downstream from this point have not been found; either they have been eroded by Meager Creek, or they have been buried by the aggrading river bed. The volume of the original debris deposits can be roughly estimated by taking the thickness and extent of remnant terraces in the valley, and extending this volume to cover the entire creek floodplain. This procedure gives a minimum volume of about $3 \times 10^6$ $m^3$, assuming the deposits extended as far downstream as Capricorn Creek (Fig. 4.4). The actual volume may have been considerably greater, as this estimate does not account for the debris which entered Lillooet River.

Figure 4.12 is an air photo, taken before the 1975 debris avalanche, which shows the surface of the 1931 debris flow deposit, and the superelevation at the confluence of Devastation and Meager Creeks. Figure 4.13 is a sketch map of the same area.

The deposits and trim lines have been correlated to the 1931 event on the basis of vegetation age, damage to surviving trees, and debris lithology. A cedar tree adjacent to the channel of Boundary Creek was scarred by the debris flow; a wedge was cut out of the scar, which gave a date of 1931 ±1 year. Two of the largest cottonwood trees growing on deposits further downstream were cut down, and gave dates (for sections about 0.5 m above ground) of 1935 and 1937. I was able to cross Meager Creek on one occasion in 1990 (the 1989 Boundary Creek debris flow temporarily placed a log across the river channel), and visit the area of

superelevation on the south valley wall. There were several scarred trees along the edge of the debris flow, but I was unable to cut them down or extract suitable wedges with the small saw I was carrying, due to the large size of the trees. However, debris caught up against the tree trunks was positively identified as belonging to the 1931 event on the basis of lithology. A dense alder jungle now covers most of the deposits and the areas deforested by the debris flow (see Fig. 7.3), which inhibits detailed investigation of the surface and perimeter of the deposit.

Approximately 42% of the stones in the debris flow deposits are of one lithology (a distinctive light grey-green dacite) which is not found in significant quantity in any other sediments. This allows identification of the deposits of this debris flow, and also supports the observation of Carter (1932) that it originated from a single landslide. I have not visited the landslide source, which is in an area where travel is dangerous.

Upper Lillooet River

On the north side of the Mount Meager complex, a debris flow terrace covers about 1.9 $km^2$ of the broad Lillooet River floodplain, to a depth of about 4 to 6 m where exposed. The deposit, and the sections examined, are shown in Figs. 4.14, 4.15, and 4.16. This deposit has been dated at 900 years B.P., from uprooted trees which are abundant in the base of the deposit (GSC-3498, 900±60; GSC-4290, 890±80).

The debris is texturally similar to other volcanic-source debris flows in the volcanic complex, although it is somewhat lower in clay content and in the proportion of coarse clasts. It consists mostly of rhyodacitic material typical of the late Pleistocene eruptive phase which comprises the northern part of the volcanic complex (Read, 1990), and it includes some entrained fluvial gravel. The exact source of the debris flow is unknown, and nothing is known of its flow dynamics or its downstream extent. By extending the thickness of the terrace across the remainder of the river floodplain, the debris flow is estimated to have had a volume of at least $10^7$ $m^3$, and it was probably larger, as additional debris must have flowed downstream into the Lillooet River canyon. The river valley is constricted at the lower end of the deposit by the fan of Salal Creek, a major left-bank tributary. This fan acted as a dam, increasing the depth and decreasing the slope of the debris flow deposit behind it.

No surveying was conducted on this deposit. Its longitudinal slope is less than the gentlest slope which can be measured by a hand-held clinometer (0.5°). Based on the 1:20,000 contour base map used for the geological map of Read (1978), its average slope is estimated to be 0.4°.

The deposit is normally graded (coarsening downward), and the proportion of coarse clasts appears to decrease in the downstream direction, at least at the three exposures which were inspected. This structure has been reported in some non-cohesive lahars which have flowed down other river valleys; as the lahar overtakes and mixes with river water, its shear strength decreases, and coarse clasts slowly fall to the base of the flowing debris (Pierson and Scott, 1985; Scott, 1988; Pierson *et al.*, 1990). However, no evidence was found of finer-textured hyperconcentrated flow deposits underlying the debris flow deposits, as has been observed at Mount St. Helens and other locations where the transition from debris flow to hyperconcentrated flow has been described (Scott, 1988). Such deposits, if they exist, may be confined to the pre-existing river channel, and may not have been observed because exposures of the base of the debris flow are limited.

There are few accessible sections where this deposit can be viewed and sampled. However, it is likely that with some effort and helicopter support, additional information could be obtained on this debris flow and other possibly related events. There are several isolated sections downstream on the left bank which contain a variety of fluvial and colluvial deposits, but these have not been dated or described, and they cannot be correlated clearly with the debris flow deposit. The inaccessible right bank of the river has numerous terrace deposits (visible in Fig. 4.14) which may contain additional sections. Most of the large deposit on the left bank is covered with peat and is below the water table, which discourages digging pits.

Although nothing is known of the dynamic behaviour of this debris flow, it is of interest because it provides a second example of the very large and destructive debris flows which can occur in the volcanic complex. The origin of such a large event is somewhat mysterious, as it is hard to explain the sudden appearance of a sufficient volume of water to mobilize such a quantity of debris. No volcanic eruption of this age is known; however, it is possible that an undocumented, small, pyroclastic or phreatic eruption could have triggered a lahar by melting

snow and ice on the flanks of the volcano. Another possible origin could be the failure of a lake dammed by a landslide or a glacier in the valley of Job Creek. Most of the volcanic rocks on the north side of the complex are not hydrothermally altered, and therefore large landslides in soft, saturated debris such as occur in the Devastation Creek drainage are unlikely. Extensive colluvial activity and Neoglaciation have obscured any clues of possible triggering events which might have been found at higher elevations in the volcanic complex.

Canyon Creek

This creek drains a partly glacier-covered basin on the southeast side of the Mount Meager volcanic complex. About half the basin is underlain by quartz diorite and metamorphic rocks, and the main debris sources are rockfall gullies and small slides in these basement rocks. Two debris flows occurred on the creek, in August 1987 and October 1990, with magnitudes of about 10,000 and 20,000 $m^3$ respectively. The second flow buried a logging maintenance camp on the creek fan, causing extensive damage (Fig. 4.17). The one occupant of the camp escaped injury because he was warned by the loud noise of the approaching debris flow.

The coarse clasts of the debris flows are about 84% basement rocks and 16% volcanic rocks, with the latter consisting of relatively unaltered andesite. The proportion of more friable volcanic rocks in the debris flow matrix appears, from colour and texture, to be much higher. In morphology and sedimentology, the deposits are similar in many ways to those of the coarse-textured debris flows. There is an inversely graded coarse surface layer in all but the most distal part of the deposits, and the average slope of the deposits on the fan is 9° to 12°. The proportion of coarse clasts (see Chapter 5 for details) is similar to that found in most of the plutonic-source debris flows; however, the debris matrix is much higher in clay, and drains very slowly. The 1990 deposit was sampled two days after the event, at which time it was still partially undrained. In this state, the debris tended to flow when disturbed, and in the more distal portions where a clast-supported surface layer was lacking, it would not bear the weight of a person. These debris flows, therefore, appear to have some physical characteristics typical of both the volcanic-source and the plutonic-source debris flows found elsewhere in the study area.

The deposits of the 1987 Canyon Creek event included a relatively coarse-textured, cobble and boulder dominated, frontal portion which formed several thick, irregular lobes near the apex of the fan, as well as somewhat finer-textured portions which travelled further down the fan. A clast-depleted, mobile, hyperconcentrated flow phase followed the initial debris surge, and flowed along shallow depressions in the fan for several hundred metres. The deposits suggest that this event may have included several distinct surges. The 1990 deposit, by contrast, is much more uniform, with no indication of separate surges and with only a very minor hyperconcentrated afterflow phase. Like the 1987 event, it left a zone of bouldery, coarse-textured material near the fan apex, suggesting a coarser frontal portion of the flow. The 1990 deposits suggest that the debris was somewhat more fluid and mobile than that of the 1987 event.

Figure 4.18 shows the areas covered by the two debris flows. The 1987 deposits were thoroughly covered by theodolite surveys and compass traverses, with numerous observations of thickness, as well as by low-level air photographs, so the map and the volume estimate are relatively reliable. The 1990 deposits were covered only by a quick compass survey, so the volume estimate and the map are less precise. However, the compass survey was tied into points from the earlier survey, so thickness estimates in the area where the newer debris flow covers the 1987 deposits are accurate.

Hot Springs Creek

A debris flow of about 60,000 $m^3$ in volume occurred during the October 1984 rainstorm on Hot Springs Creek, a right-bank tributary of Meager Creek. The deposit is well preserved, and has been incised in several locations by creek erosion, exposing sections through the debris. The source of debris is a set of rockfall gullies in a 1000 m high escarpment which is probably an ancient rockslide scar. The ridge containing the escarpment has numerous scarps and other linear features, suggesting that active sackung is taking place. The slope of the fan, in the area of debris deposition, is 9° to 10°. Several debris flows of similar size have occurred in the last 50 years or so, as deduced from the age of deciduous trees growing on the older deposits.

The deposits of the 1984 event are similar in texture to those of other debris flows derived from plutonic rocks throughout the southern Coast Mountains, except that the matrix contains a relatively high proportion of fine sand and silt, reflecting a high degree of alteration and deformation in the quartz diorite of the source area. The deposits are inversely graded, with two distinct zones, a lower matrix-supported layer, uniformly topped by a clast-supported layer consisting mainly of cobbles and boulders (see Fig. 5.9A). The deposits are quite irregular in morphology, with thickness ranging from 1 to 4 m, and with several prominent wave-like lobes of coarser clasts (Fig. 4.19). The coarse surface layer, inverse grading, and irregular thickness and morphology, are typical of many other coarse-textured debris flow deposits in the study area and elsewhere.

Figure 4.20 is a map of the deposits, based on low-level air photos and on a theodolite survey. There are about four large waves of debris, each with frontal accumulations of boulders and cobbles, separated by thinner, relatively uniform, deposits. These waves may be evidence of multiple debris surges. The debris is covered everywhere with a coarse surface layer, however this is quite variable in thickness and in maximum clast size. The deposits have been cut through by a network of channels, which probably formed immediately after emplacement of the debris, as the event occurred during a heavy rainstorm when discharges in local creeks were very high. Approximately 20% of the deposit volume appears to have been removed by this erosion, and carried further downstream as bedload, where it caused considerable damage to logging roads and a campsite at the hot springs downstream (Fig. 4.4). The volume of the event was estimated from observations of debris thickness along these channels, and wherever else thickness could be reasonably estimated. Upstream from the main deposition area, the channel is filled with debris flow and fluvial gravel deposits, probably from minor surges which followed the main event. This is unlike most of the other debris flow channels studied, in which the debris flows had scoured the channels clean of almost all moveable debris. Also unlike most coarse-textured debris flows, there are no lateral levées along the channel.

Terraces bounding the deposition area are part of a higher fan surface, about 5 to 8 m above the presently active fan. This higher fan consists, in part, of deposits of a rock avalanche

which apparently originated from the escarpment at the head of the channel. These deposits are partly covered by subsequent debris flow and fluvial deposits. From limited exposures along logging roads further down the fan, this rock avalanche appears to be older than volcanic-source deposits originating from the other side of the valley, which have been dated at 4100 years or younger (Figure 4.4). A sample of the rock avalanche deposit showed that it contains considerably more silt and fine sand, and fewer cobbles and boulders, than the debris flow deposits. This result supports the observation, made in Chapter 5, that debris flows are typically of coarser texture than rock or debris avalanches derived from the same geologic material.

At the mouth of Hot Springs Creek, about 1.4 km downstream from the 1984 deposit, there is a complex of debris flow deposits which range from about 25 to 100 years old, based on the age of deciduous trees growing on them. No major debris flows appear to have reached the mouth of the creek in the last 25 years. The Meager Creek Hot Springs emerge from these deposits, and from a fluvial terrace consisting of gravel of Hot Springs Creek provenance, which was probably emplaced when one of the debris flows blocked Meager Creek. This event occurred in about 1955 (± 5 years), based on the age of vegetation and on air photos taken in 1962.

A debris flow occurred in late 1990 or early 1991, and covered about half the area of the 1984 debris flow deposits. I observed this on a brief visit in September 1991, but I did not make any detailed observations or take samples. The event probably took place during a major rainstorm in November 1990.

Capricorn Creek

Capricorn Creek drains a relatively large (15 $km^2$), partly glacier-covered basin, underlain in its upper one-third by volcanic rocks. The lower two-thirds of the basin is underlain by fractured quartz diorite. On the steep northern wall of the valley, a large rock avalanche has filled at least a 1 km length of the valley with slide debris. This landslide has two adjacent source areas, and could be two separate events. Discontinuous remnants of the slide debris form terraces at least 20 m high and extend to 0.9 km above the mouth of the creek, just above the

apex of its fan. This landslide was investigated by Croft (1983), who estimated its age at less than a century.

The fan of Capricorn Creek is covered with a recent deposit which has the appearance of a large debris flow (Figure 4.21). It consists almost entirely (95% of coarse gravel) of material of quartz diorite origin. This deposit has encroached on the forest which once covered the left side of the fan, leaving a number of standing dead trees. The age of the event is estimated at about 1970 to 1972, based on air photos taken in 1973. No debris flow activity occurred on the fan from 1977, when the logging road was built, until 1990. Several damaged living trees along the edge of the fan, scarred by debris flow or flood event, were cut down; these gave several dates of about 1971 to 1973 ($\pm$ 2 years), as well as dates of about 1909, 1932, and 1961. The toe of the fan constricts Meager Creek against its right valley wall, and high water marks at this location show that Meager Creek was blocked to a depth of about 6 m by the *ca.* 1972 event. This, and the massive nature of the deposit at the toe of the fan, suggest that all or most of the fan deposit was emplaced as a single event.

Several pieces of evidence lead to the conclusion that the event was probably not a debris flow, but rather a "debris flood" (a flood carrying an unusual volume of bedload). These include:

- the deposits seen in section and in sample pits show weak stratification at some locations;
- the coarse surface layer of cobbles and boulders is discontinuous, and is only one stone thick where present;
- the surface of the deposit, as seen on low-level air photos, has surface features which resemble the pattern of a braided channel;
- at some locations where seen in section, the deposit appears to be clast-supported rather than matrix-supported (although this distinction is not easy to make for coarse-textured debris);
- there are no levées, or prominent lobes of coarser debris, in the deposit.

However, features typical of braided river deposits, such as imbrication of surface gravel, cross-bedding, and well-developed bars and pool-riffle sequences, are lacking. These features

are obvious in the fluvially reworked part of the fan along the active channel. Therefore, although the recent deposit appears to be more of fluvial than of debris flow origin, it was probably emplaced as a result of a single, catastrophic event. The total depth of the deposits is not known, so the volume estimate in Table 4.2 is rather approximate. The evidence of scars on trees suggests that deposits of earlier events may underlie the recent deposit.

In October 1990, a relatively small debris flood event covered about 20% of the fan with a deposit which is quite similar to the one described above (Figure 4.22). The stratification of the fresh deposit can be seen in photo B of this figure. However, at one location about 300 m below the apex of the fan, the former creek channel is filled with a deposit about 2 to 2.5 m thick which appears to be a debris flow, as it consists of massive, unstratified sandy gravel with a coarse surface layer. Thus it is possible that the *ca.* 1972 event, as well as the earlier ones, included some debris flow surges as well as fluvial transport.

The most likely origin of the events which formed the Capricorn Creek deposits is that during high flows of the creek, the landslide deposits which border the channel were undercut and slumped into the creek, partially or completely blocking it and introducing a very large volume of sediment. This process could result in an outburst flood, which would carry the introduced bedload to the fan as a single surge.

Lower Ryan River

This debris flow channel is included as a study site because it is easily accessible, has a sinuous channel which enables velocity estimates to be made from superelevation, and is typical of many debris flows originating in plutonic rocks in the study area. The channel drains a small, steep basin at the mouth of the Ryan River valley near Pemberton. The debris flow event under study occurred in October 1984, as a result of the heavy rainstorm which caused many other debris flows in the study area. A similar event in the same channel occurred in 1975, and was described by Hart (1979).

Figure 4.23 shows the channel and its drainage basin, and the debris flow fan. The main sources of debris in the basin are areas of rockfall, and a talus slope which appears to have been steepened into an indistinct moraine by a small Neoglacial glacier, which has since wasted away.

The lower part of the channel crosses a small, steep (12° to 16°) fan bordering Ryan River (Figure 4.24). Most of the debris from the 1984 event entered the river and was carried downstream, so the magnitude of the event cannot be readily estimated. About 7000 $m^3$ of debris were deposited in levées and small lobes along the channel; the total event volume was probably 20,000 $m^3$ or greater. The debris deposits preserved along the channel consist of an irregular lower layer of predominantly matrix-supported sandy gravel, with some zones of clast-supported gravel, topped by a fairly regular layer of clast-supported cobbles and boulders about 1 m or more in thickness. The coarse surface layer contains frequent boulders larger than 1 m in diameter, with very little matrix.

The 1975 event appears to have been slightly larger, based on the extent of its deposits on the fan. Another debris flow event occurred, probably in November 1990; I observed it from the air in September 1991, but did not study it on the ground. It appears to have been smaller than the 1984 event.

## 4.4 MINOR STUDY SITES

The following section gives brief descriptions of additional sites at which debris flow deposits were observed and sampled. The data on each site are summarized in Table 4.2. As in the previous section, the sites are given in order of texture, with fine-textured debris flows first and coarse-textured ones last. Maps and detailed descriptions of each site are not given here. References are given where further information is available from other sources.

### Turbid Creek

Turbid Creek drains an extremely steep drainage on the precipitous southwest flank of Mount Cayley. In June, 1984, a debris avalanche occurred in Quaternary pyroclastic deposits near the head of the basin. Two large debris flows followed this event, one immediately or soon after, and one during the October 1984 rainstorm. The landslide and debris flows are described in more detail by Jordan (1987a; 1987b) and by Cruden and Lu (1989). An earlier landslide is described by Clague and Souther (1982). Souther (1980) gives further information on the Mount Cayley volcanic complex, including an interesting eye-witness description of a small debris flow.

The June 1984 debris flow was witnessed by several people, who described a series of surges entering Squamish River, lasting for 4 or 5 hours. Their descriptions are corroborated by the hydrograph of Squamish River at the gauging station 34 km downstream, which shows several partial blockages of the river. Based on these descriptions and on the calculated peak discharge of 4000 $m^3$ (see data in Chapter 7), the volume of the event was probably in the order of $10^6$ $m^3$. The October 1984 event was not witnessed.

The lower channel of Turbid Creek is very straight, and is incised into a complex fan of mid-Holocene debris flow and debris avalanche deposits (Evans and Brooks, 1991). The channel feeds material from debris flows directly into Squamish River at a location where it is confined between the fan and a rock mountainside on the opposite bank (Figure 4.25). Very little material from the debris flows is preserved, as the flows entered Squamish River and were dispersed downstream. A sample was taken from a small terrace of debris just above the mouth of the channel; it is likely from the second event. There is a sharp bend in the channel 1.8 km above the mouth, upstream from the fan, which gives an opportunity for superelevation measurements.

Cheekye River

The Holocene Cheekye Fan, below Mount Garibaldi, consists largely of a sequence of two or more very large debris flows, the lowest exposed unit of which has been dated at under 6000 years B.P. (5890±100; Eisbacher, 1983). The fan slopes at a gradient of about 2.5°, and is topped with fluvial gravels and smaller debris flow deposits. Debris flow hazards on the fan have recently been the subject of considerable study, since the fan is occupied in part by the villages of Brackendale and Cheekye, and by several industrial and transportation facilities (Thurber Engineering Ltd. and Golder Associates Ltd., 1993). An early description of the fan and of Quaternary volcanism at Mount Garibaldi is given by Mathews (1958).

In 1958 an event described as a mudflow descended Cheekye River to its mouth (Jones, 1959). The deposits which remain near the mouth of the river are not obviously distinguishable from fluvial deposits, and it is likely that this event was a debris flood, not a debris flow, at least near the mouth. Several debris flow exposures, which may be from this event or from other

unreported events, line the channel near the fan apex and further upstream, but I have not attempted to study them.

The major rainstorm and flood of October 1984 transported large quantities of fluvial sediment, and completely rearranged the river channel deposits. In 1985 I found a small debris flow deposit amongst the new bars in the channel, just upstream from the apex of the fan. In 1989 I returned and sampled it. This deposit is unusual in that it is extremely bimodal in grain-size distribution, and consists of two very distinct layers: a lower, obviously matrix-supported, silt-rich, debris flow layer, and a surface layer consisting of cobbles and boulders with little or no matrix (Figure 4.26A). The unusual structure of this deposit may be due to floodwaters winnowing out the finer material from the clast-supported top layer. This event is probably best described as a debris flood, although it obviously included some material which had travelled as a debris flow. More detail on the 1958 and 1984 events is given in Jordan (1987b).

In 1991, a large debris flow deposit on the fan was discovered by Frank Baumann, a geological engineer living in Squamish. The deposit was previously undiscovered because of the dense second-growth forest which covers the fan. I assisted him in the initial excavation and survey of this deposit, which is described in detail by Baumann (1991). The debris flow was dated at 1100 years B.P. from samples taken from two well-preserved logs at the base of the deposit (details in Baumann, 1991). The debris flow material is fine-textured, with sparse cobbles and boulders in a clay-rich matrix (Fig. 4.26B). Baumann estimated the volume of the debris flow at $5 \times 10^6$ $m^3$, but my more conservative estimate, based on field notes taken during our survey, is $3 \times 10^6$ $m^3$.

Angel Creek debris flows

Near Angel Creek in the Meager Creek valley, two steep gullies drain an area of lava bluffs (Figure 4.4). These deliver fairly frequent, small debris flows, with an estimated 1 - 5 year return period. The deposits of two of these were surveyed and sampled. Texturally, they are similar to other debris flows in the volcanic complex. They are included in the study in order to extend the data set to events of smaller magnitude.

In one of these events, most of the debris was deposited in levées which confine the channel in its course on the fan. This pattern of deposition is typical of many debris flows in semi-arid environments (see following example), but has not been observed elsewhere in the Meager Creek study area.

Fountain Ridge and McGillivray Creek

These two sites are located on the east side of the Fraser Canyon near Lillooet (a town which has no geographic relation to Lillooet River). This semi-arid area is quite different in geomorphology and hydrology to that of the main study area. There are numerous debris flow fans, mainly of late Pleistocene to early Holocene age, which have been studied by Ryder (1971). The two sites are on debris flow fans which are presently active, as they drain small, steep basins containing eroding bluffs of friable rock, and extensive talus slopes which feed the debris flow channels. Debris flows in these channels appear to occur annually or more frequently, based on extensive fresh deposits and damage to vegetation on the fans.

These debris flows were selected because on initial observation, they appeared to be of a texture intermediate between the volcanic and plutonic source materials of the main study area; however, on sampling them, their matrix proved to resemble more the volcanic-source materials. The rocks of the source areas are intensely fractured, and therefore the coarse fraction of the debris flows is dominated by pebbles and small cobbles, with relatively few coarser fragments.

Debris flows on these fans typically flow in levée-confined channels, in which most deposition takes place on the levées and in occasional small lobes which break through them. Repeated small debris flows are confined in the same channels, causing multiple ridges of deposited debris on the levées. Larger events avulse from the channels, forming a new channel and set of levées. The cross-sectional dimensions of the channels typically declines downstream, as the discharge of the event declines, and the debris texture becomes finer downstream as coarser material is preferentially deposited in the levées. These features are especially well-developed in the Fountain Ridge channel (Figure 4.27). This depositional behaviour may be due to a relatively low water content, as discussed in Chapter 7. The data in Table 4.2 were collected in October 1989, on the two most recent debris flows which occurred that summer.

Mount Currie

A series of steep, rockfall-fed, debris flow channels drains the north face of Mount Currie near Pemberton, below a 2000 m high crumbling rock face which is undergoing toppling and slow gravitational displacement (Evans, 1987b). One of these channels experienced a debris flow of approximately 20,000 $m^3$ in the late 1980s, and a slightly larger event several years earlier (probably in the October 1984 rainstorm). The rock in the source area is altered diorite and gneiss of the Pemberton Diorite Complex. The debris matrix is finer than that of other debris flows from plutonic rock sources (5.5% clay in the matrix); otherwise, the deposits are similar in sedimentology to those of other plutonic-source debris flows. This debris flow has unusually large levées in the upper part of the fan (Fig. 4.28).

Affliction Creek

This 13 $km^2$ drainage on the north side of the Meager Creek volcanic complex is underlain by volcanic and basement rocks in roughly equal proportions, and about one-third is glacier-covered. The drainage includes a large failing slope, where fractured plutonic rock, capped by a thin lava flow, are undergoing gradual deformation and failure. This site has been studied by Bovis (1990). Debris from this site, and from Neoglacial moraines, feed predominantly plutonic debris to the creek, which has built up a large fan consisting of fluvial and debris flow material. A very large debris flow event occurred in October 1984; I briefly visited the site by helicopter on two occasions in 1985 and 1989. Most of the deposit surface consists of coarse, bouldery waves and lobes, typical of coarse-textured debris flows. Sections through the deposit are confined to a few locations bordering the creek in its distal portion. Here, the deposits appear to be of debris flow origin, with a matrix-supported lower zone and a clast-supported surface layer. However, there is some stratification at a few exposures, suggesting a possible debris flood origin for some of the debris.

Middle Lillooet River fans (Pebble Creek area)

Downstream from Meager Creek, on the left bank of Lillooet River, three unnamed fans lie below a steep mountainside of competent quartz diorite. They are fed by joint-controlled gully systems, in which rockfall debris produces debris flow events at intervals of several years.

On two of these, the centre and east fans, debris flow events occurred as a result of the October 1984 rainstorm. A smaller event occurred on the east fan in August 1989. Figure 4.29 shows the two fans. The 1984 debris flow on the centre fan produced a main depositional lobe with an extremely coarse surface layer, which made it impossible to sample the subsurface material. Finer debris continued further down the channel and produced smaller lobes; these were sampled, but the material is not representative of the entire deposit.

Upper Ryan River

This site is typical of large, plutonic-source debris flows in the study area. The sampled event occurred in October 1984, and was selected for study because of easy road access. Many similar debris flows occurred at other less accessible locations in the study area, during the same 1984 rainstorm.

## 4.5 COMMENTS ON THE INITIATION OF DEBRIS FLOWS

Debris flow source areas

The investigation of debris sources and initiating mechanisms was not a major objective of this study. However, some casual observations were made in the course of the study which are worth summarizing. In the first season of field work, traverses were made of the full length of the channels of Boundary and No Good Creeks, and a descriptive inventory was made of sediment sources. However, this activity proved to be excessively dangerous, so no further detailed investigations were made.

In both Boundary and No Good Creeks, a high proportion of the drainage basins consist of talus slopes and steep, actively disintegrating, rock faces (Figure 4.10). Furthermore, the valley walls contain zones of deep-seated, slow-moving, bedrock slumping, which tends to confine the creek channels with banks of unstable, dilated rock which are prone to undercutting and collapse. Small debris flows occur frequently on the talus slopes, as indicated by the small levées they produce; these add to the sediment which accumulates in the channels. In both channels, the supply of readily available sediment is essentially infinite. Debris flows probably occur when a hydrologic event capable of mobilizing some of the sediment takes place, which by chance is combined with a channel blockage or bank collapse which enables the debris flow to

grow as it moves downstream. It is likely that many small debris flows occur in the channels which do not travel as far as the lower valley; instead they add to the volume of debris which builds up in the middle reaches of the channel. No debris flow events which occurred during the study could be attributed to specific mass movement events which could be noted from distant observation; however, no detailed inspections of the basins were made following the events.

Loggers working in the Meager Creek valley took some interest in debris flow processes because of the inconvenience caused by repeated destruction of their road. The logging company foreman, who flew a small airplane, occasionally inspected the basin of No Good Creek from the air. He reported that debris raveling from the talus slopes tended to accumulate in the channel throughout the summer, and that the first major rainstorm following a long dry period tended to produce a debris flow (Decker, pers. comm.). This observation is supported by the fact that in the volcanic-source basins, most reported or observed debris flows occurred during minor late summer rain showers, rather than during the major fall storms.

In the mainly plutonic-source debris flow channels, rockfall from joint-controlled gullies or unstable cliffs appears to be the main mechanism which causes sediment to accumulate in the channels. In some of the basins, including Canyon, Affliction, and upper Ryan, steep Neoglacial moraines may provide additional sources of sediment. The large clast size of the sediment produced from competent plutonic rock may inhibit debris flow initiation in all but the heaviest rainstorms, which may explain why debris flows in these basins are most frequent during major autumn storms.

Most of the debris flow channels in the study area are filled with avalanche snow until mid-summer. This dense snow appears to have the effect of "gluing" mobile sediment to the channel sides, and of protecting it from small debris flows from upslope; these tend to travel over the snow surface rather than eroding through it. Apparently for this reason, no debris flow events have been recorded in the study area in spring or early summer.

Hydrologic events leading to debris flow initiation

A recording rain gauge was operated near No Good Creek during the field seasons of 1988 and 1989. The data from this gauge, and some other miscellaneous observations, are

given in Table 4.3. There are insufficient data in this record to come to any firm conclusions. However, the observation can be made that heavy rainfalls (greater than 40 mm in 24 hours), during which many debris flows occur, failed to cause debris flows in most channels, while some debris flows occurred during relatively minor rainfall events.

Unrecorded "cells" of high-intensity rainfall are often invoked as an explanation for debris flows during moderate rainfalls (*e.g.* Church and Miles, 1987). This hypothesis cannot be tested for past events. However, it is possible that heavier rain may have occurred in parts of the Lillooet River watershed during the October 1984 rainstorm, since the return period of the flood is believed to be in excess of 100 years, while the recorded rainfall at Pemberton and Alta Lake was only about a 20 year event (Nesbitt-Porter, 1985).

## 4.6 SUMMARY OF FIELD OBSERVATIONS

In addition to the measurements reported in this chapter, some qualitative observations were made which are useful in explaining the factors affecting debris flow mobility.

The debris flows examined in this study tend to fall into two general categories: coarse-textured debris flows which have a sandy matrix, a high proportion of coarse clasts, and a clearly-defined, coarse, clast-supported surface layer; and fine-textured debris flows, which have a muddy matrix with a significant clay content, fewer coarse clasts, and little or no vertical grading. The fine-textured debris flows tend to deposit on gentler slopes than the coarse-textured debris flows; the division between the two populations is around 7°. There also appears to be a scale factor, with the larger debris flows coming to rest on gentler slopes. There are some intermediate events between the two extremes. For example, the Canyon Creek and Fountain Ridge debris flows have fine-textured, clay rich, matrix material, but have coarse surface layers typical of coarse-textured debris flows.

In many of the debris flow deposits examined, three facies of deposition can be distinguished. These are the clast-supported, coarse deposits of the frontal portion of the surges and the levées; the poorly sorted, matrix-supported debris which forms the bulk of the event; and a fine-textured afterflow facies, consisting almost entirely of sand and fines, which is probably the hyperconcentrated flow phase which follows the main surge. These three facies

can be identified in almost all events, although the relative abundance and degree of preservation of each facies varies considerably.

Some debris flows develop levée-confined channels as they flow across alluvial fans, depositing almost all of their debris in the levées. These channels become smaller with increasing distance down the fan, as discharge decreases. In some cases, the clast size of the coarse fraction also decreases down-channel, as coarse material is selectively deposited in the levées. This behaviour is best developed in the Fountain Ridge debris flows, but it occurred in several other events as well. This behaviour is most typical of debris flows in semi-arid regions, although there is no immediately apparent reason why this should be the case. Most of the studied events, where they deposited on alluvial fans, spread out in an unconfined manner in a broad lobe on the fan, unless they were so small that they remained contained in a pre-existing channel. The tendency of a debris flow to remain confined between levées of its own construction has implications for attempting to model the distance of travel of debris flows on fans; if so confined, a debris flow will travel much further than if it escapes from its levées and spreads over the fan surface. There was no evidence collected during this study which would explain why a debris flow should behave in one way or the other, although it is possible that the mode of deposition is controlled by water content (see Chapter 7).

Several of the debris flows were visited in the field within a few days of their occurrence. The fine-textured debris flows remained in an undrained state for up to a week after emplacement, and were unable to bear the weight of a person. While in this state, they could be easily re-liquefied by disturbing them, and would begin to flow again. This behaviour was especially obvious in the 1990 Canyon Creek event, which partially buried a logging camp. When the material was moved by heavy equipment, it began flowing again, and excavation could not be successfully undertaken until about a week after the event. Only one coarse-textured debris flow was observed shortly after the event; this was the small Lillooet River east fan event of 1989, which was quite well consolidated after about two days. This slow drainage of fine-textured debris can be explained by the low permeability of fine-textured sediment.

In all cases where freshly deposited debris was observed over a period of time, only clear water emerged from the base and surface of the deposits as drainage and consolidation took place. This indicates that water is slowly draining through the pores of the consolidating debris, as would be expected for poorly sorted sediment. (In geotechnical engineering terms, poorly sorted sediment acts as a filter; such material will resist piping erosion, and flow through it should be laminar.) This observation also confirms that the material sampled in debris deposits is representative of the debris during flow. If fine sediment had escaped with water from the debris following emplacement, one would expect to see evidence of piping erosion; no such evidence was observed in this study. The exception to this dewatering behaviour occurs in the open framework, clast-supported coarse facies, that is, in levées and boulder fronts, where fine sediment is eroded from between the stones by turbulent flow of rainwater or streamflow.

The separation of debris flow events into two populations, one with inverse grading and a coarse surface layer, and one without, provides a qualitative indication of the rheologic model which applies to the debris. The dilatant flow model predicts that coarser clasts should migrate to the surface of a debris flow, due to the greater dispersive stress on larger particles (Takahashi, 1980). If this supposition is correct, the presence of a coarse surface layer may be taken as evidence that dilatant flow exists, and the absence of any vertical grading may be evidence that the flow behaviour is dominantly viscous, meaning that the Newtonian or Bingham model applies. Bagnold's parameter "N" (Bagnold, 1954) predicts that the dilatant, or inertial, regime is favoured by larger grain size and lower viscosity of the interstitial fluid; this is consistent with the properties of coarse-textured debris which develops a coarse surface layer. The role of grain-size distribution, and other features of debris flow sedimentology such as vertical grading, are discussed further in the following chapter.

TABLE 4.1 MORPHOMETRIC AND GEOLOGIC DATA FOR DEBRIS FLOW BASINS

| Basin | Area ($km^2$) | Total relief (m) | Glacier cover | Main geologic formations; remarks |
|---|---|---|---|---|
| Boundary Cr | 2.5 | 1500 | - | MCVC |
| NoGood Cr | 2.0 | 1600 | - | MCVC |
| Devastation Cr | 25 | 1700 | 22% | MCVC |
| Upper Lillooet R | ? | ? | ? | MCVC (source basin unknown) |
| Canyon Cr | 5.5 | 1900 | 12% | MCVC, CPC, Cadwallader Group (metamorphic rocks) |
| Hot Springs Cr | 7.1 | 1900 | 17% | CPC |
| Capricorn Cr | 15 | 2200 | 21% | CPC, MCVC |
| Lower Ryan R tributary | 1.6 | 1800 | - | CPC |
| Turbid Cr | 8.3 | 2100 | - | GVG, CPC |
| Cheekye R | 55 | 2500 | < 1% | GVG, CPC |
| Angel A gully | 0.4 | 800 | - | MCVC |
| Angel B gully | 0.2 | 700 | - | MCVC |
| Fountain Ridge gully | 1.2 | 1300 | - | Jackass Mtn Group (sedimentary rocks) |
| McGillivray Cr gully | 2.2 | 1300 | - | Mt Lytton Plutonic Complex (altered granodiorite) |
| Mount Currie gully | 1.9 | 1700 | - | Pemberton Diorite Complex (part of CPC) |
| Affliction Cr | 13 | 1500 | 40% | MCVC, CPC, Affliction Cr Stock, Cadwallader Group |
| Lillooet R fan centre | 2.8 | 2000 | - | CPC |
| Lillooet R fan east | 2.8 | 2000 | - | CPC |
| Upper Ryan R tributary | 8.3 | 1400 | 24% | CPC |

MCVC - Meager Creek Volcanic Complex (part of Garibaldi Volcanic Group)
GVG - Garibaldi Volcanic Group
CPC - Coast Plutonic Complex

TABLE 4.2 SUMMARY OF DEBRIS FLOW DEPOSITS AT MAJOR STUDY SITES

| Location and date | Site (Fig. 3.1 or 3.4) | Volume ($m^3$) | Area covered ($m^2$) | Thickness (m) | Slope(°) average range | Grading and stratification | Circumstances of deposition | Lithology (% basement and volcanic) | Remarks |
|---|---|---|---|---|---|---|---|---|---|
| Boundary Cr 1987 | m1 | 50,000 A | 21,000 | 0.5-5 | 4.5 3.1-5.5 | none | unconfined fan, confined floodplain | B33,V67 | |
| Boundary Cr 1988 | m1 | 5000 A | 7500 | 0.4-1.0 | 4.8 3.7-6.5 | none | unconfined fan | B28,V72 | Ca. 1500 $m^3$ impounded by road |
| Boundary Cr 1989 | m1 | 25,000 A | 18,000 | 1.0-2.0 | 5.3 3.6-6.5 | none | unconfined fan | B30,V70 | Road removed |
| Devastation Cr 1931 | m3 | $3x10^6$ MB | $0.2x10^6$ R | > 3.5 | 1.9 1.8-5.2 | none | confined floodplain | B9, V91 | |
| No Good Cr, early 1980s | m2 | ? | 2000 R | 1-5 | ? 3.5-4.9 | none | river, confined fan | B33, V67 | Several events |
| No Good Cr 1988 | m2 | 100 MC | 100 R | 0.5-1 | ca. 6 | none | river, confined fan | mostly volcanic | Ca. 500 $m^3$ impounded by road |
| No Good Cr 1990 | m2 | 10,000 MB | 5000 R | 0.7-6 | 4.5 4-5 | none | river, confined fan | mostly volcanic | Road removed |
| Upper Lillooet R, ca. 900 BP | m9 | $1x10^7$ MC | $1.9x10^6$ R | 4-6 ? | ca. 0.4 | weak normal grading | confined floodplain | B21, V79 | |
| Canyon Cr 1987 | m6 | 10,000 A | 8000 | 0.5-4 | 11 8-15 | inverse grading, coarse surface layer | unconfined fan | B84,V16 | |
| Canyon Cr 1990 | m6 | 20,000 B | 10,000 | 1-5 | 9 8-10 | weak inverse grading, coarse surface layer | unconfined fan | basement and volcanic | |
| Hot Springs Cr 1984 | m5 | 60,000 A | 35,000 | 1-4 | 10 7-16 | inverse grading, coarse surface layer | partly confined fan | B100 | |
| Capricorn Cr ca. 1972 | m7 | 200,000 ? C | 70,000 | 1-3 ? | 9.6 9-10 | weak stratification, thin discontinuous surface layer | confined fan | B95, V5 | May include several events |
| Lower Ryan R tributary 1984 | 4 | 20,000 MC | 7000 R | 1.5-3 | ? 10-16 | inverse grading, coarse surface layer | river, unconfined fan | B100 | Prominent levées |

Notes: Site - m refers to Meager Creek study sites, Fig. 3.4.
Volume - M is estimated minimum volume based on deposits; total event volume may have been several times greater.
Area covered - R is area of deposit remaining; implies that most of deposit has been removed.
Lithology - B is basement rocks (plutonic and metamorphic); V is Quaternary volcanic rocks.
Reliability of volume estimates:
A - based on reasonably precise surveys of area and thickness; proportional error about 0.3 to 0.5.
B - based on less precise approximations of area and thickness; proportional error about 0.5 to 1.0.
C - very rough approximation, limited thickness observations or poor preservation of deposits; proportional error 1.0 or greater.

TABLE 4.3 SUMMARY OF DEBRIS FLOW DEPOSITS AT MINOR STUDY SITES

| Location and date | Site (Fig. 3.1 or 3.4) | Volume ($m^3$) | Thickness (m) | Slope (°) | Grading and stratification | Circumstances of deposition | Dominant lithology | Remarks |
|---|---|---|---|---|---|---|---|---|
| Turbid Cr 1984 | 2 | $1x10^6$ C | ? | 4 | none apparent | river | volcanic | Two events; volume of first event based on eyewitness descriptions. |
| Cheekye R, ca. 1100 BP | 1 | $3x10^6$ C | 2-6 | 2-3 | none | unconfined fan | volcanic | |
| Cheekye R 1984 | 1 | ? | ca. 1.5 | 3.5 | coarse surface layer, strongly bimodal | confined channel | volcanic | Poorly preserved. |
| Angel A gully, ca. 1987 | m4 | 60 B | 0.6 | 12 | thin coarse surface layer | unconfined fan | volcanic | |
| Angel B gully, 1990 | m4 | 200 C | ca. 0.5 | 12-15 | none | levée-confined channel on fan | volcanic | Most deposition in levées. |
| Fountain Ridge gully, 1989 | 6 | 3500 B | 0.5-2 | 10-15 | thin coarse surface layer | levée-confined channel on fan | sedimentary | Most deposition in levées; texture becomes finer downstream. |
| McGillivray Cr gully 1989 | 7 | 6000 C | ca. 0.7 | 7-15 | thin coarse surface layer | levée-confined channel on fan | altered plutonic -metamorhic | Most deposition in catch basin above highway. |
| Mt Currie gully, ca. 1984 | 5 | 20,000 C | 1-3 | 8-17 | inverse grading, coarse surface layer | unconfined fan and levée-confined channel | altered plutonic | |
| Affliction Cr 1984 | m10 | 200,000 C | 1-2 | 6-8 | coarse surface layer, some weak stratification | unconfined fan | 60% plutonic, 40% volcanic | |
| Lillooet R centre fan 1984 | m8 | 15,000 C | 0.5-4 | 7-13 | inverse grading, coarse surface layer | unconfined fan, partly confined channel | plutonic | |
| Lillooet R east fan 1989 | m8 | 2000 B | 0.4-1.5 | 7-13 | inverse grading, coarse surface layer | partly confined channel on fan | plutonic | |
| Upper Ryan R tributary 1984 | 3 | 50,000 B | 1-2 | 8-12 | inverse grading, coarse surface layer | unconfined fan | plutonic | |

Notes: Site - m refers to Meager Creek study sites, Fig. 3.4.
Reliability of volume estimates:
A - based on reasonably precise surveys of area and thickness; proportional error about 0.3 to 0.5.
B - based on less precise approximations of area and thickness; proportional error about 0.5 to 1.0.
C - very rough approximation, limited thickness observations or poor preservation of deposits; proportional error 1.0 or greater.

TABLE 4.4 SUMMARY OF RAIN GAUGE INFORMATION

| Year | Date | Maximum rainfall in 24 hrs (mm) | | Debris flow events |
|---|---|---|---|---|
| | | No Good Cr | Pemberton | |
| 1984 | Oct. 7-9 | | 68 | 8 events in Tables 4.1 and 4.2, numerous other unstudied events |
| 1988 | Aug. 15 | 16 | | - |
| | Sept. 6 | 18 | | Boundary Cr, No Good Cr |
| | Sept. 18-19 | 16 | | - |
| | Sept. 26 | 25 | | - |
| | Oct. 9 | 14 | | - |
| | Oct. 15 | 20 | | - |
| | Oct. 20 | 12 | | - |
| 1989 | Aug. 1-4 | missing | | Lillooet R east fan |
| | Aug. 21 | 13 | | - |
| | Oct. 10 | 17 | | - |
| | Oct. 11 | 23 | | - |
| | Oct. 12 | 13 | | - |
| | Oct. 17-18 | 42 | | small debris flood, No Good Cr |
| | Oct. 22-24 | 17 | | - |
| | Oct. 25-26 | 20 | | - |
| | Nov. 8-9 | 87 | | Boundary Cr (large debris flow), No Good Cr (small debris flood) |

Note: All rainfall events in 1988 and 1989, for which over 10 mm of rainfall in 24 hours was recorded, are included.

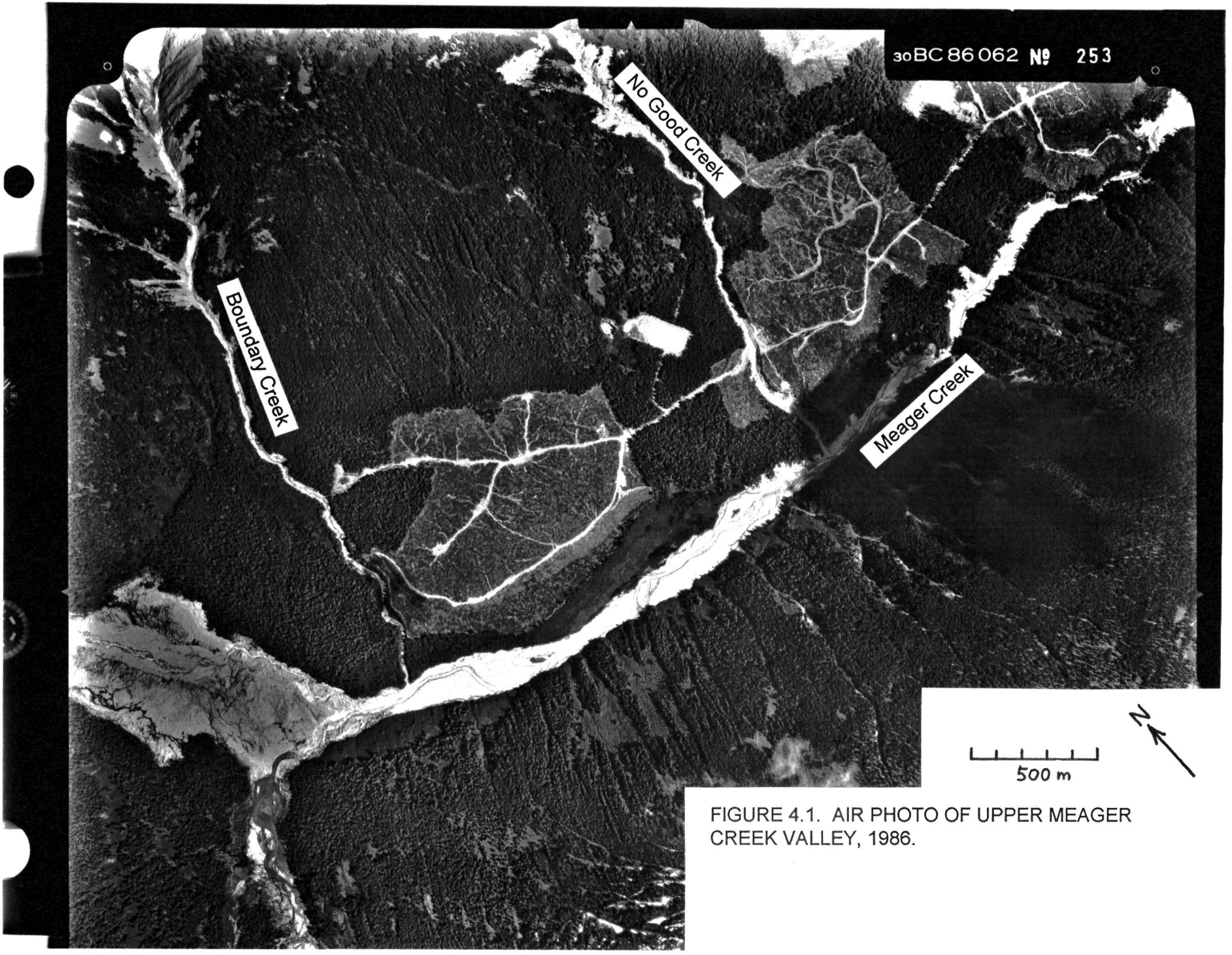


FIGURE 4.1. AIR PHOTO OF UPPER MEAGER CREEK VALLEY, 1986.

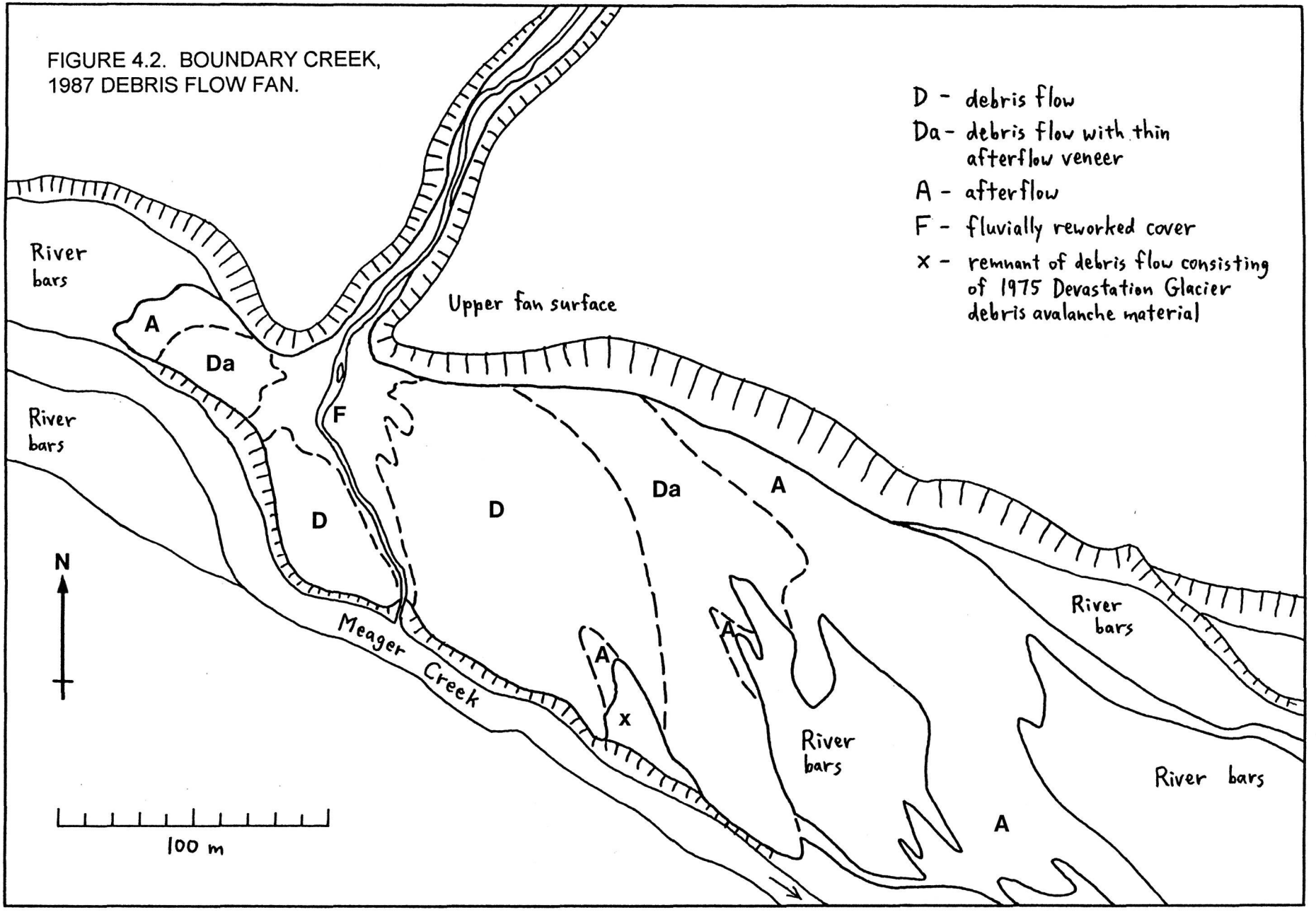
FIGURE 4.2. BOUNDARY CREEK,
1987 DEBRIS FLOW FAN.
D - debris flow
Da - debris flow with thin afterflow veneer
A - afterflow
F - fluvially reworked cover
x - remnant of debris flow consisting of 1975 Devastation Glacier debris avalanche material
River bars
Upper fan surface
A
Da
F
D
D
Da
A
River bars
River bars
N
Meager Creek
A
x
A
River bars
River bars
A
100 m

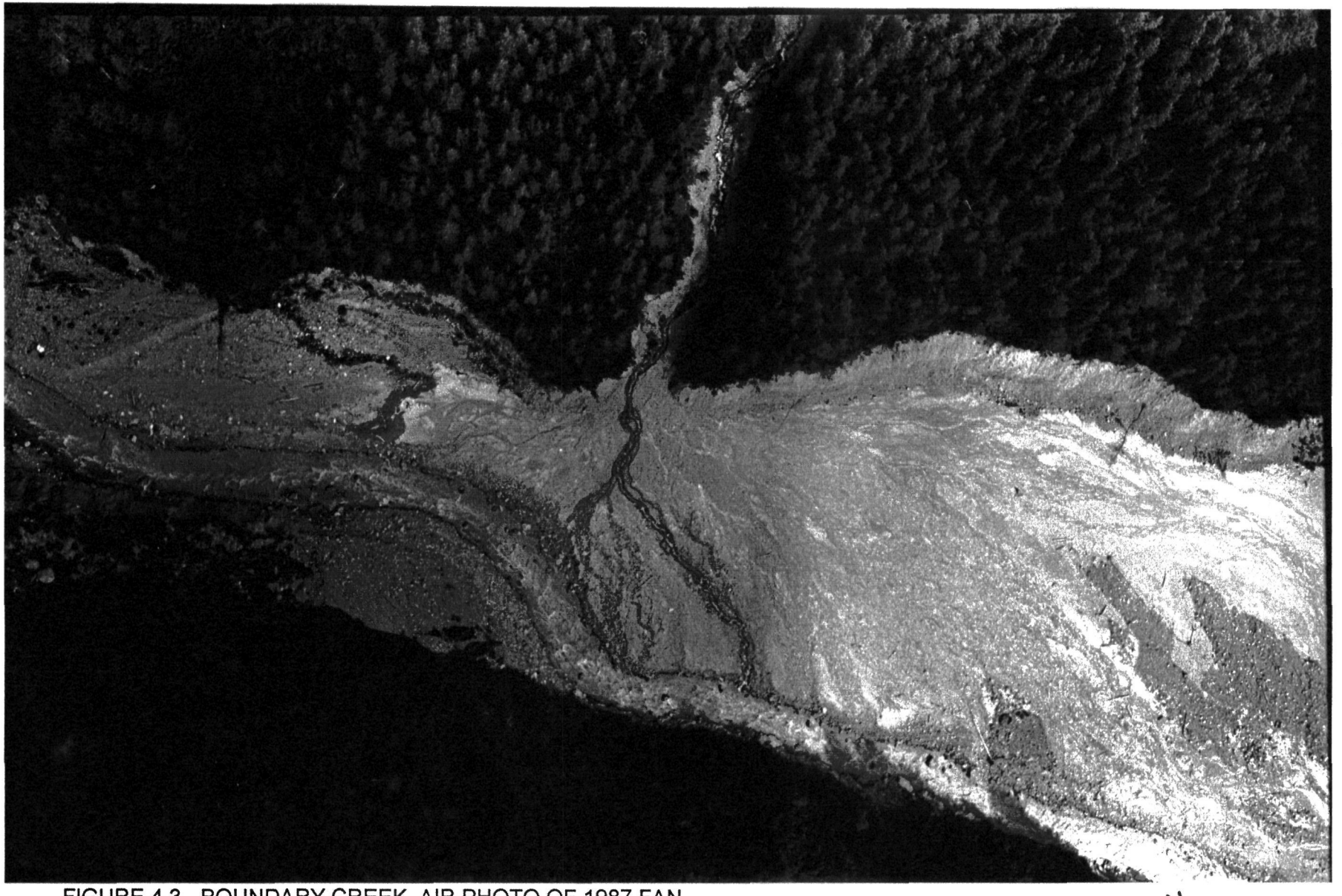


FIGURE 4.3. BOUNDARY CREEK, AIR PHOTO OF 1987 FAN.
35 mm photo taken in August 1987.


FIGURE 4.4. BOUNDARY CREEK, AIR PHOTO OF FAN AFTER 1988 DEBRIS FLOW. 35 mm photo taken in October 1988.

FIGURE 4.5. BOUNDARY CREEK, VIEW OF 1987 DEBRIS FLOW FAN FROM WEST. Photo taken from deposit of 1975 Devastation Glacier landslide, looking east down Meager Creek.

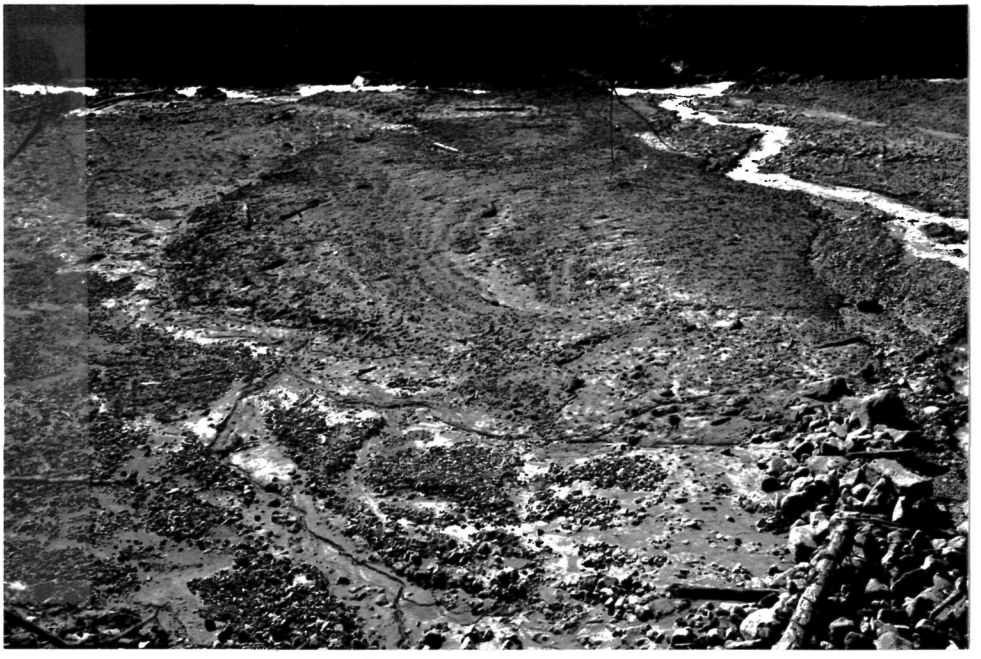

A. View looking south-west over fan, from upper fan terrace. Lobe in middle distance is about 30 m wide. Levée shown in photo B is at top centre.

B. Terminal levée of 1988 debris flow.

FIGURE 4.6. BOUNDARY CREEK, 1988 DEBRIS FLOW DEPOSITS.

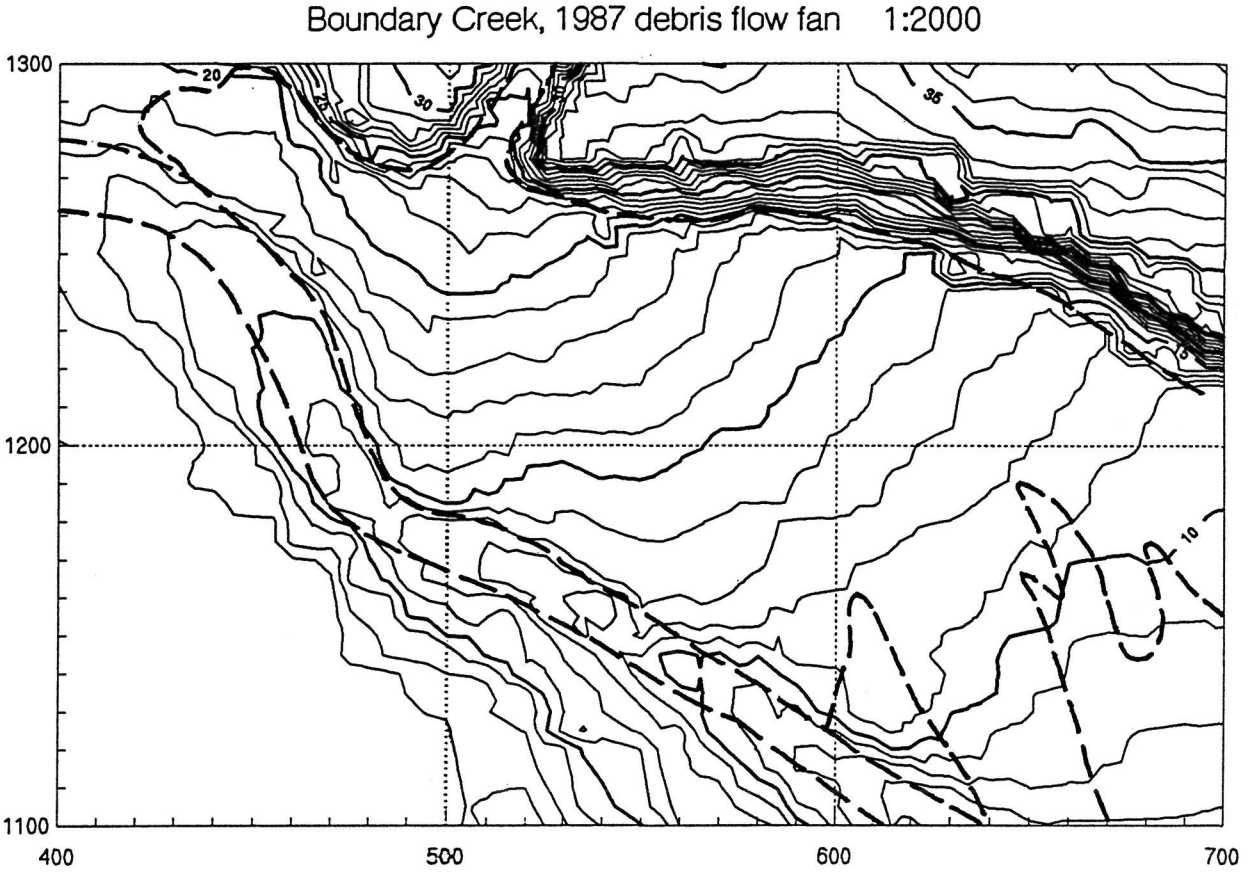


FIGURE 4.7. BOUNDARY CREEK, COMPUTER-GENERATED CONTOUR MAP OF 1987 FAN. Contour interval 1 m. Grid is labeled in metres.

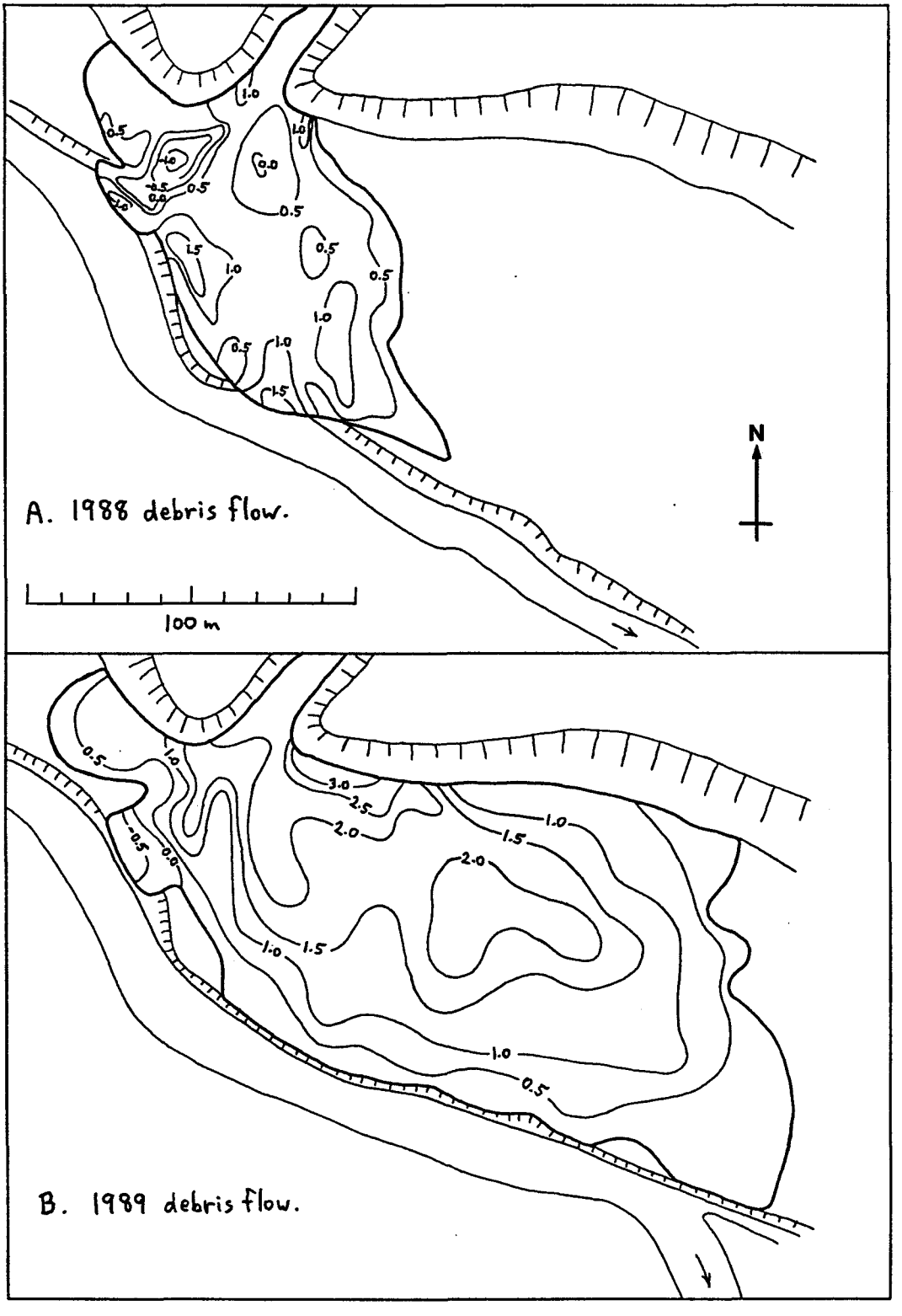


FIGURE 4.8. BOUNDARY CREEK, CONTOUR MAPS OF DEPOSITION BY 1988 AND 1989 DEBRIS FLOWS.

A. View looking east, down Meager Creek.

B. View looking north, at fan apex. 1989 debris flow forms most of upper half of section. Thin 1988 debris flow, fluvial cover, and 1987 debris flow form lower half.

FIGURE 4.9. BOUNDARY CREEK, CROSS-SECTION THROUGH FAN FOLLOWING FLOOD. Photo taken in June, 1992.

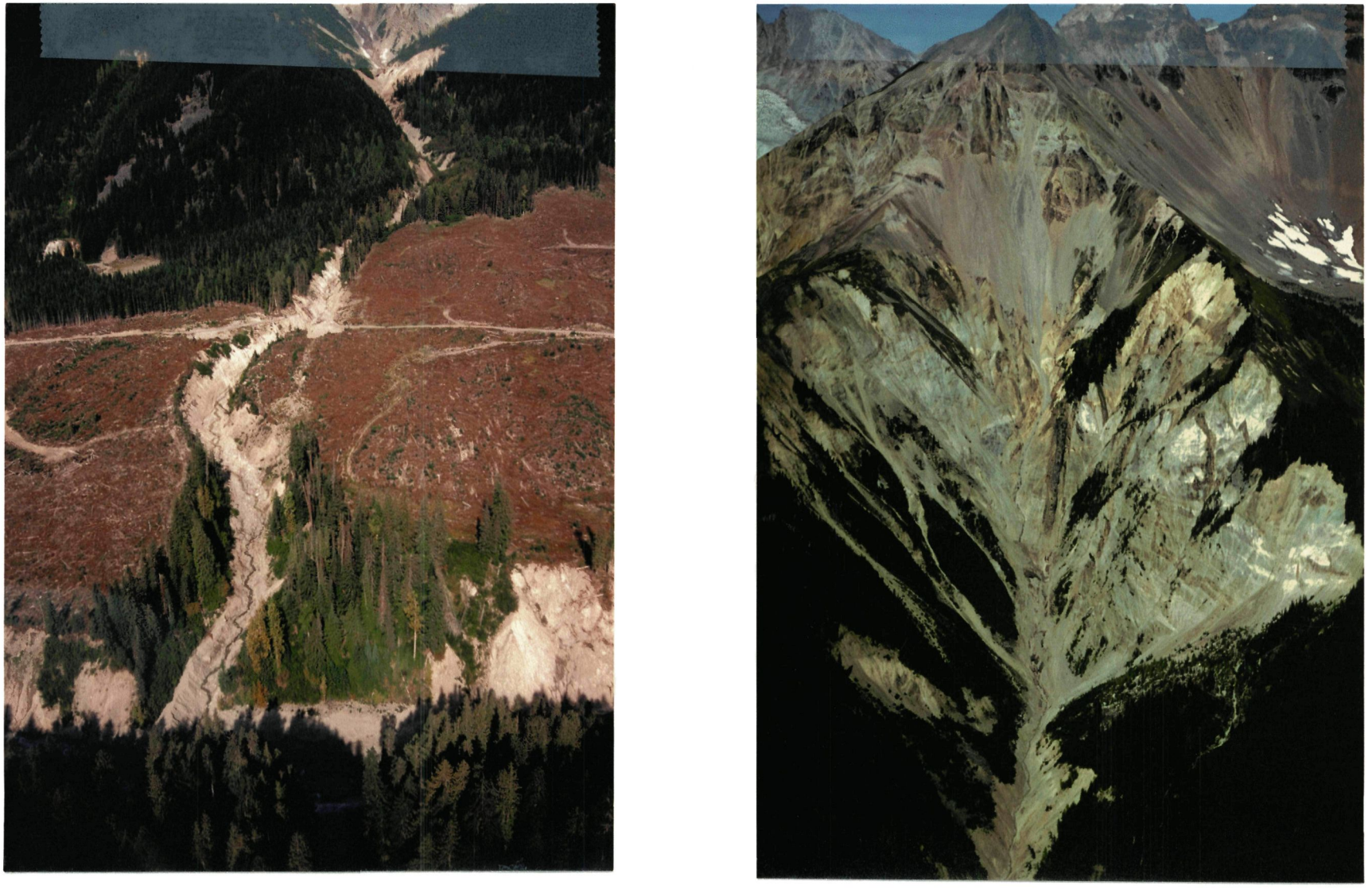

FIGURE 4.10. NO GOOD CREEK, AERIAL VIEWS OF CHANNEL (LEFT) AND UPPER BASIN (RIGHT).

A. Channel in early summer, 1988, with newly reconstructed logging road crossing.

B. Channel following October 1990 debris flow, from same vantage point. Person standing on road to right of channel shows scale.

FIGURE 4.11. NO GOOD CREEK CHANNEL IN 1988 AND 1990.

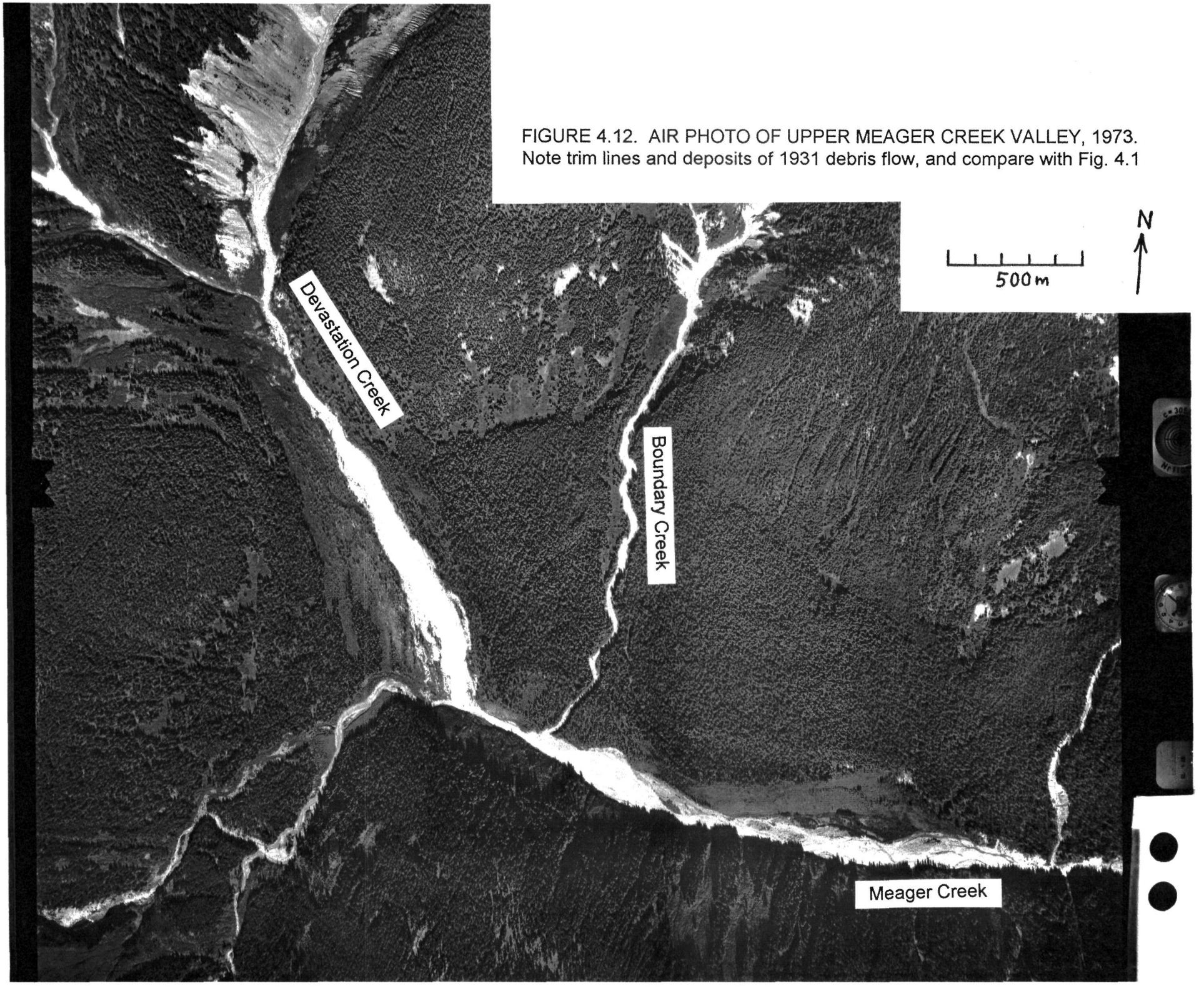


FIGURE 4.12. AIR PHOTO OF UPPER MEAGER CREEK VALLEY, 1973.
Note trim lines and deposits of 1931 debris flow, and compare with Fig. 4.1

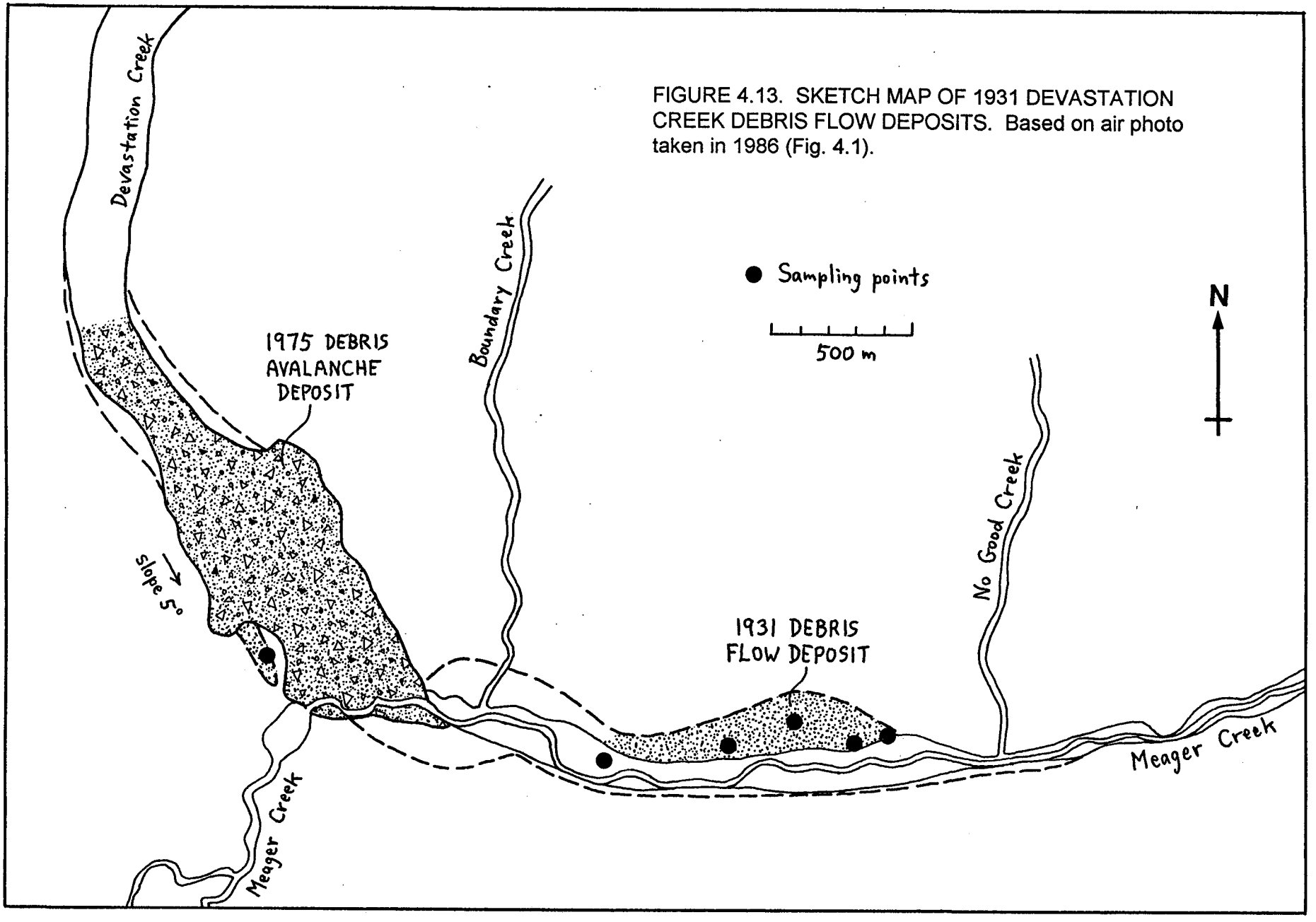


FIGURE 4.13. SKETCH MAP OF 1931 DEVASTATION CREEK DEBRIS FLOW DEPOSITS. Based on air photo taken in 1986 (Fig. 4.1).

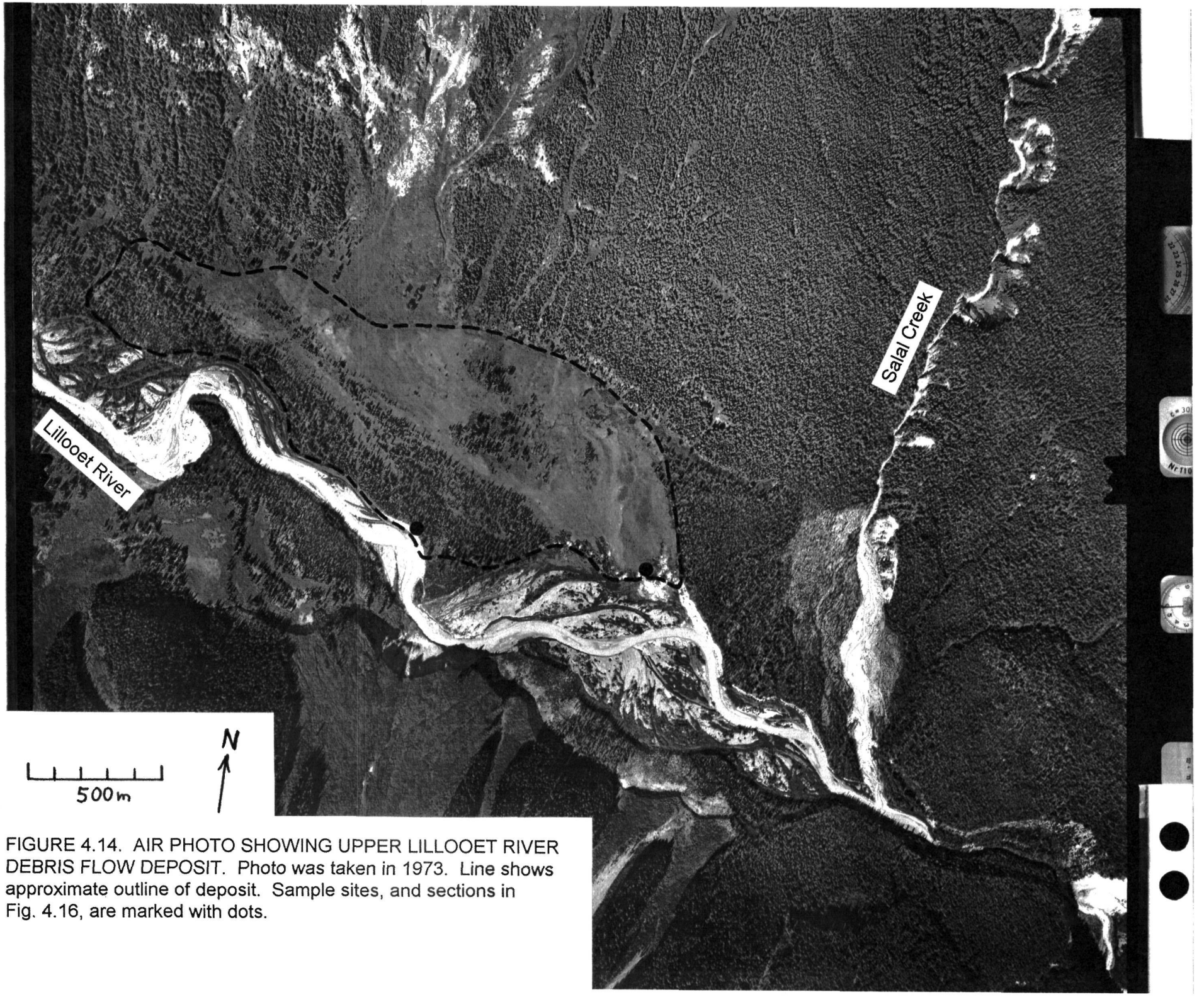


FIGURE 4.14. AIR PHOTO SHOWING UPPER LILLOOET RIVER DEBRIS FLOW DEPOSIT. Photo was taken in 1973. Line shows approximate outline of deposit. Sample sites, and sections in Fig. 4.16, are marked with dots.

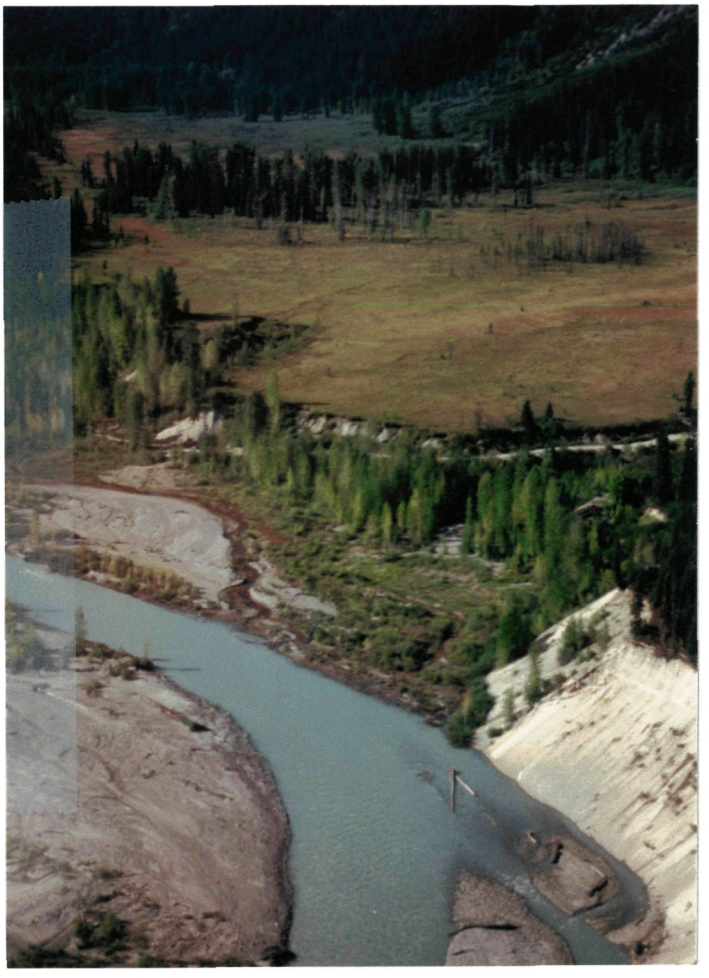

FIGURE 4.15. VIEW OF UPPER LILLOOET RIVER VALLEY, SHOWING DEBRIS FLOW DEPOSIT. Photo taken from air above mouth of Salal Creek, looking west-north-west.

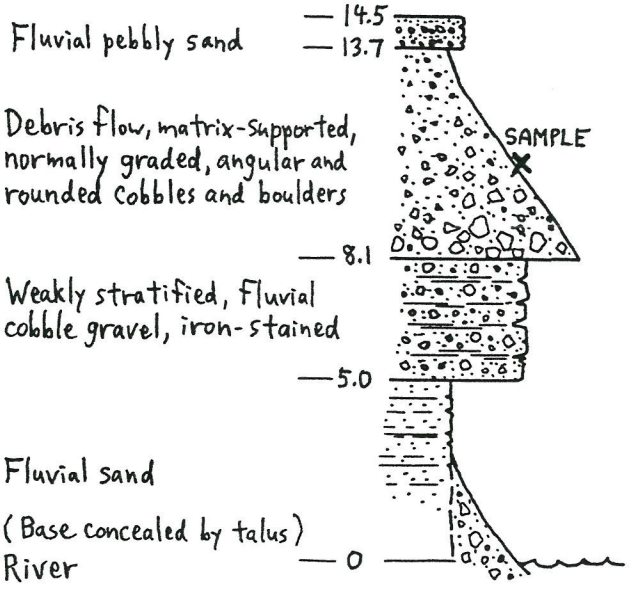


A. UPSTREAM SECTION

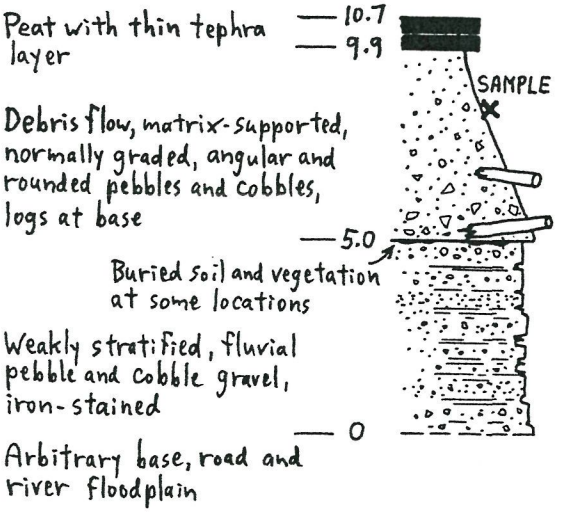


B. DOWNSTREAM SECTION

FIGURE 4.16. STRATIGRAPHIC SECTIONS OF UPPER LILLOOET RIVER DEBRIS FLOW. Elevations are in metres. Locations are shown on FIGURE 4.14.

A. (Above) View up fan from toe, several days after event.

B. (Right) Aerial view of logging maintenance camp during clean-up. Arrow shows position from where photo A was taken.

FIGURE 4.17. CANYON CREEK, 1990 DEBRIS FLOW.

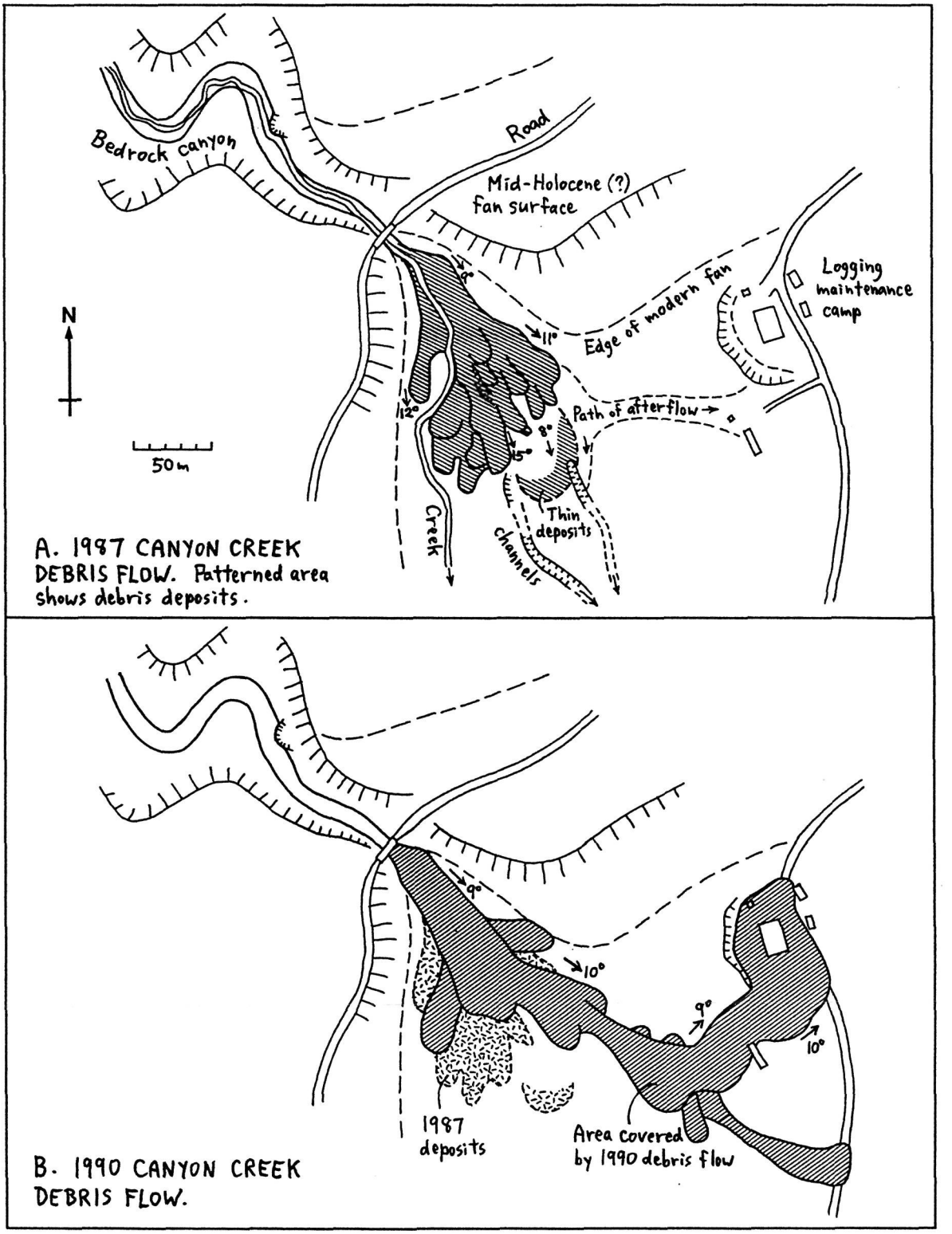


FIGURE 4.18. CANYON CREEK, SKETCH MAPS OF 1987 AND 1990 DEBRIS FLOWS.

FIGURE 4.19. HOT SPRINGS CREEK DEBRIS FLOW DEPOSIT. View looking upstream near centre of deposit.

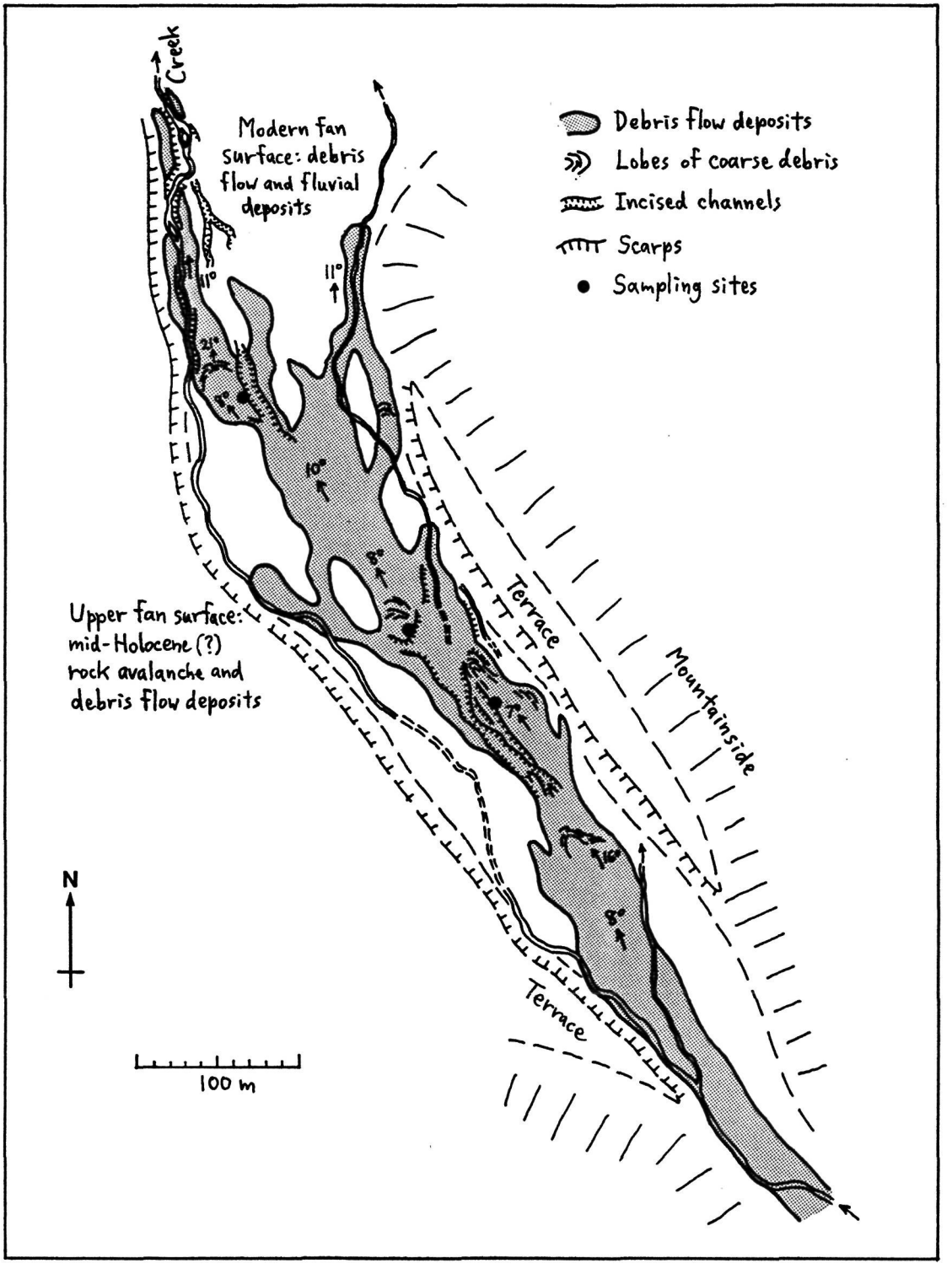


FIGURE 4.20. HOT SPRINGS CREEK, MAP OF 1984 DEBRIS FLOW.

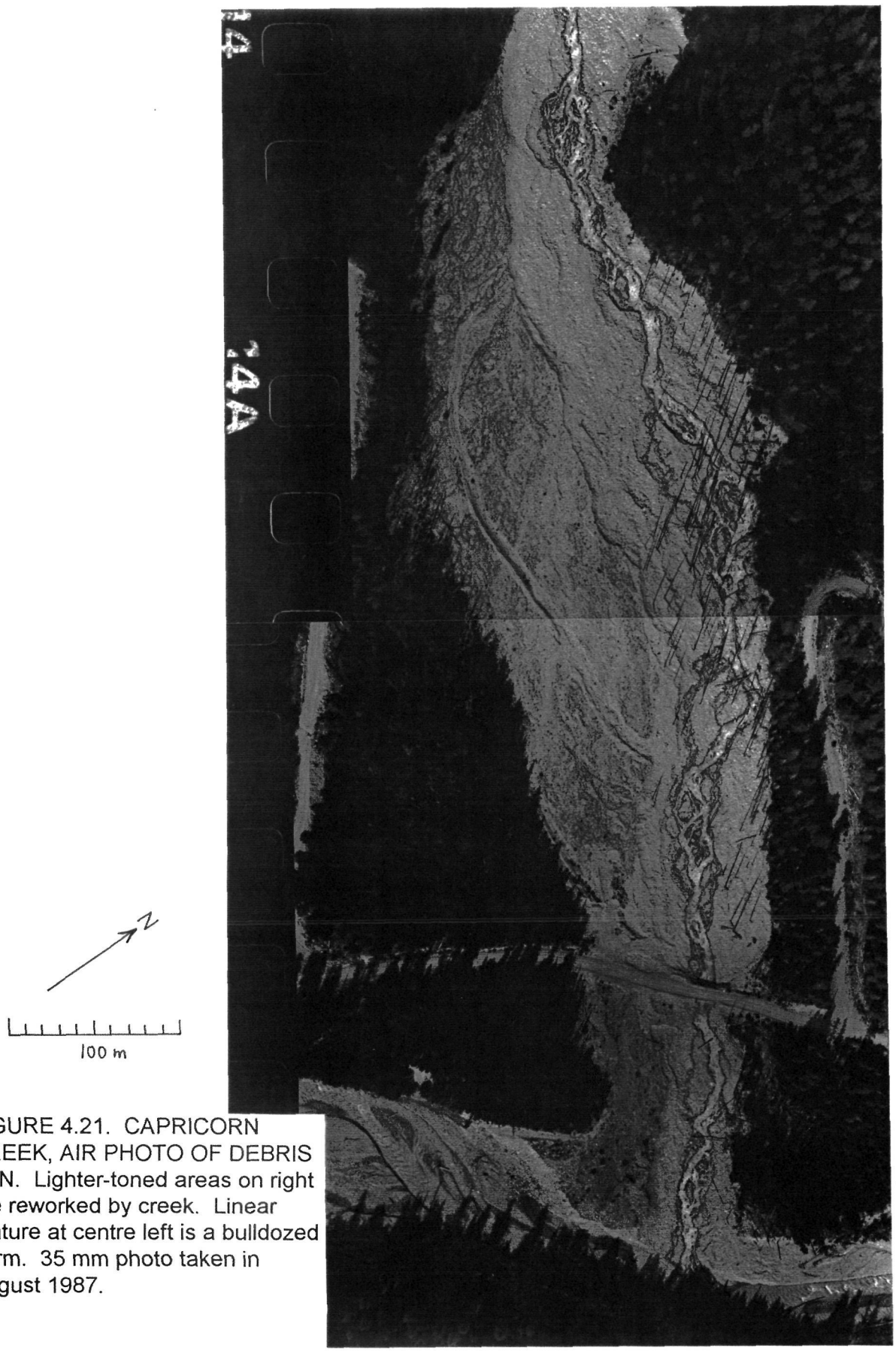


FIGURE 4.21. CAPRICORN CREEK, AIR PHOTO OF DEBRIS FAN. Lighter-toned areas on right are reworked by creek. Linear feature at centre left is a bulldozed berm. 35 mm photo taken in August 1987.

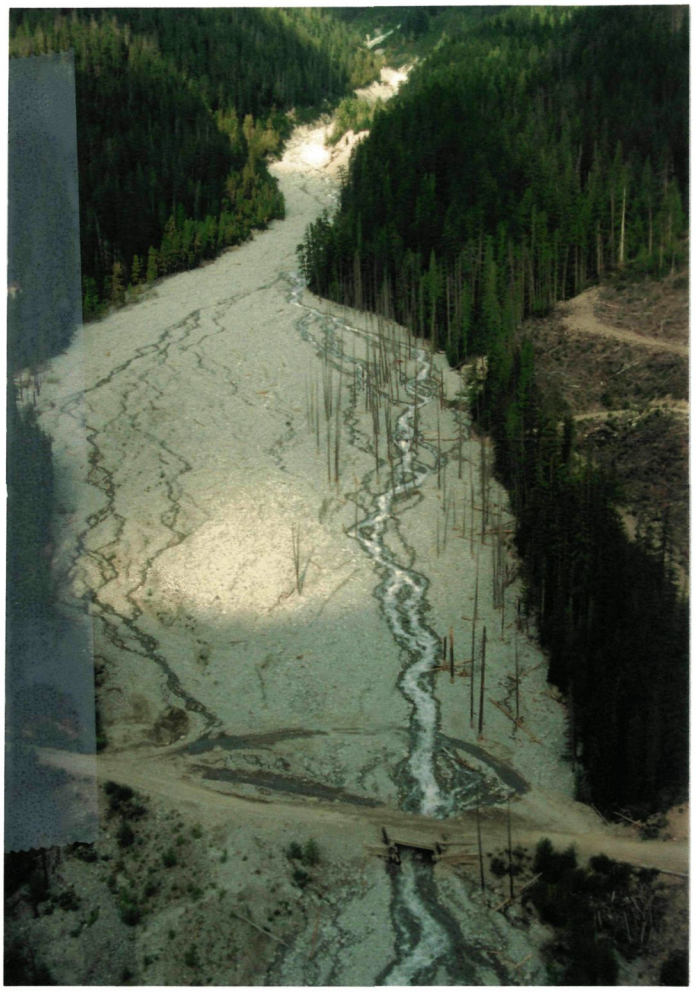

A. (Left) Aerial view after 1990 flood. 1990 deposits form a shallow veneer, covering about half the fan, over deposits of early 1970s event(s).

B. (Below) Deposits of 1990 debris flood, just above road.

FIGURE 4.22. CAPRICORN CREEK, 1990 DEBRIS FLOOD.

A. (Left) View of debris flow channel from Pemberton Valley.

B. (Below) 1984 debris flow deposits. Photo taken in October 1984.

FIGURE 4.23. LOWER RYAN RIVER DEBRIS FLOW CHANNEL AND FAN.

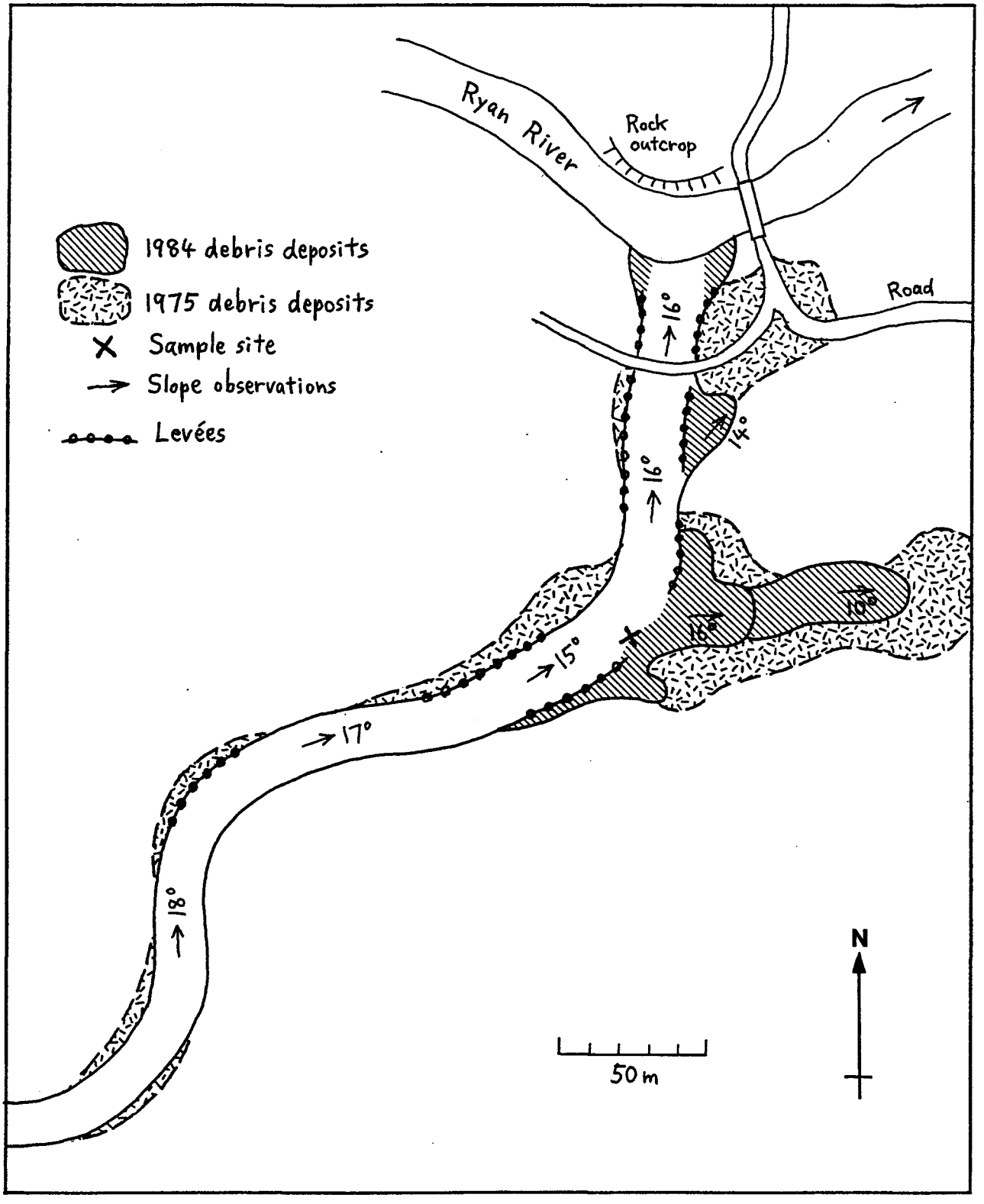


FIGURE 4.24. LOWER RYAN RIVER, SKETCH MAP OF DEBRIS FLOW FAN.

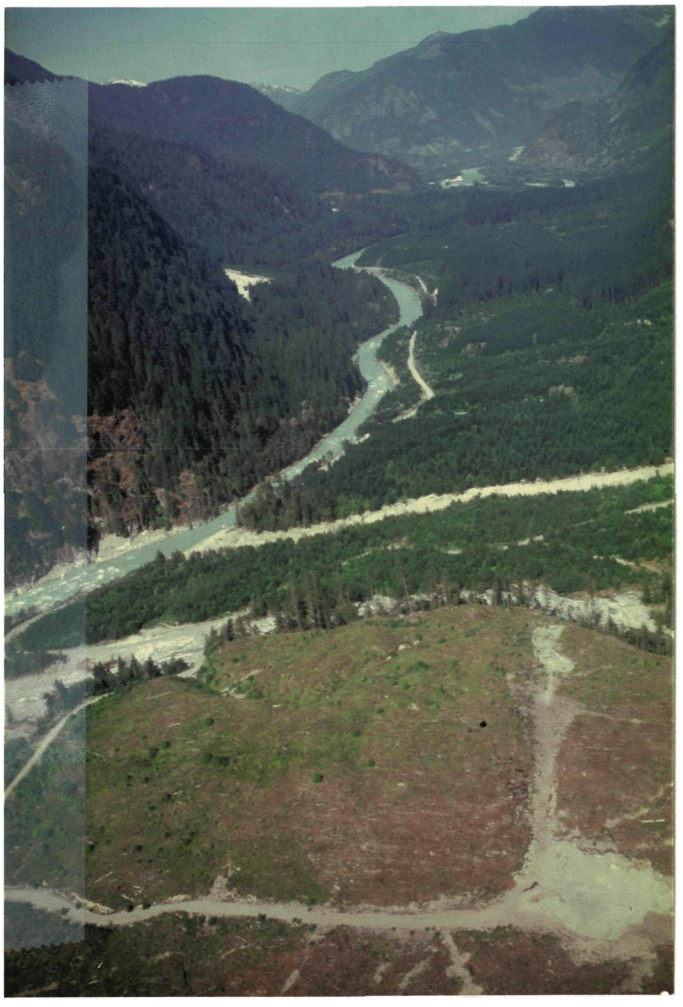

A. (Left) Aerial view of lower channel and Squamish River, looking north up river. Note superelevation of debris flow on opposite river bank.

B. (Below) Looking down debris flow channel, about 600 m above mouth.

FIGURE 4.25. TURBID CREEK DEBRIS FLOW CHANNEL. Photos taken in 1985.

A. (Above) 1984 debris deposit in Cheekye River channel. Rock hammer (centre) shows scale.

B. (Right) Debris flow deposit of 1100 years BP, in garbage dump excavation on Cheekye Fan. (Photo by F. Baumann.)

FIGURE 4.26. CHEEKYE RIVER DEBRIS FLOW DEPOSITS.

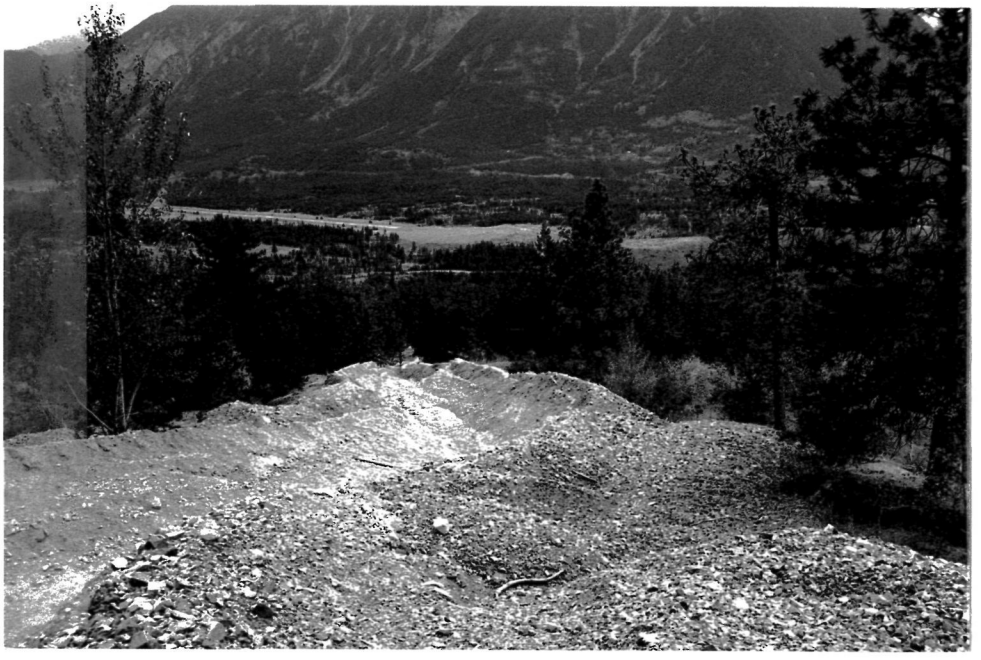

A. View down channel from near apex of fan.

B. Distal end of channel, looking downstream.

FIGURE 4.27. FOUNTAIN RIDGE DEBRIS FLOW CHANNEL.

FIGURE 4.28. MOUNT CURRIE DEBRIS FLOW FAN. (Photo by M. Bovis.)

A. (Above) Centre fan, view of 1984 deposits, looking downstream from near apex. Person (centre right) shows scale.

B. (Right) East fan, aerial view showing 1989 debris flow.

FIGURE 4.29. MIDDLE LILLOOET RIVER DEBRIS FLOW FANS.

# CHAPTER 5. SEDIMENTOLOGY OF DEBRIS FLOW DEPOSITS

In this chapter, the results of grain-size analysis of debris flow samples are described, and observations are presented on other sediment attributes, such as grading and stratigraphy. Texture is the primary characteristic of debris flow sediments which directly results from source area lithology, and it can be described quantitatively using standard measures and methods of analysis.

Texture is also the main characteristic which controls the geotechnical properties of sediments, such as permeability and shear strength. Based on the work of Johnson (1970), Takahashi (1981), and others, it is reasonable to assume that texture has a controlling influence on debris flow rheology.

## 5.1 SAMPLING METHODS AND ANALYSIS OF SAMPLES

The general approach to sampling debris flow deposits was described in the previous chapter. At most sites, there was not a wide choice of good sampling locations, either because of limited preservation of the deposit, or because of a coarse surface layer of boulders which limited sampling locations to natural sections. At the detailed study sites, an attempt was made to find two or more suitable sampling locations. A location was considered "suitable" if it appeared, on visual inspection, to be about average in terms of deposit thickness and proportion of cobbles and boulders, and if it was accessible and could be sampled without excessive labour or danger. At most sites, therefore, sample design was opportunistic rather than planned. Surface stone count locations were selected in a similar way, by a subjective judgment as to whether or not the location was representative of the average texture of the surface layer.

Figure 5.1 shows schematically, for a typical coarse-textured deposit, the types of samples which were collected. These include bulk samples of subsurface material, and stone counts on the deposit surfaces and on the faces of sections. Figure 5.2 is an illustration of bulk sampling procedure on a fine-textured deposit.

Definitions and standard procedures

The texture of debris flow material sampled in this study is described and analyzed using terminology and methods summarized by Folk (1966) and by Church *et al.* (1987). The Wentworth grain-size classification is used, in which terms for the general size categories can be defined as:

| | |
|---|---|
| boulders | larger than 256 mm |
| cobbles | 64 - 256 mm |
| pebbles | 4 - 64 mm |
| granules | 2 - 4 mm |
| sand | 0.063 - 2 mm |
| silt | 0.004 - 0.063 mm |
| clay | smaller than 0.004 mm. |

The dimensions refer to sieve mesh size, which corresponds approximately to b-axis diameter, or to the length of the intermediate axis. These definitions of textural classes are not unanimously agreed upon in the sedimentology and geomorphology literature. Pebbles are often defined as the 2 - 64 mm size class. The term "gravel" is sometimes used interchangeably with "pebbles"; however, in this study, "gravel" is used as a general term to include all sizes larger than 2 mm, which is consistent with many sources in geomorphology (for example, Howes and Kenk, 1988).

The Wentworth size scale is based on base 2 logarithms. Grain-size (D) is given in millimetres or in phi ($\phi$) units, where phi is defined as

$$\phi = -\log_2 D \quad (\text{mm}) \tag{5.1}$$

Numerous measures of mean grain-size and sorting have been proposed by sedimentologists, and are reviewed by Folk (1966). In this study, the graphic mean, $M_Z$, and the inclusive graphic standard deviation, $\sigma_I$, are used. They are defined as

$$M_Z = (D_{16} + D_{50} + D_{84})/3 \tag{5.2}$$

$$\sigma_I = (D_{16} - D_{84})/4 + (D_5 - D_{95})/6.6 \tag{5.3}$$

where $D_i$ is the size in phi units of the *i*th percentile, or the grain-size at which i percent of the sample is finer. Additional measures are defined for skewness and kurtosis, but they are not used in this study.

The size distribution of coarse gravels was normally determined in the field by grid samples, or stone counts. The principles of this type of sampling are discussed by Church *et al.* (1987). Fine gravels and sand were analyzed by sieving, using standard methods, either in the lab or the field. Fines (silt and clay) were analyzed by sedimentation, using the hydrometer method. The procedure and calculation methods given by Lambe (1951) were used for sedimentation analysis. Some further details of sieving methods are given in the following sections.

All grain-size statistics and graphs are based on 1 $\phi$ intervals on the Wentworth scale. Some samples collected early in the study were physically processed at 1/2 $\phi$ intervals, but later were analyzed mathematically using 1 $\phi$ intervals. It was decided that the extra information gained by 1/2 $\phi$ analysis did not justify the additional effort required in sieving.

Bulk samples

Bulk samples are defined here as large samples which were chosen to be representative of the subsurface layer of a deposit displaying a distinct coarse surface layer, or representative of the average texture of a deposit with no such surface layer. Since all deposits contained abundant cobbles and many contained boulders, samples had to be large enough to be representative of the larger size classes (see discussion below). A sample size of about 200 kg was found to be a reasonable compromise between representativeness and practicality, although some samples of about 1000 kg were taken at detailed study sites. All bulk samples were truncated at 256 mm, since larger size classes could not be represented except by sample sizes of several tonnes.

Smaller grab samples, considered representative to 32 mm, were also taken at many sites. These are useful for characterizing the debris matrix (material smaller than 4 mm), but do not provide sufficient information to characterize the total grain-size distribution, unless they are extended to coarser grades by means of stone counts.

Samples were processed in the field by passing the material through a set of field sieves ranging in size from 64 mm down to a convenient lower size, usually 32 mm but sometimes 22 or 16 mm. Cobbles were sized individually using a template consisting of square holes cut in a piece of sheet metal. A spring scale capable of weighing to 22 kg was used for field sieving. The weights of occasional cobbles larger than 22 kg were estimated by measuring the dimensions of the cobble. Field processing was done with the material in a moist state. The moisture content was critical for successful handling of fine-textured samples. Samples were excavated, and then left to dry in the sun (if present) or under a tarp (if not) until the moisture content was suitable. This moisture content was typically about 4 to 6% by weight of sub-32 mm material. A split of several kilograms of the finer material was returned to the lab for further processing.

Many of the fine-textured debris flow samples, which consisted mostly of sand with sufficient silt and clay to make the sample cohesive, presented some preparation difficulties for hydrometer and sieve analysis. The following method proved to be effective. A split of about 100 g of material under 2 mm was treated with dispersant, and washed through a 0.5 mm sieve using less than 1 litre of distilled water. Mechanical agitation was not used, to avoid breaking friable particles. The fine portion was then analyzed in the sedimentation cylinder. Finally, it was washed through a 0.063 mm sieve with an excess of water, and the fine sand was recombined with the coarse sand for sieving.

The proportion of organic material in the samples was, in all cases, well below 1% by weight. The samples were not treated to remove organic material before sedimentation analysis. The fine organic material consisted mostly of undecomposed, shredded wood, which could not readily be removed by chemical treatment. If organic material was present in visible quantities, it was removed from the sand before sieving by flotation in water, and then dried and weighed. Organic fragments were removed manually from gravel during sieving, and weighed separately.

Specific gravity

Several calculations in sediment testing, including hydrometer analysis and the geotechnical tests described in Chapter 6, require knowledge of the specific gravity of the

sediment particles. Since specific gravity can vary considerably with lithology, it was measured directly in several of the samples. The results are shown in Table 5.1.

For fine sediment, a sample of sand produced from sieving was immersed in water and weighed in a small, calibrated, volumetric flask, according to the method described by Lambe (1951). This specific gravity was assumed to represent all of the finer sediment in the sample, and was used in hydrometer analysis calculations.

For coarse clasts, pebbles in the 16-32 mm size class were grouped by lithology, and weighed both in air and submerged in water. The specific gravity measured in this way varied considerably with some of the volcanic rocks, depending on whether the rocks were initially wet or dry, due to the high porosity of pyroclastic rocks. The measurement of rocks soaked in water is probably the more representative of rocks in debris flows under field conditions. For calculations on whole debris flow volume, an estimated average specific gravity was used, based on the proportions of stones and matrix in the material. The error in the measured specific gravity of the porous volcanic rocks is of the order of $\pm$ 0.2.

The problem of mud on stones

Most fine-textured samples were difficult to sieve in the field because cohesive material ("mud") tended to stick to the stones. Most of it could be brushed off if the sample was at the optimum moisture content; however, if it was too dry or too wet, the mud could not be removed. This coating of mud would introduce a bias in the analysis if it were not corrected. After some experimentation, the following procedure was developed.

During field sieving, as much of the loose mud as possible was brushed off. For most samples at the detailed study sites, and at several other sites, one or two buckets of stones were washed in water after sieving and weighing, and then were dried and reweighed. The weight of mud was converted to a dry weight using the moisture content of the split brought back to the lab. The amount of mud was expressed as a mass per unit surface area, using the surface areas of equivalent spherical particles of diameter equal to the midpoint of the size class (Table 5.1). Typical mud coatings were 0.02 to 0.15 g/cm$^2$. (C.g.s. units were used for working calculations in grain-size analysis.) The measured mud coatings were used to correct the weights of all the

size classes of stones, and the calculated weight of mud was added to the fine portion of the sample during calculations. These measurements were performed on 25 samples. The results were used to derive a subjective scale ranging from 1 (very clean, 0.01 $g/cm^2$) to 5 (extremely muddy, 0.16 $g/cm^2$), which was applied to samples for which the measurements were not made.

Several samples of the mud washed from stones were returned to the lab for grain-size analysis. The mud was found to consist almost entirely of material smaller than 0.5 mm, and its grain-size distribution below this size matched the distribution of the actual samples very closely. A simple algorithm was written in a computer program used for grain-size analysis, which in effect took the "missing" mud washed from stones in the field, and added it to the fraction finer than 0.5 mm.

The amount of mud on stones in most fine-textured samples, computed by this procedure, ranged from about 2 to 6% of the total material under 2 mm, and in some samples which were analyzed at wetter than optimum moisture content, it was greater than 10%. This would be a significant error were it not corrected.

Required size of samples

Church *et al.* (1987) discuss several criteria for determining the required size of a grain-size sample. For samples with stones larger than 32 mm, the recommended sample size is 100 times the weight of the largest stone in the sample. According to this recommendation, a sample representative to 128 mm should weigh 290 kg in size, and to be representative to 256 mm, it should weigh 2300 kg (from weights of spheres of equivalent sieve size; Table 5.1). These recommendations are based on 1/2 $\phi$ grain-size analyses (Church *et al.*, 1987). For 1 $\phi$ analyses, samples could be smaller (half the recommended size or less), to achieve the same number of stones in the largest sieve size. Based on this reasoning, 1000 kg was initially chosen as the optimum size for samples representative to 256 mm. This sample size was later reduced to 200 kg for practical reasons. An analysis of errors (section 5.3) shows that this reduced size was sufficient to give reasonably precise results for summary grain-size measures. For most samples which were field sieved to 32 mm, the split of material smaller than 32 mm returned to the lab was 6 to 12 kg, well in excess of 100 times the weight of a 32 mm stone.

Stone counts, and calculation of total size distributions

The grain-size distribution of coarse material was measured by stone counts. The application of stone count methods, including statistical considerations and sample sizes, is discussed by Church *et al.* (1987). Kellerhals and Bray (1971) showed that the distribution of a grid stone count is statistically equivalent to the distribution of a sample sieved by weight. Three techniques were used in this study.

For the coarse surface layers of coarse-textured debris flows, surface counts were made by laying a tape over the surface, and measuring the b-axis of each stone at regular intervals (usually 1 m or 0.5 m). Most surface stone counts numbered 50 to 100 stones. This method was also used on the surface of some fine-textured debris flow deposits, which did not have a coarse surface layer, so as to extend the representativeness of these samples to the boulder size class. At detailed study sites, several stone counts were taken at different locations on the deposit surface.

At some locations, where samples were taken on vertical sections through deposits, stone counts were taken along the face of the exposure. This method was used on the No Good (early 1980's), Hot Springs 1984, Canyon 1987, and Capricorn (early 1970's) debris flow sites. The method was the same as that used in the surface counts, except that the sample size was smaller (50 stones or fewer), and the interval along the tape was smaller, typically 0.2 m. The face had to be cleaned of loose material before the count could be taken, which made the process laborious. This method enabled extension of the grain-size distributions of bulk samples to the boulder size class, for both fine-textured and coarse-textured deposits.

Stone counts of the faces of sections were also made using photographs. This method was less satisfactory, because the sample size was usually smaller, individual stones could not be examined to identify the b-axis, and hiding of stones by loose material or other stones was a problem. The method was used mainly at sites examined late in the study (1990), as time did not permit stone counts at each site.

Stone counts were combined with the results of bulk sample analysis to calculate the estimated total size distributions of the debris flow deposits. The procedure for achieving this was as follows:

a) The distributions of each type of sample (bulk samples and stone counts) were averaged, where more than one sample was taken.

b) For stone counts made along sections at sites where bulk samples were taken, the ratio of boulders to cobbles was used to extend the bulk sample distributions to include the boulder size class. The working assumptions are that the proportion of cobbles in the bulk sample is representative, and that the distributions of the stone counts are not representative of size classes smaller than 64 mm. (The latter assumption is often the case for fine-textured material, especially with counts made from photographs.)

c) The same procedure was employed, using surface stone counts, on the Boundary 1987 deposit, and on samples of the Meager Creek fluvial deposits.

d) The size distribution of the coarse surface layer, where present, was calculated from surface stone counts. These were combined with stone counts of the subsurface part of the surface layer, which were made from photographs taken of sections through several deposits (Hot Springs 1984, Capricorn, early 1970s, and Canyon 1987 and 1990). It was desirable to use both types of counts, since the coarse surface layers were inversely graded, and surface stone counts therefore were biased towards larger sizes.

e) An estimate was made, based on photographs and field notes, of the average ratio of the thickness of the coarse surface layer, to that of the subsurface layer. This ratio was used to combine the size distributions of the two layers. This step is the main source of error in the procedure, as the relative thicknesses of the two layers often varied considerably, and there were limited exposures where the full thickness of the debris flow deposits could be observed.

As Church *et al.* (1987) show, the sieve size of a stone is smaller than its b-axis diameter, when the b-axis and c-axis are not equal. Therefore the stone counts are not exactly equivalent to sieve analyses, but are biased towards larger sieve sizes. This error is small when compared

with other sources of error in the procedure described above, and no attempt was made to correct for it.

Boundary Creek fan sampling design

The fan of the 1987 Boundary Creek debris flow was an exception to the comments made at the beginning of Section 5.1 on sample location, because it was very fresh and well preserved, and pits could be dug anywhere on its surface. Therefore, a more systematic sampling design was used on this deposit. The sample locations are shown on Fig. 5.11. Early in the 1987 field season, three sample locations were chosen spaced roughly equidistant along a radial line near the centre of the fan, and very large (1000 kg or more) samples were taken. These samples revealed little variation in texture. Later, to determine if there was any systematic variation in texture across the fan, additional sample locations were randomly chosen. To do this, a grid consisting of four parallel transects was laid out across the fan. Ten locations along these lines were randomly selected (using the random number generator of a calculator, and measured distances along the transects). Pits were dug at the first five locations chosen, and surface stone counts were taken at nine of the ten locations. (One stone count site was not used because it was covered with afterflow material, and there were no surface stones.) The sample sizes were smaller (approximately 200 kg) than those of the original three samples because, following processing of these larger samples, it was decided, rather subjectively, that the smaller size would be adequately representative of the clasts up to 256 mm. The number of samples was arbitrarily chosen to provide a reasonable amount of data without requiring an unreasonable amount of labour.

## 5.2 DISCUSSION OF RESULTS

Summary grain-size parameters of the debris flow deposits are given in Table 5.2. The table gives statistics for both the total distribution, computed for the entire deposit as described above, as well as the distribution of subsurface material truncated at 256 mm. This latter set of truncated statistics is given to provide a common basis for reporting the texture of all deposits, including those for which stone counts were not made. Since boulders were a minor constituent

of most subsurface deposits, the distribution truncated at 256 mm gives a reasonable description of the texture, which is useful when comparing different deposits.

No attempt is made in this chapter to compare grain-size statistics with those reported in other studies. Very few total grain-size distributions of debris flows, which include cobbles and boulders, have been reported in the debris flow literature. Scott (1988), and Scott *et al.* (1992), give total grain-size distributions and statistics of several lahars which include cobbles. In the literature, however, grain-size statistics and cumulative curves are sometimes reported for samples truncated at an arbitrary size, typically about 30 to 100 mm (for example, Sharp and Nobles, 1953; Pierson, 1985; Pierson, 1986). Statistical measures such as $M_Z$ and $\sigma_I$ are relatively meaningless for truncated samples which exclude a major part of the sample, and they are totally meaningless if the truncation size varies amongst different samples, or if it is unreported. $M_Z$ is strongly affected by the largest size classes, especially in fine-skewed samples. In strongly fine-skewed samples, the apparent $\sigma_I$ of truncated samples is simply a measure of the proportion of fines in the sample.

In this study, therefore, $M_Z$ and $\sigma_I$ are reported only for those deposits in which the total distribution was sampled, or in which the samples are representative to 256 mm, an upper size which includes most of the deposit material. For samples truncated at some smaller size, such as 32 mm, other non-statistical measures such as the relative proportions of sand, silt, and clay, are appropriate, and are included in several figures in this chapter.

Grain-size distributions

Table 5.2 includes grain-size statistics for all debris flow events described in Chapter 4, for which sufficient sampling was done to describe the distribution to 256 mm. In addition, samples taken of river bars in Meager Creek at three locations, and in the Lillooet River a short distance below Meager Creek, are included for comparison. The identification numbers in the table refer to points on some of the graphs which follow. The table includes a classification of debris flows as to type, including fine-textured (A), intermediate or other (B), and coarse-textured (C). This preliminary classification is based on field observations of the sedimentology of the deposits, as described in Chapter 4.

Cumulative curves of debris flow deposits at the detailed study sites are given in Figure 5.3. The same data are given in the form of histograms in Figure 5.4, for these deposits, and for some additional deposits for which total distributions were calculated. At sites where more than one sample was taken, each grain-size distribution is an average of the distributions of the individual samples.

The cumulative curves and histograms show that the fine-textured debris flows closely approximate a normal distribution (*i.e.* they are linear on a probability graph) for sizes below about -5 $\phi$ (32 mm), but are non-normal over larger sizes. Coarse-textured debris flows are strongly bimodal. The Canyon Creek debris flows resemble the fine-textured deposits in the sand and smaller sizes, and coarse-textured deposits in the gravel sizes; this is to be expected, given that volcanic and coarse plutonic-metamorphic rock types are of about equal abundance in the source area of this basin. Almost all the distributions are strongly fine-skewed. Typical values of the Inclusive Graphic Skewness (Folk, 1966) are 0.45 to 0.65, although several fine-textured debris flows with relatively low contents of cobbles and boulders have lower skewness values.

Most of the distributions are bimodal, although bimodality is much more pronounced in coarse-textured deposits. The minimum point in many of the distributions is at approximately -1 to -2 $\phi$ (2 to 4 mm). For this reason, 4 mm was chosen as an arbitrary dividing point for the definition of "matrix" and "clasts" in all deposits.

In some bimodal deposits, most notably Cheekye 1984, Upper Lillooet 900 B.P., and No Good 1990, the coarse fraction (large pebbles to boulders) is derived largely from stream-bed gravels entrained by the debris flow. This observation is based on the presence of rounded stones in the deposits, which in some cases were of contrasting lithology to the more angular, colluvial-source clasts in the deposits. Fluvially derived stones were very abundant in the Turbid 1984 deposit (not included in Fig. 5.4). They were also observed, although not in abundance, in the most distal deposits of the Devastation 1931 debris flow deposit. The presence of fluvially derived stones is evidence of downstream bulking (increase in volume) of some debris flows.

The summary statistics in Table 5.2 are more readily compared in textural triangles (Figure 5.5), or on graphs of $M_Z$ vs. $\sigma_I$ (Figure 5.6). Graphs of mean vs. standard deviation, or other measures of central tendency and sorting, are commonly used in sedimentology, and have sometimes been used in studies of debris flows (for example, Innes, 1983; Costa, 1984; Scott *et al.*, 1992).

On both types of diagram, the fine-textured, volcanic-source debris flows and the coarse-textured, plutonic-source debris flows are clearly distinguishable as different populations. The limits of the two types of debris flow can be summarized as follows (with two minor exceptions):

- on the < 2 mm textural triangle, 75% sand, 20% silt, and 5% clay;
- on the < 256 mm $M_Z$ vs. $\sigma_I$ diagram, $M_Z = -4\ \phi$ and $\sigma_I = 4\ \phi$.

On the latter diagram, two fine-textured debris flows, No Good 1990 (9) and Turbid 1984 (10), are close to the coarse-textured cluster of points. This is probably because these two events contained a relatively high proportion of entrained stream-channel gravel.

The two populations are not as clearly distinguished on the two graphs representing total debris flow material. This is because the proportion of boulders in the debris flows varies greatly, especially in deposits with coarse surface layers, and the coarsest size classes exert a strong influence on the grain-size statistics. However, on the $M_Z$ vs. $\sigma_I$ diagram, $\sigma_I = 4\ \phi$ remains a useful division between the two populations. On the textural triangle, the two populations can be distinguished by a fines content of about 4%.

Figure 5.7 shows the proportion of matrix in the subsurface material, plotted against the proportion of clay in the matrix. "Matrix" is defined here as all material finer than 4 mm. The clay content is less than 3% in the coarse-textured group, and greater than 6% in the fine-textured group. (This is essentially the same result as that given by the < 2 mm textural triangle, since the proportion of clay in the < 2 mm fraction and in the < 4 mm fraction are very highly correlated.)

The debris flow deposits initially classified as "intermediate or other" cover a relatively wide range of values in all the statistics shown on the graphs. One of the deposits, McGillivray

(16), can be included in the fine-textured category on the basis of these statistics. Several others, including Angel A (11), Fountain (15), and Mount Currie (17) are similar to the fine-textured group in most respects. They were not originally included in this group because they had a thin, clast-supported, surface layer, and because they had well-developed, coarse, lateral levées. Two of the debris flows, Cheekye 1984 (14) and Canyon 1987 (12), could be grouped with the coarse-textured category on the basis of most, but not all, of the statistics. These two events contained a high proportion of entrained stream channel cobbles and boulders, which produced a grain-size distribution resembling the coarse-textured, plutonic-source debris flows, despite their relatively fine matrix textures. The Cheekye 1984 event is difficult to interpret because the sample was collected from a small remnant of the deposit which had been affected by streamflow, and so may not be representative of the original deposit.

The two samples of fluvial gravels cannot be readily distinguished from the coarse-textured debris flows on the basis of grain-size statistics alone. On the cumulative curve (Fig. 5.3 B), the curve of the Meager Creek fluvial gravels closely resembles those of the plutonic-source debris flows, except that it is slightly depleted in fine sand and silt. Fluvial gravels and coarse-textured debris flows apparently can be distinguished only on the basis of sedimentologic features observed in the field, such as bedding and bar structure, not on the basis of texture. The Capricorn Creek event (22), which is believed to be the result of a "debris flood", or a process intermediate between debris flow and fluvial transport, cannot be distinguished from the other coarse-textured deposits on the basis of texture alone.

Vertical grading, stratification, and coarse surface layers

Grading refers to a systematic vertical variation in grain-size, either as normal grading (coarsening downward) or as inverse grading (coarsening upward) (Scott, 1988). Inverse grading is frequently observed in debris flows, especially coarse-textured ones, and the presence of inverse grading in a deposit is sometimes used to infer that the dilatant, or granular, flow law applies to a debris flow (Takahashi, 1981; see Chapter 2).

Inverse grading is a feature of many of the debris flows observed in the study area. It takes the form of a clearly defined, coarse-textured, clast-supported, surface layer, in which

matrix is often totally lacking, and which is itself inversely graded. Examples of this surface layer are shown in Figs. 5.9 and 5.10. The subsurface layer invariably has no systematic grading. In this study, no examples were seen of deposits with gradual inverse grading in their basal zone or through their entire thickness, as have been documented in some other areas (for example, Scott, 1988).

Most of the fine-textured debris flows showed no systematic grading whatsoever. This uniformly mixed nature is illustrated in Figure 5.8, and can also be seen in Figs. 4.9B and 4.26B.

The Upper Lillooet (*ca.* 900 B.P.) debris flow deposit is unique in that it is normally graded throughout its observed thickness. Furthermore, at the three sections examined, it displayed a decrease in the proportion of coarse clasts in the downstream direction. At one section, in addition to the large bulk sample taken at about the middle of the section, a small grab sample was taken of the finer material near the top. This showed an almost identical grain-size distribution in material smaller than 32 mm, indicating that the grading is a feature of the coarse clasts only. This type of grading is known as "coarse tail grading" (Middleton and Hampton, 1976; Scott, 1988). As was noted in Chapter 4, this normal grading, and the downstream decrease in coarse clast content, may be evidence that the debris flow gradually dropped its coarse clasts as competence was lost by being diluted with river water.

No stratification was observed in the deposits of any single debris flow (with the exception of Capricorn Creek; see discussion following). (The coarse surface layers discussed above are considered here to be a feature of inverse grading, not of stratification.) Such stratification as is observed in some fan and channel margin deposits is the result of several debris flow units of different age, or of alternating debris flow and fluvial deposits. As noted by Major and Iverson (1993), in their experiments on model debris flows in a large flume, debris flows with multiple surges do not leave evidence of the separate surges in the deposit statigraphy. If multiple surges had occurred in the debris flows of this study, then it is likely that the surges displaced each other laterally, rather than forming a vertical sequence; the latter behaviour, had it occurred, should have left evidence in the form of stratification.

Figure 5.14 shows deposits of the older (early 1970's) and the 1990 Capricorn Creek events. The older deposit has weak stratification in some locations (not apparent in Photo A), and the 1990 deposit has prominent stratification (Photo B). In addition, the deposits are very close to being clast-supported (Photo A). These features, combined with other evidence discussed in Chapter 4, led to the conclusion that this event was not a true debris flow, but was rather a "debris flood".

Lateral variability of debris flow deposits

Most of the debris flow deposits showed relatively little lateral variability in the texture of the main deposit. However, many debris flows showed variability in the form of several distinct facies of deposition, as discussed in Chapter 4 (section 4.3, Boundary Creek). These facies are:

a) the main deposit, which forms most of the volume of the debris flow deposits, and consists of the material in the main surge (or surges) of the debris flow;
b) the coarse, often clast-supported, frontal lobe, which is usually a relatively small volume of material at the front of each surge;
c) lateral levées of coarse material, similar in texture to the frontal lobe, which often border the channel upstream of the depositional area;
d) a fine-textured afterflow facies, resulting from the relatively fluid, hyperconcentrated flow phase which follows the main debris flow surge.

The main deposit facies comprises a large majority of the volume of all debris flows studied. The other facies are present at most, but not all, of the study sites. They correspond to the phases of debris flow surges which have been described in many eye-witness observations of debris flows (for example, Sharp and Nobles, 1953; Takahashi, 1981; Costa, 1984; Costa and Williams, 1984; Pierson, 1986).

Coarse frontal lobes and lateral levées are commonly present in both fine-textured and coarse-textured debris flows. Coarse frontal lobes are, on average, more abundant and better developed in coarse-textured debris flows. Some fine-textured debris flow deposits are lacking frontal lobes, but this may be simply because they were deposited in a river and not preserved (*e.g.* Boundary 1989, Devastation 1931). The fine afterflow facies is abundant in only a few

deposits, (especially Boundary 1987 and Canyon 1987), but this may be an accident of deposition; if the afterflow phase happened to flow down a creek channel, instead of being diverted onto a dry part of the fan or floodplain, it would not be preserved. In addition to these facies, many debris flow deposits include an area of fluvially reworked material, the abundance of which depends on the streamflow discharge which followed the debris flow event as well as the time elapsed since the event. This is not a facies of the debris flow deposit, as it is formed after, not during, deposition.

Within the main deposit, lateral variability is usually very low, and is confined to the coarse (cobble and boulder) fraction and to the coarse surface layer (if present). In deposits from which multiple samples were taken, the grain-size distribution of the sub-32 mm fraction is almost identical in all samples (see discussion of sampling errors below).

Three samples were taken of the afterflow facies of the Boundary 1987 deposit (see Figure 5.15). These showed a nearly identical grain-size distribution to the main deposit in the sub-4 mm fraction, suggesting that this facies consists of the same matrix material as the main surge, but is lacking coarser clasts.

The results from multiple samples taken of the Boundary 1987 deposit are shown in Figure 5.11. The stone count data show an apparent tendency for the proportion of cobbles and boulders to decrease from the apex of the fan towards its edges. The mean size ($M_Z$) data of the small (200 kg) samples does not show such a trend, although there is a trend apparent in both $M_Z$ and the cobble-boulder content of the large (1000 kg) samples. (The proportion of cobbles and boulders in the stone counts appears to be lower than that in the large bulk samples, because fine debris on the surface conceals many stones, and therefore the stone counts are biased toward a lower proportion of stones.)

There is an anomalous concentration of coarse clasts (52%) shown by the stone count most directly in front of the mouth of the creek. This may indicate that there was a coarse frontal accumulation, deposited near the mouth of the creek, and then covered by later, finer debris. It is difficult to draw firm conclusions from these data, because the differences in cobble and boulder contents are probably not statistically significant, given the sampling errors involved

(see section 5.3). Also, the deposit is quite deep (about 5 m deep near its apex), and most of the deeply buried material therefore could not be sampled.

Matrix-supported and clast-supported deposits

The presence of matrix-supported material is often used as a criterion to distinguish debris flow deposits from fluvial deposits (Costa, 1984). However, the meaning of matrix-supported as opposed to clast-supported, structure is in question if matrix and clasts cannot be clearly defined. In the case of fine-textured debris flows in Fig. 5.3, there is only a very weak bimodality, if any, and there is therefore little basis for defining matrix and clasts. However, visually, these deposits are clearly matrix-supported, because stones in the larger size classes do not touch each other (Fig. 5.8). The cumulative curves of these deposits are sufficiently flat (*i.e.* $\sigma_I$ is high enough) that the abundance of stones in any size class is small compared with the volume of finer material. A $\sigma_I$ greater than about 3.8 to 4.0 $\phi$ appears to be diagnostic of matrix-supported deposits, in cases where the material is not strongly bimodal.

Coarse-textured debris is often highly bimodal, and therefore stones and matrix can be clearly defined. In deposits that are positively identified as debris flows, for example Hot Springs (Fig. 5.9) and Lower Ryan, the subsurface debris has the visual appearance of being matrix-supported. However, the grain-size distributions are not greatly different from those of fluvial deposits, which are clearly clast-supported with boulders and cobbles in contact. The distinction between matrix-supported and clast-supported appears to be a result of the orientation and spatial arrangement of large clasts, and the presence of a thin coating of matrix surrounding the large clasts in the debris flow deposits. This can be inferred from qualitative observations, but not from quantitative sampling.

Examples of matrix-supported debris flow deposits, with high contents of boulders and cobbles, are shown in Figs. 5.9, 5.10, and 5.12. By contrast, Fig. 5.13 shows one of the sample sites of fluvial deposits in the Meager Creek channel. It is clearly clast-supported, although the content of boulders and cobbles is similar to that in the debris flows (see Table 5.2).

Distinguishing debris flow deposits from fluvial and landslide deposits

From the observations made in this study, it is possible to make some generalizations which are useful in identifying deposits of debris flow origin, to distinguish them from other types of deposit. Costa (1984) reviews the criteria for distinguishing debris flow from fluvial deposits. These include structural features of fluvial deposits, such as bars, imbricated surface stones, cross-bedding, etc., which are generally lacking in debris flow deposits, and the presence of muddy matrix material which typically surrounds individual stones in debris flow deposits.

As mentioned in the preceding section, coarse-textured, plutonic-source debris flow deposits can be quite difficult to distinguish from fluvial deposits. This is because of the lack of fines in the sediment, and because fluvial deposits resulting from floods in steep mountain creeks are often quite chaotic, lacking the organized structural features found in the fluvial deposits of large, low-gradient streams. The most reliable characteristics to distinguish coarse-textured debris flows are: the presence of a prominent, coarse, surface layer which is usually at least several stones thick and inversely graded; the presence of lobes and levées of coarse clasts; and a matrix-supported appearance as well as a lack of grading and stratification in the subsurface material. However, there is a continuous gradation of deposit types which ranges from obvious debris flow deposits to obvious fluvial deposits. The Capricorn Creek "debris flood" described above is a good example of a deposit with intermediate structural features.

Fine-textured debris flow deposits can be readily distinguished from fluvial deposits because of their texture. Fluvial deposits in this study area contain very little material finer than 0.25 mm, while fine sand, silt, and clay are abundant in debris flows derived from fine-textured material.

There is also a continuous gradation of processes, and associated deposit types, from debris flows to debris avalanches and rock avalanches. True debris flow is the flow of a saturated slurry under its own weight, which can take place on quite gentle slopes if the slurry possesses Newtonian or Bingham properties. Debris and rock avalanches differ from debris flows in that they move in a largely unsaturated state, in which high pore water pressures do not develop. Rapidly moving debris or rock avalanches can travel on gentle slopes only as a result

of momentum, or as a result of poorly understood mechanisms of dry granular flow in high velocity, high volume events (Hsu, 1975; Hungr and Morgenstern, 1984). The "fahrböschung" (or ratio of maximum vertical height to maximum horizontal distance of travel; Hsu, 1975) of rock and debris avalanches is far lower than that of debris flows of comparable volume.

In the study area, the most common types of large landslides are debris avalanches, originating in incompetent volcanic rocks and pyroclastic debris, and rock avalanches, originating in competent plutonic rocks. The two differ only in texture, with the rock avalanches containing a higher proportion of large clasts and a lower proportion of clay than debris avalanches. The most useful identifying features which distinguish debris flow deposits from debris and rock avalanche deposit in this study area are:

a) debris and rock avalanches are often lithologically zoned, with areas of distinct lithology reflecting the distribution of lithology in the source area, unlike debris flow deposits which are uniformly mixed;
b) debris avalanches have a hummocky surface, often with cones of debris and isolated large boulders on the surface, while fine-textured debris flows have a smoother, more regular surface;
c) debris avalanche deposits often contain very angular boulders, split boulders with matching pieces a short distance apart, and very weak boulders which are crumbling in place, unlike debris flow deposits, in which surviving boulders are usually relatively competent and are slightly rounded;
d) rock avalanche deposits originating in competent rocks sometimes have inverse grading, although they do not have the distinct, matrix-deficient surface layer typical of coarse-textured debris flow deposits;
e) debris and rock avalanche deposits are finer textured than debris flow deposits originating from the same source materials.

Grab samples (< 32 mm) of debris and rock avalanche deposits were taken at three study sites: Hot Springs, Capricorn, and Devastation. They are shown on the sub-2 mm textural triangle of Fig. 5.5. In each case, the debris or rock avalanche deposit contains more clay and

silt than the debris flows (or debris flood in the case of Capricorn) originating from the same source area. In Devastation Creek, the 1975 debris avalanche is unusually clay-rich compared to the 1931 debris flow; this may reflect sources in different lithologic units within the same general source area. The same observation of debris and rock avalanches which are finer textured than adjacent debris flows has been made by visual inspection and hand texturing at several other locations in the study area, including No Good Creek, Turbid Creek, and Cheekye River. The coarser texture of debris flows may be due to several factors: debris flow source areas may include material which has accumulated in gullies and channels, and been depleted of fines; and most debris flows increase in volume considerably by bulking with fluvial sand and gravel as they erode their channels. Also, higher fines content in debris and rock avalanches may be explained by rapid shear rates or intense vibration which cause greater comminution of clasts.

## 5.3 SAMPLING ERRORS

Errors in the grain-size distributions can be attributed to several sources, including:

a) random errors in the grain-size analysis procedure, such as those associated with splitting;
b) systematic errors in the grain-size analysis procedure, such as mud on stones which are field sieved, or inaccurate hydrometer analysis procedure, or bias which may be inherent in making stone counts from photographs;
c) inaccurate estimates of the proportions of the surface and subsurface layers when calculating combined grain-size distributions;
d) random variability of sediment texture in the deposit;
e) selection of unrepresentative sample locations in the deposit.

Most of these sources of error have been described in section 5.1. In this study, the last three are probably the most important sources of error. Church *et al.* (1987) give a detailed discussion of errors involved in the sampling and analysis procedure itself. In this study, an effort was made to minimize these sources of error (categories a and b), by using adequately large sample and split sizes, and by replicating samples. However, because of the amount of time and labour required to properly sample debris flow deposits, the analyses of many deposits

are subject to quite large errors. In Table 5.2, a qualitative indication is given of the reliability of each grain-size analysis.

Several deposits were sampled at 3 or more locations, enabling quantitative estimates to be made of sampling errors. Table 5.3 gives a summary of the variability in some of the grain-size statistics, for samples truncated at 256 mm. On the Boundary 1987 deposit, 3 large samples (about 1 tonne to 512 mm) and 5 smaller samples (about 200 kg to 256 mm) were taken, which enable the effect of sample size to be investigated. A sample number of 3 gives a poor estimate of the population standard deviation ($\sigma$), so the results in the table give a very approximate indication of the variability of the statistics. The variability of most statistics is expressed as the coefficient of variation ($C_v$, or sample standard deviation, s, divided by the mean). For statistics expressed in phi units, s is given in the table, since phi units are logarithmic.

The statistics most sensitive to sample size are the proportion of sediment in the two largest 1 $\phi$ size classes (*i.e.* cobbles). The variability within these classes is 2 to 4 times greater for the small samples relative to the large samples from the Boundary Creek deposit. However, variability in the total proportion of cobbles, and of $M_Z$ and $\sigma_I$, are not greater in the small samples.

The statistics of the fine-textured end of the grain-size curve (percent matrix and percent clay in matrix) show much less variability than the other statistics in Table 5.3. This reflects the observation made in the field that the matrix texture varies very little from place to place in debris flow deposits. The coefficient of variation of percent clay in matrix in Table 5.3 corresponds to about $\pm$ 0.5 to 0.7% in the last column of Table 5.2, for both fine-textured and coarse-textured debris flows.

Part B of Table 5.3 shows that the $C_v$ of individual 1 $\phi$ pebble classes, in splits from one sample, is about 0.12 to 0.15. This is comparable to the results of more extensive tests of fluvial samples reported by Church *et al.* (1987), which gave $C_v$ values of about 0.04 to 0.20 for individual size classes which contained more than 100 grains. The large samples of the Boundary Creek deposit gave similar $C_v$ values in the largest size classes, indicating that a sample size of about 1 tonne is sufficient to represent all size classes of the grain-size

distribution up to about 256 mm. For summary statistics such as $M_Z$ and $\sigma_I$, the smaller sample size of 200 kg appears to be adequate.

The coarse-textured Hot Springs deposit (Table 5.3) showed greater variability in most statistics than did the fine-textured deposits. There is no apparent reason for this, since one would expect sieve analysis of non-muddy, granitic sediment to be more precise than that of muddy sediment. This result may indicate a greater local random variability in sediment texture in the coarse-textured debris flows; that is, the sediment in these debris flows may be less uniformly mixed.

Figure 5.15, graph A, gives a graphical indication of the variability of cumulative curves from multiple samples of a single deposit, in this case the Devastation 1931 debris flow, from which 7 samples were taken of material smaller than 32 mm. For any percentile, the variability in the curves is in the range of about $\pm$ 0.5 $\phi$.

Graphs B and C of Figure 5.15 illustrate the method used to combine stone counts with bulk sieving data, and show the grain-size distributions of the of deposition facies. For coarse-textured deposits, the major source of error is uncertainty in estimating the relative proportions of the two layers. For the Boundary deposit, the surface stone count curve is biased toward fine grain-sizes because many stones were concealed by fine sediment on the surface. However, this bias did not affect the combined distribution, because only the cobble and boulder classes were used to extend the combined cumulative curve.

## 5.4 WATER CONTENT AND WEIGHT-VOLUME RELATIONS

Several fine-textured debris flow events were sampled within 2 to 3 days of their emplacement. At this time, they were still in an undrained state, except for a thin surface crust. They would not support the weight of a person, and the debris could be easily mobilized by pushing or vibrating it slightly. Water content samples were taken, with reasonable confidence that they were very close to their original values. No such samples were taken of coarse-textured debris flows; samples would have to be taken immediately upon emplacement, as coarse-textured debris flows drain rapidly (see Chapter 6).

The water content measurements are given in Table 5.4. The 1988 samples were taken in 20 litre plastic paint buckets, which were sealed until analysis. The 1990 samples were taken in double plastic bags (sample size about 9 to 14 kg), and analyzed within several days of sampling.

Water content measurements are meaningful only if they are reported with respect to a consistent upper size limit. Some of the samples contained stones up to about 64 mm, but the measurements were reduced to a common upper size limit of 32 mm. This is the size to which grab samples of several kilograms are representative, and therefore the water content measurements at 32 mm are probably comparable with most other measurements that have been reported in the literature. The values of water content on a dry weight basis (w), and concentration of solids by weight ($C_s$) in Table 5.4 are consistent with most of the measurements from other studies reported in Table 2.1.

It is of interest to report water content measurements to an upper size limit of 256 mm in order to estimate the water content of the entire debris flow, and also to calculate the matrix (< 4 mm) water content for comparison with some of the geotechnical tests described in Chapter 6. These calculations can be made simply by adding the proportional weights of the 32 to 256 mm fraction, or subtracting the 4 to 32 fraction, respectively. However, it is probably not reasonable to assume that all the water content is associated with the matrix material; a small amount of water is probably adsorbed on the surface of the stones. To get a rough idea of what this might be, non-porous stones (quartz diorite) were weighed dry, then reweighed after soaking them and shaking off the excess water. The amount of adsorbed water per unit surface area was approximately 0.008 g/cm$^2$. Using this correction, the water content can be adjusted to any upper size limit, provided the grain-size distribution is known, by:

$$w = \frac{w_0 + \sum(Aa_i s_i)}{1 + \sum s_i} \qquad (5.4)$$

where w is the water content (dry weight basis) at the new size limit, $w_0$ is the water content at the standard size limit (32 mm in this case), A is the adsorbed surface water as noted above, $a_i$ is the surface area per unit mass for size class i (Table 5.1), and $s_i$ is the proportion of particles by weight in size class i, relative to a total weight of 1 at the standard size limit. (If the calculation

is for a smaller, rather than for a larger, upper size limit, then the "+" signs in the formula become "–" signs.) The correction for surface water makes a negligible difference for the 32 to 256 mm particles, but it makes a difference of about 0.01 to 0.02 in the calculated water content at 4 mm, since the smaller size classes have a relatively high surface area. The amount of water absorbed in porous volcanic stones is unknown; this may introduce a substantial error in calculated water contents and void ratios.

The water contents of the Boundary sample in Table 5.4 are somewhat higher (by 50% or more) than the liquid limit at 4 mm ($w_L = 0.18$), as well as the water contents at which permeability and shear strength tests were conducted (Chapter 6). However, they are only slightly higher than the water contents at which consolidation tests were done.

In calculations involving water content, including the geotechnical tests described in Chapter 6, it is useful to make use of some formulae from soil mechanics relating water content, void ratio, and unit weight. These include (after Craig, 1987), where e is void ratio, $G_s$ is particle specific gravity, $\gamma$ is unit weight, $\gamma_w$ is the unit weight of water (9.8 kN/m$^3$), and $S_r$ is the degree of saturation (the proportion of the void space which is occupied by water):

$$w = \frac{S_r e}{G_s} \tag{5.5}$$

$$\gamma = \frac{G_s(1+w)\gamma_w}{1+e} \tag{5.6}$$

If V and M are the total volume and mass of a sample respectively, $M_s$ is the mass of solids, and $\rho_w$ is the density of water, then the following formulae are also useful:

$$M_s = \frac{M}{1+w} \tag{5.7}$$

$$e = \frac{VG_s\rho_w}{M_s} - 1 \tag{5.8}$$

The degree of saturation, $S_r$, was typically about 0.9 for samples reconstituted in the lab for geotechnical tests. The calculated $S_r$ of the water content samples collected in 20 litre buckets was approximately 0.7 to 0.8. These low values may represent the actual field degree of saturation, or they may be affected by air included in the bucket during sampling. The samples could also include air in the pore spaces of volcanic rocks.

## 5.5 SUMMARY OF SEDIMENTOLOGY

The texture of debris flows was measured by taking bulk samples of subsurface material, and by making stone counts of coarse surface layers where present. At detailed study sites, several samples were taken if time permitted. The results of replicate sampling indicated that the texture of subsurface material showed very little lateral variability within debris flow deposits. After some experimentation, it was determined that a sample size of about 200 kg was sufficient to represent the grain-size distribution to 256 mm.

The two main populations of events in this study, coarse-textured, plutonic-source debris flows, and fine-textured, volcanic-source debris flows, can be distinguished on the basis of texture and grading. A graphic mean of $M_Z = -4\ \phi$, an inclusive graphic standard deviation of $\sigma_I = 4\ \phi$, and a matrix clay content of 4 to 5%, separates coarse-textured from fine-textured deposits. Coarse-textured debris flows have a well-defined, clast-supported, inversely-graded, surface layer. This layer is lacking in fine-textured debris flows, which are typically ungraded.

Three facies of deposition can be identified in many debris flows: coarse, frontal levées and lobes: the main, poorly sorted, deposit; and a fine afterflow deposit. These facies correspond with the bouldery front, the main surge, and the following hyperconcentrated flow, which have been described in previous studies where debris flows have been observed in motion.

Fluvial gravels and "debris flood" deposits cannot be readily distinguished from coarse-textured debris flow deposits on the basis of average texture. However, the lack of stratification, and the well-defined, coarse, surface layer, are distinguishing features of debris flows.

TABLE 5.1 WEIGHT AND SPECIFIC GRAVITY OF STONES

A. THEORETICAL WEIGHTS OF STONES IN WENTWORTH SIZE CLASSES. Weights are for spheres of the given dimension, with a specific gravity of 2.65.

| Sieve size | | Mass | Size class | Class midpoint | Mass | Surface area per |
|---|---|---|---|---|---|---|
| (mm) | (phi) | (g) | (mm) | (mm) | (g) | unit mass ($cm^2/g$) |
| 1024 | -10 | $1.5x10^6$ | 512-1024 | 724 | 530,000 | 0.031 |
| 512 | -9 | 190,000 | 256-512 | 362 | 66,000 | 0.063 |
| 256 | -8 | 23,000 | 128-256 | 181 | 8200 | 0.125 |
| 128 | -7 | 2900 | 64-128 | 90.5 | 1030 | 0.25 |
| 64 | -6 | 360 | 32-64 | 45.3 | 130 | 0.50 |
| 32 | -5 | 46 | 16-32 | 22.6 | 16 | 1.0 |
| 16 | -4 | 5.7 | 8-16 | 11.3 | 2.0 | 2.0 |
| 8 | -3 | 0.71 | 4-8 | 5.66 | 0.25 | 4.0 |
| 4 | -2 | 0.089 | 2-4 | 2.83 | 0.031 | 8.0 |
| 2 | -1 | 0.011 | | | | |

B. SPECIFIC GRAVITY OF SAMPLED DEBRIS FLOW MATERIAL

| Sample location | Dominant lithology | Specific gravity of sand | Specific gravity of pebbles* |
|---|---|---|---|
| Boundary | dacite | 2.69 | 2.47-2.73 |
| No Good | dacite, rhyolite | 2.69 | 2.40-2.73 |
| Devastation 1931 | dacite, tuff | 2.67 | 2.34-2.90 |
| Upper Lillooet ca. 900 BP | dacite | 2.62 | |
| Canyon | gneiss, andesite | 2.70 | |
| Hot Springs | quartz diorite | 2.73 | 2.73 |
| Capricorn | granodiorite, dacite, andesite | 2.69 | 2.74 |
| Lower Ryan | quartz diorite | 2.71 | 2.71 |
| Fountain | greywacke, sandstone | 2.76 | 2.75 |

* Pebbles include a variety of lithologies for volcanic-source debris flows. Low values are for porous pyroclastic rocks. High values are for minor types of basement rock (e.g. amphibolite).

TABLE 5.2 SUMMARY OF GRAIN SIZE STATISTICS

| Event or Location | ID | Type of Event | Relia-bility | No. of bulk samples | Total debris flow material | | | | Subsurface material < 256 mm | | | | | | |
|---|---|---|---|---|---|---|---|---|---|---|---|---|---|---|---|
| | | | | | Graphic mean | Inc.gr. St.Dev. | D50 | % cobbles & boulders | Graphic mean | Inc.gr. St.Dev. | D50 | % matrix | % fines | % clay | % clay in matrix |
| Angel B 1990 | 1 | A | D | 1 | | | | | -3.04 | 4.41 | -4.71 | 31.1 | 10.7 | 3.9 | 12.5 |
| Boundary 1987 | 2 | A | A | 8 | -4.25 | 4.71 | -5.74 | 47.3 | -3.13 | 4.57 | -4.68 | 33.3 | 10.5 | 3.4 | 10.3 |
| Boundary 1988 | 3 | A | B | 3 | -2.58 | 4.73 | -4.03 | 25.1 | -2.31 | 4.64 | -3.72 | 39.1 | 12.9 | 4.2 | 10.7 |
| Boundary 1989 | 4 | A | B | 3 | -4.11 | 4.65 | -5.78 | 47.3 | -3.44 | 4.52 | -5.18 | 31.1 | 10.0 | 3.2 | 10.2 |
| Cheekye ca. 1100 BP | 5 | A | D | 0 | -0.59 | 4.76 | -1.23 | 10.0 | -0.59 | 4.76 | -1.23 | 55.0 | 19.7 | 4.6 | 8.4 |
| Upper Lillooet, ca. 900 B | 6 | A | B | 2 | -1.04 | 4.48 | -1.22 | 12.2 | -1.04 | 4.48 | -1.22 | 57.3 | 14.7 | 3.8 | 6.7 |
| Devastation 1931 | 7 | A | B | 3 | -2.30 | 5.02 | -3.31 | 30.2 | -1.80 | 4.86 | -2.59 | 46.4 | 14.7 | 4.7 | 10.2 |
| No Good, early 1980s | 8 | A | A | 3 | -3.99 | 4.94 | -5.52 | 45.0 | -2.94 | 4.78 | -4.34 | 36.2 | 11.9 | 4.0 | 11.1 |
| NoGood 1990 | 9 | A | D | 0 | -4.71 | 4.01 | -6.00 | 50.0 | -4.03 | 4.04 | -5.46 | 23.2 | 7.7 | 2.5 | 10.9 |
| Turbid 1984 | 10 | A | D | 1 | | | | | -4.00 | 3.76 | -5.67 | 24.2 | 6.0 | 1.5 | 6.4 |
| Angel A, ca. 1987 | 11 | B | B | 1 | -3.96 | 3.70 | -4.87 | 28.4 | -3.74 | 3.76 | -4.68 | 25.0 | 7.1 | 2.2 | 8.7 |
| Canyon 1987 | 12 | B | A | 2 | -6.82 | 2.49 | -7.05 | 75.8 | -5.32 | 3.07 | -6.38 | 15.8 | 4.1 | 0.9 | 5.6 |
| Canyon 1990 | 13 | B | C | 1 | -5.22 | 3.42 | -6.31 | 56.0 | -4.24 | 3.81 | -5.74 | 21.7 | 5.7 | 1.3 | 5.8 |
| Cheekye 1984 | 14 | B | D | 1 | -5.50 | 3.82 | -7.33 | 80.3 | -4.38 | 4.06 | -6.76 | 29.6 | 5.5 | 1.0 | 3.4 |
| Fountain 1989 | 15 | B | C | 1 | -3.21 | 3.64 | -3.85 | 21.1 | -2.37 | 3.76 | -3.31 | 31.9 | 9.9 | 2.8 | 8.6 |
| McGillivray 1989 | 16 | B | C | 1 | -1.74 | 4.55 | -3.46 | 12.0 | -1.35 | 4.60 | -3.07 | 41.7 | 17.8 | 3.8 | 9.0 |
| Mt Currie, ca. 1984 | 17 | B | C | 1 | -3.08 | 4.44 | -5.25 | 35.0 | -2.58 | 4.39 | -4.81 | 33.8 | 13.7 | 1.7 | 5.2 |
| Affliction 1984 | 21 | C | D | 1 | | | | | -4.31 | 2.91 | -5.15 | 23.0 | 1.2 | 0.1 | 0.5 |
| Capricorn, ca. 1972 | 22 | C | A | 2 | -5.02 | 3.29 | -6.24 | 55.3 | -4.36 | 3.34 | -5.77 | 23.9 | 2.1 | 0.2 | 1.0 |
| Hot Springs 1984 | 23 | C | A | 3 | -6.43 | 2.71 | -6.69 | 66.3 | -4.13 | 3.54 | -5.82 | 19.1 | 3.4 | 0.5 | 2.6 |
| Lillooet fan centre 1984 | 24 | C | D | 1 | | | | | -4.66 | 2.87 | -5.39 | 25.2 | 0.4 | 0.0 | 0.0 |
| Ryan lower 1984 | 26 | C | C | 1 | -5.99 | 3.73 | -7.09 | 67.3 | -4.30 | 3.39 | -5.63 | 28.1 | 2.5 | 0.1 | 0.4 |
| Ryan upper 1984 | 27 | C | C | 1 | -5.58 | 2.79 | -6.33 | 56.7 | -4.74 | 3.05 | -5.98 | 20.8 | 0.9 | 0.1 | 0.3 |
| Meager Creek fluvial | 31 | F | A | 3 | -5.26 | 3.13 | -6.23 | 53.8 | -4.64 | 3.03 | -5.65 | 21.0 | 0.8 | 0.1 | 0.6 |
| Lillooet River fluvial | 32 | F | C | 1 | | | | | -4.83 | 3.00 | -5.94 | 19.5 | 0.8 | 0.1 | 0.5 |

Notes:

1. Type of Event - A = Fine-textured (no surface layer, and muddy matrix), B = Intermediate (thin or intermittent surface layer, or surface layer and muddy matrix), C = Coarse-textured (well-defined, coarse, surface layer and sandy matrix), F = fluvial gravels
2. Reliability - A = Very good (suffiicient bulk samples and stone counts to represent total material), B = Good (reasonably representative to 256 mm, photo estimates or limited stone count for boulders), C = poor (one bulk sample, poor representation of cobbles, photo estimate of boulders), D = very poor (rough photo or field estimate of cobble-boulder fraction, or poor sample site, or poorly preserved deposit).
3. No. of bulk samples - Number of samples of subsurface material representative to 256 mm. "0" indicates that a photo estimate was used for cobbles.
4. Total debris flow material - Subsurface material, averaged with coarse surface layer where present.
5. Subsurface material - truncated to 256 mm. "Matrix" is material smaller than 4 mm.
6. All grain size statistics are in phi units, except those reported in %.

TABLE 5.3 SAMPLING ERRORS

A. VARIABILITY OF GRAIN SIZE STATISTICS AMONGST MULTIPLE SAMPLES. All samples are trucated to 256 mm. Standard deviation (s) is given for statistics reported in phi units, and coefficient of variation ($C_v$) is given for other statistics.

| Statistic | Boundary 1987 | | | Devastation | Hot Springs |
|---|---|---|---|---|---|
| | all samples | large samples | small samples | | |
| n (number of samples) | 8 | 3 | 5 | 3 | 3 |
| Mean sample size (kg) | 464 | 890 | 208 | 480 | 385 |
| $D_{50}$ - s (phi) | 0.43 | 0.56 | 0.39 | 0.38 | 0.50 |
| $M_z$ - s (phi) | 0.32 | 0.41 | 0.30 | 0.22 | 0.21 |
| $\sigma_I$ - s (phi) | 0.16 | 0.16 | 0.17 | 0.14 | 0.43 |
| % cobbles - $C_v$ | 0.13 | 0.13 | 0.13 | 0.18 | 0.31 |
| % matrix - $C_v$ | 0.11 | 0.15 | 0.10 | 0.05 | 0.09 |
| % clay in matrix - $C_v$ | 0.05 | | | 0.06 | 0.26 |
| % in 128-256 mm - $C_v$ | 0.43 | 0.12 | 0.49 | 0.47 | 0.97 |
| % in 64-128 mm - $C_v$ | 0.26 | 0.15 | 0.33 | 0.04 | 0.27 |
| average $C_v$, size classes in 0.063-32 mm range | 0.14 | | | 0.10 | 0.29 |

B. VARIABILITY OF SAMPLE SPLITS. Statistics are for 8 splits of a 60 kg sample of < 32 mm material, sample Devastation 1931-3.

| Statistic | | Value |
|---|---|---|
| n | | 8 |
| mean split size (kg) | | 7.5 |
| % in 16-32 mm class | - mean | 12.6 |
| | - $C_v$ | 0.15 |
| % in 8-16 mm class | - mean | 9.9 |
| | - $C_v$ | 0.12 |

TABLE 5.4 WATER CONTENT OF DEBRIS FLOW SAMPLES

| Sample | Measured water content of < 32 mm material | | Calculated equivalent water contents: < 256 mm | | < 4 mm | |
|---|---|---|---|---|---|---|
| | w | $c_s$ | w | $c_s$ | w | $c_s$ |
| Boundary 1988 | 0.194 | 0.84 | 0.126 | 0.89 | 0.31 | 0.76 |
| No Good 1988 | 0.214 | 0.82 | - | - | 0.29 | 0.78 |
| Canyon 1990 | 0.168 | 0.86 | 0.063 | 0.94 | 0.32 | 0.76 |
| No Good 1990 | 0.206 | 0.83 | 0.090 | 0.92 | 0.37 | 0.73 |

Notes: Samples were collected 2 to 3 days after debris flow event.
No Good 1988 was not sampled to 256 mm.
w = water content, dry weight basis.
$c_s$ = concentration of solids by weight = 1/(1+w)

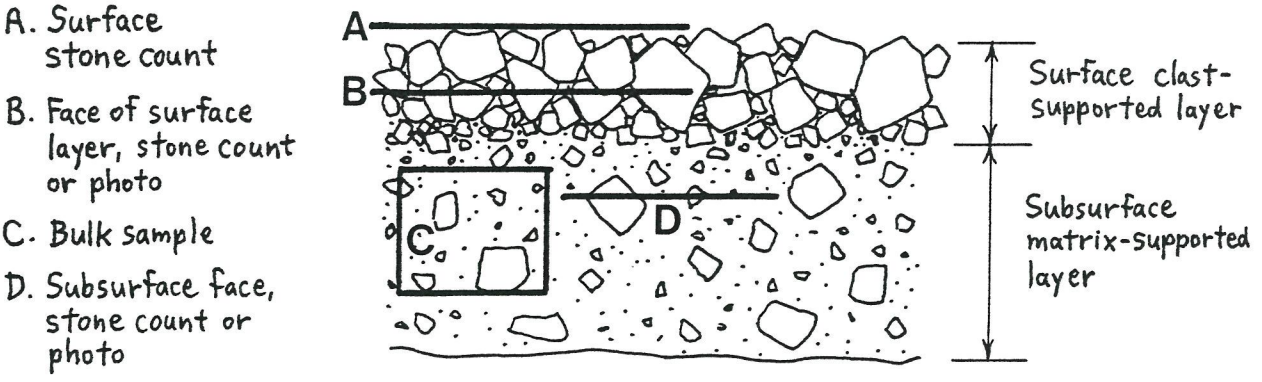


FIGURE 5.1. SKETCH SHOWING TYPES OF SAMPLES TAKEN IN A TYPICAL COARSE-TEXTURED DEBRIS FLOW DEPOSIT.

FIGURE 5.2. PHOTO SHOWING BULK SIEVING PROCEDURE ON BOUNDARY CREEK FAN.

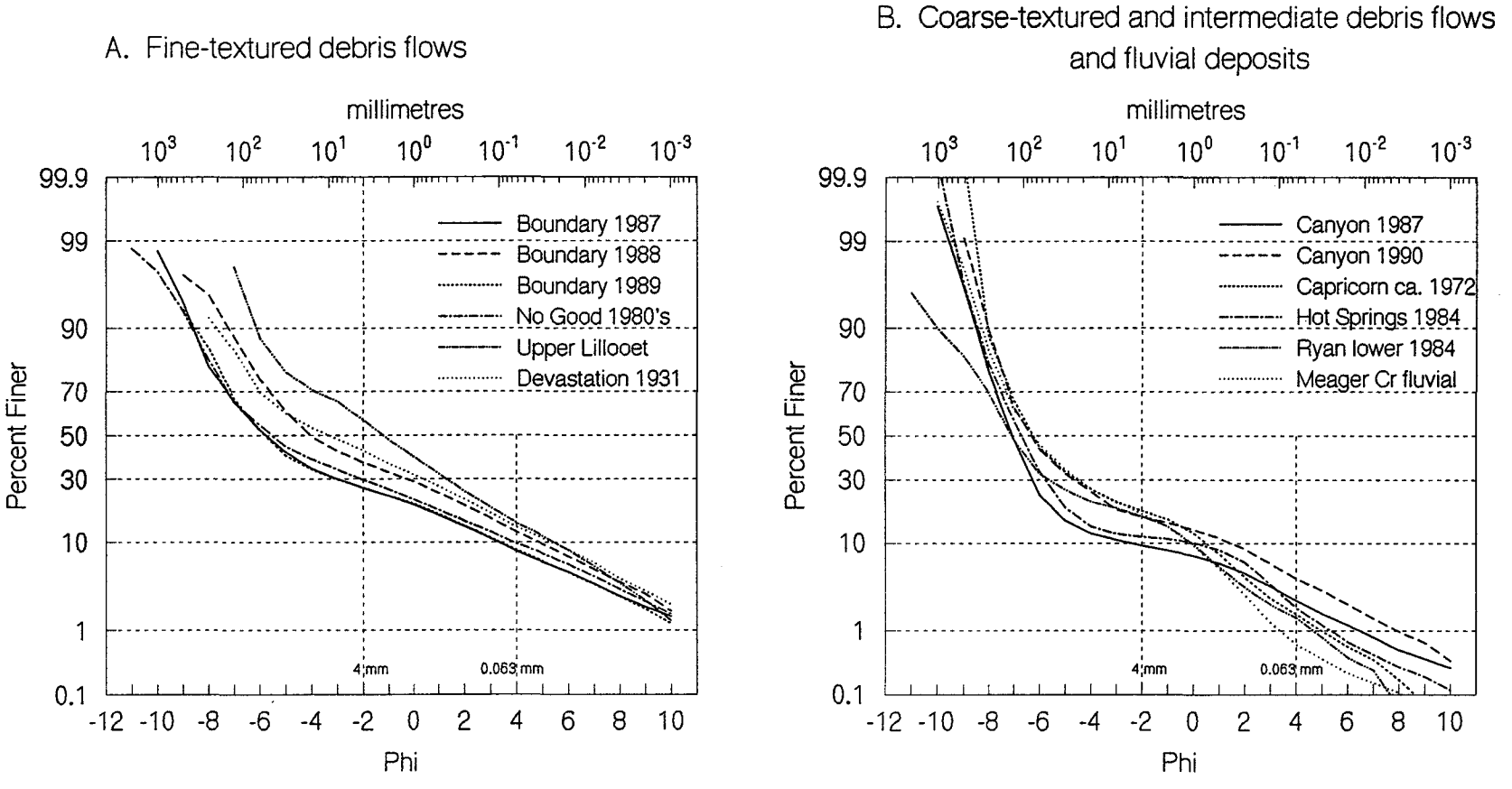


FIGURE 5.3. CUMULATIVE CURVES OF GRAIN-SIZE DISTRIBUTIONS.

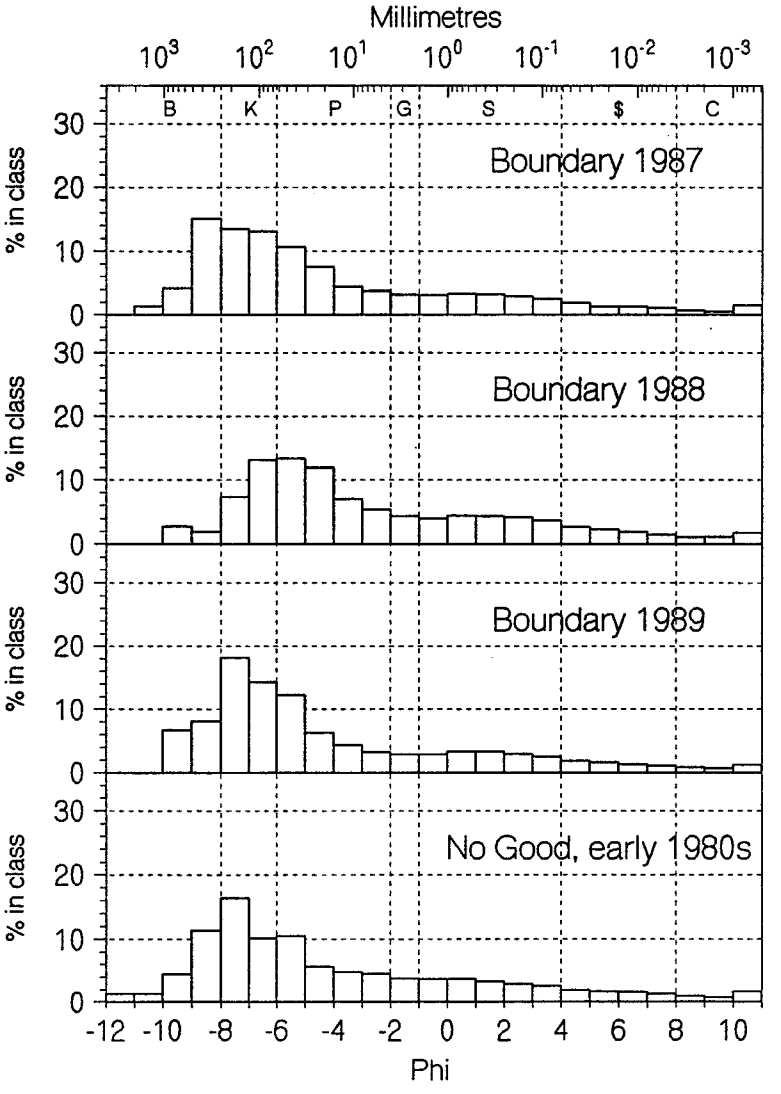


FIGURE 5.4.
HISTOGRAMS OF GRAIN-SIZE DISTRIBUTIONS.

All distributions in Figures 5.3 and 5.4 are combined distributions of total debris flow material, including coarse surface layers where present.

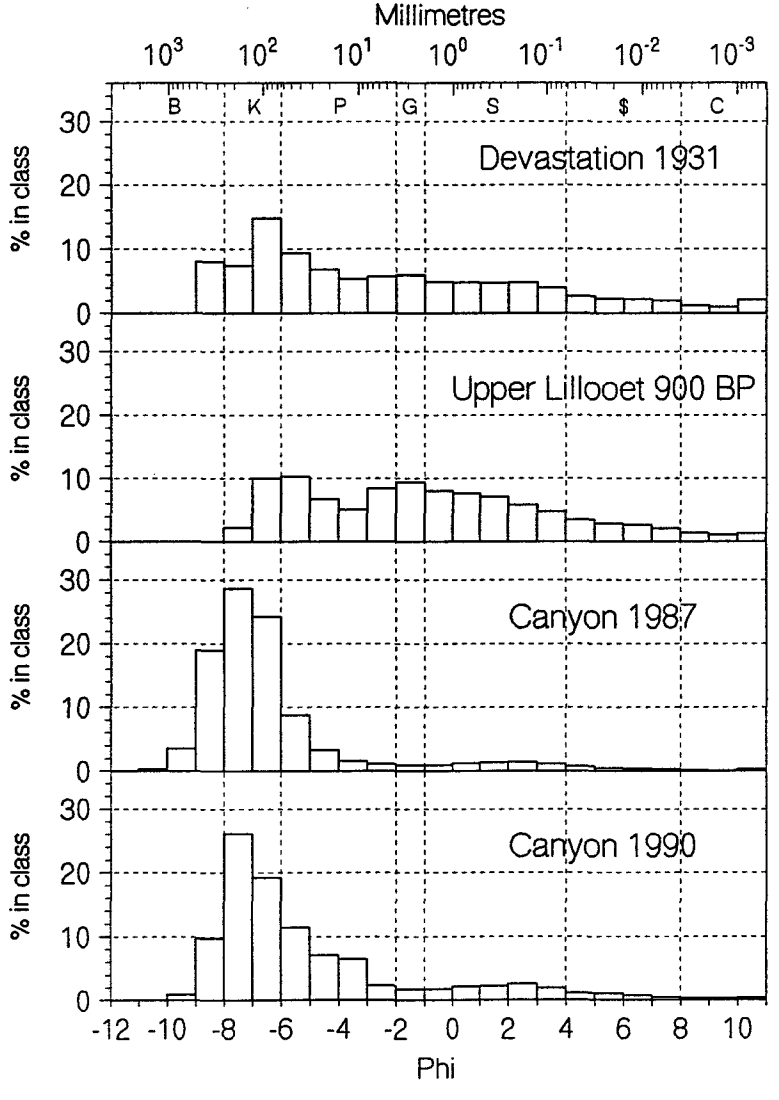
Millimetres
10^3 10^2 10^1 10^0 10^-1 10^-2 10^-3
B K P G S $ C
Devastation 1931
Upper Lillooet 900 BP
Canyon 1987
Canyon 1990
% in class
0 10 20 30
-12 -10 -8 -6 -4 -2 0 2 4 6 8 10
Phi

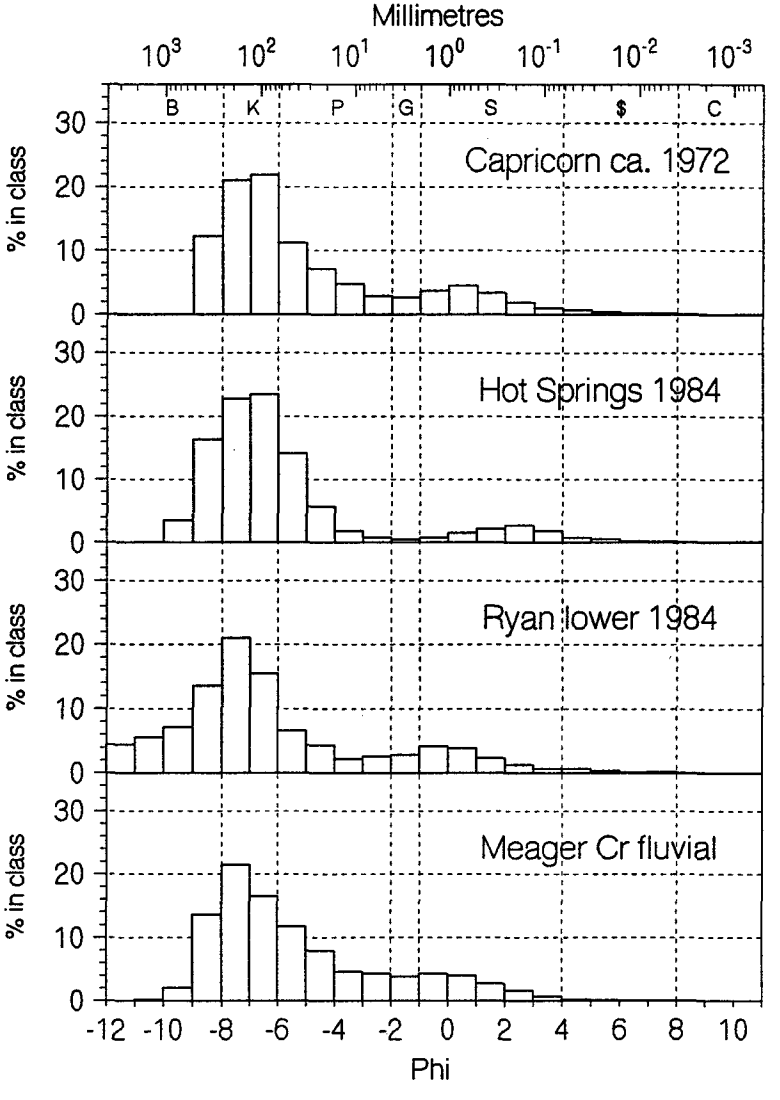
Millimetres
10^3 10^2 10^1 10^0 10^-1 10^-2 10^-3
B K P G S $ C
Capricorn ca. 1972
Hot Springs 1984
Ryan lower 1984
Meager Cr fluvial
% in class
0 10 20 30
-12 -10 -8 -6 -4 -2 0 2 4 6 8 10
Phi

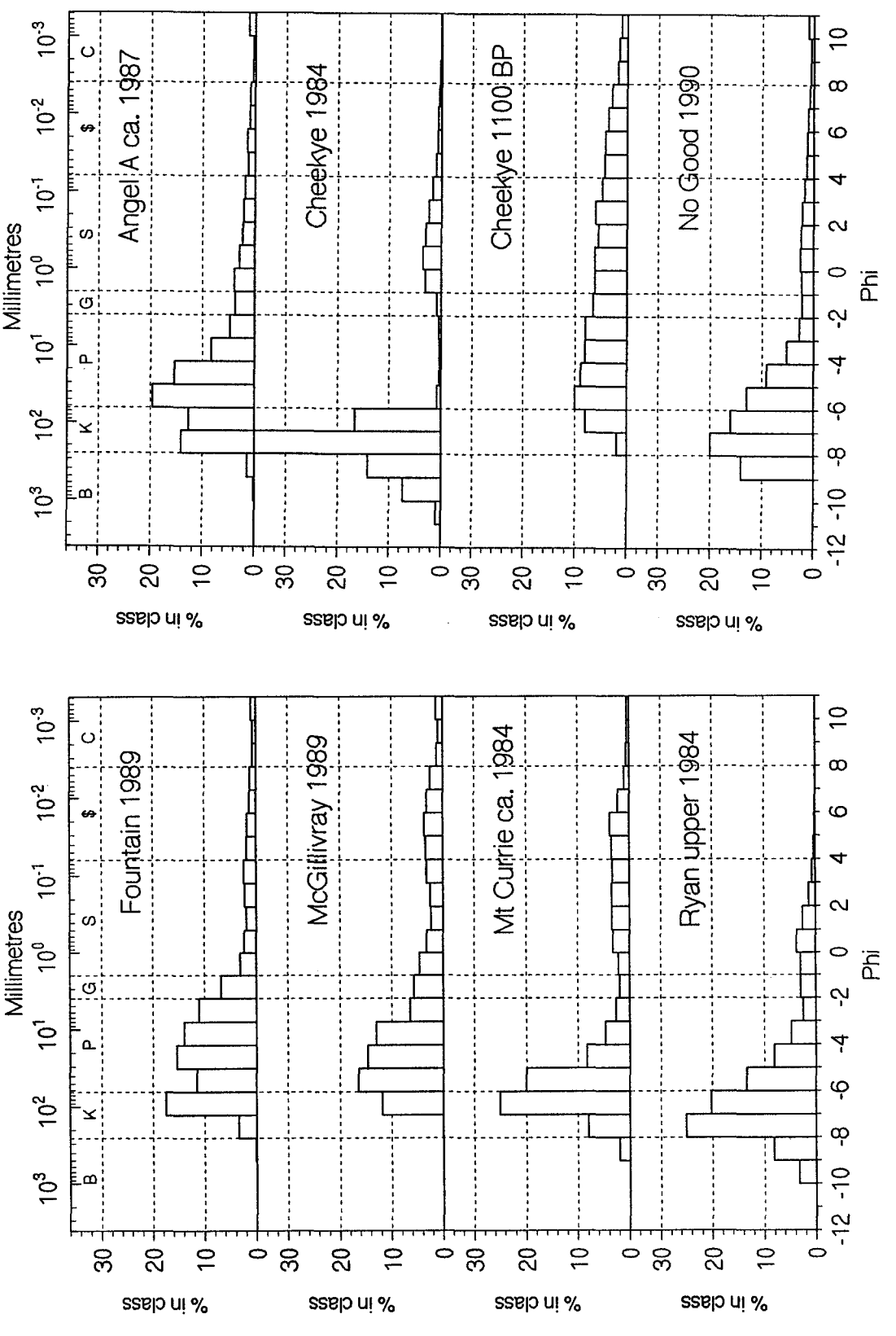
Millimetres
Phi
% in class
Angel A ca. 1987
Cheekye 1984
Cheekye 1100 BP
No Good 1990
Fountain 1989
McGillivray 1989
Mt Currie ca. 1984
Ryan upper 1984

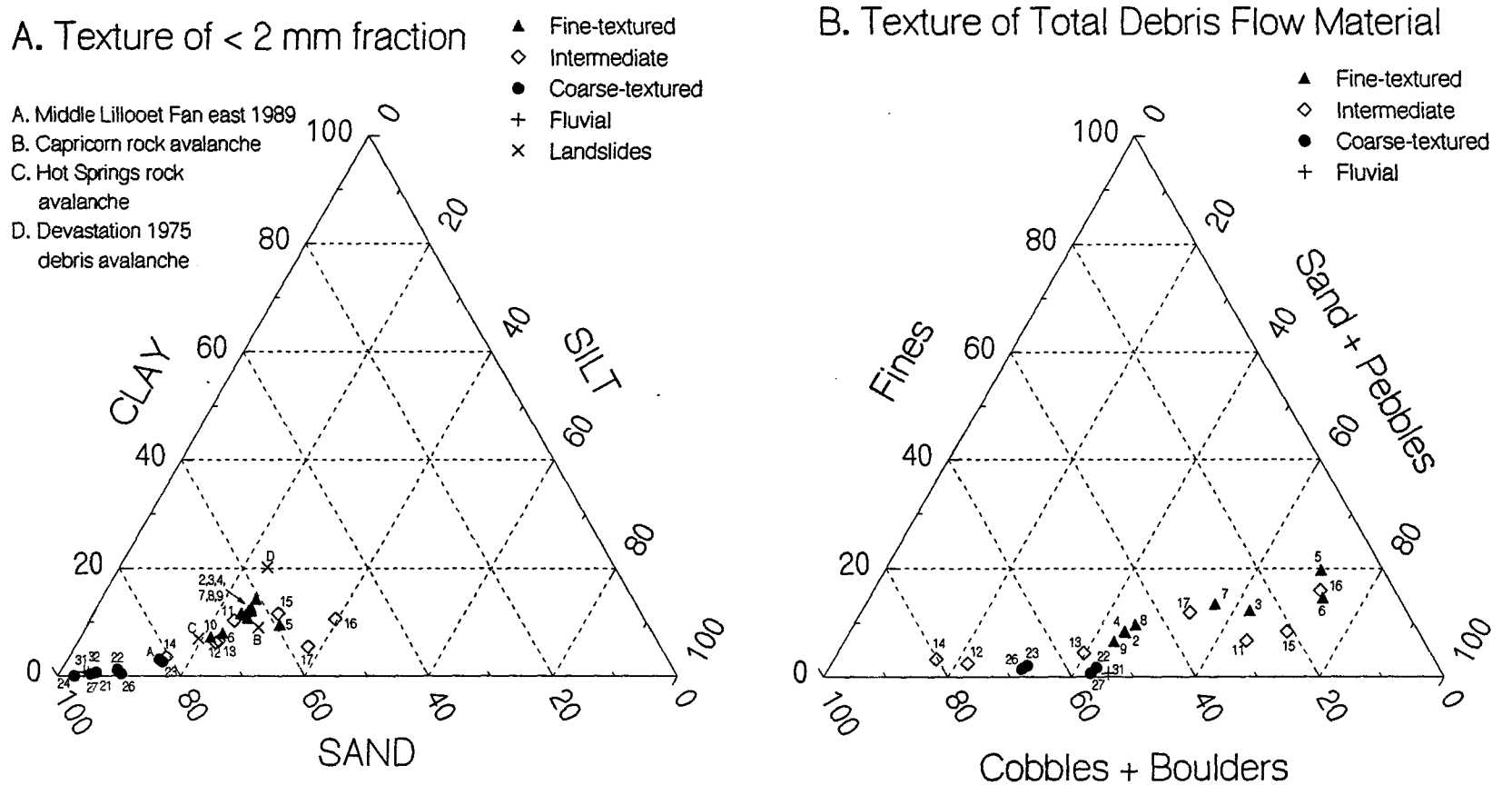


FIGURE 5.5. TEXTURAL TRIANGLES OF DEBRIS FLOW MATERIAL.

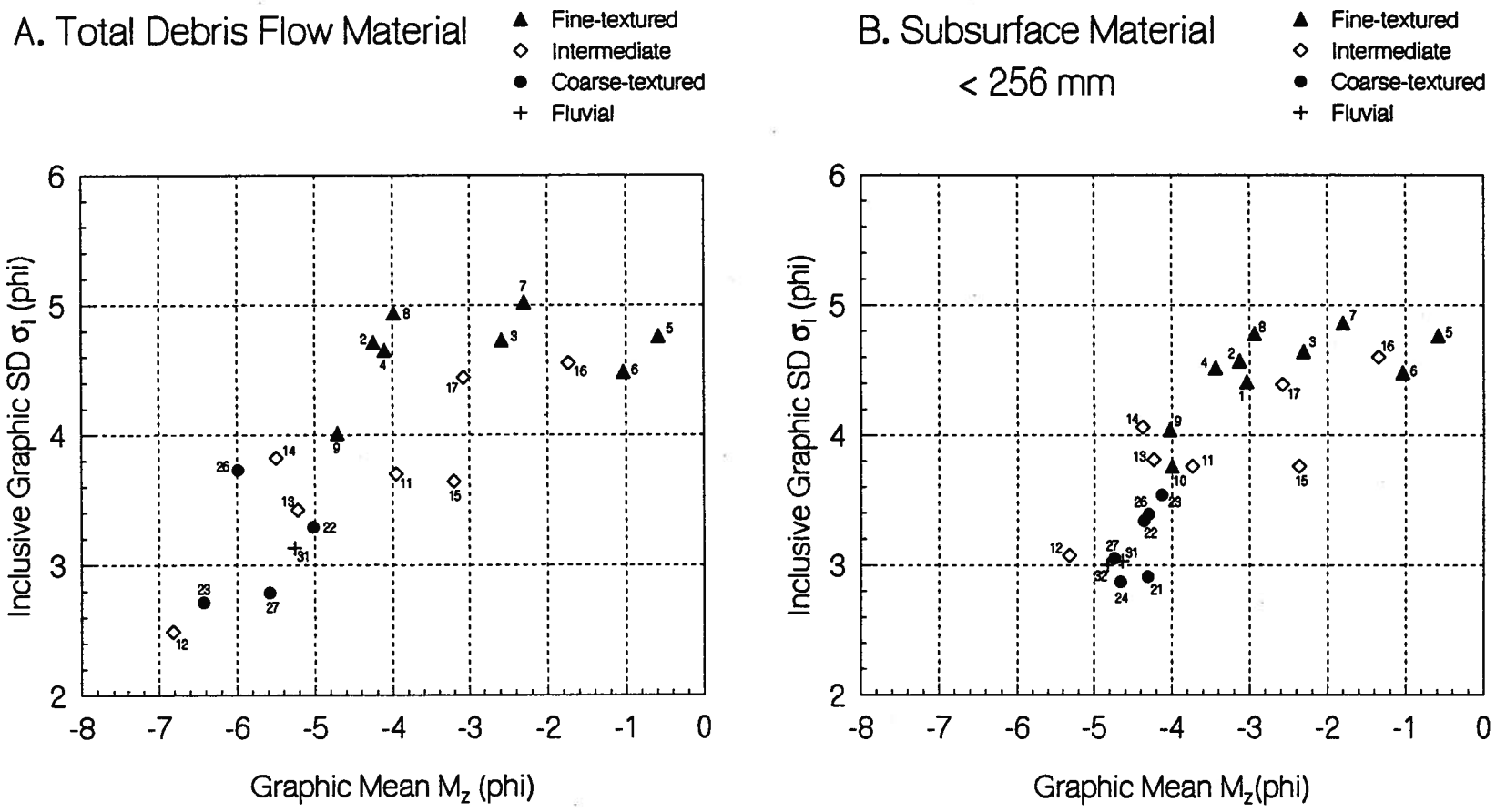


FIGURE 5.6. GRAPHS OF MEAN GRAIN-SIZE VS. STANDARD DEVIATION.

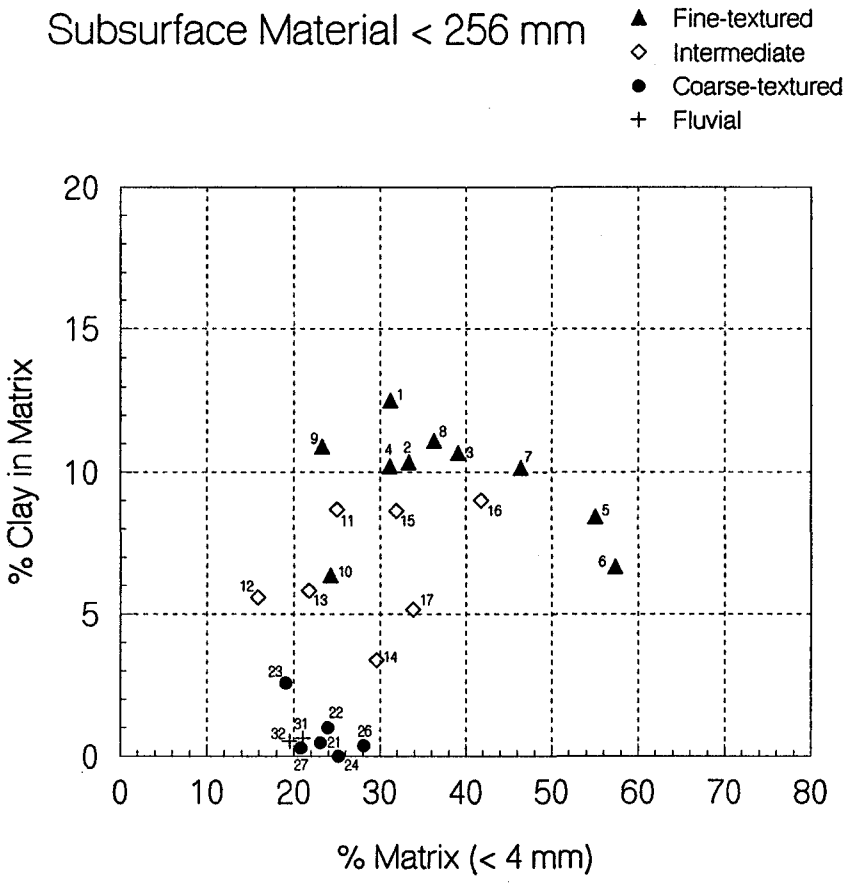


FIGURE 5.7. GRAPH OF % MATRIX VS. CLAY CONTENT IN MATRIX.

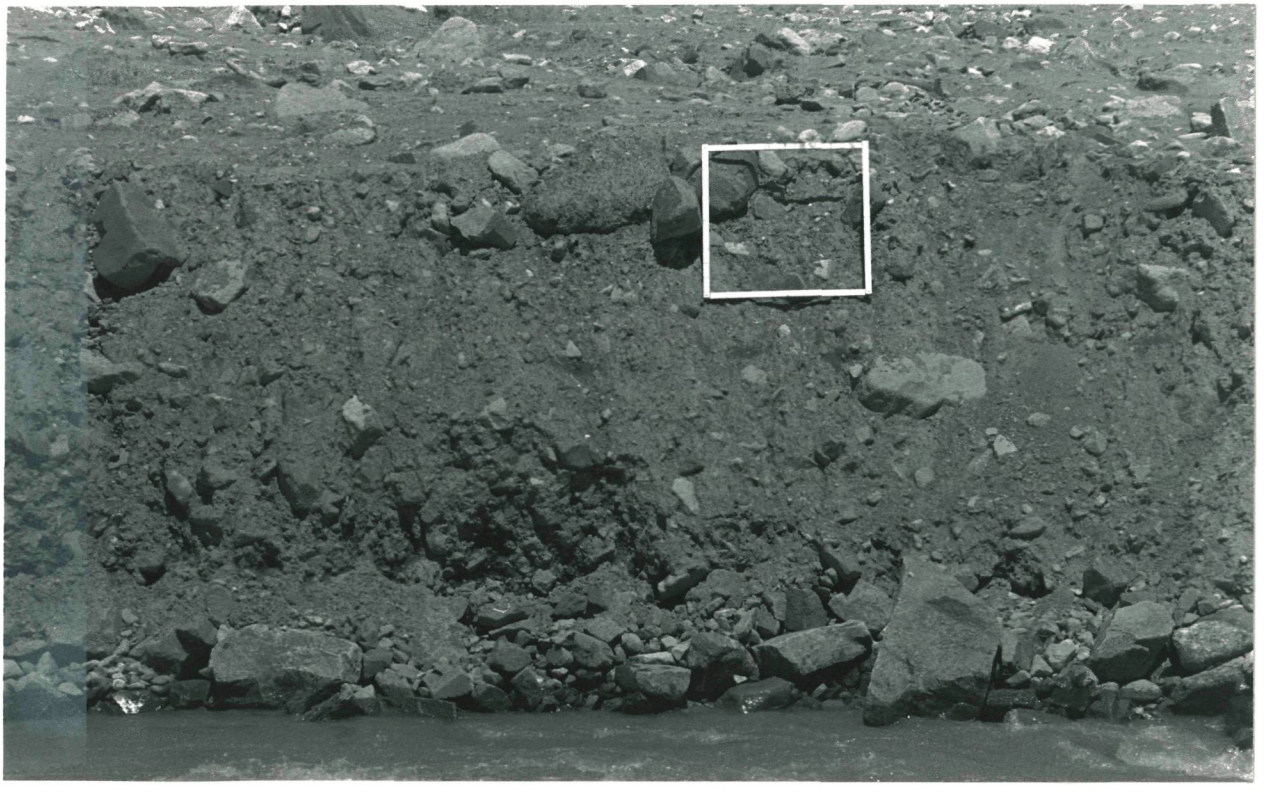

A. (Above) Boundary Creek fan debris flow deposits in section. The 1 m square frame shows scale. The line about 0.3 m below the frame is the bottom of the 1989 deposit.

B. Devastation 1931 deposit in section at a sample pit. Pole is 1 m long.

FIGURE 5.8. FINE-TEXTURED DEBRIS FLOW DEPOSITS: BOUNDARY 1989 AND DEVASTATION 1931.

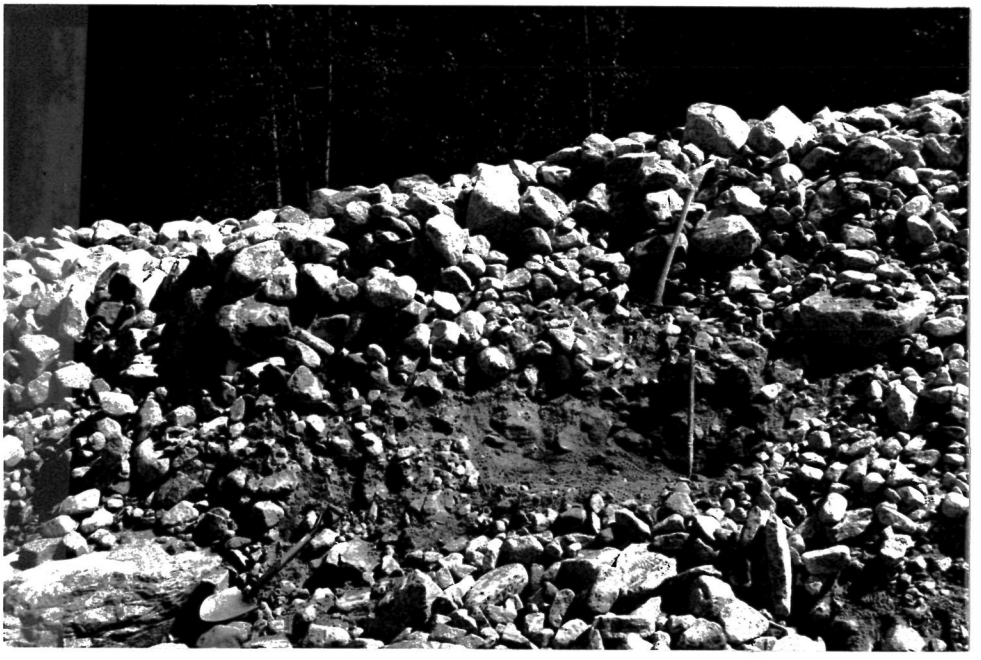

A. Hot Springs 1984. Tools are about 0.75 m long. Note inverse grading in surface layer, and matrix-supported subsurface material in excavated sample pit.

B. Canyon 1987. This deposit is classified as "intermediate" in texture, but the inversely graded surface layer is typical of coarse-textured debris flows. Tape is set up for subsurface stone counts.

FIGURE 5.9. INVERSE GRADING IN COARSE-TEXTURED DEBRIS FLOW DEPOSITS: HOT SPRINGS 1984 AND CANYON 1987.

A. Thin, inversely graded lobe near apex of fan.

B. Section through main deposit, exposed by excavation at logging maintenance camp. Deposit is about 5 m deep at this point. Rod is 1.8 m long.

FIGURE 5.10. CANYON 1990 DEBRIS FLOW DEPOSIT.

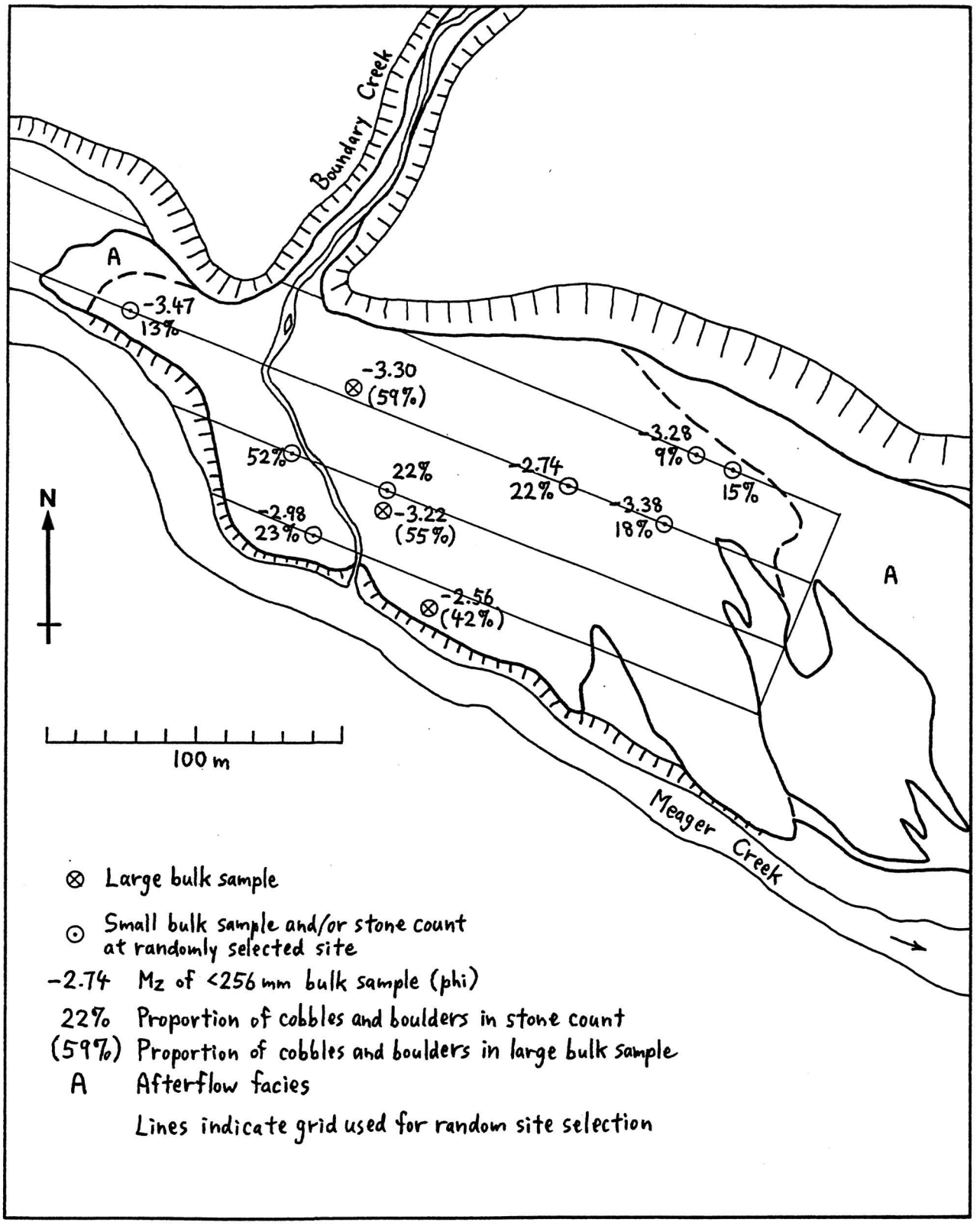


FIGURE 5.11. RESULTS OF SAMPLING ON BOUNDARY CREEK FAN.

FIGURE 5.12. NO GOOD 1990 DEBRIS FLOW DEPOSIT. Ice axe is 0.75 m long. Deposit is a small remnant in channel 250 m above mouth.

FIGURE 5.13. CLAST-SUPPORTED FLUVIAL DEPOSIT - MEAGER CREEK BARS. Rod is graduated in feet.

A. Early 1970s deposit, at sampling pit. Note the thin surface layer, and subsurface boulders which are almost in contact.

B. Stratified deposit of 1990 debris flood.

FIGURE 5.14. CAPRICORN CREEK DEBRIS FLOOD DEPOSITS.

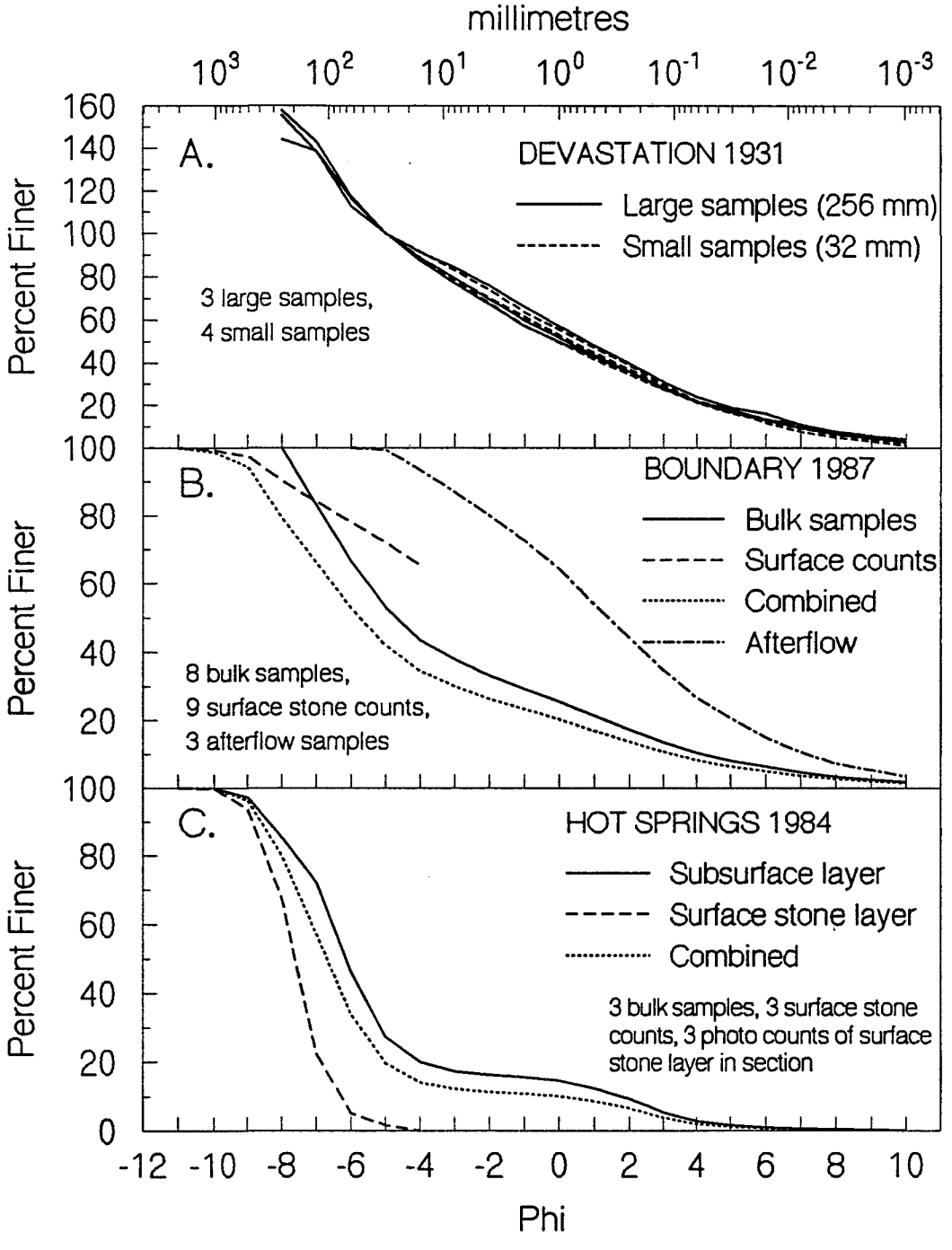


FIGURE 5.15. CUMULATIVE CURVES ILLUSTRATING COMBINED SURFACE AND SUBSURFACE SAMPLES, AND SAMPLING ERRORS.

A. Seven samples from Devastation 1931 debris flow, graphed with 100% at 32 mm.
B. Average cumulative curves for Boundary 1987 debris flow. Afterflow facies is not included in the combined curve.
C. Average cumulative curves for Hot Springs 1984 debris flow.

# CHAPTER 6. GEOTECHNICAL PROPERTIES OF DEBRIS FLOW SAMPLES

Several standard geotechnical tests were performed on selected debris flow samples, in order to investigate factors that might explain observed differences in the behaviour of fine-textured and coarse-textured debris flows. The tests included consistency limits, angle of internal friction, permeability, and consolidation. Standard soil mechanics methods as described in Lambe (1951) were used, unless otherwise noted.

Studies on debris flows which report geotechnical and material properties are rare. Owens (1973) measured the angle of internal friction, as well as performing rheologic tests. Pierson (1981) measured the rate of consolidation of debris flow material. Otherwise, most previous debris flow studies have reported only texture. Studies of other mass movement processes, however, have often examined shear strength and other geotechnical properties (for example, Hungr and Morgenstern, 1984).

## 6.1 CONSISTENCY LIMITS

Liquid limit and plastic limit tests were performed on a number of samples, using the standard apparatus. Samples were sieved to a maximum size of 0.42 mm, which is the specified standard. The results are given in Table 6.1.

The plastic limit $w_P$ and the liquid limit $w_L$ are the water contents (on a dry weight basis) at which a soil passes from the semi-solid to the plastic state, and from the plastic to the liquid state, respectively, using arbitrary definitions (Craig, 1987). These consistency limits are useful in classifying and describing fine-textured soils. The liquid limit is of relevance to debris flow, as debris must be at a water content in excess of the liquid limit in order to behave as a fluid.

The results in Table 6.1, as would be expected, show a correlation between the liquid limit and the proportion of clay in the debris flow matrix. Plastic behaviour (the capability of forming a ribbon when rolled with the hands) occurred only in those samples with a clay content of 9% or greater in the matrix (defined as material smaller than 4 mm). This corresponds to a clay proportion of about 15% in the subsample finer than 0.42 mm used for the tests.

Because the samples tested are poorly sorted and contain a high proportion of sand, the liquid limit and plasticity index do not vary greatly between the different samples, and are much lower than are typically measured for well-sorted, fine-textured sediments such as glaciolacustrine silts and clays. Therefore, the consistency limits are not an especially useful tool for discriminating between fine-textured and coarse-textured debris samples. However, the presence of cohesive material in the relatively fine-textured samples is obvious on hand-texturing, and the stickiness of wet debris to the touch is a useful characteristic to distinguish cohesive from non-cohesive samples.

The consistency limits are very sensitive to the amount of sand in a sample. To test this sensitivity, additional tests were performed on a sample of the fines only (< 0.074 mm), and on another sample of the entire matrix (< 4 mm), from one debris flow site. The results are shown in Figure 6.1. For the coarser sample, as well as for two other samples in Table 6.1, the liquid limit could not be successfully tested using the standard grooving tool. The value reported is the water content at which liquefaction of the sample could be achieved by vibrating it with a blunt instrument.

## 6.2 SHEAR STRENGTH

A possible hypothesis to explain the apparently greater mobility of fine-textured debris flows, especially the lower slope on which they are capable of flowing, is that angle of internal friction, $\phi'$, is lower than for coarse-textured debris flows. Therefore, shear strength tests were performed on two fine-textured samples, Boundary 1987-1 and Meager 1931-3, and two coarse-textured samples, Hot Springs 1984-1 and Ryan 1984-1. The matrix material (< 4 mm) of each sample was used.

(The term "angle of internal friction" is used here because the resistance to shear under discussion is specifically the resistance due to friction at very low shear rates. The alternative term "angle of shearing resistance" [Craig, 1987] includes resistance from all sources, including rate-dependent effects such as dispersive stress and intragranular collisions.)

The shear strength of a soil at failure can be expressed by the well-known Coulomb strength model, in terms of effective normal stress (Craig, 1987, after Terzaghi, 1943):

$$\tau_f = c' + \sigma'_f \tan\phi' \qquad (6.1)$$

where $\tau_f$ is the shear strength at failure, c' is cohesion, $\sigma'_f$ is effective normal stress ($\sigma' = \sigma - u$, where $\sigma$ is total normal stress and u is pore water pressure), and $\phi'$ is the angle of internal friction. This model is not applicable to flowing debris; however it has been used to describe the failure of stream channel sediment at the point of debris flow initiation (Takahashi, 1978). The model should also be applicable to debris flow termination, at the point where the debris stops flowing.

Most natural soils exist at a density which is greater (*i.e.* a void ratio which is smaller) than occurs at the point of failure. Thus the soil must expand, or dilate, as it is sheared. If a relatively dense soil is sheared to the point of failure, the angle of internal friction at failure is $\phi'_p$, or peak angle, which depends on the initial void ratio. On continued shear, the ratio of shear stress to normal stress will decline to a lower value which can be expressed by $\phi'_{cv}$ (constant volume friction angle), which should be independent of the initial void ratio. If the soil is initially less dense than the critical state, on shear it will fail gradually and contract until the critical void ratio, $e_{cv}$, is reached. This concept is relevant to debris flow behaviour, in that during flow and deposition, the debris must be at a void ratio equal to or greater than $e_{cv}$.

Shear strength can be measured by two standard methods, the direct shear test and the triaxial compression test. Both tests apply normal stress and shear stress to a small sample under controlled conditions, enabling the determination of all the terms in eq. 6.1. Both methods are described in detail in a number of soil mechanics references (including Lambe, 1951, and Craig, 1987); therefore, they will not be described here.

The two coarse-textured samples were tested using a variation of the triaxial compression test, known as the vacuum triaxial test, at the Civil Engineering Department of the University of British Columbia. This test is performed on a dry sample of a cohesionless material (*i.e.* a sand). The confining pressure is provided by a vacuum applied to the sample, instead of a pressurized, water-filled, surrounding vessel as is used in the standard triaxial test. Each sample was tested two or three times, at initial densities ranging from moderately well packed, to as loosely packed as possible. The volume of the test sample (hence the density and the void ratio) were

determined at the start and end of each test by directly measuring the dimensions of the sample cylinder. The samples were about 135 mm long and 70 mm in diameter. The tests could be conducted at only one confining pressure, which was that provided by the vacuum line. The values of $\phi'$ were calculated assuming that $c' = 0$.

The two fine-textured samples were tested in a standard direct shear apparatus, in the laboratory of an engineering firm (Golder Associates, of Vancouver). The shear box was 50 mm square, and the samples tested were about 25 mm thick. Each sample was mixed with water to a content approximating the liquid limit, and then consolidated in the apparatus under the normal stress used for the test. The initial volume (hence void ratio) was measured following consolidation. The sample was then sheared at a rate slow enough (about 0.4 mm/hr) to ensure that it remained in a completely drained condition. The friction angles were calculated assuming that $c' = 0$, since the samples were remolded and tested in a normally consolidated state.

It would have been desirable to test all the samples using the same method. However, the vacuum triaxial test is designed only for cohesionless material, and a standard triaxial apparatus or direct shear apparatus was not available for use at U.B.C. The direct shear apparatus which was used was not available for sufficient time to enable additional tests to be made on the coarse-textured samples.

The results of the tests are summarized in Table 6.2. The errors in the results are estimated, approximately, to be about $\pm 2°$ for $\phi'$, and $\pm 0.02$ for void ratio. Examples of test results for one sample using each test procedure are shown in Figures 6.2 and 6.3. These results clearly show the peak and residual strength behaviour described above.

The results show that the $\phi'_{cv}$ values of fine-textured and coarse-textured materials do not differ significantly from each other. The abundance of sand in the fine-textured samples is apparently sufficient that the clay in the material does not significantly influence the shear strength. The friction angles are relatively high compared to many natural sandy sediments (for example, typical values for $\phi'_{cv}$ of 27-35° given by Craig, 1987). The high values are probably due to the angular nature of the sand, which is largely derived from freshly broken rock. Owens (1973) measured comparable values (41-46°) in debris flow material derived from talus slopes.

## 6.3 PERMEABILITY

The hydraulic conductivity of a saturated soil or other porous material is a measure of the rate of flow of water under a hydraulic head, according to Darcy's law:

$$q = K\frac{dh}{dx} \tag{6.2}$$

where K is the hydraulic conductivity of the soil, q is the discharge of water per unit cross-sectional area through the soil, and dh/dx is the gradient of hydraulic head, h, with respect to length x parallel to the direction of flow. The term "permeability" refers to the conductivity of a porous medium to the flow of any fluid, and is a property of the porous medium alone (Freeze and Cherry, 1979). It is related to hydraulic conductivity by:

$$K = \frac{k\rho g}{\mu} \tag{6.3}$$

where $\rho$ and $\mu$ are the density and viscosity of the fluid, and permeability, k, has units of $m^2$. It is common in soil mechanics practice to use the term "permeability" in place of hydraulic conductivity (Lambe, 1951; Craig, 1987). In this chapter, the term "hydraulic conductivity" is used for quantitative purposes. It has units of velocity, and is not constant with temperature. The term "permeability" is used in a qualitative context as a property of the porous medium.

The hydraulic conductivity of a sample can be measured directly by applying eq. 6.2 if the hydraulic head is kept constant across the sample. However, it is often more convenient to use an apparatus known as a falling-head permeameter, in which the hydraulic head varies during the test (Lambe, 1951). Using such an apparatus, the hydraulic conductivity is calculated from

$$K = \frac{aL}{A}\frac{\Delta(\ln h)}{\Delta t} \tag{6.4}$$

where a and A are the cross-sectional areas of the standpipe and sample, respectively, L is the length of the sample, and t is time.

Figure 6.5 is a diagram of the falling-head permeameter which was built for this study. For each test, a sample of debris matrix (< 4 mm) was mixed with water to a water content reasonably close to the liquid limit, and packed into the permeameter cylinder. The sample was separated from the rest of the apparatus by two filters, each consisting of a piece of nylon dish-scrubbing pad, with a disk of filter paper for fine-textured samples, or of 0.074 mm sieve mesh

for coarse-textured samples. Tests were done on several debris flow samples and, for comparison, a sample of sandy gravel sieved to < 4 mm, from the channel of the Lillooet River.

The results of the tests are given in Table 6.3, and show several orders of magnitude variability in hydraulic conductivity. The permeability of a sediment is controlled mainly by the finer portion of the grain size curve. In Figure 6.4, hydraulic conductivity is graphed against the proportion of fines (silt + clay) in the sample, and against $D_{10}$. (In soil mechanics, $D_{10}$ is sometimes used as an index which is related to permeability .) The hydraulic conductivity of several samples was also measured by the constant-head method (eq. 6.2) following consolidation tests (see next section). These results are included in Table 6.3 and Figure 6.4.

Complete saturation of the samples was not achieved in the tests, and therefore the measured values may be slightly lower than the true saturated hydraulic conductivity. However, the saturation levels are probably comparable to those normally occurring in debris flows.

As explained in the following section, the permeability of debris may be relevant in debris flow behaviour, as it controls the rate of dissipation of excess pore water pressure in undrained debris.

## 6.4 CONSOLIDATION TESTS

Consolidation, in soil mechanics, is the amount and rate of settlement of a compressible sediment under a change in effective stress. If a load is applied to a saturated soil, the change in stress is borne first by the pore water, and then as drainage occurs and the soil compresses, the stress is transferred to the soil particles. The rate of settlement is determined by the rate of dissipation of excess pore water pressure.

During debris flow, it is a reasonable assumption that the debris is totally undrained, *i.e.* effective stress $\sigma'$ is zero. A possible hypothesis for the mobility of a debris flow as it spreads out on an alluvial fan is that $\sigma'$ may not be zero, if excess pore water pressure is being dissipated, and thus frictional strength may develop. Therefore, consolidation theory may be a useful tool in investigating debris flow mobility. (Hutchinson, 1986, used a consolidation model to explain the behaviour of the coal waste failure of 1966 in Aberfan, Wales.)

The standard consolidation test in soil mechanics is an empirical procedure, designed to give results which enable the prediction of the amount and rate of settlement of a compressible soil under a load. The test is based on the one-dimensional consolidation theory of Terzaghi (1943), and is described in Craig (1987) and Lambe (1951). According to the theory, consolidation can be described by:

$$\frac{\partial u}{\partial t} = c_v \frac{\partial^2 u}{\partial z^2} \tag{6.5}$$

where u is pore water pressure, z is depth below the surface of the soil layer, and t is time. $c_v$ is the coefficient of consolidation, a property of the soil, which is proportional to permeability and inversely proportional to compressibility. Thus, if a soil is both highly compressible and of low permeability, the rate of consolidation will be low. The rate of consolidation depends directly on $c_v$ and inversely on the square of the length of the drainage path.

For this study, a simple apparatus was built (Figure 6.6) to measure the consolidation and the dissipation of excess pore water pressure in freshly deposited debris. It consists of a piece of nominal 8-inch plastic water pipe with a solid base, connected to a pressure transducer. A pressure transducer was used to avoid the slow response which would result from the use of an open manometer. The base of the cylinder contains a filter consisting of fine gravel, separated from the sample by a metal screen. In each test, a sample of debris was mixed to a water content at which it would flow, which is slightly greater than the liquid limit. The base of the cylinder was filled with water to the top of the filter, and the debris was poured in and thoroughly mixed. As it consolidated, pore water pressure was recorded by the pressure transducer, and periodic measurements were made of the surface level of the debris. The density and void ratio of the sample were measured by weighing the sample in the apparatus, assuming the sample was completely saturated. The pressure transducer measurements were found, during calibration, to be precise to about ± 0.2 kPa over the range of pressures recorded.

The samples tested were from three debris flows (Boundary 1987, Hot Springs 1984, and Ryan 1984), sieved to smaller than 16 mm.

The test described here is different than the standard soil mechanics test (the oedometer test) in that the sample is loaded only by self-weight, and the range of stresses over which consolidation is measured is very low. However, this is the stress range of interest for the debris flow problem. In the standard soil mechanics test, the sample is very thin compared to the pressure head to which it is subjected; thus $\sigma'$ can be assumed equal throughout the sample. This is not the case in this experiment.

Figure 6.7 shows the results of the pore water pressure measurements. The graphs clearly show that the rate of excess pore water pressure dissipation is at least two orders of magnitude slower in the fine-textured sample (Boundary) than in the coarse-textured samples. If the results are plotted on a logarithmic axis of excess pore water pressure, they plot as a relatively straight line for the central part of the consolidation curve. The inverse slope of this line, t*, is a measure of the rate of consolidation. It is given in Table 6.4. For each test, the pressure eventually equilibrated at a level slightly above the hydrostatic water level. The reason for this is not clear; it is possible that minor ambient vibrations or temperature fluctuations prevented complete drainage. The graph of the Boundary sample shows a diurnal pattern, probably due to temperature changes.

Following each consolidation test, the cylinder was shaken slightly. This resulted in an increase in pore water pressure to the geostatic level (*i.e.* liquefaction). Only a slight tap was required to cause liquefaction. The rate of subsequent consolidation was much faster than the initial rate, because only a very small decrease in void ratio was necessary during consolidation.

For the debris flow problem, the rate of change of pore water pressure is the relevant quantity. However, the other parameters of the consolidation theory can be calculated, given frequent measurements of the sample thickness. The coefficient of consolidation $c_v$ is calculated by one of two empirical methods, using graphs of thickness versus the logarithm of time or the square root of time. These graphs are shown for the Boundary sample in Figure 6.8. The graphs are very similar to those for theoretical curves, and for "textbook examples" of standard consolidation tests on clay samples (Lambe, 1951; Craig, 1987), although the results for the coarse-textured samples are less perfect.

From the coefficient of consolidation, the hydraulic conductivity can be indirectly calculated. If this calculation is carried out for the Boundary sample, the calculated hydraulic conductivity is $1.7 \times 10^{-8}$ m/s, very similar to the directly measured value. This result, and the graphs in Figure 6.8, suggest that the consolidating debris in this experiment behaves in a manner very similar to consolidation in the standard oedometer test. However, the experiment differs from the standard test in that consolidation takes place under self-weight; the thickness of the sample is not small compared to the applied stress, and the amount of compression is not constant throughout the thickness of the sample. Therefore, it is probably not reasonable to calculate the coefficient of consolidation and other parameters from this test.

Following each test, the hydraulic conductivity was directly measured by opening the tube at the base of the cylinder, and adding water at the top. The water draining from the bottom of the cylinder during the final permeability test was clean, indicating that the fluid moving through the pores is water, not a clay-water slurry. On emptying the cylinder following each test, the density of the sample appeared to have increased with depth, due to higher $\sigma'$ near the bottom. There was no visible sign that differential settling of coarse clasts had occurred.

An experiment similar to this one was performed by Pierson (1981), on samples of a debris flow which consisted of about 14% clay as a proportion of < 2 mm material. He used open tube piezometers in samples 87 to 200 mm deep, with slurries ranging from the silt + clay fraction only, to a sample with stones to cobble size. For the coarser samples, most of the dissipation of excess pore water pressure occurred in about 1 to 2 hours, faster than for the clayey (Boundary) sample in the present study. The faster drainage may be explained by the shorter drainage path.

## 6.5 DISCUSSION OF GEOTECHNICAL TESTS AND IMPLICATIONS FOR DEBRIS FLOW MOVEMENT

The tests described above show that permeability is the most significant characteristic which distinguishes the fine-textured and coarse-textured debris samples. The content of cohesive material (clay and possibly fine silt) in the Boundary and Meager samples causes permeability to be at least two orders of magnitude lower than in the sandy samples (Hot

Springs and Ryan). This in turn causes the rate of consolidation, or dissipation of excess pore water pressure, to be proportionately slower.

The angle of internal friction is about the same for the fine-textured and coarse-textured samples, since both types of material are predominantly sand. This quantity, therefore, does not help in explaining the different mobility of fine-textured and coarse-textured debris flows. However, greater effective normal stress in partially drained, coarse-textured debris flows would contribute to frictional strength.

The question which remains to be answered is whether the rate of drainage of excess pore water pressure could have a significant effect on debris flow mobility. From the graphs in Figure 6.7, some reduction in excess pressure, about 20%, takes place very quickly. This initial drainage took about 30 seconds in the coarse-textured samples, and about 5 minutes in the fine-textured sample. When mixing the samples, it was quite difficult to keep the coarse-textured debris in an undrained state; unless the mixing was continuously vigorous, the debris would suddenly stiffen, indicating that some drainage and development of frictional strength were taking place. However, the fine-textured debris would remain completely undrained for at least several minutes following mixing. This behaviour was quite noticeable during the flume tests (Chapter 8). Thus, it is reasonable to speculate that, in the time it takes to flow in the order of 100 m on an alluvial fan, some drainage might take place in coarse-textured debris, which would allow significant frictional strength to develop. However, a contrary observation is that following consolidation, it was easy to liquefy the samples by vibrating them. The constant vibration to which debris would be subject during even slow flow might prevent any dissipation of excess pore water pressure from taking place.

As an example, suppose that a debris flow 1 m thick, with $\gamma = 21$ kN/m$^3$ and $\phi' = 42°$, initially completely undrained, flows across a 10° fan and comes to rest through the development of frictional strength. From the Coulomb shear strength equation (eq. 6.1) with $c' = 0$, it can be calculated that the pore water pressure, u, would have to drop from 20.7 to 16.6 kPa for equilibrium to be reached. A 1 m thickness of debris, draining to both the top and bottom, would have a drainage path length of 0.5 m, the same as in the consolidation experiments. This

amount of drainage could take place, for coarse-textured material, in several minutes or less, but would require an hour or longer in fine-textured debris.

The above discussion suggests that consolidation of coarse-textured debris might possibly contribute to frictional strength during debris flow deposition. However, consolidation of fine-textured debris is so slow that no significant frictional strength is likely to develop in the several minutes required for deposition. This latter statement is supported by the field observation that, on several occasions during this study, fine-textured debris flows were found to be in an almost completely undrained state several days after emplacement.

TABLE 6.1 CONSISTENCY LIMITS

| Sample | $w_L$ | $w_P$ | $I_P$ | sand:silt:clay in sample <4mm | Remarks |
|---|---|---|---|---|---|
| Boundary 1987-1 | 24 | 21 | 3 | 69:21:10 | |
| Boundary 1987-1, <0.074mm | 44 | 27 | 17 | 69:21:10 | |
| Boundary 1987-1, < 4 mm | 18 | NP | | 69:21:10 | Liquifaction water content |
| Boundary 1988-2 | 25 | 21 | 4 | 67:23:10 | |
| No Good, early 1980s-1 | 25 | 21 | 4 | 69:20:11 | |
| No Good 1988-2 | 24 | 20 | 4 | 67:23:10 | |
| Meager 1931-1 | 21 | 20 | 1 | 68:22:10 | |
| Meager 1931-3 | 21 | 20 | 1 | 69:22:9 | |
| Upper Lillooet 900 BP - 1 | 19 | NP | | 74:19:7 | |
| Canyon 1987-2 | 19 | NP | | 74:20:6 | |
| Hot Springs 1984-1 | 19 | NP | | 81:16:3 | Liquifaction water content |
| Turbid 1984-1 | 20 | NP | | 75:19:6 | |
| Fountain 1989-2 | 19 | 16 | 3 | 69:22:9 | |

Notes: Sample: last digit is sample number, where several samples were taken.
$w_L$ = Liquid limit; $w_P$ = Plastic limit; $I_P$ = Plasticity index = $w_L$-$w_P$.
All limits are given in %.
NP = non-plastic.
"Liquifaction water content": no true liquid limit was observed; $w_L$ is the water content at which the sample could be liquified by vibrating.
"sand" in samples < 4 mm includes granules (2-4 mm).
All samples are sieved to < 0.42 mm, except as noted.

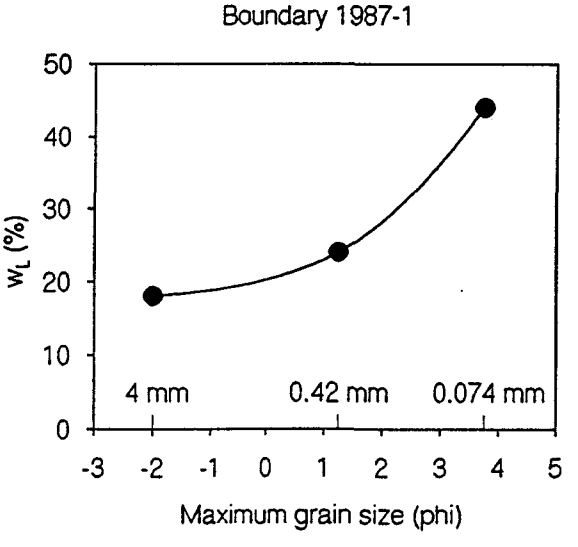


FIGURE 6.1

LIQUID LIMIT AND SAMPLE GRAIN-SIZE

TABLE 6.2 SHEAR STRENGTH TESTS

All stresses are given in kPa. Tests were performed on material < 4 mm.

A. DIRECT SHEAR TESTS

| Sample | Boundary test 1 | Boundary test 2 | Meager test 1 | Meager test 2 |
|---|---|---|---|---|
| Normal stress $\sigma'_n$ | 49.6 | 101.8 | 49.6 | 101.8 |
| Shear stress at peak, $\tau_p$ | 50.5 | 93.5 | 54.4 | 111.3 |
| Void ratio e (beginning) | 0.529 | 0.496 | 0.412 | 0.417 |
| Void ratio e (end) | 0.538 | 0.496 | 0.431 | 0.437 |
| Angle of friction $\phi'_p$ (peak) | 45.5° | 42.6° | 47.6° | 47.6° |
| Angle of friction $\phi'$ (large displacement) | 42.2° | 39.7° | 39.6° | 41.0° |
| Dilation during test | +0.6% | 0 | +1.4% | +1.4% |

B. TRIAXIAL TESTS

| Sample | Hot Springs test 1 | Hot Springs test 2 | Hot Springs test 3 | Ryan test 1 | Ryan test 2 |
|---|---|---|---|---|---|
| Confining stress $\sigma'_3$ | 68.5 | 74.2 | 67.6 | 76.9 | 75.3 |
| Deviator stress at peak $\sigma'_1-\sigma'_3$ | 461 | 401 | 269 | 512 | 368 |
| Void ratio e (beginning) | 0.496 | 0.557 | 0.692 | 0.433 | 0.553 |
| Void ratio e (end) | 0.544 | 0.571 | 0.635 | - | 0.558 |
| Angle of friction $\phi'_p$ (peak) | 50.4° | 46.9° | 41.9° | 50.2° | 45.2° |
| Angle of friction $\phi'$ (large displacement) | 49.3° | 43.5° | 41.7° | 46.6° | 44.3° |
| Dilation during test | +3.2% | +0.9% | -3.4% | - | +0.4% |

C. INTERPRETATION OF SHEAR STRENGTH TESTS

| Samples | Boundary | Meager | Hot Springs | Ryan |
|---|---|---|---|---|
| Constant volume void ratio $e_{cv}$ | 0.54 | 0.44 | 0.59-0.63 | 0.55 |
| Corresponding water content w [1] | 0.19 | 0.16 | 0.21-0.22 | 0.19 |
| Angle of friction $\phi'_{cv}$ | 40-42° | 40-41° | 42° | 44° |

[1] Assuming $S_r = 0.95$.

TABLE 6.3 PERMEABILITY TESTS

A. TESTS IN FALLING-HEAD PERMEAMETER, SAMPLES < 4 mm.

| Sample | Hydraulic conductivity K (m/s) | Void ratio e | Water content w | Satu-ration ratio $S_r$ | Proportion sand:silt:clay | $D_{10}$ (mm) | Remarks |
|---|---|---|---|---|---|---|---|
| Boundary 1987-1 | $1.2x10^{-8}$ | 0.53 | 0.188 | 0.96 | 69:21:10 | 0.0036 | |
| Meager 1931-3 | $4x10^{-9}$ | 0.50 | 0.167 | 0.90 | 69:22:9 | 0.0044 | K varied from 2.5 - 5 $x10^{-9}$ m/s |
| Canyon 1987-2 | $5.3x10^{-8}$ | 0.55 | 0.179 | 0.87 | 74:20:6 | 0.0098 | |
| Hot Springs 1984-3 | $1.3x10^{-6}$ | 0.55 | 0.178 | 0.88 | 82:15:3 | 0.028 | |
| Ryan 1984-1 | $1.8x10^{-6}$ | 0.46 | 0.148 | 0.87 | 91:9:0 | 0.78 | |
| Lillooet River fluvial | $6.3x10^{-5}$ | 0.61 | 0.192 | 0.83 | 96:4:0 | 0.149 | |

Note: Last digit of "sample" refers to sample number, where several samples were taken. "Sand" in samples < 4 mm includes granules (2-4 mm).

B. TESTS IN CONSOLIDATION CYLINDER, SAMPLES < 16 mm.

| Sample | Hydraulic conductivity K (m/s) | Void ratio e | Remarks |
|---|---|---|---|
| Boundary 1987 | $2.1x10^{-8}$ | 0.56 | e varied through sample; mean e may be lower |
| Hot Springs 1984 | $1.0x10^{-6}$ | 0.32 | |
| Ryan 1984 | $2.3x10^{-6}$ | 0.32 | |

Note: Measurements were made following consolidation tests, using constant-head formula. Proportion of pebbles > 4 mm was not recorded. Data are plotted on Fig. 6.4 using grain size parameters from part A, assuming the additional pebbles do not affect permeability.

TABLE 6.4 RESULTS OF CONSOLIDATION TESTS

| Sample | Boundary | Hot Springs | Ryan |
|---|---|---|---|
| Initial length L (mm) | 521 | 507 | 485 |
| Change in length $\Delta L$ (mm) | 21.3 | 18.0 | 14.0 |
| Initial void ratio $e_0$ | 0.582 | 0.344 | 0.339 |
| Final void ratio $e_1$ [1] | 0.567 | 0.320 | 0.319 |
| Average effective stress change $\Delta\sigma'$ (kPa) [2] | 2.7 | 3.2 | 3.1 |
| t* (hrs) [3] | 95 | 0.65 | 0.23 |

Notes:

1. Average void ratio calculated from $\Delta L$. Void ratios were not constant throughout samples following tests.
2. $\Delta\sigma'$ at base is assumed to be the difference between $\sigma'_0 = 0$, and $\sigma'_1 = \sigma - u_H$ under fully drained conditions. Average $\Delta\sigma'$ for the sample is half of this.
3. Defined as the time required for excess pore water pressure, $u - u_H$, to drop to 1/e of an initial value (where e is the base of natural logarithms), calculated from the slope of a plot of ln $(u - u_H)$ vs. time.

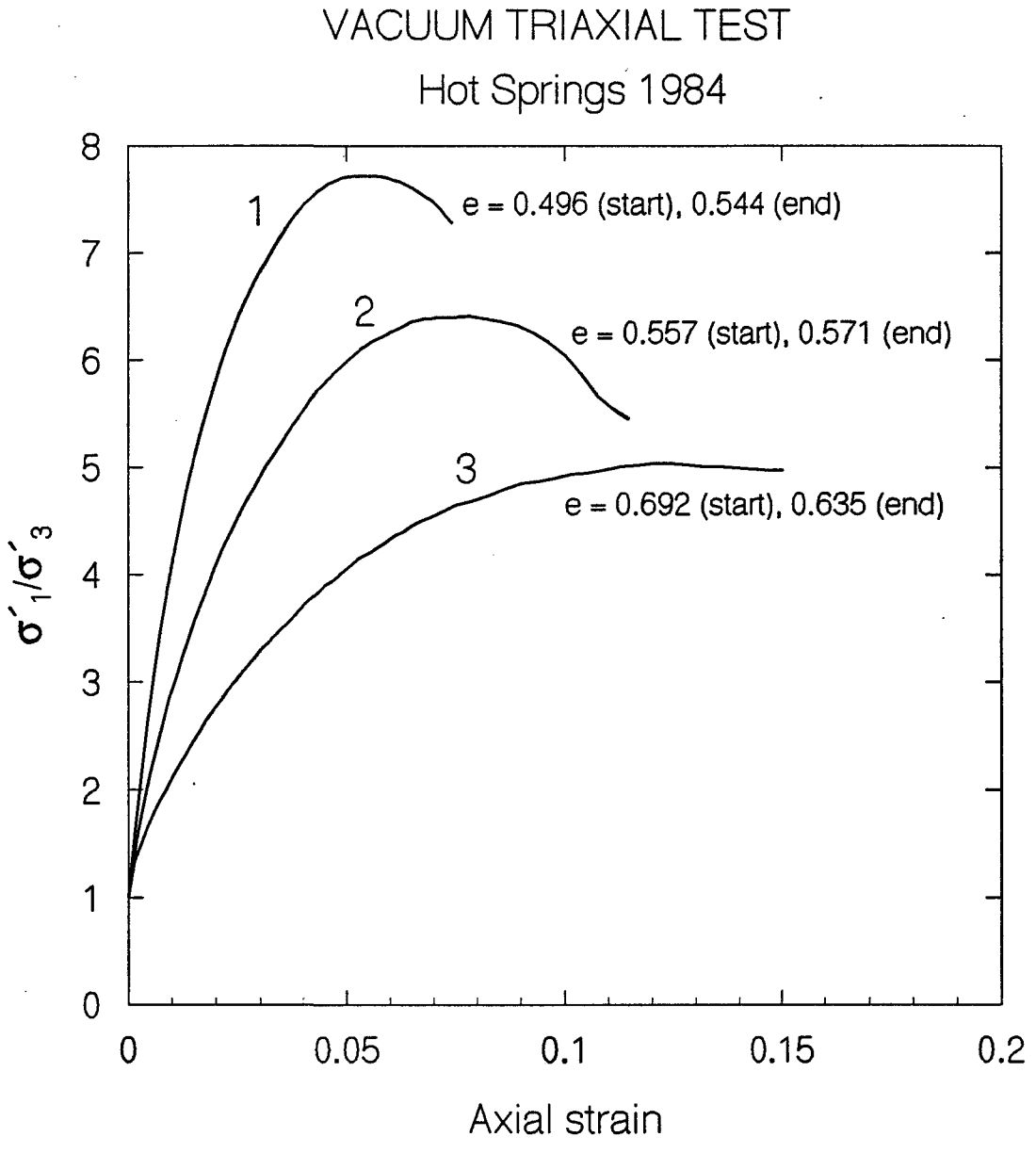


FIGURE 6.2. EXAMPLE OF TRIAXIAL SHEAR TEST RESULTS.
$\sigma_3'$ = confining stress; $\sigma_1'$ = axial stress = $\sigma_3' + \sigma_d$.

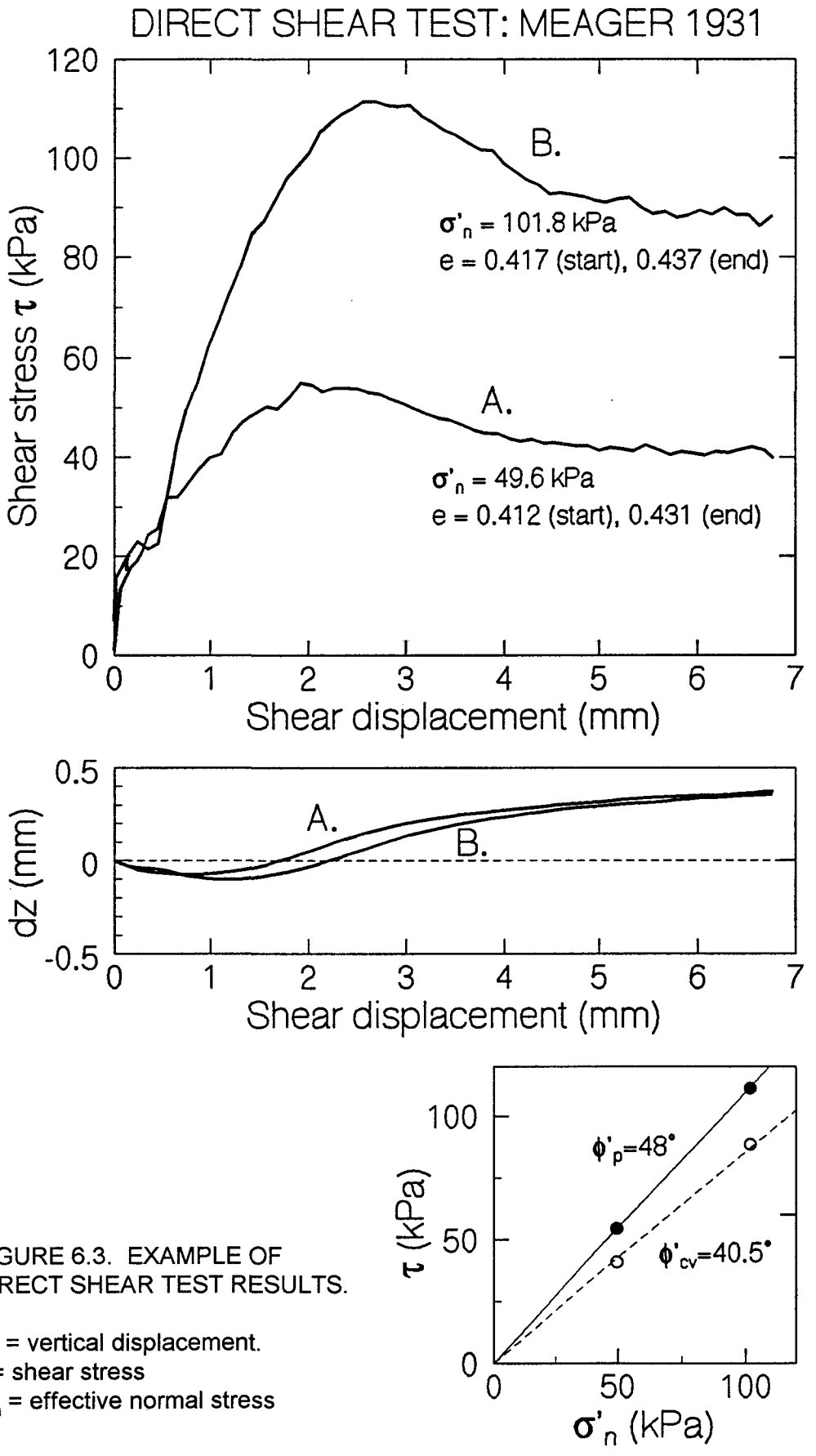


FIGURE 6.3. EXAMPLE OF DIRECT SHEAR TEST RESULTS.

dz = vertical displacement.
$\tau$ = shear stress
$\sigma'_n$ = effective normal stress

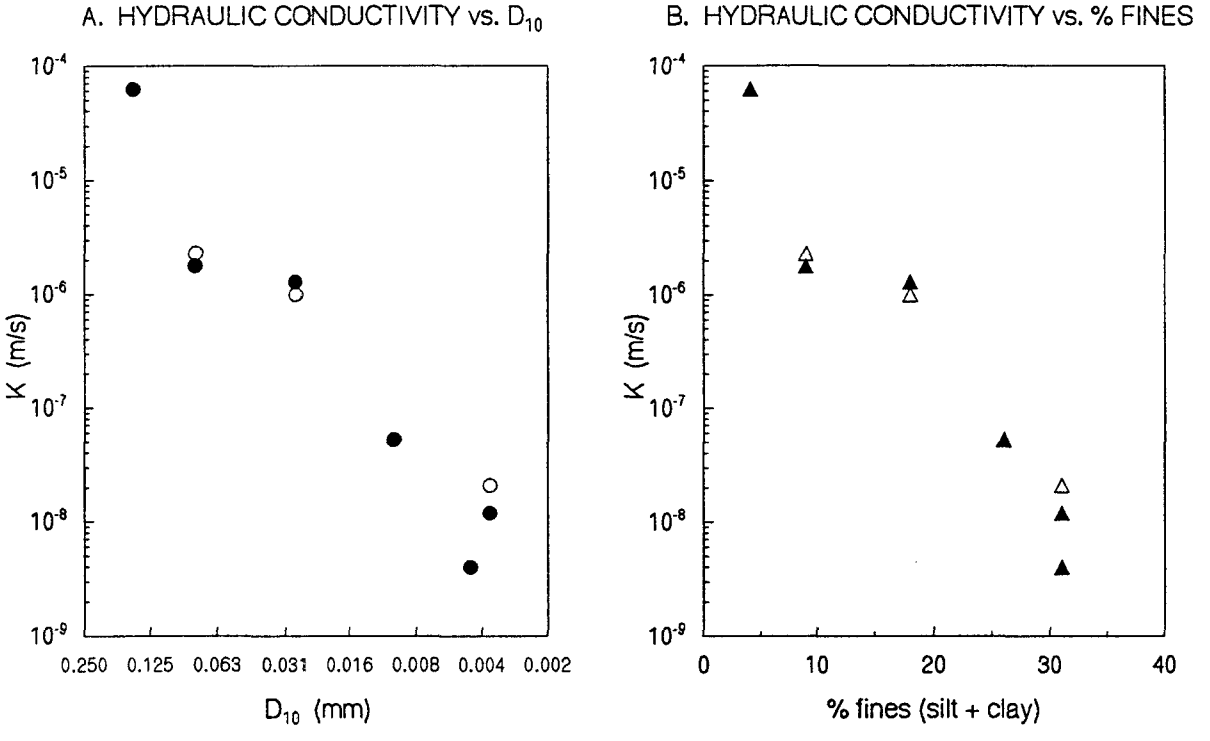


FIGURE 6.4. HYDRAULIC CONDUCTIVITY AND GRAIN-SIZE PARAMETERS.
Closed symbols are measurements made with the falling head permeameter. Open symbols are measurements made in the consolidation cylinder. Grain size parameters are for samples < 4 mm.

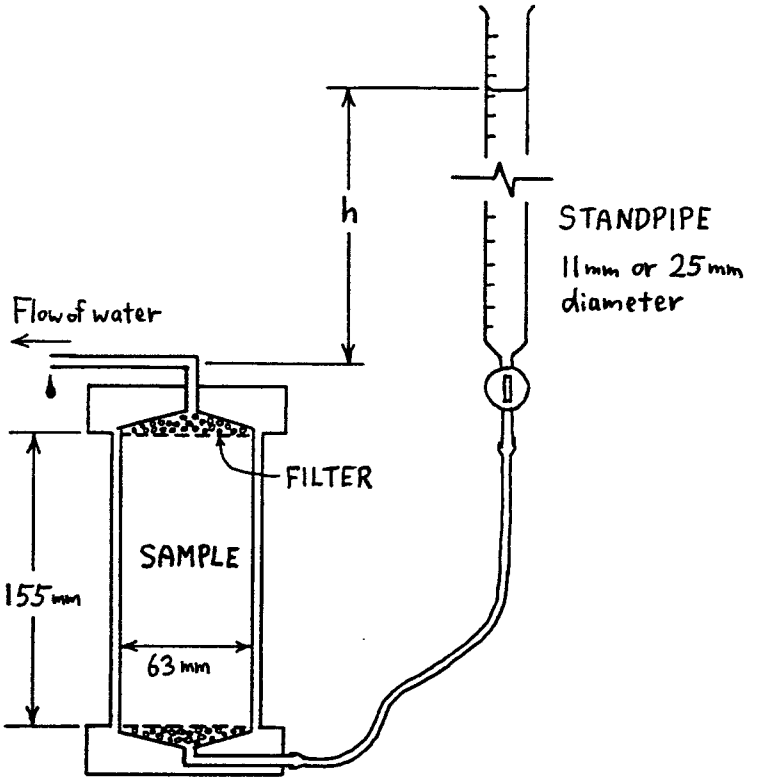


FIGURE 6.5. SKETCH OF PERMEAMETER.

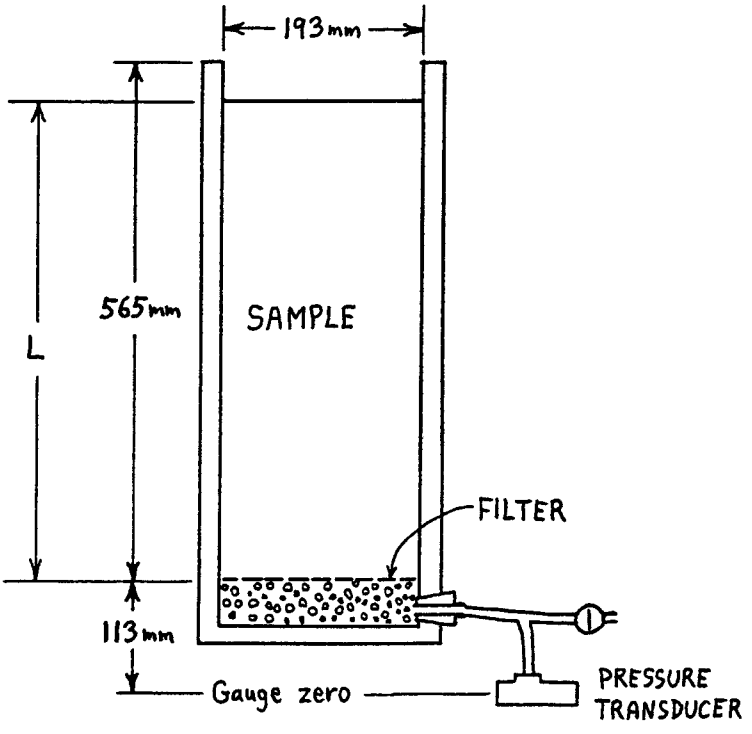


FIGURE 6.6. SKETCH OF CONSOLIDATION CYLINDER.

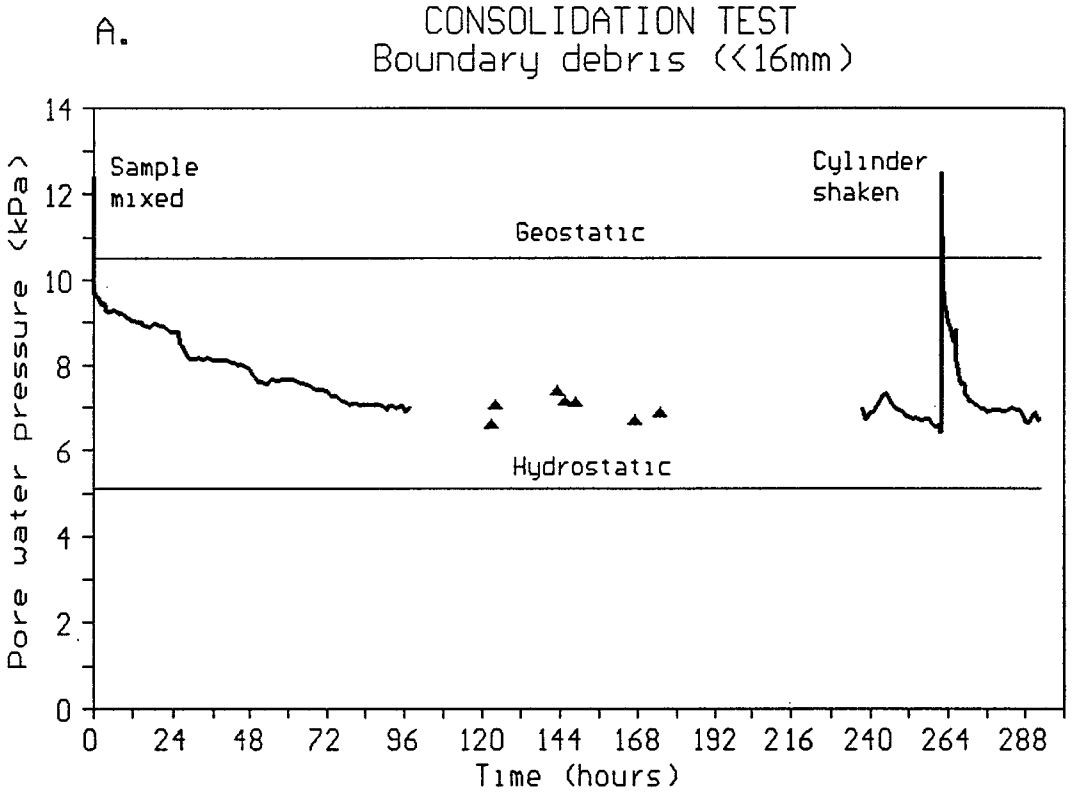


FIGURE 6.7. CONSOLIDATION TESTS: PORE WATER PRESSURE. Geostatic water pressure = $\sigma = \gamma L$. Hydrostatic water pressure = $\gamma_w L$. Triangle symbols in graph A indicate point readings when recorder was not running.

B.

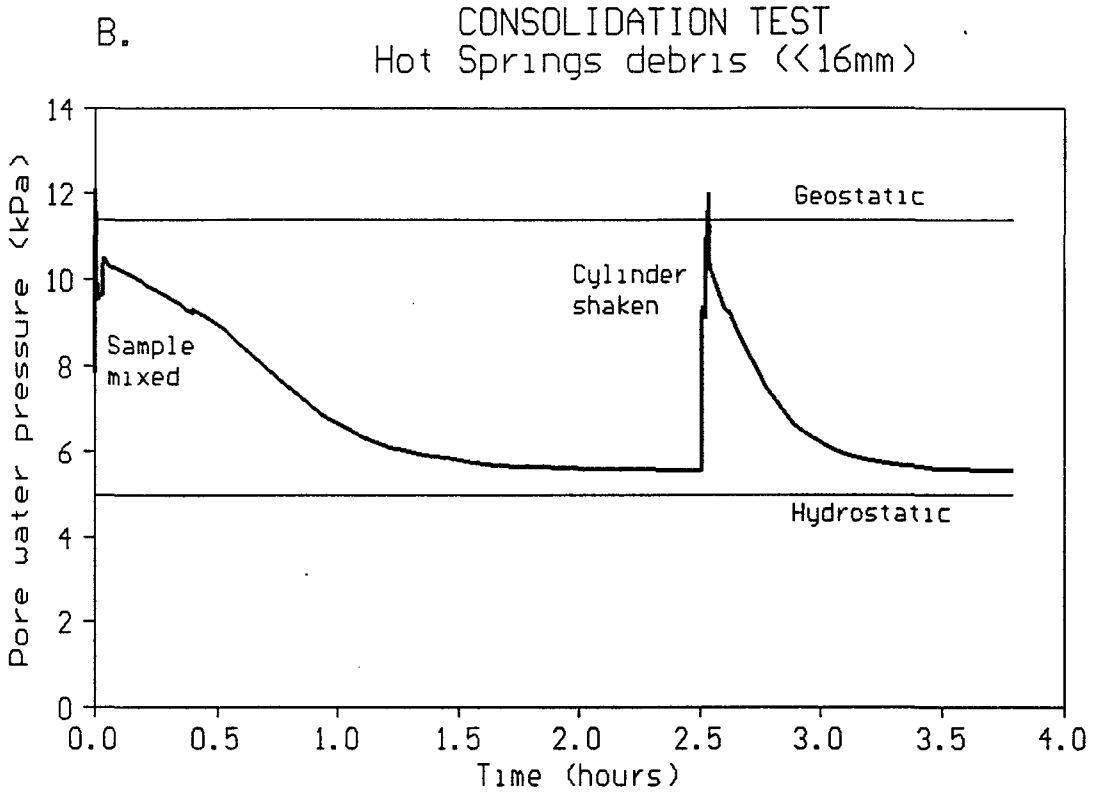
CONSOLIDATION TEST
Hot Springs debris (<16mm)
Pore water pressure (kPa)
Time (hours)
Geostatic
Hydrostatic
Sample mixed
Cylinder shaken
0
2
4
6
8
10
12
14
0.0
0.5
1.0
1.5
2.0
2.5
3.0
3.5
4.0

C.

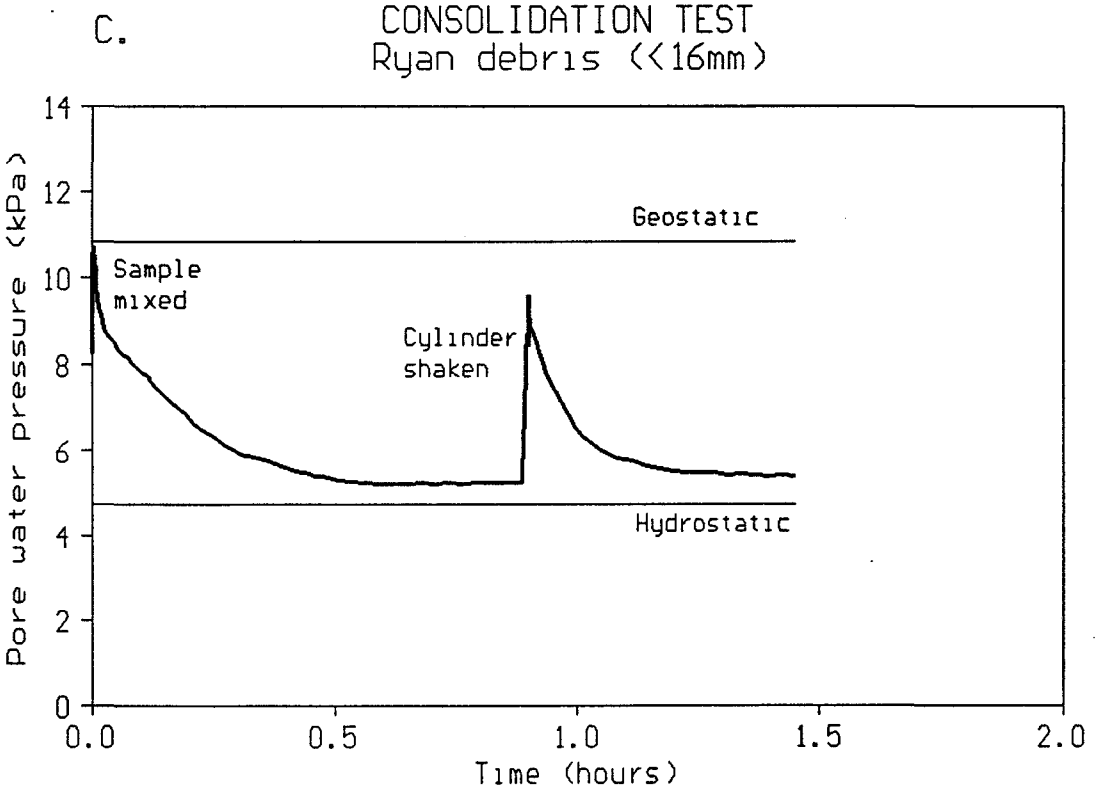
CONSOLIDATION TEST
Ryan debris (<16mm)
Pore water pressure (kPa)
Time (hours)
Geostatic
Hydrostatic
Sample mixed
Cylinder shaken
0
2
4
6
8
10
12
14
0.0
0.5
1.0
1.5
2.0

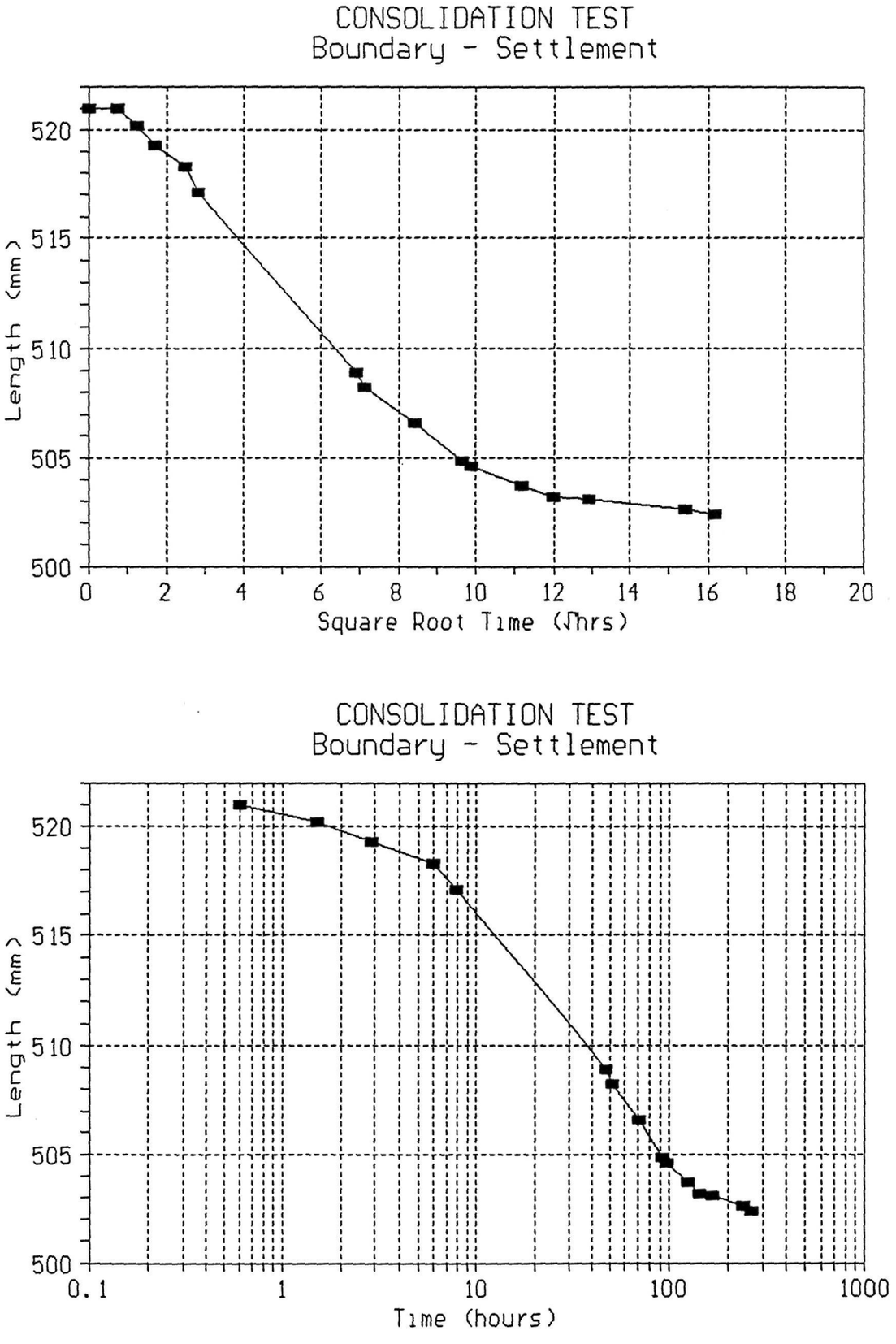


FIGURE 6.8. CONSOLIDATION TESTS: RATE OF SETTLEMENT.

# CHAPTER 7. DYNAMIC BEHAVIOUR OF DEBRIS FLOW EVENTS

Chapters 5 and 6 described the sedimentological and geotechnical properties of debris flow deposits, which are debris flow material at rest. In this chapter, an attempt is made to reconstruct the properties of the debris flows in motion. In the absence of direct observation of moving debris flows, this reconstruction relies on calculations of velocity based on the superelevation equation (eq. 2.34). The assumptions inherent in this calculation are discussed in section 2.4. The channel dimensions for superelevation and discharge calculations are based on measurement of mud lines left by debris flows. These reflect the peak flow stage of the largest surge. As discussed earlier, debris flows often consist of numerous surges, so the properties calculated from the peak flow of one surge may not be representative of the average properties of the entire event. Information on lesser flow stages is rarely available from evidence in the channel following an event.

Velocity calculations could not be made for all debris flow events, due to a lack of suitable cross-sections. For example, the channel of Hot Springs Creek is nearly straight, with no bends of short radius in which superelevation could be measured.

## 7.1 DEBRIS FLOW VELOCITY

Table 7.1 lists the channel cross-sectional data for all the sites at which superelevation measurements were made. The channel dimensions were surveyed with a theodolite, or with a tape and hand-held clinometer and compass, as described in Chapter 4. The hand surveys are sufficiently precise for superelevation calculations, although the theodolite surveys allow more precise calculation of cross-sectional area, and also allow the location of maximum superelevation to be more precisely determined. Details of several of the sites are given below.

### Boundary Creek

A number of cross-sections in the Boundary Creek channel were surveyed on three occasions, following the debris flow events of 1987, 1988, and 1989. The locations are shown on Figure 7.1. Two channel bends, marked A and B, were suitable for superelevation

measurements. Only section A was surveyed following the 1989 event. Figure 7.4 shows a photograph taken at section B following the 1988 event.

The 1987 and 1988 events were quite similar in velocity and cross-sectional area, although the estimated total volume of the 1987 event is 10 times greater. This suggests that the 1988 event consisted of a small number of surges, perhaps only one, while the 1987 event may have consisted of many surges. The 1989 event was intermediate in total volume but had the greatest peak discharge. This poor correlation between total volume and peak discharge creates difficulties in trying to develop empirical methods for predicting velocity, depth of flow, and runout distance (see Hungr *et al.*, 1984, and section 7.3 below). The larger volume of the 1987 event is consistent with the fact that this was the first major debris flow in 5 or more years, while the 1988 event occurred in a channel which had been stripped clean of debris the previous year.

At both bends on Boundary Creek, several cross-sections were surveyed on two or three occasions (Figure 7.1). These surveys showed that during each of the 1988 and 1989 events, the channels were deepened by 0.5 to 2 m. This erosion did not take place uniformly, which explains why, in Table 7.1, the slope is different for each event at site A.

Devastation Creek 1931 debris flow

This debris flow event is unique because of its great size, and because it stripped a path though mature forest, enabling its trim lines to be clearly visible 60 years later. Figure 7.2 shows a map of the debris flow path in the upper valley of Meager Creek, and several cross-sections of the channel. As the debris turned the corner at the confluence of Devastation and Meager Creeks, it banked up the valley wall to an elevation of 105 m above the valley floor. Figure 7.3 shows photographs of the trim lines of this debris flow at its point of greatest superelevation, and in the reach between Boundary and No Good Creeks.

The geometry of the bend is not ideal for the application of the superelevation equation, since it is not of uniform radius but instead consists of an approximately planar mountainside which the debris flow intercepted at a horizontal angle of about 40°. Using the superelevation equation, an approximate velocity of 36 m/s is calculated. The main uncertainty in the calculation is the radius of curvature of the bend. This estimate, however, is believed to be

reasonable, since the velocity-head equation gives a figure of about 40 m/s; the latter equation, however, is not as applicable, since the debris struck the mountainside obliquely and did not completely stop. Proceeding around the bend, the debris sloshed across to the other side of the valley and crossed the fan of Boundary Creek, stripping off the forest and leaving a thin veneer of debris. Application of the superelevation equation at this site gives a velocity estimate of 24 m/s. The debris flowed down Meager Creek at an average depth of about 12 m, as shown by the average elevation of trees stripped from above the river channel. Based on this average depth and a velocity of 24 m/s, the peak discharge was in the order of 70,000 $m^3$ $s^{-1}$.

In this reach of Meager Creek, the flow was highly unsteady, as it was decelerating rapidly where the channel gradient decreased from 5° in the Devastation Creek valley to 2° in the Meager Creek valley. This factor, combined with the approximations inherent in the application of the superelevation equation, make the calculation of flow parameters subject to considerable uncertainty. However, the estimated velocity and peak discharge appear to be reasonable; they are comparable to those calculated from lahars of similar magnitude resulting from the 1980 eruption of Mount St. Helens (Janda *et al.*, 1981; Pierson, 1985).

The velocity and peak discharge of this event, and its estimated minimum volume of 3 x $10^6$ $m^3$, make it the largest known debris flow in historic time in North America that was not associated with a volcanic eruption.

Canyon Creek

The channel of Canyon Creek immediately above the debris flow fan consists of a bedrock canyon with a sharp S-shaped bend, shown in Figure 4.18. The upper bend is not suitable for velocity calculations, as the channel slope and cross-section are not uniform and there is a waterfall just above the bend. However, the channel slope and width are quite uniform from the centre of the S-bend to the fan. The two cross-sections given in Table 7.1 are the lower part of the S-bend, and a bend of lesser arc just downstream. Figure 7.4 shows a photograph of the superelevation in the canyon.

Velocity can also be estimated from observations of runup on tree trunks in the path of the flow, using eq. 2.36. Runup was measured on 18 trees on the Canyon Creek fan, shortly after

the 1990 debris flow event. These measurements yielded a mean velocity of 4.2 m/s, with a standard deviation of 0.9 m/s. This is about half the velocity calculated in the canyon upstream, and is reasonably consistent with the decrease in velocity that would be expected as debris spreads out on the fan.

Turbid Creek 1984

The lower channel of Turbid Creek is very straight and uniform, with a width of 40 to 50 m and a depth of 10 to 14 m (Fig. 4.25). Although the highest trim lines are clearly visible, it was not possible to distinguish between those left by the June and October events of 1984. However, there is one sharp bend in the channel 1.8 km above its mouth, which enables velocity estimates to be made. The bend of Turbid Creek is not ideal for application of the superelevation equation; the radius of the bend varies, and it contains a steep bank perpendicular to the approach direction. In this situation, the velocity-head equation (eq. 2.35) might be equally applicable, although it should give a minimum velocity since the debris did not stop at its point of greatest runup. At this bend, the superelevation equation gives a velocity of 8 m/s, while the velocity-head equation gives 12 m/s. The average of the two, 10 m/s, is used as the most reasonable estimate of velocity.

Other sites

Several debris flow channels which had apparently suitable bends did not show measurable superelevation. The smallest amount of superelevation which can reasonably be surveyed, for channels in the order of 10 m wide and with relatively uniform and fine-textured debris levées, is about 0.2 m. Based on this lower limit, the velocity of the No Good Creek 1988 debris flow must have been less than 5 m/s, while that of the Fountain 1989 and McGillivray 1989 events must have been less than 3 m/s. The bends in the latter two channels were near the apex of their respective fans. As discussed in Chapter 4, the cross-sectional area and velocity of these debris flows apparently decreased down the fan through deposition of levées. The Newtonian viscosity of these debris flows, calculated from these velocity ranges, would be greater than 400 Pa.s for No Good, and greater than 3000 Pa.s for Fountain and McGillivray.

The superelevation site for the Angel Creek B 1990 debris flow is near the apex of its fan. Another bend lower on the fan did not show measurable superelevation, and the velocity is therefore estimated at less than 2 m/s (Table 7.1). The cross-sectional area of this channel decreased down the fan as levées were deposited, and the superelevation results also indicate that velocity dropped.

## 7.2 RHEOLOGIC PARAMETERS AND FLOW REGIME

From the estimated velocity and measured cross-sections, the apparent Newtonian viscosity of each debris flow can be calculated from eq. 2.26. Table 7.2 gives the Newtonian viscosity, and other flow parameters, of each debris flow event. Average values are given for those events in which velocity was calculated at two sections. The range of velocities in Table 7.1 gives an indication of the error to which the calculations are subject. The error in the calculated viscosity is estimated to be about ± 20% to 50% or more, depending on the quality of the superelevation measurements at each section.

The Bingham yield strength can be calculated from eq. 2.9, for debris flow deposits which are fairly uniform in thickness, and the Bingham viscosity can then be calculated from eq. 2.33. This calculation assumes that the debris properties at the location where the deposit thickness is measured are representative of the debris at its peak flow stage in the channel upstream. Only four debris flows had uniform deposits from which the Bingham parameters could be calculated (Table 7.2). The Boundary 1988 debris flow left a very uniform deposit, which may have been the result of a single surge. The Boundary 1989 deposit was somewhat more uneven, with an average thickness ranging from about 0.8 to 2.0 m (Fig. 4.8). The parameters given in Table 7.2 are based on an average thickness of 1.4 m. It is possible that this deposit is the result of multiple surges containing material of varying yield strength, or that coarse frontal lobes from some surges underlie part of the deposit, causing variations in thickness. A yield strength cannot be calculated for the Boundary 1987 event, since its deposit forms a tapering wedge shape, and no detailed information is available on the underlying floodplain surface.

The rheologic parameters of the Devastation 1931 debris flow are given as ranges, since as noted above, there is considerable error attached to the velocity and cross-sectional area estimates.

There is a tendency for the apparent Newtonian viscosity to be greater for coarser-textured debris flows. (The logarithm of viscosity is highly correlated with the matrix clay content, with $r = -0.853$, but it is not significantly correlated with mean grain size.) The Turbid Creek 1984 event has an unusually high viscosity for a volcanic-source debris flow. Its deposits were poorly preserved, and it is possible that the debris at the peak flow stage contained a higher proportion of entrained channel gravel than was in the small debris flow remnant which was sampled. It is also possible that the two 1984 events had different texture and flow properties.

The granular resistance term for the dilatant flow model (eq. 2.32) can be calculated from the same data used for the Newtonian model. It is included in Table 7.2 only for those debris flows which have evidence, in the form of inversely graded deposits, that the dilatant or granular flow model is applicable.

The Reynolds number and Froude number are also tabulated in Table 7.2. They are calculated using the hydraulic radius, not the peak depth which is listed in the table. All Reynolds numbers are clearly in the laminar flow range, except for the Devastation 1931 event, which borders on the transitional range of 500 to 2500. Most Froude numbers are in the critical or supercritical range. The calculation for Lillooet fan east 1989 is based on a section of a minor runout channel in the distal part of the deposit, and is probably not representative of the main flow. With this exception, all Froude numbers are in the range of $Fr > 0.6$ which Davies (1986) suggests can result in multiple surges spontaneously forming within a flow.

There is no basis in the flow data themselves to assess whether either the Bingham or the dilatant flow model is more appropriate for any particular debris flow. As discussed in Chapter 5, sedimentological properties of the deposit can be used to infer which model is more appropriate. The presence of inverse grading, and the lack of uniform layers of debris on the fan or in the channel, suggest that the dilatant flow model is applicable. Ungraded debris deposits of uniform thickness imply that the Bingham model is applicable. The Newtonian model is not

suggested as being appropriate to fully describe the behaviour of any of the debris flows. However, it is a convenient single-parameter approximation of the Bingham model which is reasonable to use for flows in confined channels, where the critical depth is small compared to the flow depth. As pointed out by Hungr *et al.* (1984), for practical purposes of predicting debris flow behaviour, it makes little difference whether the Newtonian or the dilatant model is used, since the two models are rheologically quite similar.

The "Bagnold number" (eq. 2.41) has been suggested by some authors (Takahashi, 1980; Davies, 1986; Major and Pierson, 1992) as an indicator of whether debris flow is in the inertial (dilatant model) or viscous (Newtonian or Bingham model) regime. In practice, it is not possible to calculate meaningful values of this number for poorly sorted debris, since it was originally defined by Bagnold (1954) on the basis of uniform-sized spheres in a liquid. The main problems of using the Bagnold number are defining the composition of the interstitial fluid, and assigning a single, meaningful value of grain diameter.

Some sample calculations of the Bagnold number are shown in Table 7.3, for some hypothetical but typical fine-textured and coarse-textured debris flows. The linear grain concentration term, $\lambda$, is somewhat arbitrary for poorly sorted debris, but by using some typical void ratios calculated in Chapters 5 and 6, it is possible to estimate it from eq. 2.20. Generally, it will be greater for coarser textured debris. Typical viscosities for the debris matrix (< 4 mm) are taken from the flume results reported in Chapter 8. Bagnold (1954) defined the viscous regime as $N < 40$, and the inertial regime as $N > 450$. As the sample calculations show, if the interstitial fluid is assumed to be water, the flow regime is clearly inertial, but if the interstitial fluid is assumed to be a slurry of fine debris, then the regime is likely to be viscous or transitional. The actual numbers are probably meaningless for poorly sorted debris, but the calculations show that N will be lower for fine-textured than for coarse-textured debris. Therefore, there is some theoretical justification, supporting the sedimentologic evidence, that a viscous (*i.e.* Bingham) model may be applicable to fine-textured debris flows, and an inertial (*i.e.* dilatant) model may be applicable to coarse-textured debris flows.

## 7.3 SLOPE OF DEPOSITION AND DISTANCE OF TRAVEL

Two parameters which are important in hazard assessment on debris flow fans are the slope of deposition and the distance of travel. Existing techniques which are used to model these quantities use an approach based on momentum and frictional resistance (Takahashi, 1981; Hungr *et al.*, 1984). This approach has been found to work reasonably well for coarse-textured debris flows in southwestern British Columbia (Hungr *et al.*, 1984). However, as discussed in Chapter 6, the effective friction slope of fine-textured debris during deposition may be zero, and as pointed out in Chapter 2, the Bingham model predicts that a debris flow which is sufficiently large can flow long distances on very gentle slopes. This behaviour has been observed in several large fine-textured debris flows in this study (for example, Devastation Creek and Upper Lillooet River), and has also been documented in numerous fine-textured volcanic-source debris flows elsewhere (for example, Crandell, 1971; Niyazov and Degovets, 1975; and many others).

An attempt was made to test the runout model of Takahashi and Yoshida (Hungr *et al.*, 1984), using a friction slope of tan 10° as suggested by these authors. Only two locations in this study, Boundary Creek and Canyon Creek, have sufficient data (approach velocity and runout distance on an unconfined fan) to permit use of this model. Application of the model to the five events on these two fans gave very poor correspondence to the observed runout distances. The model can be made to fit by adjusting the friction slope; reasonably good correspondence was achieved by using a friction slope ($\tan^{-1} S_f$) of 6 to 8° for Boundary Creek and 11 to 13.5° for Canyon Creek. However, it is probably not reasonable to apply the model to Boundary Creek, since the available evidence shows that these debris flows behave according to the Bingham model, not the dilatant or granular flow model.

It should be possible to calculate the friction slope from eq. 2.42c (Takahashi, 1980, and Hungr *et al.*, 1984, after Bagnold, 1954). However, this model was originally developed for uniform-sized grains in liquid. The main limitation is using it to calculate the friction slope of poorly sorted debris is that it is difficult or impossible to define what constitutes the grains and the interstitial fluid. Table 7.3 includes example calculations, using typical parameters for coarse-textured and fine-textured debris flows observed in this study. The table shows that a

wide range of friction slopes can result from assuming that the interstitial fluid is water, a slurry of fines, or a slurry of matrix (< 4 mm) material. For fine-textured debris which remains fully undrained during deposition, it may be reasonable to assume that the fluid phase is the entire debris material, in which case $S_f = 0$.

The other major limitation of the runout model of Takahashi and Yoshida is that the friction slope must be greater than the slope of deposition ($S_f > \tan \theta$). If the slope of deposition $\theta$ is within about 1° of the friction slope, which is likely to be the case, then the error in the calculation of the runout distance becomes so great that the model is of no practical use. The runout distance becomes infinite if $S_f = \tan \theta$. In practice, it is not possible to determine $\theta$ more precisely than about ± 1°, since most fans have some variability in slope.

A simple statistical analysis was performed on the data assembled in this chapter, to investigate the factors which are most significant in controlling the slope of deposition and the runout distance. The data used for this analysis are summarized in Table 7.4. Several grain size parameters from Table 5.2 were used in the analysis, as shown in Table 7.5. The choice of grain size parameters is somewhat arbitrary, as there are a large number to choose from, and many parameters are highly inter-correlated. For statistical analysis, it was desirable to reduce the number of variables to less than the sample number. Correlation matrices of the variables used are given in Table 7.5. It is apparent from this table that volume is the variable most highly correlated with both slope and distance of travel, although there are also significant correlations between slope and some grain size parameters. The correlation of volume with slope and distance of travel is also evident from graphs of these variables (Figure 7.5).

On Figure 7.5A, which plots deposit slope against volume, most of the points lie on a linear trend, with the exception of four fine-textured debris flows which lie to the left (lower deposit slope) of the trend. These four points are the Boundary and No Good debris flows, and their position would appear to suggest there may be an upper limit of about 5° to the deposit slope of fine-textured debris flows. Point no. 1 (the very small Angel B debris flow), however, is anomalous. The poor fit of some of the fine-textured debris flows to the general trend can be explained by the fact that deposit slope is correlated with texture as well as volume.

A regression analysis was performed on the data using the all subsets method of multiple regression. The best model for deposit slope (highest $r^2$ with no non-significant variables) was found to be with volume, $M_{z(256)}$, and % $clay_{(256)}$ (Figure 7.6A). However, $M_{z(256)}$ is barely significant at the 0.05 level, and its inclusion in the model may be spurious, since it is in fact negatively correlated with slope (*i.e.* finer grain size or larger $M_z$ in phi is associated with lower slopes). The best model with two variables is slope versus volume and % $clay_{(4)}$ (or percent clay in the matrix) (Figure 7.6B). The latter model is preferable since both variables are highly significant, and $r^2$ is only slightly lower. Also, in practical terms, the clay content of the matrix is a much simpler measure to obtain than grain size parameters based on large bulk samples. One should not attach too much importance to the actual coefficients in the regression equation, since it is probably not reasonable to use it as a predictive equation in other geologic or hydrologic environments.

If viscosity is included in the regression analysis, it is a significant variable. However, the use of viscosity reduces the sample size from 21 to 10, and since it is highly correlated with matrix clay content, it was not used.

Figure 7.5B shows that there is a good relation between distance of travel and volume of event, for debris flows which were deposited on unconfined fans. Events which were confined by levées or valley walls flowed for somewhat greater distances. Regression analysis showed that volume was the only variable tested which contributed significantly to a relation with distance of travel.

## 7.4 DISCUSSION

The calculated velocities, and the Newtonian and Bingham parameters, are generally comparable to those calculated from other debris flows of similar magnitude elsewhere (Table 2.1). Most of the debris flows examined in this study, including the fine-textured ones, have a greater proportion of coarse clasts than those studied elsewhere; however, that may be partly a result of inadequate sampling of the coarse fraction in previous studies.

There is a strong tendency for coarser textured debris flows to have a greater resistance to flow, as indicated by the apparent Newtonian viscosities. The reason for this is not obvious. It

may be due to properties of the matrix, in particular the clay content, which may retain more water and which may cushion collisions between large grains, thus reducing resistance due to grain interactions. Or, more abundant coarse clasts may increase inertial resistance due to frequent collisions. Major and Pierson (1992) found in their rheometer studies that coarse particles were important in increasing viscosity. The statistical analysis done in this chapter (which may be misleading due to small sample size) suggests that clay content is the most significant factor explaining the slope of deposition, and it is also more highly correlated with viscosity than is either mean grain size or cobble and boulder content.

Both total debris flow volume and debris texture are significant factors in the slope of deposition. Total volume was found to be the only significant factor in the runout distance of debris flows on unconfined fans. The runout equation of Takahashi and Yoshida was found to be of little value in predicting the runout distances observed in this study.

In the data reported in this chapter, as well as in the debris flow examples from the literature given in Table 2.1, there is a surprisingly low range of velocity and viscosity. There is less than one order of magnitude in the values of velocity and apparent Newtonian viscosity given in Table 7.2, despite the fact that velocity is proportional to the square of flow depth, and despite the sensitivity of viscosity to water content. There is a slight tendency, apparent in the data of Table 7.2, for larger debris flows to have a higher viscosity. This may partly explain the low range of flow velocities. A possible explanation for this behaviour is that there may be a negative feedback mechanism operating in debris flow movement, that causes debris to flow only under a restricted range of water contents. If flow velocity is high, a debris flow will tend to erode its bed, entraining more sediment, which will reduce its water content and increase its viscosity, causing it to slow down. A debris flow with too high a sediment concentration and viscosity may simply stop, whereupon more fluid afterflow and streamflow would catch up to it and mix with it, causing it to begin flowing again with reduced viscosity. Larger debris flows, which have a greater shear stress at their base due to greater depth, would be more erosive and would presumably be able to achieve this equilibrium flow condition at a higher sediment concentration.

An additional factor that may cause an upper limit to the velocity is the tendency for debris flows to spontaneously form a series of surges. Davies (1986) pointed out that this tendency is a function of the Froude number. If a debris flow reaches a high velocity, then its Froude number increases, and it is likely to break down into a series of smaller surges, each of which would have lower velocity due to lower depth.

Although there is no firm evidence in this study to support these explanations, there is some support from casual observations. There are many examples of small debris flows which have stopped in a channel and not continued. Relatively few of them were seen in this study area, but I have seen many of them in channels in the drier climate of the British Columbia interior, where there may be insufficient water in a channel to remobilize a "stalled" debris flow. There are also examples, including several in this study area, of debris floods which apparently formed when a debris flow mixed with too much water to remain a coherent debris flow. At least one such event occurred on No Good Creek in 1989. These observations suggest that many mass movement and sediment transport events take place which do not succeed in achieving the narrow range of water contents required for debris flow.

The two study sites located in the drier interior climate, Fountain and McGillivray, had debris flow events which appear to have relatively low velocities and high viscosities. They also had especially well developed levées, in which much of their sediment was deposited. This morphology and mode of deposition is quite common in dry interior climates, but is relatively unusual in wet coastal environments. This may reflect the low availability of water in the dry interior channels; these debris flows may be flowing at the "dry" end (*i.e.* high viscosity) of the possible range of water contents. Whipple and Dunne (1992), studying debris flow deposits in an arid environment, concluded that sediment concentration influenced both runout distance and depositional features such as confining levées.

The multiple events in the Boundary Creek channel show that there is a poor relation between total debris flow volume and peak discharge, which may be due to a tendency for debris flows to occur as a series of surges. For prediction and design purposes, depth of flow, velocity,

and superelevation are functions of the largest surge in an event. The distance of travel on a fan is a function of the total debris flow volume.

TABLE 7.1 CHANNEL CROSS-SECTIONAL DATA AND VELOCITY CALCULATIONS

| Site, event, and section | Slope θ (°) | Peak depth H (m) | Total width B (m) | Area A ($m^2$) | Shape factor K | Radius $r_c$ (m) | Superelevation Δh(m) | Velocity U (m/s) |
|---|---|---|---|---|---|---|---|---|
| Boundary 1987 - A | 8.1 | 3.0 | 20 | 32 | 4.8 | 80 | 1.8 | 8.4 |
| - B | 6.2 | 3.4 | 16 | 32 | 5.3 | 40 | 1.6 | 6.2 |
| Boundary 1988 - A | 8.6 | 3.3 | 15 | 35 | 5.0 | 80 | 1.0 | 7.2 |
| - B | 6.2 | 3.6 | 15.5 | 37 | 5.2 | 40 | 1.25 | 5.6 |
| Boundary 1989 - A | 7.8 | 4.3 | 20 | 50 | 5.4 | 80 | 1.7 | 8.1 |
| Devastation 1931 - A | 5 | ? | 280 | - | - | ca. 450 | 85 | ca. 36 |
| - B | 2.1 | ca. 15 | 290 | ca. 3000 | ca. 4 | ca. 600 | 30 | ca. 24 |
| Canyon 1987 - A | 9.1 | 3.8 | 22 | 45 | 5.0 | 17 | 4.3 | 5.7 |
| - B | 9.1 | 4.5 | 15 | 55 | 5.3 | 22 | 2.4 | 5.8 |
| Canyon 1990 - A | 9.1 | 5.7 | 22 | 65 | 6.5 | 17 | 9.3 | 8.3 |
| - B | 9.1 | 5.4 | 16 | 78 | 5.4 | 22 | 4.6 | 7.8 |
| Lower Ryan 1984 - A | 19 | 5.0 | 19 | 70 | 5.3 | 47 | 1.5 | 5.9 |
| - B | 15 | 4.1 | 20.5 | 56 | 4.9 | 65 | 1.1 | 5.7 |
| No Good 1988 | 8 | 1.8 | 12 | 15 | | 180 | 0 | |
| Angel B 1990 [1] | 23 | 1.7 | 5.2 | 5.6 | 6.6 | 15 | 0.55 | 3.8 |
| Lillooet fan east 1989 [2] | 10 | 1.9 | 7.5 | 11 | 5.0 | 20 | 0.23 | 2.4 |
| Mt Currie ca. 1984 [3] | 15 | 4.5 | 18 | 50 | 5.5 | 70 | 1.1 | 6.3 |
| Turbid 1984 [4] | 4.8 | 13 | 57 | 400 | 5.6 | 50 | 7.5 | 8 |
| Fountain 1989 | 15 | 3.0 | 9 | 20 | | 40 | 0 | |
| McGillivray 1989 | 15 | 2.5 | 10 | 16 | | 40 | 0 | |

Notes:
1. Angel B - a cross-section further downstream showed no measurable superelevation.
2. Lillooet fan east - section is for a reach below area of main deposition, and is not representative of average flow cross-section.
3. Mount Currie - data are averages of mesurements at three similar bends.
4. Turbid Cr - velocity head formula gives U = 12 m/s; an average of U = 10 m/s is used in subsequent calculations.

TABLE 7.2 VELOCITY AND RHEOLOGIC DATA

| Event | Reliability | Slope θ (°) | Velocity U (m/s) | Peak discharge Q ($m^3/s$) | Newtonian viscosity $\mu_N$ (Pa.s) | Granular resistance $\mu_G$ ($Pa.s^2$) | Yield strength k (Pa) | Bingham viscosity $\mu_B$ (Pa.s) | Reynolds number Re | Froude number Fr |
|---|---|---|---|---|---|---|---|---|---|---|
| Boundary 1987 | A | 7.2 | 7.3 | 230 | 730 | | | | 47 | 1.6 |
| Boundary 1988 | A | 7.4 | 6.4 | 230 | 990 | | 1100 | 870 | 36 | 1.3 |
| Boundary 1989 | B | 7.8 | 8.1 | 410 | 1200 | | 2700 | 740 | 40 | 1.5 |
| Devastation 1931 | C | 1.9 | 24-36 | ca. 70,000 | 1000-2000 | | 2400 | 500-1500 | ca. 400 | ca. 2 |
| Canyon 1987 | A | 9.1 | 5.8 | 290 | 2100 | 600 | | | 20 | 1.1 |
| Canyon 1990 | A | 9.1 | 8.1 | 580 | 2300 | 620 | | | 34 | 1.3 |
| Lower Ryan 1984 | A | 17 | 5.8 | 370 | 4700 | 1500 | | | 10 | 1.0 |
| Angel B 1989 | C | 23 | 3.8 | 21 | 950 | | 2500 | 570 | 10 | 1.1 |
| Lillooet fan east 1989 | C | 10 | 2.4 | 26 | 1200 | 390 | | | 8 | 0.6 |
| Mount Currie ca. 1984 | B | 15 | 6.3 | 320 | 3500 | 950 | | | 14 | 1.1 |
| Turbid 1984 | B | 4.8 | 10 | 4000 | 5300 | | | | 40 | 1.0 |

Notes:
1. Average values of θ, U, Q, and $\mu_N$ are given where more than one cross-section was measured.
2. A unit weight of 21,000 $kN/m^3$ is used for volcanic-source debris, and 23,000 $kN/m^3$ for plutonic-source debris.
3. Reliability: A - good channel geometry, more than one section measured, U and $\mu_N$ are ± 20%.
   B - poor channel geometry, or only one section, U and $\mu_N$ are ± 40%.
   C - very poor geometry, and/or poor estimate of superelevation, U and $\mu_N$ are ± > 50%.

TABLE 7.3 EXAMPLE CALCULATIONS, BAGNOLD NUMBER AND FRICTION SLOPE

A. BAGNOLD NUMBER $N = \frac{\lambda^{1/2}\rho_s D^2}{\mu}\frac{du}{dz}$

Assumptions for typical debris flows:
- $\rho_s$ = 2700 kg/m$^3$
- du/dz = 4 s$^{-1}$
- D is the median diameter of clasts larger than the interstitial fluid.

1. Coarse debris in water
   $\lambda$ = 100
   D = 32 mm
   $\mu$ = 0.001 Pa.s N = 100,000

2. Coarse debris in < 4 mm slurry
   $\lambda$ = 50
   D = 64 mm
   $\mu$ = 1 Pa.s N = 300

3. Fine debris in < 4 mm slurry
   $\lambda$ = 25
   D = 32 mm
   $\mu$ = 2 Pa.s N = 30

B. FRICTION SLOPE $S_f = \frac{(\rho_s - \rho_f)c_v}{(\rho_s - \rho_f)c_v + \rho_f}\tan\alpha$

Assumptions: $S_r$ = 1, $\alpha$ = 30°
Coarse debris: $G_s$ = 2.72, w = 0.09, e = 0.272,< 4 mm content = 20%, fines content = 3%
Fine debris: $G_s$ = 2.67, w = 0.14, e = 0.415,< 4 mm content = 35%, fines content = 12%

| Interstitial fluid: | Water | < 0.063 mm slurry | < 4 mm slurry | All debris |
|---|---|---|---|---|
| 1. Coarse debris | | | | |
| $c_v$ | 0.786 | 0.763 | 0.629 | 0 |
| $\rho_f$ (kg/m$^3$) | 1000 | 1170 | 1730 | 2350 |
| $S_f$ | tan 18.4° | tan 16.2° | tan 8.7° | 0 |
| 2. Fine debris | | | | |
| $c_v$ | 0.707 | 0.622 | 0.459 | 0 |
| $\rho_f$ (kg/m$^3$) | 1000 | 1370 | 1760 | 2180 |
| $S_f$ | tan 17.3° | tan 12.1° | tan 6.3° | 0 |

TABLE 7.4 MOBILITY DATA USED IN STATISTICAL ANALYSIS

| Event | ID | Type of Event | Volume (m3) | average deposit slope (deg.) | distance of travel (m) | type of deposition | channel slope (deg.) | channel velocity (m/s) | Newtonian viscosity (Pa.s) |
|---|---|---|---|---|---|---|---|---|---|
| Angel B 1990 | 1 | F | 200 | 13.5 | 120 | LC | 23 | 3.8 | 950 |
| Boundary 1987 | 2 | F | 50,000 | 4.5 | 250 | U | 7.2 | 7.3 | 730 |
| Boundary 1988 | 3 | F | 5000 | 4.8 | 130 | U | 7.4 | 6.4 | 980 |
| Boundary 1989 | 4 | F | 25,000 | 5.3 | 220 | U | 7.8 | 8.1 | 1200 |
| Cheekye ca. 1100 BP | 5 | F | 3,000,000 | 2.5 | 1200 | U | | | |
| Upper Lillooet ca. 900 BP | 6 | F | 10,000,000 | 0.4 | | CC | | | |
| Devastation 1931 | 7 | F | 3,000,000 | 1.9 | 8000 | CC | 1.9 | 24 | 1500 |
| NoGood 1990 | 9 | F | 10,000 | 4.5 | | | | | |
| Turbid 1984 | 10 | F | 1,000,000 | 4 | | | 4.8 | 10 | 5500 |
| Angel A ca. 1987 | 11 | I | 60 | 12 | 30 | U | | | |
| Canyon 1987 | 12 | I | 10,000 | 11 | 160 | U | 9.1 | 5.8 | 2100 |
| Canyon 1990 | 13 | I | 20,000 | 9 | 350 | U | 9.1 | 8.1 | 2400 |
| Fountain 1989 | 15 | I | 3500 | 12.5 | 1100 | LC | | | |
| McGillivray 1989 | 16 | I | 6000 | 11 | 1000 | LC | | | |
| Mt Currie ca. 1984 | 17 | I | 20,000 | 12.5 | 700 | LC | 15 | 6.3 | 3500 |
| Affliction 1984 | 21 | C | 200,000 | 7 | 1000 | U | | | |
| Capricorn ca. 1972 | 22 | C | 200,000 | 9.6 | 800 | U | | | |
| Hot Springs 1984 | 23 | C | 60,000 | 10 | 600 | U | | | |
| Lillooet fan centre 1984 | 24 | C | 15,000 | 10 | 150 | U | | | |
| Ryan lower 1984 | 26 | C | 20,000 | 13 | | | 17 | 5.8 | 4800 |
| Ryan upper 1984 | 27 | C | 50,000 | 10 | 700 | U | | | |

Type of event: F - Fine-textured; I - Intermediate; C - Coarse-textured
Type of deposition: U - Unconfined; LC - Levée-confined; CC - Confined in channel
For grain size statistics, see Table 5.2

## TABLE 7.5 CORRELATION MATRICES

A. Slope of Deposition (all events)
n=21

| | Log Volume | Mz (256) | % matrix (256) | % fines (256) | % clay (256) | % clay (4) | Slope (degrees) |
|---|---|---|---|---|---|---|---|
| Log Volume | **1** | | | | | | |
| Mz (256) | 0.307 | **1** | | | | | |
| % matrix (256) | **0.458** | **0.947** | **1** | | | | |
| % fines (256) | 0.176 | **0.937** | **0.855** | **1** | | | |
| % clay (256) | 0.092 | **0.849** | **0.791** | **0.915** | **1** | | |
| % clay (4) | -0.230 | **0.555** | 0.432 | **0.728** | **0.883** | **1** | |
| Slope (degrees) | **-0.734** | -0.431 | **-0.554** | -0.396 | **-0.497** | -0.309 | **1** |

B. Distance of travel (events on unconfined fans only)
n=12

| | Log Volume | Slope (degrees) | Mz (256) | % fines (256) | % clay (256) | % clay (4) | Log Distance |
|---|---|---|---|---|---|---|---|
| Log Volume | **1** | | | | | | |
| Slope (degrees) | -0.549 | **1** | | | | | |
| Mz (256) | 0.325 | **-0.824** | **1** | | | | |
| % fines (256) | 0.185 | **-0.784** | **0.934** | **1** | | | |
| % clay (256) | 0.033 | **-0.780** | **0.881** | **0.969** | **1** | | |
| % clay (4) | -0.272 | -0.548 | **0.628** | **0.825** | **0.910** | **1** | |
| Log Distance | **0.935** | -0.346 | 0.141 | -0.033 | -0.187 | -0.456 | **1** |

Notes:

1. Correlation coefficients shown in bold type are significant at the 0.05 level.
2. (256) and (4) indicate grain-size paramaters for material < 256 mm and < 4 mm respectively.
3. Mz is in phi units; a larger phi value indicates a smaller sediment size.

FIGURE 7.1. MAP OF BOUNDARY CREEK CHANNEL.

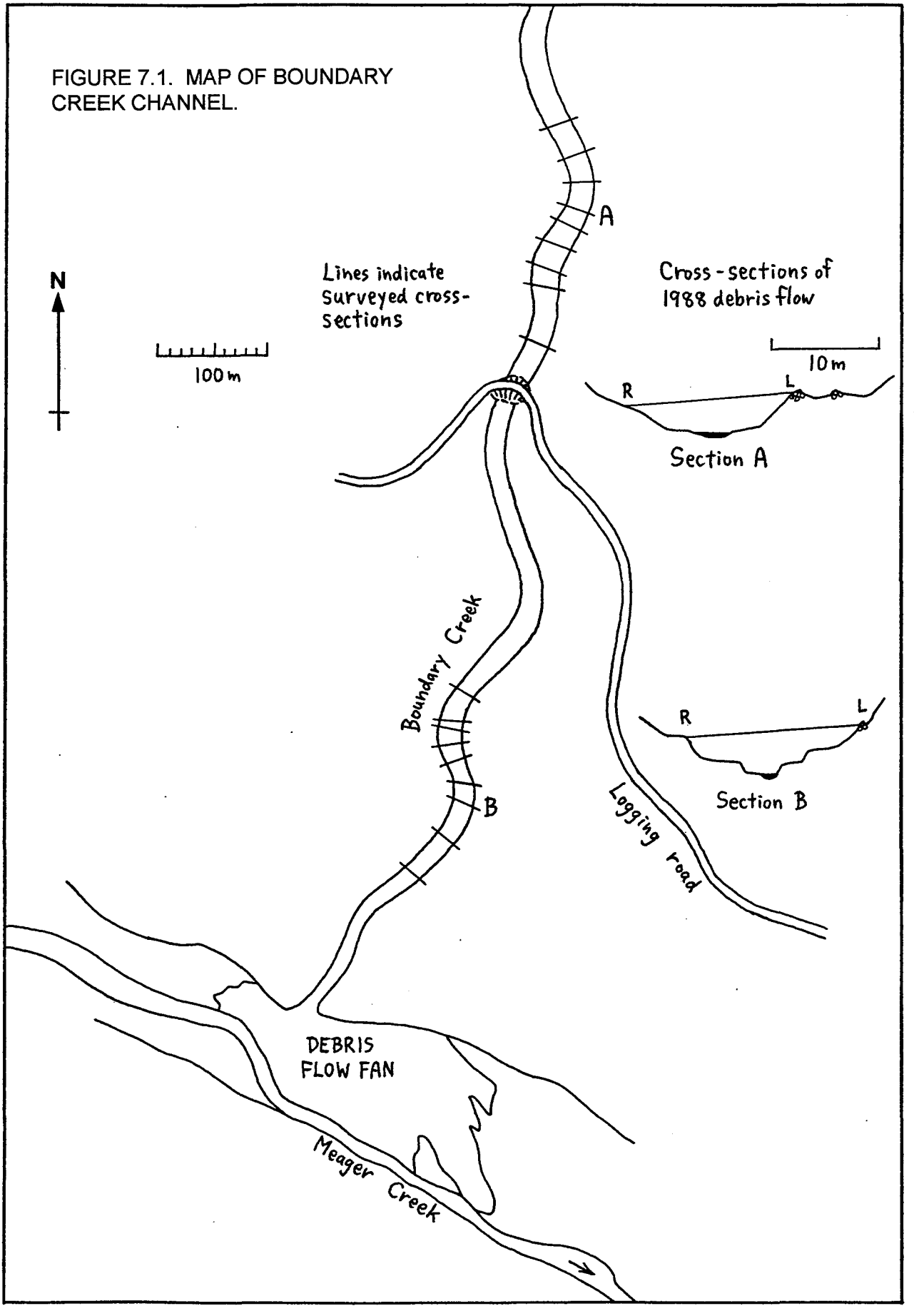

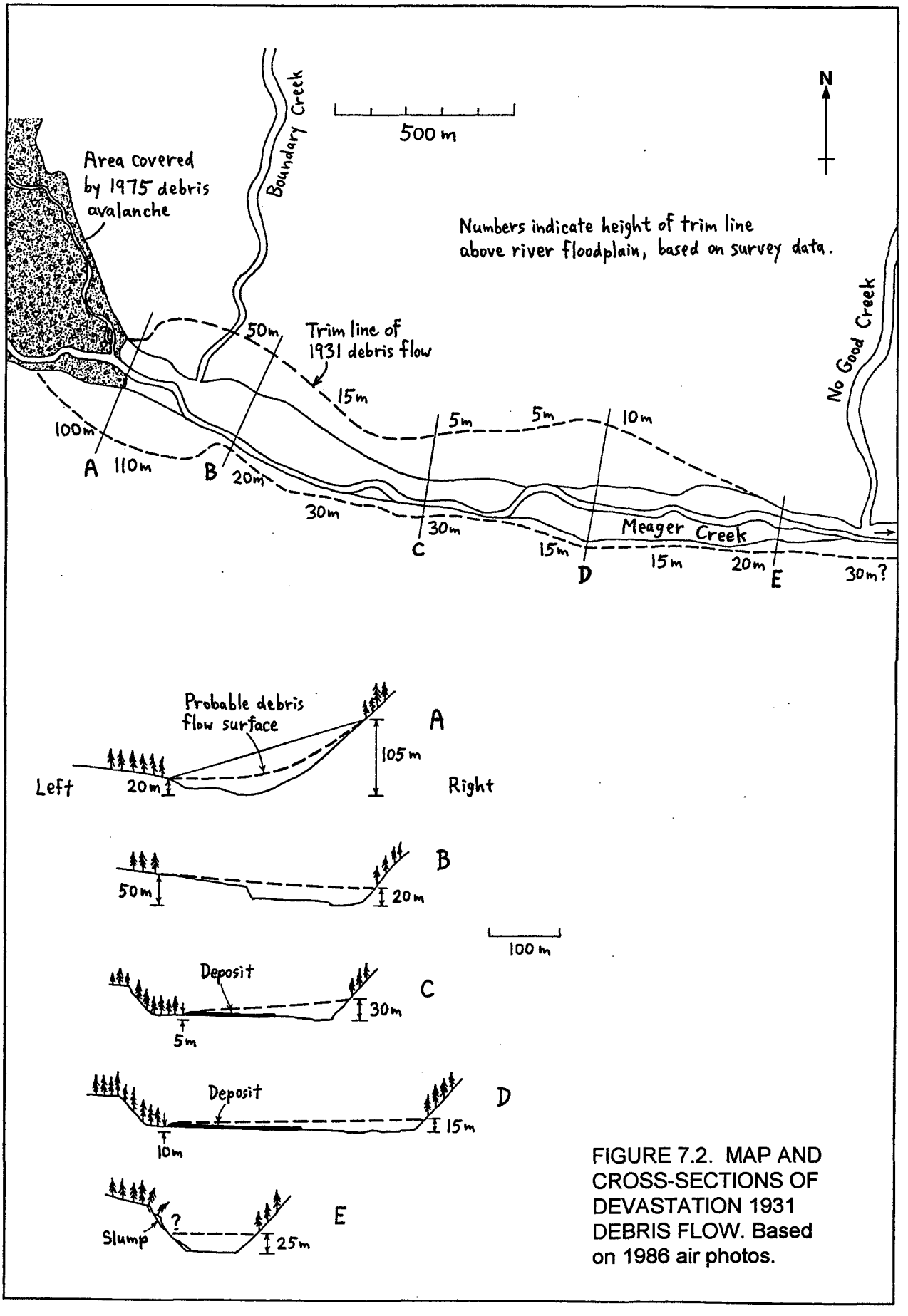


FIGURE 7.2. MAP AND CROSS-SECTIONS OF DEVASTATION 1931 DEBRIS FLOW. Based on 1986 air photos.

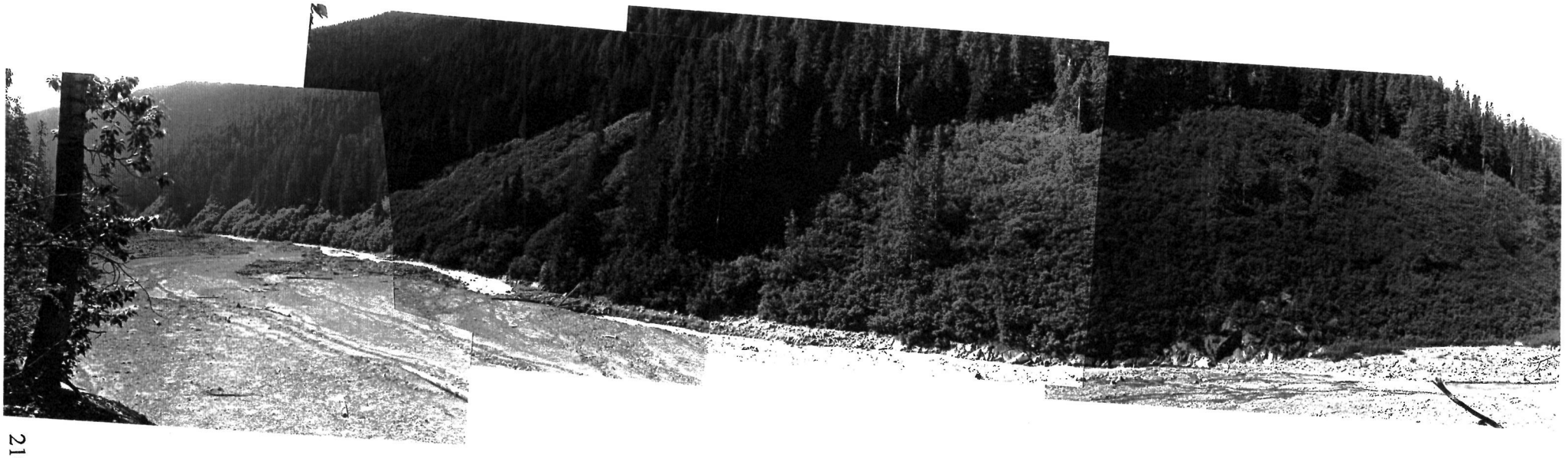

A. View from Boundary Creek fan to right bank of Meager Creek, showing maximum superelevation (right). Deposits of 1989 Boundary Creek debris flow are in foreground. (Note: Higher brush area in centre left was not caused by Devastation Creek debris flow; all other brush areas were.)

FIGURE 7.3. PHOTOGRAPHS OF TRIM LINES OF DEVASTATION 1931 DEBRIS FLOW IN MEAGER CREEK CHANNEL.



B. View across Meager Creek valley from terrace between Boundary and No Good Creeks. Low ridge in foreground, at edge of deciduous trees, is the levée marking the left edge of the Devastation Creek debris flow. Mature forest in immediate foreground has been clear-cut.

FIGURE 7.3 (continued).

A. (Left) Boundary Creek channel following 1988 debris flow, at site of section B, looking upstream.

B. (Below) Canyon Creek channel following 1987 debris flow, looking upstream. Arrows show height of flow on each bank.

FIGURE 7.4. PHOTOGRAPHS OF SUPERELEVATION IN BOUNDARY CREEK AND CANYON CREEK CHANNELS.

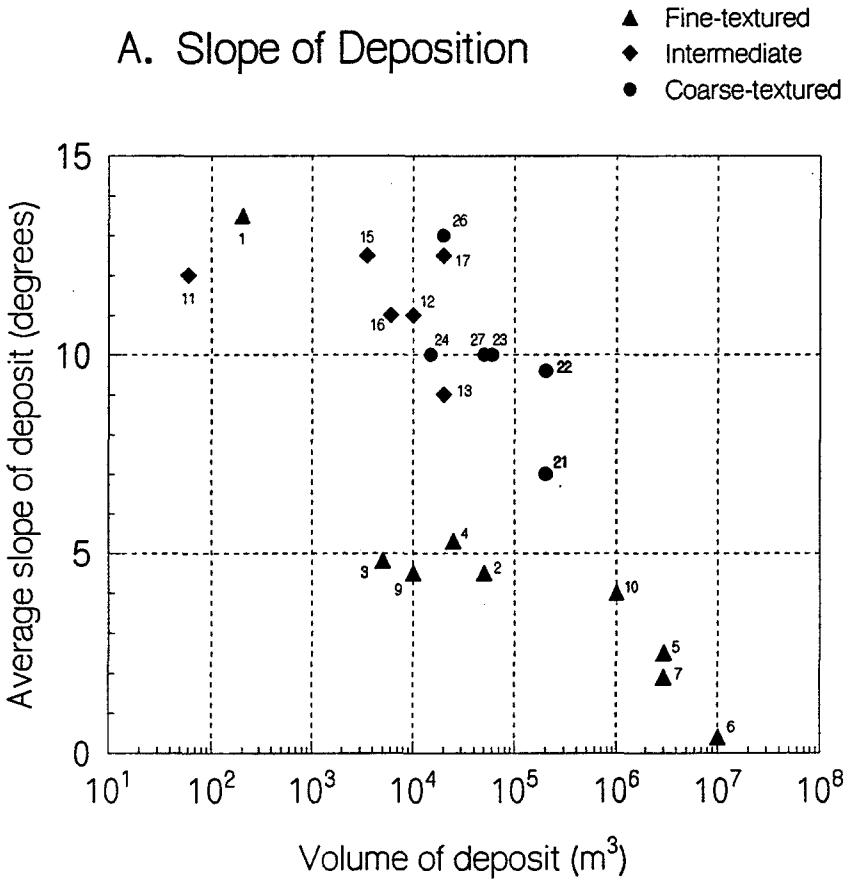


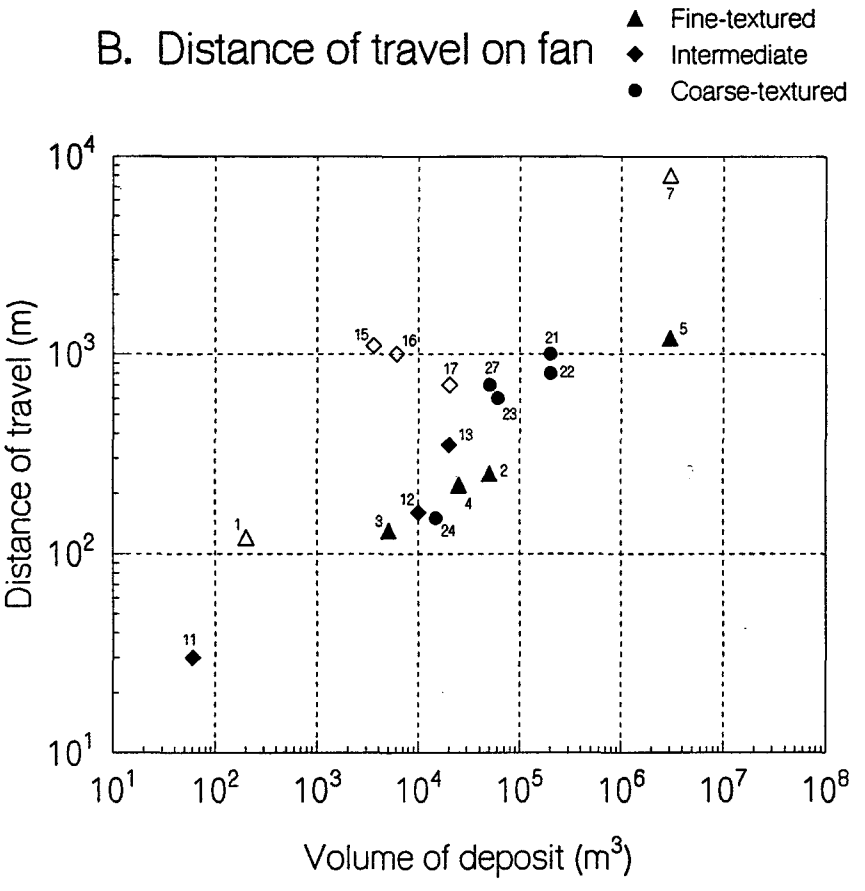


FIGURE 7.5. SLOPE OF DEPOSITION AND DISTANCE OF TRAVEL. Numbers refer to event ID in Table 7.4.

Open symbols on graph B are debris flows in confined channels.

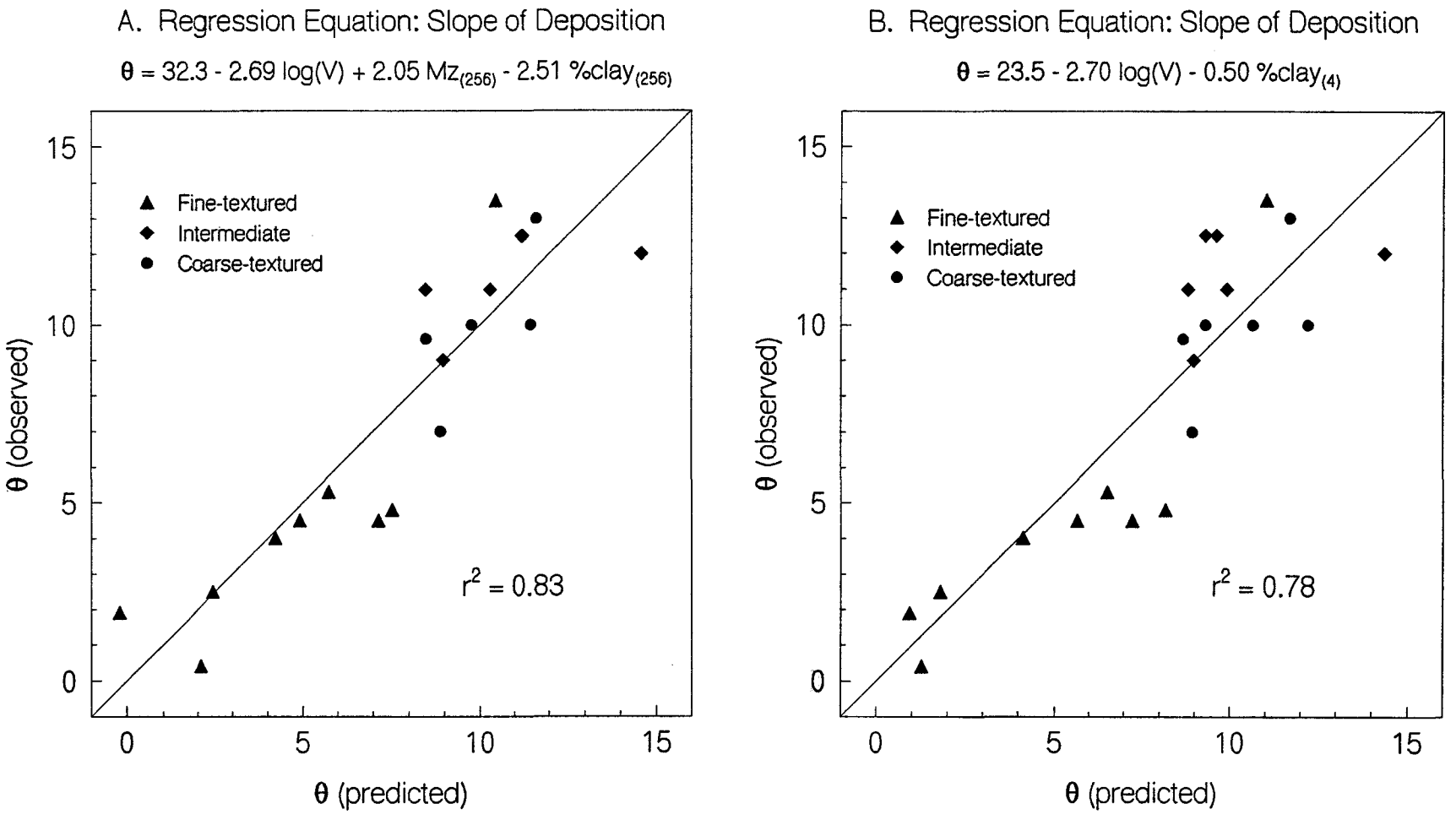


**FIGURE 7.6. REGRESSION EQUATIONS: OBSERVED AND PREDICTED VALUES OF SLOPE OF DEPOSITION.**

# CHAPTER 8. FLUME RESULTS, AND REVIEW OF EXPERIMENTS ON DEBRIS RHEOLOGY

In the previous chapters, some field evidence was presented which indicates, somewhat indirectly, that fine-textured debris flows can be described by a Bingham flow model, while coarse-textured debris flows behave according to a dilatant model. It may be possible to perform experiments on model debris flows in the laboratory to support the field observations, and to provide additional information on flow processes by observing the flows in motion.

The objective of laboratory experiments on the rheology of debris samples has usually been to measure rheologic parameters such as viscosity, yield strength, and the flow behaviour index, and to determine how these vary with sediment concentration and sediment composition. Two approaches have been taken: measurement of parameters in a rheometer (or viscometer); and observing the behaviour of debris slurries in a flume.

The first approach uses standard engineering technology to measure rheologic parameters under controlled conditions of steady, uniform shear. The second approach is more comparable to real debris flows in natural channels; however, it is less controlled, as flow tends to become unsteady and non-uniform. In both approaches, scaling is an important consideration. Both the scale of the apparatus, and the grain size of the material tested, are much smaller in the experiment (model) than in natural debris flows (prototype). Scaling considerations are discussed below in section 8.2.

In this study, a simple flume was built to model debris flow surges of different compositions. Also, an attempt was made to build a large concentric-cylinder viscometer, but this was unsuccessful. A brief review of previous studies of debris flow rheology is given here, followed by the results of the flume experiments.

## 8.1 REVIEW OF LITERATURE ON EXPERIMENTS

Table 8.1 gives a summary of experimental studies on the rheology of debris flow material, which have been published in English. Most of these studies assumed the Bingham model, and calculated the Bingham viscosity and yield strength for material over a range of water contents.

The most frequently used apparatus has been the concentric-cylinder viscometer. To obtain repeatable measurements from this device, the gap size should be at least 10 times the diameter of the largest particle in the sample, and the size of the gap should be small compared to the diameter of the inner cylinder (Van Wazer *et al.*, 1963). These requirements place obvious limitations on the feasibility of performing measurements on realistic debris flow samples; either testing is limited to very fine material, or a very large viscometer must be constructed.

The behaviour of non-Newtonian fluids is often highly dependent on shear rate; therefore the laboratory tests should be done at shear rates comparable to those of natural debris flows. Average shear rates (velocity:depth ratios) are commonly 10 $s^{-1}$ or less (Phillips and Davies, 1991). The data in Table 2.1 indicate typical average shear rates of 4 $s^{-1}$ or less. Maximum shear rates at the base of a flow are 3 times the average shear rate for a Newtonian fluid (eq. 2.43), and somewhat greater for a Bingham fluid, so a range of shear rates of up to about 30 $s^{-1}$ appears to be appropriate for rheometer tests.

The results of several sets of measurements are summarized in Figure 8.1. Data in the original references have been converted to solids concentration by weight where necessary, assuming $G_s$=2.65. Several selected results from each of the three references which used viscometers are shown in the figure, to illustrate the range of material textures tested. The data points are not shown; in most cases there was considerable scatter about each regression line.

Owens (1973) used a commercially available viscometer, with an outer cup volume of 200 ml. He does not report the gap size; since he tested material up to 8 mm, it is apparent that he violated the 10:1 gap to particle size guideline. He also performed tests in a small flume with a semi-circular cross-section, or "channel viscometer". He used the method of Johnson (1970) to compute the Bingham flow parameters, by photographing reflective streaks on the flow surface.

O'Brien and Julien (1988) used a custom-built viscometer in which they tested the fines fraction (less than 0.072 mm) from several debris flows, at relatively low solids concentrations and high shear rates. They added sand to the fines for some tests (with insufficient data reported

to include in Figure 8.1). The sand did not affect viscosity significantly until the volume added exceeded 20% of the total sample volume, above which point viscosity increased sharply.

Major and Pierson (1992) constructed a large concentric-cylinder viscometer, capable of testing samples of up to 0.3 $m^3$. Their published results used a smaller outer cylinder, about 230 mm in diameter, and only material smaller than 2 mm was tested. They added sand in various proportions to the fines fraction separated from the 1980 North Toutle River lahar.

Phillips and Davies (1991) built a large cone-and-plate viscometer, with a diameter of 2 m, capable of testing debris flow material with clasts up to about 120 mm. A smaller, 1/5 scale model was also used to test finer samples. Their data are not reported in a form which can be included in Figure 8.1. Their results, however, were similar to others reported here in that they observed great sensitivity of viscosity to water content. They achieved considerably higher sediment concentrations and viscosities with the large viscometer and coarser sediment, than were reported for fine sediment tested in smaller devices.

Major and Pierson (1992) and Phillips and Davies (1991) both concluded that debris flows cannot be described by a single rheologic model, and they found that at low shear rates (below about 5 $s^{-1}$) the shear behaviour of debris was quite variable and departed from ideal rheologic models. Typical behaviour in their viscometers at low shear rates included hysteresis, rapid random fluctuations in shear resistance (torque), a decrease in torque over time, and poor reproducibility of results. Also, both studies reported some cases where, in plots of torque vs. shear rate, torque decreased from the initial yield stress and then increased, whereas under the Bingham model, a steady increase would be expected.

Fairchild (1985) performed two types of flume experiments. First, he ran batches of debris from the 1980 North Toutle River lahar down a simple rectangular flume, and calculated the Bingham flow parameters for these surges. Then, he constructed a recirculating flume, in which he achieved steady, uniform flow of slurries made from various proportions of commercially-available clay, silt, and sand. A principle objective of these tests was to determine the rheologic model which best described the flow; as the Bingham model was not assumed, his results cannot readily be compared with the data shown in Figure 8.1. He found that the yield strength was

sensitive to clay content; that the flow behaviour index (the exponent n in eq. 2.24) varied from well under 1 for a clay slurry, to approximately 2 for the higher sand contents; and that the behaviour of clay slurries was significantly different from that of slurries with a high concentration of poorly-sorted granular sediment. (Since steady, uniform flow is not typical of real debris flows, his device should be considered a type of viscometer or rheometer, rather than a flume for debris flow simulation.)

The most consistent result shown by the data in Figure 8.1, is that both yield strength and viscosity are extremely sensitive to water content, ranging over about two orders of magnitude for only a few percent change in solids concentration. This behaviour of debris slurries is familiar to anyone who has mixed pancake batter or concrete. For any particular sediment composition, there is a limited range of water contents over which the debris can behave as a single-phase, viscous slurry. If water content is lower, the material deforms as a frictional soil, failing along discrete planes. If water content is too high, coarser sediment settles out, and the material behaves as two phases, with a fluid entraining coarse sediment as bedload. (See also the discussion in section 7.4.)

Another common result is that clay-rich sediment has a higher water content for a given range of yield strengths and viscosities than does sandy sediment. This result can be explained simply by the relative surface areas of fine-textured and coarse-textured sediment.

The results of the rheologic experiments have little direct practical applicability, in that the measured flow parameters cannot be used directly for modeling real debris flows. Each particular viscometer or flume appears to have a particular range of viscosities it is capable of testing; if too viscous, slippage occurs at the inner cylinder or the flume base, and if too fluid, sediment in the slurry separates out. This range determines the water content at which a given sediment composition can be tested in the device. Of the experiments summarized in Table 8.1, only those of Phillips and Davies (1991) have apparent viscosities comparable to those calculated for actual debris flows with significant amounts of coarse gravel, as listed in Table 2.1.

Numerous flume experiments have been performed by Japanese researchers (Takahashi, 1980; and several studies reviewed by Chen, 1987). Most of them have based their analyses on the dilatant, or granular, flow model, and have performed experiments using gravel and sand in water. Some of the Japanese experimental results are reviewed by Takahashi (1991). The reported results describe in some detail the profiles of grain concentration and velocity, but values of flow resistance are not reported in a form that can be included in Table 8.1.

Some Chinese researchers also have done experimental work on the rheology of debris flow slurries, and have generally favoured the Bingham model (O'Brien and Julien, 1988).

Nasmith and Mercer (1979) used bentonite slurries, with a scale model of a debris flow channel and fan, to simulate debris flow behaviour for the design of protective dykes. However, they did not calculate any rheologic parameters, nor did they attempt to ensure that the slurries behaved rheologically in a manner similar to the actual debris flows.

Davies (1988, 1990) performed a unique experiment, in which he used a moving belt as a flume, keeping a debris surge in stationary equilibrium, in effect creating an infinitely long flume. Also, he reduced the experiment to two-dimensional form by replacing grains with cylindrical rods. The objective of this experiment was to investigate certain fundamental properties of debris flow surges, including the distributions of grain concentration and shear rate, and the tendency for roll waves to form. There was no intent to apply a rheologic model, and the experimental surges did not sufficiently resemble real debris flows to be able do so.

The U.S. Geological Survey has recently built a 95 m long flume for debris flow experiments. Results from these experiments have not yet been published (as of early 1994, the time of this writing); however, Major and Iverson (1993) give a brief qualitative description of some experiments. They report that debris flows invariably develop multiple roll waves or surges, and that little or no evidence of these multiple surges is recorded in the internal structure of deposits.

## 8.2 SCALING CONSIDERATIONS

In constructing scale models of hydraulic phenomena, it is necessary that certain quantities such as slope, flow velocity, and flow depth be scaled in such a way that the hydraulic behaviour

of the model remains similar to that of the real world (or prototype). This subject has received considerable attention in the modeling of bedload transport by rivers (Graf, 1971). For flumes designed to model rivers, it is considered necessary to keep the Reynolds number (eq. 2.37) and the Froude number (eq. 2.38) respectively as similar as possible.

For models of debris flows, the Reynolds number is obviously relevant because it describes whether flow is laminar or turbulent. The relevance of the Froude number is less obvious; however, as discussed in section 2.5, it may be important in describing the formation of roll waves in debris flows. Since in many debris flows, the Froude number is close to the critical value of 1, Froude number similarity may be important in modeling.

If both the Reynolds and Froude numbers are kept constant, then the following must hold:

$$\left(\frac{U}{(gH)^{1/2}}\right)_{model} = \left(\frac{U}{(gH)^{1/2}}\right)_{prototype}$$

and

$$\left(\frac{UH\rho}{\mu}\right)_{model} = \left(\frac{UH\rho}{\mu}\right)_{prototype} \qquad (8.1)$$

The ratio of a quantity in the model to that in the prototype can be defined by the symbol $\lambda$ (after Graf, 1971). If $\lambda_U$, $\lambda_H$, and $\lambda_\mu$ are the ratios for velocity, depth, and viscosity respectively, then the equations above become

Froude number: $\lambda_U^2 \lambda_H^{-1} = 1$

Reynolds number: $\lambda_U \lambda_H \lambda_\mu^{-1} = 1$ (8.2)

For Newtonian laminar flow, U is proportional to $SH^2\mu^{-1}$ (eq. 2.6). If this is substituted into eq. 8.2, the equations become

Froude number: $\lambda_H^3 \lambda_s^2 \lambda_\mu^{-2} = 1$

Reynolds number: $\lambda_H^3 \lambda_s \lambda_\mu^{-2} = 1$ (8.3)

Both equations are true if

$\lambda_s = 1$ and $\lambda_H^3 \lambda_\mu^{-2} = 1$ (8.4)

or, if slope is the same in the model and the prototype, and the term $H^3\mu^{-2}$ is kept constant. This is easily accomplished in practice; as the physical dimensions of the model channel (H) are reduced, viscosity can be reduced by increasing water content.

The result that slope should be kept constant is somewhat contrary to field experience; small debris flows on talus slopes of 30° or steeper appear to behave similarly to large debris flows in channels of 10° or less.

The Bingham flow equations do not lend themselves to similar analysis because of the additive terms. However, if the ratio of plug thickness to flow depth ($T_0/H$) is kept constant, then the above analysis for Newtonian flow should apply.

For dilatant flow, the Reynolds number is not applicable, since the "viscosity" term ($\mu_G$) is not given in the appropriate units. The "Bagnold number", N (eq. 2.41), may be relevant. It distinguishes the viscous regime ($N < 40$) from the inertial regime ($N > 450$), and it has been used for this purpose by some authors (Takahashi, 1980; Major and Pierson, 1992). Unfortunately, it is difficult to apply this number in practice, because for poorly sorted debris for which matrix and grains cannot be readily defined, it is impossible to select meaningful values for D (the representative grain size) and $\mu$ (the viscosity of the interstitial fluid). Bagnold (1954) performed the experiments on which the derivation of this number is based, using uniformly sized spheres in a viscous liquid. It is not reasonable to extend his empirical results to slurries of poorly sorted granular material. However, if the general form of the Bagnold number is considered to be valid (although the numerical value may not be), one should attempt to keep the term $D^2(du/dz)\mu^{-1}$ similar in both the model and prototype.

In these experiments, the slope was similar to that of many natural debris flow channels, the depth of flow was reduced by a factor of about 100, and the viscosity was in the order of 1000 times less than that calculated for natural debris flows in this study. Therefore, the condition of Eqs. 8.4 was adhered to reasonably well. Furthermore, the maximum size of gravel was about 10 to 30 times smaller than typical large clasts in debris flows, and the shear rates in the flume were several times greater than in most natural flows. Therefore, approximate Bagnold number similarity was also observed. Reynolds numbers for the experiments were about 3 to 120, well within the laminar range, and Froude numbers ranged from 0.5 to 3, similar to those calculated for natural debris flows in Chapter 7. Average shear rates were about 10 to 50 $s^{-1}$, greater by a factor of about 10 than the average shear rates of natural debris flows.

If experiments are performed on mixtures of sand and gravel in water, grain size can be scaled along with model scale. However, this is not possible with poorly sorted slurries containing cohesive material. If the grain size of a debris slurry is reduced by truncation, as in this study, the overall grain size distribution changes. In these experiments, by truncating the samples to 16 mm, half or more of the total volume was removed; thus, clay content is about twice as great. However, clay behaves rheologically like clay in both the model and the prototype; it does not start behaving like sand because the scale of the model has been reduced 100 times.

## 8.3 FLUME EXPERIMENTS

In the present study, a simple flume was constructed to test debris flow samples collected from several of the study sites. These included two fine-textured debris flows (Boundary Creek 1988, and Meager Creek 1931), and two coarse-textured debris flows (Hot Springs Creek 1984 and Lower Ryan River 1984). For each sample, about 40 kg of the matrix (finer than 4 mm) material was separated and used in the flume tests. Pebbles in the 4-16 mm size range from the same samples were added for further tests. In the tables and figures which follow, samples consisting of matrix are called "fine", and samples with pebbles added are called "coarse". Table 8.2 gives information on the texture of the various samples.

### Apparatus and experimental method

The flume was 4.9 m long, and 95 mm wide at the base with 60° side walls. Samples of about 20 litres were mixed in a bucket, and placed in a hopper at the head of the flume. While keeping the sample mixed, a trap door was opened to let the debris flow down the flume. This resulted in a single surge, which attenuated downstream in a manner similar to a dam-break flood wave. A video camera was used to record each test. Figure 8.2 shows the apparatus, from the usual position of the video camera. A 35 mm camera with a motor drive was also used to take pictures of some surges, perpendicular to the flow direction (as shown in Figure 8.3). Lines were marked on the flume walls to indicate depth, and distance from the head of the flume, to facilitate making measurements from the photographs.

The base of the flume was slightly rougher than the sides, since it was made of rough-sawn lumber while the sides were made of planed lumber. Theoretically, for laminar flow, small-scale roughness of the channel should not affect flow behaviour as long as slippage does not occur at the base. Slippage was observed in some flows with low water contents, and the results of these tests were not used. To test the assumption that roughness has no effect, a rough bed was constructed of slabs of concrete with embedded pebbles, and some tests were run with this bed inserted in the flume. Only one test was successfully completed; due to the increased width of the flume base, flows tended not to reach the end of the flume. The rough bed made measurement of flow depth less precise, and it also made the flume very difficult to clean between tests.

Following each test, the peak height of the surge was recorded at the 2, 3, and 4 m marks by measuring the height of the mud lines. A shadow cast by a small stick, placed across the flume for some tests, showed that the flow surface was always convex at the surge peak. The average height of this bulge, 4 mm, was added to the mud-line height to obtain the peak flow depth.

To determine the velocity of the surge front for each test, the video tape was replayed in slow motion. The video camera had an internal clock which recorded the time on the tape, and this was used to note the position of the front as it progressed down the flume. A graph was drawn of distance versus time, which was differentiated graphically to calculate velocity. The procedure is illustrated in Figure 8.4 for two examples.

For each test, rheologic parameters of the surge peak were calculated using Eqs. 2.26, 2.32, or 2.33, for the Newtonian, dilatant, and Bingham models respectively. Peak flow depths for most tests were in the range of 35 to 60 mm. From these depths, and the cross-sectional geometry of the flume, average shape factors K of 5.8 for the Newtonian model and 3.9 for the dilatant model were calculated. For simplicity, a single average value of K was used for each model; individual values are in the range of about ± 10% of the average value.

The rheologic parameters were calculated at the 2, 3, and 4 m distances along the flume. Because the flow was sometimes quite unsteady at the 2 m point (see discussion below), the parameters for each test were taken as the average of the 3 and 4 m calculations.

It is also possible to calculate the rheologic parameters for the recession, or declining flow, part of the surge, using the surface velocity and eq. 2.11. The surface velocity was measured by tracing pebbles visible in successive photographs (Fig. 8.3).

The Bingham yield strength (k) was calculated following each test, by measuring the depth of debris deposited in the flume and applying eq. 2.9. Below the flume, the debris spread out on a plywood sheet of lesser slope than the flume. Immediately following each test, 3 small samples were taken from the deposit for measurement of water content. At the end of the flume, there was a drop of about 5 cm to the plywood sheet. Because of this discontinuity, it was not possible to extend these experiments to an analysis of debris flow runout.

Results

A summary of the test results is given in Table 8.3. All tests which were successfully completed (that is, flows reached the end of the flume, and exhibited flow rather than sliding) are included in the summary.

The assumptions made in calculating the flow parameters from observations of the surge velocity are as follows:

- The velocity of the wave front, and the average velocity at the peak depth, are equal. Therefore, velocity can be calculated as if for steady, uniform flow. (This is the roll wave assumption discussed in section 2.5.).
- Acceleration terms are negligible.
- The behaviour of the surge is controlled by the average sediment concentration and composition in the deepest part of the flow; or, non-uniform sediment concentration and composition can be ignored in calculating flow parameters. (This assumption may not be valid, considering the observations of frontal accumulation of coarse clasts described below.)
- The selected model (Bingham, Newtonian, or dilatant) actually describes the behaviour of the material.

The resistance parameters (viscosity and granular resistance) are averages of the values calculated at the 3 and 4 m distances. The individual values at these points range up to about ± 50% from the average, although most are within ± 20%. At the 2 m point, the flow depth was often dropping rapidly from its initial peak depth, and the calculated resistance parameters, which are highly sensitive to flow depth, were therefore sometimes inconsistent with values calculated further down the flume, where depth varied less rapidly. Therefore, only the values at the 3 and 4 m distances were used in the calculations.

For several tests with fine-textured material, rheologic parameters are not given because the flow displayed very unsteady behaviour. For example, one flow (BF4) suddenly decelerated almost to a stop, and then accelerated slowly. Generally, most flow surges attenuated as they flowed down the flume, with both depth and velocity decreasing. Some surges flowed with essentially constant velocity and depth. Some attenuated very rapidly at first, and then flowed with very slow, almost constant, velocity to the end. The coarse-textured samples (Hot Springs and Ryan) flowed in a more steady manner than the fine-textured samples (Boundary and Meager). All three "RC" (Ryan coarse) tests, inexplicably, did not attenuate, but increased slightly in both depth and velocity as they flowed.

All of the tests using fine-textured material left a uniform layer of debris in the flume, the thickness of which varied inversely with flume slope. If this layer of stationary debris was pushed ahead into a bulge, it would resume flowing to the end of the flume until its depth once again declined to the critical thickness. This behaviour is typical of Bingham substances.

The tests using coarse-textured material did not show this behaviour. In these tests, flow continued until only a very thin coating of debris remained, which was comparable in thickness (2 to 5 mm) to the largest particles in the matrix (4 mm). In the case of samples containing larger pebbles, the layer was about the same thickness, but it included isolated stranded pebbles. If this layer was pushed, it did not resume flowing, indicating that it was in a drained or partly drained state. This behaviour suggests that the coarse-textured material does not possess a true Bingham yield strength. The deposition of the thin layer is probably due either to the stranding of coarse sand grains as the depth approached zero, or to partial drainage (*i.e.* loss of pore water

pressure) as the flow velocity approached zero. (The apparent yield strengths are shown in Table 8.3 for comparison.)

From these observations, it was concluded that the Bingham model is applicable to the fine-textured samples, but not to the coarse-textured samples. There was no evidence from these tests to indicate which of the single-parameter models is more applicable to coarse-textured debris; however, on the basis of field evidence discussed earlier, the dilatant (or granular flow) model is used. Table 8.3 gives the Bingham and granular flow parameters as appropriate for each sample. The "granular resistance" given in the table is square root of $\mu_G$ in eq. 2.32. The apparent Newtonian viscosity is also given for all samples, to provide a single index of flow resistance for purposes of comparison.

In most of the tests on material which included pebbles, a noticeable concentration of coarse clasts formed at the front of the surge. For three runs, large (1 to 2 kg) samples were taken at the front, middle, and rear of the deposit below the flume, for grain size analysis. These samples show the systematic variation in pebble content (Table 8.2). The Ryan (RC) tests did not show this systematic variation. A vertical gradient of pebble content was not noticed in the deposits; however, the debris flowed over a small drop before being deposited, so if such a gradient existed in the flows, it may have been destroyed by mixing.

Figure 8.5 shows a plot of Bingham viscosity against sediment concentration for the Boundary and Meager tests. The relation for the group of tests as a whole is good ($r^2 = 0.81$), although it is poor for some materials in the group (especially BC).

The sediment concentrations of the "coarse" (added pebbles) tests are higher than those of the "fine" (matrix only) tests. The sediment concentrations can be adjusted by calculating the water content on the basis of matrix weight only. It seems to be reasonable to do this; the pebbles should absorb a negligible amount of water compared to the finer matrix, and if the debris viscosity is due to the properties of the matrix, the adjusted sediment concentrations should give a better relation. However, the overall relation (graph B) is much poorer. The viscosities for the "coarse" samples are almost an order of magnitude higher than they would be

if they fell on the same trend as the "fine" samples. This demonstrates that content of coarse particles, as well as the water content of the matrix, controls the apparent viscosity.

Figure 8.6 shows the calculated Bingham yield strength plotted against sediment concentration. The coarse-textured materials (Hot Springs and Ryan) are shown for comparison, although as discussed above, these values are probably not true Bingham yield strengths. For the Boundary and Meager samples, each individual group of tests (BF, BC, MF, and MC) show good relations, although there is no overall relation. If the yield strengths are plotted against adjusted sediment concentration (matrix water content only), the points for the added-pebble ("coarse") tests move much closer to the corresponding points for the matrix-only ("fine") tests. This implies that the Bingham yield strength is mainly due to the properties of the matrix, and is affected only to a minor extent by the pebble content.

Figure 8.7 shows the granular resistance term (graph A) for the Hot Springs and Ryan tests, and also the apparent Newtonian viscosity (graph B) for all tests. There is a weak trend to increasing resistance with increasing sediment concentration for the coarse-textured materials. However, the overall relations are poor; $r^2 = 0.32$ for both granular resistance (Fig. 8.7A), and apparent Newtonian viscosity (Fig. 8.7B, coarse-textured samples only).

Table 8.3 also shows rheologic parameters calculated from recession flows. Figure 8.3 shows an example of the photographs used to obtain the data, and Figure 8.8 gives two examples illustrating the calculation procedure. For each data point, the surface velocity U, and the term $\gamma S(H-T_0)^2/2$, were tabulated in a spreadsheet. The critical thickness $T_0$ was varied by trial and error until the correlation coefficient was maximized. A regression line was then calculated, forced through the origin; U was taken to be the independent variable in the regression since the term $(H-T_0)$ is subject to considerable error. The Bingham viscosity is the slope of this regression line, and yield strength is calculated from the best-fit value of $T_0$. A similar procedure was used to calculate granular resistance for the dilatant model, except that yield strength is assumed to be zero.

The Bingham parameters calculated by this curve-fitting procedure differ considerably from those calculated from the velocity of the wave front. The calculated Bingham viscosity is

highly sensitive to the chosen value of $T_0$, especially for the shallowest flows for which $(H-T_0)$ is close to zero. The differences in calculated values may be due to inaccuracies in estimating flow depth from the photographs, or they may reflect different debris properties or flow behaviour in the frontal and recession parts of the surges. Both Major and Pierson (1992) and Phillips and Davies (1991) found that at low shear rates, the behaviour of debris flow material may depart considerably from the ideal Bingham model, so the parameters calculated by the two methods may not be comparable. The calculation of Bingham parameters from recession flows is probably not as satisfactory a method as measuring the depth and velocity of the wave front, because of the low shear rates and because the recession portion of the flow may not be representative of the coarser frontal portion. However, the data in Figure 8.8 lend support to the conclusion that the Bingham model can be used to describe the behaviour of fine-textured debris.

## 8.4 SUMMARY OF FLUME RESULTS

The most significant conclusion that can be drawn from the flume experiments is that the fine-textured materials (Boundary and Meager) demonstrate a well-defined Bingham yield strength, which for each material is positively correlated with sediment concentration. The coarse-textured materials (Hot Springs and Ryan) do not appear to possess a Bingham yield strength. This result suggests that the Bingham model is appropriate for modeling the behaviour of the fine-textured debris, but is not appropriate for the coarse-textured debris. However, no conclusion can be drawn as to which single-parameter model, the Newtonian or the dilatant model, is more appropriate for coarse-textured debris.

If all the fine-textured samples tested are treated as one population, there is a good relation between Bingham viscosity and sediment concentration. There are some indications from the data that Bingham viscosity is significantly influenced by the concentration of coarse clasts (larger than 4 mm), while Bingham yield strength is controlled mainly by the water content of the debris matrix (material smaller than 4 mm).

In most of the tests which included pebbles, the coarser clasts became concentrated at the front of the surge wave. No information was obtained on the mechanism which caused this sorting.

The sediment concentrations, Bingham yield strengths, and Bingham viscosities measured in this study are reasonably comparable to those measured in flume and viscometer tests by Owens (1973), Fairchild (1985), and Major and Pierson (1992). However, the values of the Bingham and Newtonian parameters are much lower (by one to three orders of magnitude) than those calculated for natural debris flows in Chapter 7. This difference is expected, according to the scaling relations discussed above. The purpose of flume and viscometer tests is not to calculate parameters that can be used in modeling real debris flows, but to investigate the applicability of various rheologic models that can be used to explain debris flow behaviour.

## TABLE 8.1 REVIEW OF PUBLISHED RHEOLOGIC EXPERIMENTS

| Reference | Type of rheometer | Size | Material tested | Range of $c_s$ (%) | Range of shear rate ($s^{-1}$) | Range of k (Pa) | Range of $\mu_B$ (Pa.s) | Range of $\mu_N$ (Pa.s) | Remarks |
|---|---|---|---|---|---|---|---|---|---|
| A. Viscometer tests | | | | | | | | | |
| Owens, 1973 | Concentric cylinder | 200 ml (gap not reported) | Debris flow samples < 8 mm | 60-80 | 1-6 | 5-71 | 0.8-23 | - | Silty fines; sand & small pebbles added |
| O'Brien and Julien, 1988 | Concentric cylinder | not reported | Debris flow fines | 30-70 | up to 150 ? | 0.2-100 | 0.04-10 | - | Sand added for some tests; clay 3-32% |
| Phillips and Davies, 1991 | Cone and plate | 1. 2 m diameter | Debris flow samples < 120 mm | 88-90 | 0.5-4 | - | - | 300-1800 | Samples collected from two debris flows in motion; 12-24% fines, up to 11% clay |
| | | 2. 0.4 m diameter | < 35 mm | 75-83 | 1-18 | 15-300 | - | 0.4-238 | (same as above) |
| Major and Pierson, 1992 | Concentric cylinder | 230 mm diam., 31 mm gap | Debris flow samples < 2 mm | 68-84 | up to 50 | 12-405 | 0.2-28 | - | Fines and sand mixed in varying proportions |
| B. Flume tests | | | | | | | | | |
| Owens, 1973 | Semi-circular flumes | 9.4 cm and 16.2 cm wide, slope 10-20° | Debris flow samples < 16 mm | 66-82 | not reported | 3.2-160 | 0.001-11 | - | Velocity profile measured photographically |
| Fairchild, 1985 | 1. Batch flume | not reported | Debris flow samples < 23 mm | 83-84 | not reported | 50-280 | 3-48 | - | k from deposit thickness |
| | 2. Recir-culating flume | 4.9 m long, 13.5 cm wide, 25 cm deep | Synthetic slurries | 15-56 | not reported | 12-200 | - | - | Uniform steady flow; Bingham model not assumed |
| Takahashi, 1991 | Various flume experiments | various; typical 5-20 cm wide, slope 7-25° | Sand and fine gravel in water | 30-80 | typical 10-30 ? | - | - | - | Numerous experiments reviewed. Dilatant (granular) flow model used. |

TABLE 8.2 MATERIAL USED IN FLUME TESTS

A. TEXTURE OF SAMPLES

| Tests | Run numbers | Proportions sand:silt:clay in matrix [1] | Proportions pebbles:matrix for coarse tests [2] |
|---|---|---|---|
| Fine-textured debris | | | |
| Boundary fine | BF 2-6 | 69:21:10 | - |
| Boundary coarse [3] | BC 2-8, 11-12 | 69:21:10 | 38:62 |
| Boundary coarse, extra stones | BC 10 | 69:21:10 | 54:46 |
| Meager fine | MF 2-5 | 68:22:10 | - |
| Meager coarse | MC 1-5 | 68:22:10 | 33:67 |
| Coarse-textured debris | | | |
| Hot Springs fine | HF 3-5 | 83:15:2 | - |
| Hot Springs coarse | HC 1-3, 5-6 | 83:15:2 | 54:46 |
| Ryan fine | RF 2 | 91:9:0 | - |
| Ryan coarse | RC 1-3 | 91:9:0 | 39:61 |

Notes: 1. Material < 4 mm; "sand" includes granules (2-4 mm)
2. Measured from debris deposits following tests. "Coarse tests" refers to debris to which pebbles were added, for both fine-textured and coarse-textured debris.
3. Run BC 8 used a 40 litre sample. All other runs used 20 litre samples. BC 12 used a rough-bed flume insert.

B. VARIATION IN TEXTURE OF COARSE TESTS

| Test | Percentage of pebbles sampled in: [1] | | |
|---|---|---|---|
| | Front | Middle | Rear |
| BC 4 | 50 | 34 | 31 |
| MC 4 | 43 | 30 | 25 |
| HC 3 | 57 | 54 | 51 |

Notes: 1. Samples taken from debris deposits following tests.

TABLE 8.3 SUMMARY DATA FROM FLUME TESTS

| test | S | w | $C_s$ | k (Pa) | $\mu_B$ (Pa.s) | $\mu_G$ (Pa.s$^2$) | $\mu_N$ (Pa.s) | H (m) | $k_{(R)}$ (Pa) | $\mu_{B(R)}$ (Pa.s) or $\mu_{G(R)}$ (Pa.s$^2$) |
|---|---|---|---|---|---|---|---|---|---|---|
| BF2 | 0.54 | 0.283 | 0.779 | 249 | | | | 0.028 | | |
| BF3 | 0.54 | 0.296 | 0.772 | 205 | 0.42 | | 1.41 | 0.039 | | |
| BF4 | 0.43 | 0.291 | 0.775 | 197 | | | | 0.036 | | |
| BF5 | 0.43 | 0.297 | 0.771 | 114 | 0.57 | | 1.17 | 0.039 | | |
| BF6 | 0.34 | 0.308 | 0.765 | 135 | 0.34 | | 1.28 | 0.038 | | |
| BC2 | 0.54 | 0.194 | 0.838 | 187 | 0.78 | | 2.12 | 0.038 | | |
| BC3 | 0.43 | 0.200 | 0.833 | 201 | | | | 0.041 | | |
| BC4 | 0.43 | 0.203 | 0.831 | 157 | 1.26 | | 2.79 | 0.047 | | |
| BC5 | 0.34 | 0.201 | 0.833 | 159 | | | | 0.044 | | |
| BC6 | 0.34 | 0.221 | 0.819 | 103 | 0.88 | | 1.63 | 0.047 | | |
| BC7 | 0.34 | 0.211 | 0.826 | 117 | 0.93 | | 1.91 | 0.048 | 117 | 0.67 |
| BC8 | 0.34 | 0.217 | 0.822 | 117 | 1.38 | | 2.45 | 0.056 | 93 | 2.36 |
| BC11 | 0.34 | 0.208 | 0.828 | 124 | 1.31 | | 2.49 | 0.055 | | |
| BC10 | 0.34 | 0.174 | 0.852 | 129 | 2.36 | | 4.69 | 0.053 | | |
| BC12 | 0.34 | 0.211 | 0.826 | 193 | 1.79 | | 4.76 | 0.064 | | |
| MF2 | 0.54 | 0.228 | 0.814 | 151 | 0.93 | | 2.30 | 0.034 | | |
| MF3 | 0.43 | 0.225 | 0.816 | 267 | | | | 0.032 | | |
| MF4 | 0.43 | 0.243 | 0.805 | 102 | 0.78 | | 1.38 | 0.040 | 76 | 1.24 |
| MF5 | 0.34 | 0.242 | 0.805 | 147 | 0.65 | | 2.76 | 0.039 | 117 | 4.26 |
| MC1 | 0.54 | 0.178 | 0.849 | 180 | 2.04 | | 4.05 | 0.047 | | |
| MC2 | 0.43 | 0.176 | 0.850 | 206 | 2.19 | | 9.00 | 0.042 | | |
| MC3 | 0.43 | 0.187 | 0.842 | 106 | 1.50 | | 2.46 | 0.045 | 71 | 2.67 |
| MC4 | 0.34 | 0.186 | 0.843 | 140 | 1.71 | | 4.34 | 0.047 | | |
| MC5 | 0.34 | 0.197 | 0.835 | 78 | 1.05 | | 1.62 | 0.046 | | |
| HF3 | 0.54 | 0.230 | 0.813 | 33 | | 0.017 | 1.83 | 0.040 | | |
| HF4 | 0.43 | 0.226 | 0.816 | 44 | | 0.070 | 3.57 | 0.046 | | 0.130 |
| HF5 | 0.43 | 0.242 | 0.805 | 26 | | 0.024 | 2.03 | 0.044 | | |
| HC1 | 0.54 | 0.110 | 0.901 | 49 | | 0.066 | 3.34 | 0.031 | | |
| HC2 | 0.54 | 0.118 | 0.894 | 18 | | 0.042 | 3.07 | 0.041 | | |
| HC3 | 0.43 | 0.119 | 0.894 | 49 | | 0.140 | 4.95 | 0.040 | | |
| HC5 | 0.34 | 0.120 | 0.893 | 38 | | 0.289 | 7.68 | 0.060 | | 0.194 |
| HC6 | 0.43 | 0.129 | 0.886 | 38 | | 0.133 | 5.53 | 0.054 | | |
| RF2 | 0.54 | 0.186 | 0.843 | 34 | | 0.053 | 3.20 | 0.038 | | |
| RC1 | 0.54 | 0.145 | 0.873 | 28 | | 0.020 | 1.83 | 0.034 | | |
| RC2 | 0.43 | 0.136 | 0.880 | 24 | | 0.430 | 10.25 | 0.057 | | |
| RC3 | 0.43 | 0.125 | 0.889 | 24 | | 0.152 | 5.74 | 0.050 | | |

S : slope = sin (flume angle)
w : water content, dry weight basis
$C_s$ : Solids concentration by weight
k : yield strength (Pa) = $\gamma.T_0.S$
$\mu_B$ : Bingham viscosity (Pa.s)
$\mu_G$ : resistance term in granular flow model (Pa.s$^2$)
$\mu_N$ : apparent Newtonian viscosity (Pa.s)
H : average wave height at flume distance of 3 to 4 m (m)
$k_{(R)}$, $\mu_{B(R)}$, $\mu_{G(R)}$ : calculated from recession flow

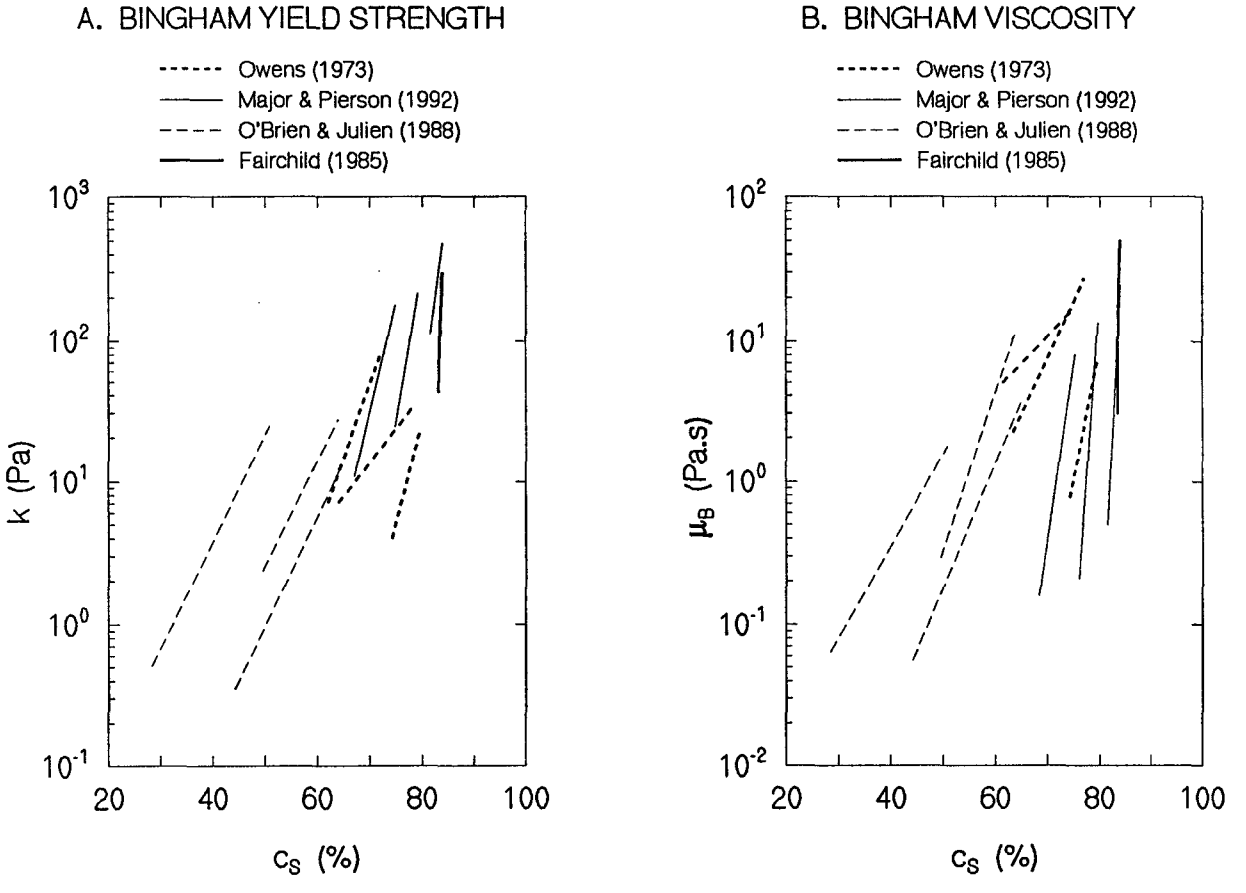


FIGURE 8.1. RESULTS OF SELECTED RHEOLOGIC EXPERIMENTS FROM THE LITERATURE.

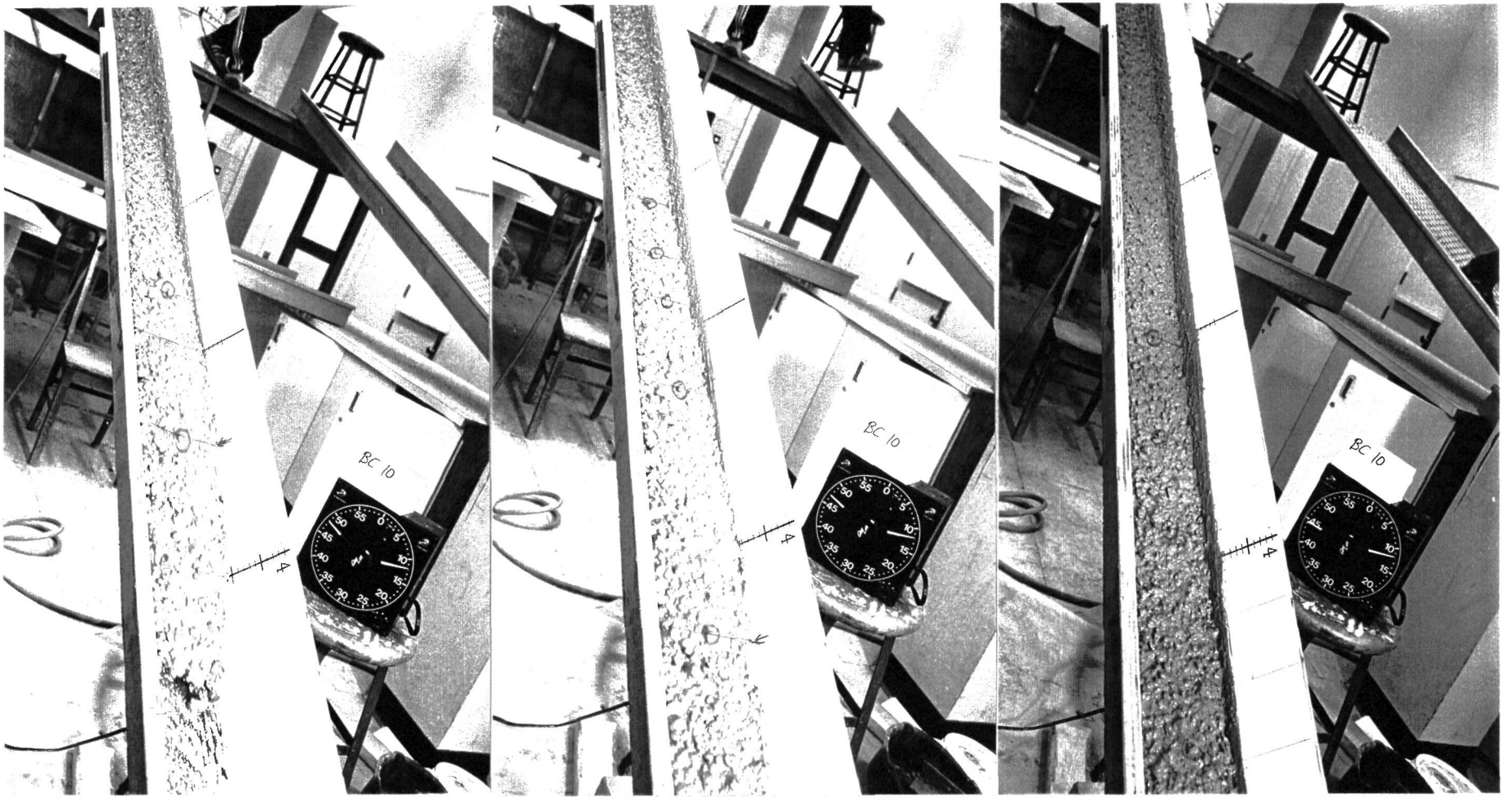


FIGURE 8.2. FLUME TESTS: OBLIQUE PHOTOS. These photos are taken from the position of the video camera used to record wave front velocity.

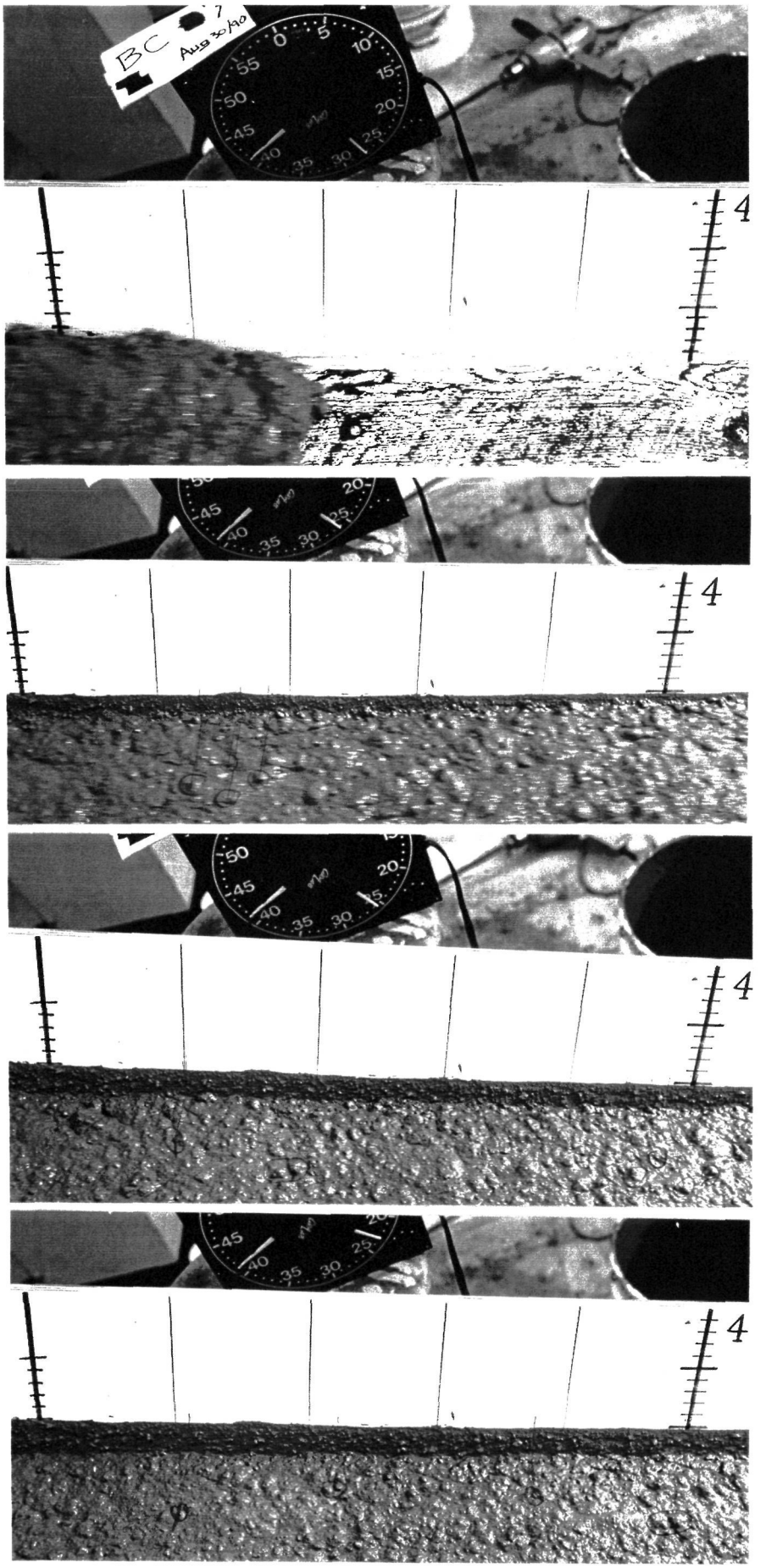


FIGURE 8.3. FLUME TESTS: CLOSE-UP PERPENDICULAR PHOTOS. These photos were used to calculate velocity and depth for recession flows.

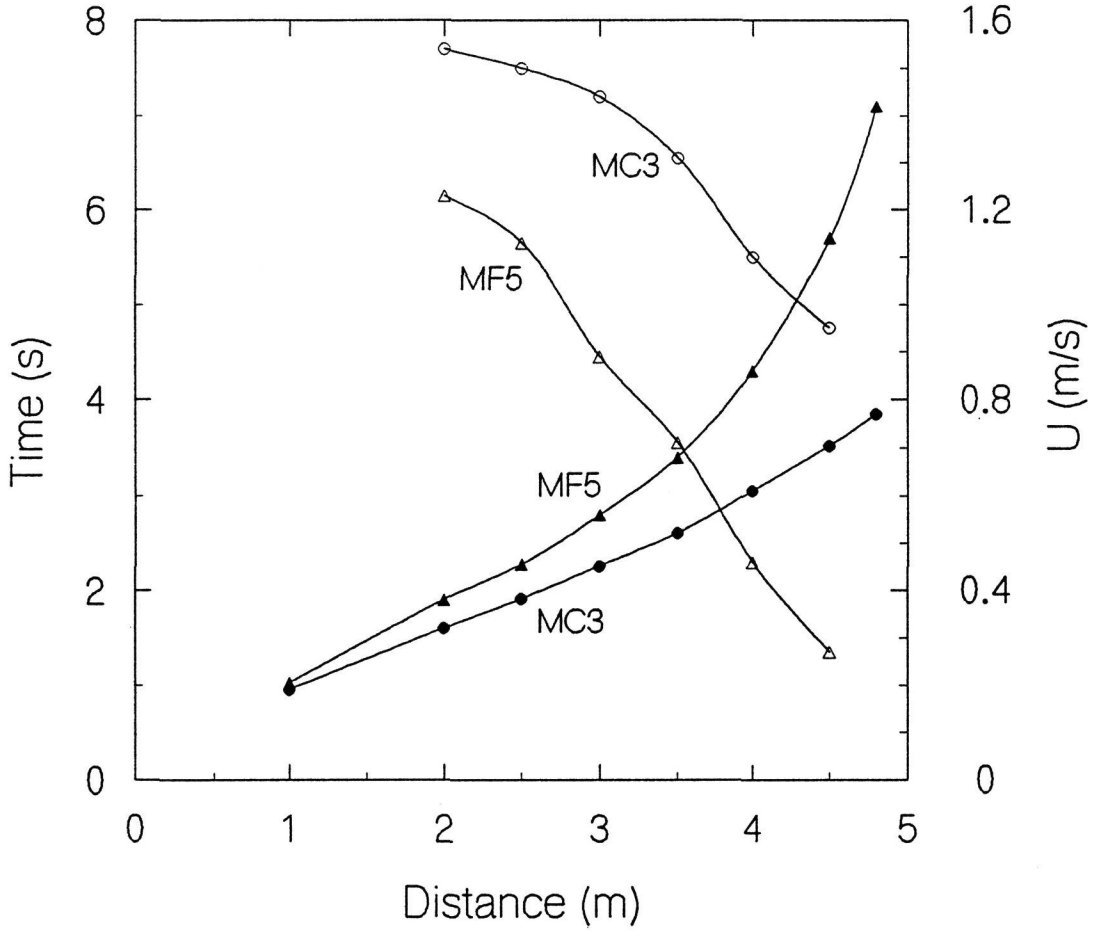


FIGURE 8.4. EXAMPLE OF PROCEDURE USED TO CALCULATE WAVE FRONT VELOCITY. Closed symbols are front position vs. time from video recording. Open symbols are calculated velocity.

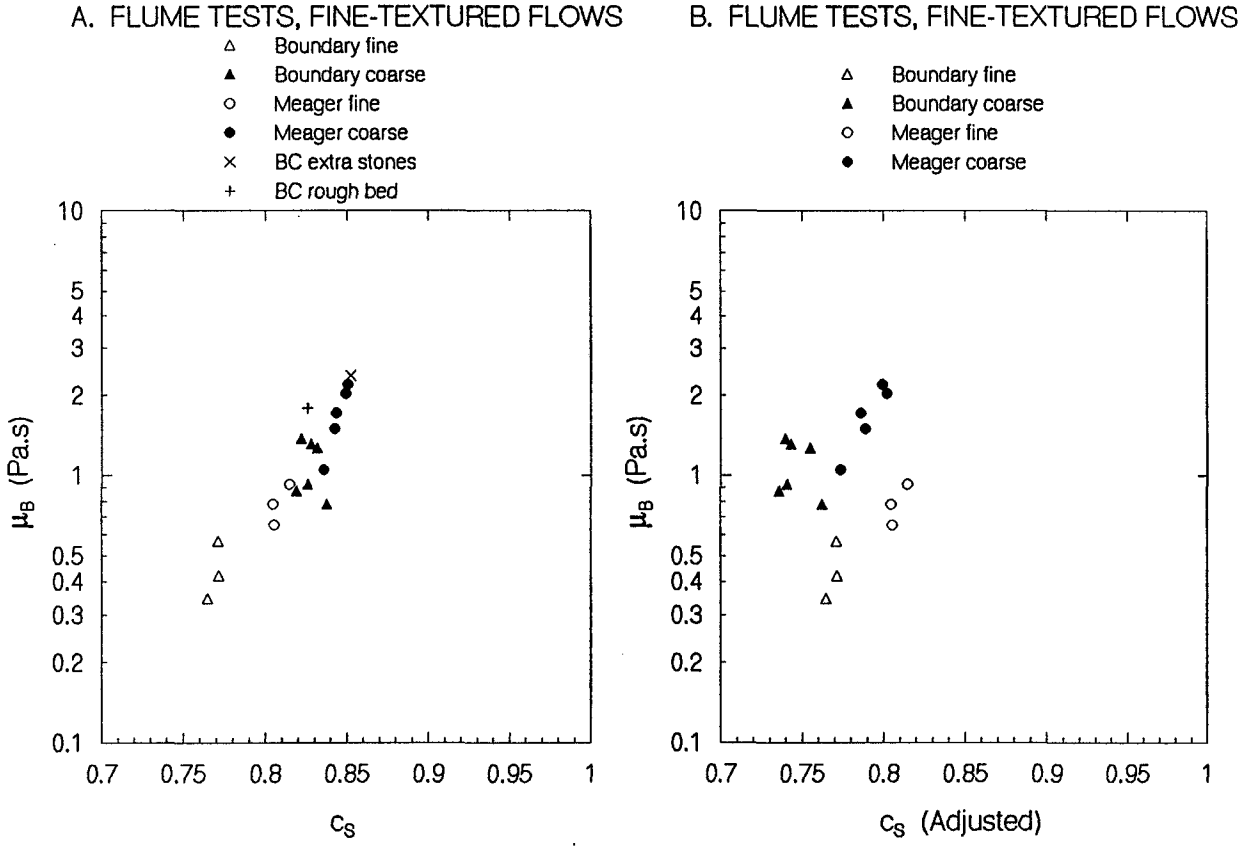


FIGURE 8.5. BINGHAM VISCOSITY VS. SEDIMENT CONCENTRATION. Samples labeled "fine" are matrix material (< 4 mm). Samples labeled "coarse" have pebbles added to matrix material. Graph B shows adjusted sediment concentration, calculated on the basis of water content of the matrix.

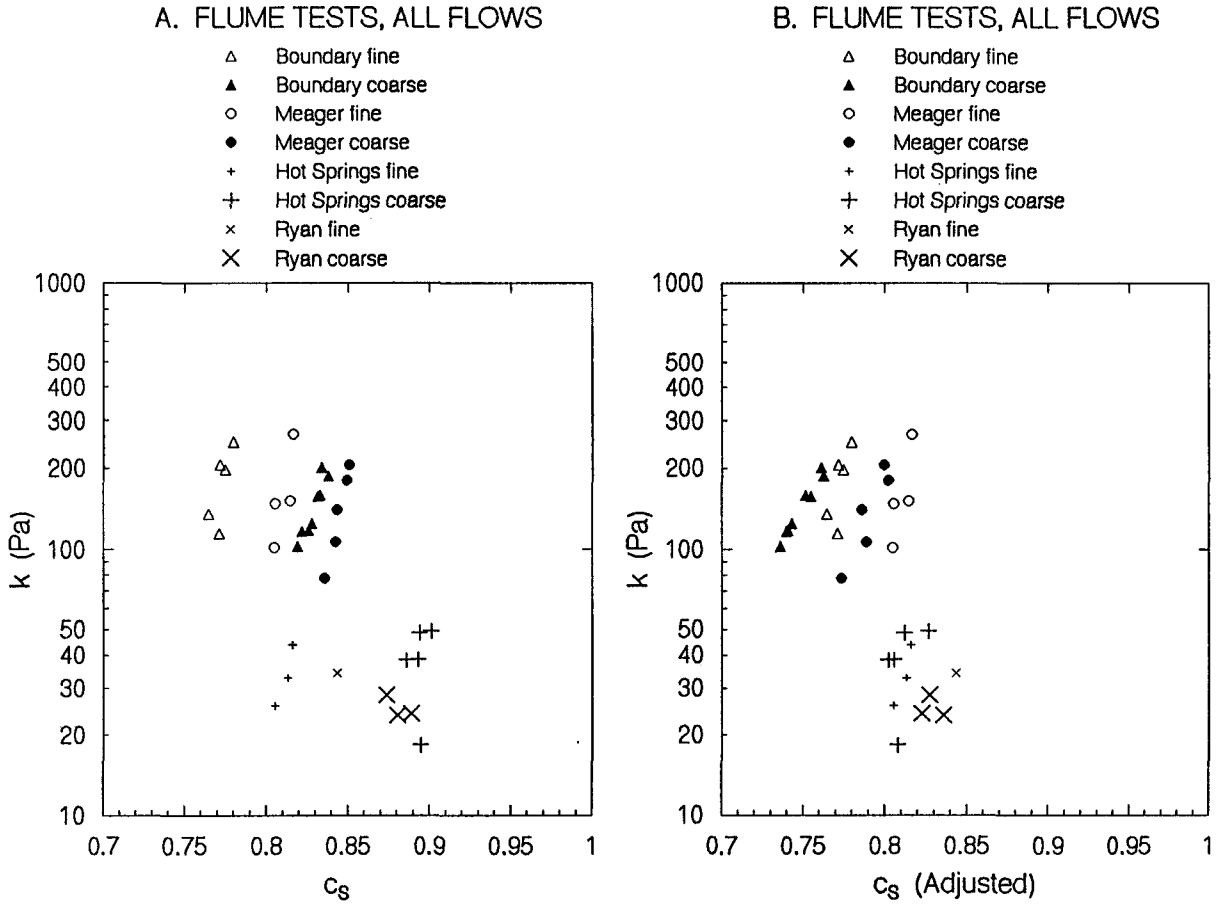


FIGURE 8.6. BINGHAM YIELD STRENGTH VS. SEDIMENT CONCENTRATION.
(See explanatory notes for Figure 8.5.)

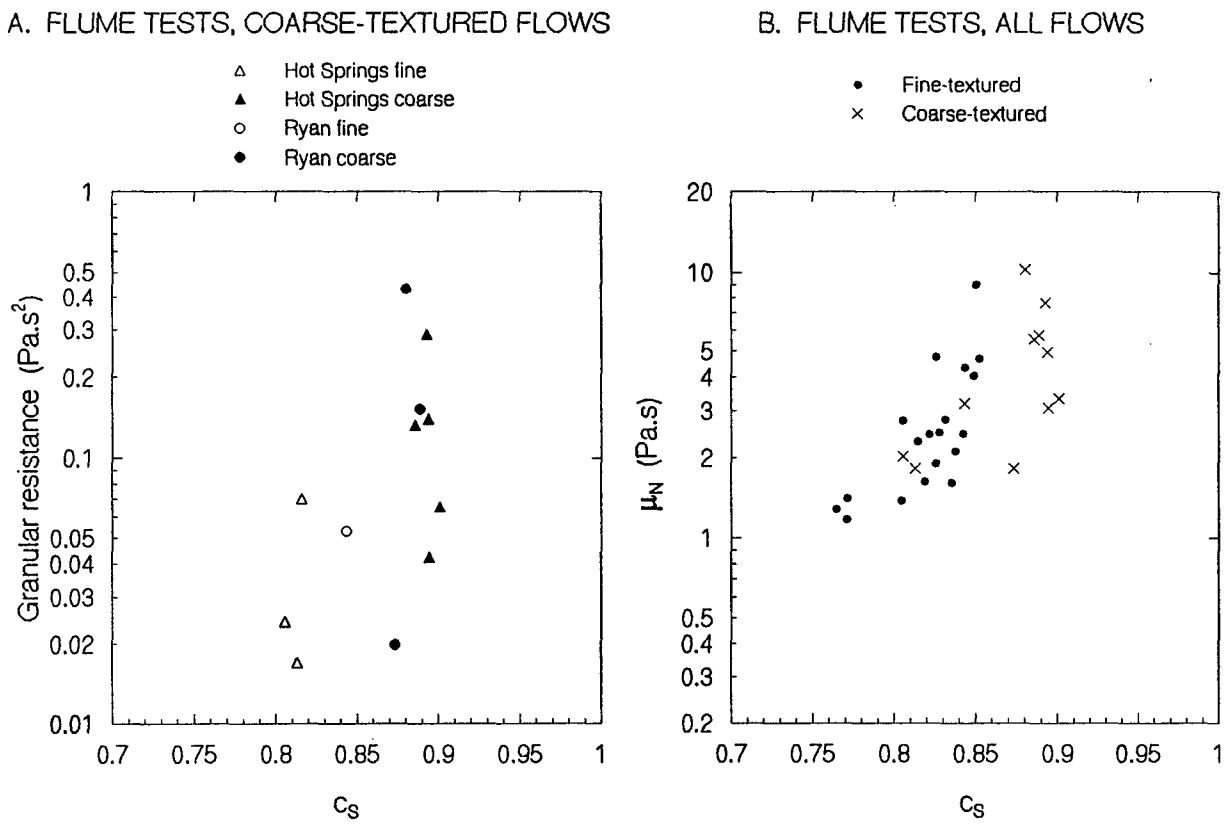


FIGURE 8.7. GRANULAR RESISTANCE AND APPARENT NEWTONIAN VISCOSITY VS. SEDIMENT CONCENTRATION.
Graph A : Granular resistance term is $\mu_G$ in dilatant model.
Graph B : Apparent Newtonian viscosity for all tests. Fine-textured samples are Boundary and Devastation, coarse-textured samples are Hot Springs and Ryan.

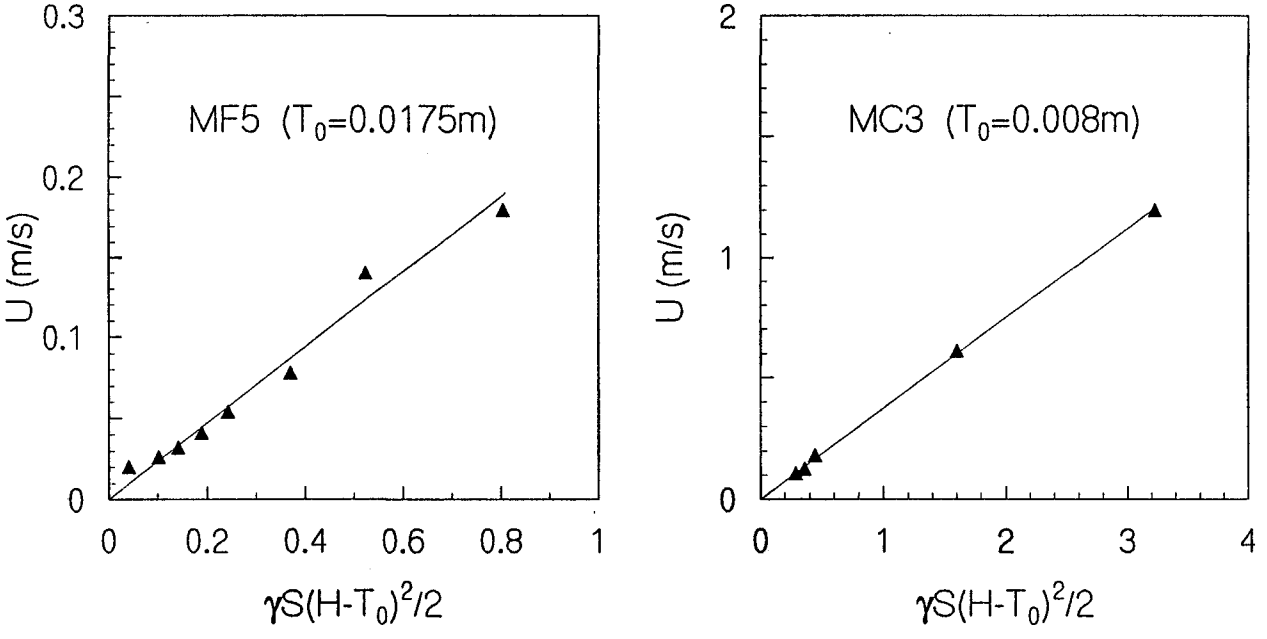


FIGURE 8.8. EXAMPLES OF VISCOSITY CALCULATION FROM RECESSION FLOW. U is surface velocity calculated from photographs. The line is a regression line forced through the origin.

# CHAPTER 9. SUMMARY, CLASSIFICATION, AND CONCLUSIONS

## 9.1 SUMMARY OF RESULTS

In this study, 25 debris flow events in or adjacent to the southern Coast Mountains were examined in the field, 13 of them in considerable detail. The volumes of these debris flows ranged from about 100 $m^3$ to over $10^7$ $m^3$. Field investigations depended on study of debris flow deposits and evidence of flow in the channels, since no events were observed in motion. Most of the debris flows fall into two distinct populations. Coarse-textured debris flows, with abundant cobbles and boulders and a sandy matrix, are derived from competent plutonic rocks. They develop depositional fans with slopes of 7 to 15°, and have inversely graded deposits with a distinct clast-supported surface layer of cobbles and boulders. Fine-textured debris flows, with a significant clay content in the matrix and less abundant coarse clasts, are derived from incompetent or altered, Quaternary, volcanic rocks. They come to rest on slopes gentler than 7°, and form deposits with no systematic grading or internal structure. These two categories reflect the two principal rock types of the study area. There are several events in the study area with intermediate debris composition, which show features of both debris flow categories. These events are derived from drainages with a mixture of plutonic and volcanic rocks, or with other lithologies such as sedimentary rocks.

At the detailed study sites, debris flow material was sampled to determine grain-size distributions representative of all size classes, including boulders. The coarse-textured and fine-textured categories of debris flow, which were initially defined on the basis of lithology, deposit morphology, and vertical grading, can be approximately distinguished by the following grain-size parameters: $M_z$ (graphic mean) = -4 $\phi$; $\sigma_I$ (inclusive graphic standard deviation) = 4 $\phi$; and a matrix clay content of about 4 to 5%. These statistics are based on subsurface material truncated at 256 mm. On the basis of bimodality in some grain-size distributions, "matrix" is defined as material smaller than 4 mm. This definition is somewhat arbitrary, as some debris flows are not bimodal, in which case there is no reasonable basis for distinguishing matrix from clasts. Bimodality is more pronounced in coarse-textured debris flows. Almost all grain-size

distributions were strongly fine-skewed, with a relatively large proportion of stones larger than 32 mm.

A distinguishing feature of the coarse-textured debris flows is a well-defined, clast-supported, inversely-graded, surface layer. Almost all the fine-textured debris flows, and the subsurface layers of coarse-textured debris flows, are ungraded and unstratified. The one exception is the fine-textured Upper Lillooet River debris flow, which is normally graded; apparently, large clasts were settling to the base of the debris flow as it moved downstream. This event had a lower matrix clay content than other debris flows classified as "fine-textured", at 6.7%. It may be an example of the downstream progression of a relatively non-cohesive debris flow to hyperconcentrated flow as it mixes with river water (as documented by Pierson and Scott, 1985).

Almost all debris flows examined showed evidence in their deposits of a frontal accumulation of coarse stones, even though there was no inverse grading in the main deposit of fine-textured debris flows. Many debris flow events left fine-textured afterflow deposits, which strongly resembled the matrix of the main deposit in its grain-size distribution.

Two events on Capricorn Creek are classified as "debris floods", rather than debris flows, on the basis of the stratigraphy of their deposits. However, they cannot be distinguished readily from coarse-textured debris flows on the basis of bulk sediment texture.

Fine-textured debris flows show very little lateral variability in the texture of their deposits. Coarse-textured debris flows have little lateral variability in the texture of subsurface material, but there is often variability in the thickness and clast size of the surface layer. Fine-textured debris flow deposits are often very uniform in thickness, which lends support to the Bingham model as appropriate to describe their behaviour. Also, they often leave thin, uniform layers of fine debris in the channel after they pass, as the Bingham model predicts. Coarse-textured debris flow deposits usually are less uniform in thickness, and usually do not leave layers of debris remaining in their channels, which implies that they are not behaving according to the Bingham model.

All debris flow deposits observed appear to be matrix-supported in their main, subsurface portions, even those derived from very coarse-textured debris flows with abundant cobbles and boulders. The reason for this appears to be, based on observation of deposits and from videos of flowing debris (*e.g.* Costa and Williams, 1984), that excess coarse clasts are ejected from the subsurface portion of flow and accumulate as an inversely graded surface layer. The mechanism responsible for this process is probably dispersive stress, as predicted by the dilatant flow model.

Geotechnical tests were performed on several samples of reconstituted debris, representative of typical fine-textured and coarse-textured debris flows. Tests included shear strength, permeability, and consolidation. The angle of internal friction was the same, about 42°, for both types of debris. Permeability, however, is strongly dependent on debris texture, ranging from about $10^{-8}$ m/s for clay-rich debris to $2 \times 10^{-6}$ m/s for sandy debris. Largely because of the low permeability, the consolidation rates of fine-textured debris are much lower than those of coarse-textured debris. The time required for excess pore pressure to dissipate sufficiently to generate significant frictional strength ranged from several minutes in sandy, coarse-textured debris, to several days in clay-rich, fine-textured debris. These tests are supported by field observations that fine-textured debris flows remain in an almost completely undrained state for several days following deposition.

It is reasonable to conclude that, during deposition of debris flows, fine-textured debris may be in a completely undrained state, with effective normal stress and frictional strength equal to, or very close to, zero. Coarse-textured debris, by contrast, drains sufficiently rapidly that significant frictional strength develops during deposition. This mechanism probably explains the ability of fine-textured debris flows to travel, and form deposits, on very gentle slopes, as low as 0.4° for large debris flows in this study, while coarse-textured debris flows tend to come to rest on slopes between about 7 and 15°.

Because of their low rate of consolidation, fine-textured deposits on a fan can be easily remobilized by additional surges, over periods of perhaps many hours. Thus, the entire deposit acts as a single body of fluid, advancing at the toe as it reaches a uniform thickness determined by the Bingham yield strength. By contrast, each coarse-textured debris surge, once at rest, is

resistant to remobilization because of its frictional strength. Multiple surges therefore tend to form irregular deposits consisting of a series of lobes.

Calculated velocities and apparent Newtonian viscosities of debris flows in this study reveal a tendency for coarser textured flows to have a greater resistance to flow. However, there is no firm evidence from the calculated flow parameters to determine whether individual debris flows behave according to a viscous (Newtonian or Bingham) flow model, or an inertial (dilatant) flow model.

Statistical analysis suggests that debris flow volume, and the proportion of clay in the debris matrix, are the most significant factors explaining the slope of deposition. Debris flow volume is the only statistically significant factor explaining runout distance on unconfined fans. Some debris flows confined by constructional levées, or by valley walls, had greater runout distances than unconfined debris flows of similar volume.

There is a poor relation between total debris flow volume and maximum discharge. This is probably explained by the tendency of debris flows to form multiple surges.

The debris flows examined in this study, and those previously reported in the literature, have a smaller range of velocities and apparent viscosities than would be expected, considering the sensitivity of velocity to flow depth, and of viscosity to water content. This may be due to a negative feedback mechanism which limits debris flow to a restricted range of water contents; fast-moving debris flows erode more channel sediment, which increases the viscosity, while slow-moving debris flows can mix with more fluid debris from behind, thereby decreasing the viscosity. An alternative explanation may be that the coarse frontal accumulation of coarse clasts which occurs in most debris flows may limit flow velocity, and thus increase the apparent viscosity of fine-textured debris flows, even though the coarse front may be only a small proportion of the total debris flow volume.

Existing approaches to describing and modeling debris flow behaviour, including the ones used in this study, assume that the entire main surge has consistent physical properties. However, the frontal concentration of stones may exert a controlling influence on some aspects of debris flow behaviour, and it may have properties very different from the main body of the

surge behind it. This problem of varying rheologic and strength characteristics within debris flow surges has yet to be studied quantitatively.

Flume tests on fine-textured debris samples showed that both the Bingham viscosity and yield strength increased rapidly with increasing sediment concentration. In coarse-textured samples, however, the apparent Newtonian viscosity and the granular flow resistance did not show a strong relation with sediment concentration. The coarse-textured debris samples appeared, from flume tests, to have a very low or nonexistent Bingham yield strength. The flume tests support the field observation that many features of fine-textured debris flows can be described by the Bingham flow model, while coarse-textured debris flows are better described by a single-parameter (dilatant or Newtonian) flow model.

## 9.2 CLASSIFICATION OF DEBRIS FLOWS AND RELATED PHENOMENA

This section deals with the classification of phenomena which fall within the category of mass movement generally considered to be debris flow, with an emphasis on events examined in this study. Chapter 1 dealt with the definition and classification of debris flow in the context of other mass movement processes.

The most widely used, early classification of mass movement processes is that of Varnes (1978, revised from the original 1958 version). In this classification, "debris flow" is identified as a single category, with one subcategory, "mudflow", defined on the basis of a gravel content less than 50%. Swanston and Swanson (1976) classified mass movement processes in steep, forested environments (of which this study area is one) using Varnes' terminology in most instances, but introducing the term "debris torrent" to describe debris flows confined in channels. VanDine (1985) presented a classification, which differs considerably from that of Varnes in that it considers processes transitional between mass movement and streamflow. VanDine also used the term "debris torrent" to describe channelized, predominantly coarse-textured, debris flows. Costa (1984) also described, without formal classification, the transition between debris flow and streamflow.

Pierson and Costa (1987) introduced a classification of sediment-water flows on the basis of sediment concentration and flow velocity. In their classification, "slurry flow" is distinguished

from granular flow, which is unsaturated or at a water content below the liquid limit, and from hyperconcentrated streamflow, which has a water content too high to carry gravel in suspension and to exhibit plastic flow behaviour. Slurry flow is divided into "viscous slurry flow", which can be described by the Bingham flow model, and "inertial slurry flow", which can be described by the dilatant flow model. They recommend the use of the term "debris flow" to describe both types of slurry flow.

Scott *et al.* (1992) divided debris flows into two categories, cohesive and noncohesive, on the basis of clay content. Cohesive debris flows contain more than about 3 to 5% clay, and resist mixing with water in stream channels; thus, if of large size they tend to be more persistent, and can travel long distances down river valleys. Noncohesive debris flows contain less than about 3 to 5% clay; they can mix more readily with water, and tend to evolve into hyperconcentrated flow as they move down valleys. In their Mount Rainier study area, cohesive debris flows resulted from large landslides in hydrothermally altered, clay-rich, volcanic rock, while noncohesive debris flows originated as flood surges which bulked to debris flows by entraining stream-channel sediment.

The classification of Pierson and Costa (1987) appears to be applicable to both the field and laboratory observations made in this study. Most debris flow events can be described by their "viscous" and "inertial" categories, which correspond, respectively, to the "fine-textured" and "coarse-textured" classes used in this study. Also, there is support for the "cohesive" and "noncohesive" categories of Scott *et al.* (1992). The debris flows derived from clay-rich, altered, volcanic rocks, such as those on Boundary, Devastation, and No Good Creeks, are clearly cohesive; they appear to have resisted mixing with water on encountering large water courses, and texture and structure did not vary downstream. Several fine-textured debris flows with relatively low clay contents fall in the noncohesive category; in particular, the Upper Lillooet River event changed in texture downstream, apparently because of dilution with water. Many events initially classed as "intermediate" fall into the noncohesive category, which may include events which display features of both Bingham and dilatant flow. The matrix clay

content of the "noncohesive" debris flows is apparently insufficient to give cohesive properties to the debris flow mass as a whole.

Table 9.1 gives a classification of debris flows observed in this study, which incorporates the terminology of the above two classifications. The figures for clay content, mean grain size ($M_Z$), and sorting ($\sigma_I$), are based on those given in Chapter 5. Although they are typical of this study area, they may not necessarily apply to debris flows in other geologic environments. The total clay content (< 256 mm basis) corresponding to the viscous categories is considerably lower than that reported in other studies; this is because the high content of cobbles typical of this study area strongly affects statistics based on the total (or < 256 mm) sample. For this reason, the clay content of the matrix (< 4 mm) is a more consistent statistic; in this study, flow behaviour appeared to be controlled more by the matrix clay content than by the content of coarse clasts. The figures for hydraulic conductivity ($K_{sat}$) in the table are order-of-magnitude estimates, as measurements were made on relatively few samples.

The table includes a category for "debris floods", a term which has been described (although not strictly defined) by Slaymaker (1988; after Aulitzky, 1980). It is defined here as a form of fluvial transport in which large quantities of bedload are rapidly transported in steep (usually > 8°) stream channels, and emplaced in massive or weakly stratified, poorly sorted deposits which have a superficial resemblance to debris flow deposits. They differ from true debris flows in that the water and sediment are distinct phases, which separate upon deposition. They differ from hyperconcentrated flow in that they have a very high proportion of coarse gravel and a low concentration of silt and clay, due to their usual origin in coarse-textured geologic materials which do not produce significant amounts of fine sediment. Debris floods may begin as coarse-textured debris flows, which progress to debris floods through mixing with streamflow. In this study, the best examples are the events on Capricorn Creek. They may also occur in some channels which normally produce fine-textured debris flows, such as No Good Creek, when a small, noncohesive, viscous debris flow, containing a relatively high proportion of gravel, mixes with large volumes of streamflow.

The phenomenon defined here as "debris flood" is often included, with coarse-textured debris flows, in the category of "debris torrent", a term in common usage in British Columbia. Pierson and Costa (1987) recommend that the term "debris torrent" be discontinued, since it has no rheologic basis. This writer concurs with this recommendation, and prefers that the more precise terms "debris flow" and "debris flood" be used.

Part B of Table 9.1 gives a very simple classification of sediment transport phenomena by water content. The processes with which debris flow can be transitional depend on debris texture. At water contents which are too high to support debris flow, fine-textured debris will be transported as hyperconcentrated flow, while coarse-textured debris will be transported as debris floods. Debris flows may evolve from noncohesive debris avalanches, or from cohesive debris slides or earthflows, if these landslides mix with sufficient water (although the reverse process is not possible). There probably exist phenomena which are transitional between all these categories of sediment movement.

The classification could also include two other factors related to flow and deposition behaviour. The first is whether the event occurs as a single surge, or as a series of surges. This factor controls the peak discharge, and therefore the peak velocity and flow depth, as compared to the total volume of the debris flow as a whole. The second factor is the mode of deposition upon losing confinement: whether the debris spreads out on its fan or valley bottom, or whether it is confined between levées which it constructs as it flows. This difference may be explained by water content; debris flows which spread out may have relatively high water contents, and some may be transitional to debris floods or hyperconcentrated flow, while levée-confined flows may be flowing near the lower limit of their possible water content.

## 9.3 CONCLUDING REMARKS

Debris flows examined in this study originated from several lithologic types, ranging from competent, coarse-grained, plutonic rocks to weak, clay-rich, Quaternary volcanic rocks. These debris flows displayed a wide range of flow behaviours. At one extreme are relatively low-mobility events consisting mostly of coarse gravel, which formed deposits on steep fans of 10-15°. At the other extreme are highly mobile, fine-textured events which flowed at high velocity

along low-gradient river valleys. This variety of behaviours can be explained in part by the different rheologic models which describe debris flows of differing texture. Both field observations and laboratory studies indicate that the Bingham flow model can describe many features of fine-textured debris flows, while the dilatant model is more applicable to coarse-textured debris flows.

The sample of debris flows studied in the field included several events with texture and depositional features intermediate between the fine and coarse textural extremes. However, laboratory tests were performed mainly on the obviously fine-textured, clay-rich, volcanic-source examples, and the obviously coarse-textured, sandy, plutonic-source examples. Most of the debris flows fell clearly into one or the other of these categories, but this may not be the case in other geologic environments. An important category of debris flows in southwestern British Columbia not included in the study is the type which originates in forested environments and includes a high proportion of organic material. All events in this study originated primarily in alpine or unvegetated areas, and contained little or no organic material.

Low permeability, low consolidation rates, and a relatively low abundance of large clasts are important factors which explain the greater mobility of fine-textured debris flows. Fine-textured debris behaves as a fluid during flow and deposition; the effective normal stress ($\sigma'$) is zero or very near zero, so there is little or no frictional strength, and collisions between large clasts are sufficiently damped by the viscous matrix that they do not contribute greatly to resistance during rapid flow. Coarse-textured debris probably also has a $\sigma'$ close to zero during flow, but frequent collisions between large clasts cause inertial resistance to flow. During deposition, significant frictional strength may develop as excess pore pressure dissipates and $\sigma'$ increases. This allows the debris to come to rest on relatively steep slopes. The clay content of the debris matrix appears to be the most important factor determining debris flow mobility and rheologic behaviour. The content of coarse clasts probably plays an important role as well; however, in this study almost all debris flows examined had relatively high proportions of gravel to matrix (50% or greater), so the effect of coarse clasts was difficult to assess.

The runout distances of all types of debris flows are strongly dependent on the total volume of the event. With fine-textured debris flows, total volume and Bingham yield strength are apparently the only significant factors determining runout distance. Therefore, large, fine-textured debris flows, derived from slope failures in weak, clay-rich, volcanic rocks, are extremely hazardous as they can flow for long distances on gentle gradients.

Several debris flows have been documented, originating in volcanic source areas, which had exceptionally large magnitudes and distances of flow. These include events in Devastation Creek, Upper Lillooet River, Turbid Creek, and Cheekye River. The behaviour of these fine-textured debris flows is not well explained by existing models developed for coarse-textured debris flows in the Coast Crystalline Complex, which underlies much of southwestern British Columbia. Understanding the flow behaviour and properties of these fine-textured debris flows is critical to hazard assessment in the valleys below the Quaternary volcanic complexes.

## TABLE 9.1 CLASSIFICATION OF DEBRIS FLOWS AND RELATED PHENOMENA

A. TEXTURE AND RHEOLOGY: Classification of events observed in this study. Classification is based on Pierson and Costa (1987) and Scott *et al.* (1992).

| Category of flow | % clay in matrix (<4 mm fraction) | % clay in <256 mm fraction | mean grain-size $M_z$ (phi) | standard deviation $\sigma_I$ (phi) | hydraulic conductivity K (m/s) | Flow behaviour and sedimentology |
|---|---|---|---|---|---|---|
| 1. Viscous slurry flow (fine-textured debris flow) | | | | | | |
| a) Cohesive | 8 to 15 | 3 to 5 | -1 to -4 | 4.2 to 4.9 | $10^{-8}$ to $10^{-9}$ | Bingham flow model; resists dilution; can flow on very gentle slopes; clayey matrix; matrix-supported; ungraded uniform deposits; drains very slowly; flow distance depends on volume and yield strength. |
| b) Noncohesive | 4 to 8 | 1 to 4 | -1 to -5 | 3.1 to 4.4 | $10^{-7}$ | Bingam and/or dilatant flow model; silty matrix; may become diluted to hyperconcentrated flow; matrix-supported; deposits may be inversely or normally graded; flow distance depends on volume, yield strength, and dilution. |
| 2. Inertial slurry flow (coarse-textured debris flow) | 0 to 4 | 0 to 1 | -4 to -5 | 2.8 to 3.6 | $10^{-6}$ | Dilatant flow model; drains rapidly; deposits on relatively steep slopes; sandy matrix; mostly matrix-supported with clast-supported surface layer; inversely graded; irregular deposits with terminal lobes and levées; flow distance depends on volume and frictional strength. |
| 3. "Debris floods" | 0 to 2 ? | 0 to 0.5 ? | ? | ? | $> 10^{-6}$ | Mechanics of flow uncertain; may be granular flow with separate fluid and sediment phases; unsteady turbulent flow; sandy matrix; largely clast-supported; massive or weakly stratified deposits. |

B. WATER CONTENT: Relation of debris flows to other sediment movement processes

| | WET ⟷ DRY | | |
|---|---|---|---|
| Fine-textured | Hyperconcentrated flow | Debris flow | Debris slide, earthflow ? |
| Coarse-textured | Debris flood | Debris flow | Debris avalanche |

Notes: 1. The matrix clay content is proposed as the measure which distinguishes between categories of debris flow. Other measures of texture show overlap.
2. Hydraulic conductivity (K) figures are order-of-magnitude estimates.

## REFERENCES


Aulitzky, H. 1980. Preliminary two fold classification of torrents. Symposium Interpraevent 1980, 4: 285-309. (Referred to by Slaymaker, 1988.)

Bagnold, R.A. 1954. Experiments on a gravity-free dispersion of large solid spheres in a Newtonian fluid under shear. Proceedings of the Royal Society of London, series A, 225: 49-63.

Baumann, F.W. 1991. Report on the garbage dump debris flow deposit and its relationship to the geologic history of the Cheekye Fan, Squamish, B.C. Unpublished report prepared for British Columbia Ministry of Environment.

Benda, L. and Cundy, T.W. 1990. Predicting deposition of debris flows in mountain channels. Canadian Geotechnical Journal, 27: 409-417.

Benda, L. and Dunne, T. 1987. Sediment routing by debris flow. *In* Erosion and Sedimentation in the Pacific Rim. *Edited by* Beschta, R.L. et al. International Association of Hydrological Sciences, Publication no. 165: 213-223.

Blackwelder, E. 1928. Mudflow as a geologic agent in semiarid mountains. Geological Society of America Bulletin, 39: 465-483.

Boussinesq, J. 1868. Memoir sur l'influence des frottements dans les mouvements reguliers des fluides. Journal de Mathématiques Pures et Appliqués, Series 2, 13: 377-424. (Referred to in discussion following paper by Straub et al., 1958.)

Bovis, M.J. 1982. Uphill-facing (antislope) scarps in the Coast Mountains. Geological Society of America Bulletin, 93: 804-812.

Bovis, M.J. 1985. Earthflows in the Interior Plateau, southwest British Columbia. Canadian Geotechnical Journal, 22: 313-334.

Bovis, M.J. 1990. Rock-slope deformation at Affliction Creek, southern Coast Mountains, British Columbia. Canadian Journal of Earth Sciences, 27: 243-254.

Bovis, M.J. and Dagg, B.R. 1988. A model for debris accumulation and mobilization in steep mountain streams. Hydrological Sciences Journal, 33: 589-604.

Broscoe, A.J. and Thomson, S. 1969. Observations on an alpine mudflow, Steele Creek, Yukon. Canadian Journal of Earth Sciences, 6: 219-229.

Buchanan, P. and Savigny, K.W. 1990. Factors controlling debris avalanche initiation. Canadian Geotechnical Journal, 27: 659-675.

Cannon, S.H. and Savage, W.Z. 1988. A mass-change model for the estimation of debris-flow runout. Journal of Geology, 96: 221-227.

Carter, N.M. 1932. Exploration in the Lillooet River watershed. Canadian Alpine Journal, 21: 8-18.

Chen, C.L. 1987. Comprehensive review of debris flow modeling concepts in Japan. *In* Debris Flows/Avalanches: Process, Recognition, and Mitigation. *Edited by* Costa, J.E. and Wieczorek, G.F. Geological Society of America, Reviews in Engineering Geology, VII: 13-29.

Chow, V.T. 1959. Open Channel Hydraulics. McGraw Hill, New York, 680 p.

Chow, V.T., Maidment, D.R., and Mays, L.W. 1988. Applied Hydrology. McGraw-Hill, New York, 572 p.

Church, M.A., McLean, D.G., and Wolcott, J.F. 1987. River bed gravels: Sampling and analysis. *In* Sediment Transport in Gravel-bed Rivers. *Edited by* Thorne, C.R., Bathurst, J.C., and Hey, R.D. Wiley, Chichester, p. 43-79.

Church, M. and Miles, M.J. 1987. Meteorological antecedents to debris flow in southwestern British Columbia; some case studies. *In* Debris Flows/Avalanches: Process, Recognition, and Mitigation. *Edited by* Costa, J.E. and Wieczorek, G.F. Geological Society of America, Reviews in Engineering Geology, VII: 63-79.

Clague, J.J., Evans, S.G., and Blown, I.G. 1985. A debris flow triggered by the breaching of a moraine-dammed lake, Klattasine Creek, British Columbia. Canadian Journal of Earth Sciences, 22: 1492-1502.

Clague, J.J. and Souther, J.G. 1982. The Dusty Creek landslide on Mount Cayley, British Columbia. Canadian Journal of Earth Sciences, 19: 524-539.

Conway, Sir M. 1907. The Fan Mountains in the Duab of Turkestan - Discussion. The Geographical Journal, 30: 501-502.

Costa, J.E. 1984. Physical geomorphology of debris flows. *In* Developments and Applications of Geomorphology. *Edited by* Costa, J.E. and Fleisher, P.J. Springer-Verlag, Berlin, Heidelberg, p. 268-317.

Costa, J.E. 1988. Rheologic, geomorphic, and sedimentologic differentiation of water floods, hyperconcentrated flows, and debris flows. *In* Flood Geomorphology. *Edited by* Baker, V.R., Kochel, R.C., and Patton, P.C. Wiley-Interscience, New York. p. 113-122.

Costa, J.E. and Williams, G.P. 1984. Debris-flow dynamics. U.S. Geological Survey, Open-File Report 84-606 (videotape).

Craig, R.F. 1987. Soil Mechanics. (4th ed.) Van Nostrand Reinhold, Berkshire, U.K., 410 p.

Crandell, D.R. 1971. Postglacial lahars from Mount Rainier volcano, Washington. U.S. Geological Survey, Professional Paper 677, 75 p.

Crandell, D.R., Mullineaux, D.R., and Miller, C.D. 1979. Volcanic-hazard studies in the Cascade Range of the western United States. *In* Volcanic Activity and Human Ecology. *Edited by* Sheets, P.D. and Grayson, D.K. Academic Press, New York, p. 195-219.

Croft, S.A.S. 1983. Stability assessment of the Capricorn Creek valley, British Columbia. Unpublished B.A.Sc. thesis, Department of Geological Sciences, University of British Columbia.

Cruden, D.M. and Lu Z. 1989. The geomorphic impact of the catastrophic October 1984 flood on the planform of the Squamish River, southwestern British Columbia: Discussion. Canadian Journal of Earth Sciences, 26: 336.

Curran, M., Chow, B., Toews, D., and Boyer, D. 1990. Landslide study - Cape Horn Bluffs area. Unpublished report, British Columbia Ministries of Forests and Environment, Nelson, B.C., 46 p.

Curry, R.R. 1966. Observation of alpine mudflows in the Tenmile Range, central Colorado. Geological Society of America Bulletin, 77: 771-776.

Davies, T.R.H. 1986. Large debris flows: a macro-viscous phenomenon. Acta Mechanica, 63: 161-178.

Davies, T.R.H. 1988. Debris flow surges - a laboratory investigation. Mitteilungen der Versuchsanstalt für Wasserbau, Hydrologie und Glaziologie, Nr. 96. Eidgenössischen Technischen Hochschule Zürich, 122 p.

Davies, T.R.H. 1990. Debris-flow surges - experimental simulation. Journal of Hydrology (New Zealand), 29: 18-46.

Driedger, C.L. and Fountain, A.G. 1989. Glacier outburst floods at Mount Rainier, Washington State, U.S.A. Annals of Glaciology, 13: 51-55.

Eisbacher, G.H. 1983. Slope stability and mountain torrents, Fraser Lowland and southern Coast Mountains, British Columbia. Geological Association of Canada - Mineralogical Association of Canada - Canadian Geophysical Union, Joint Annual Meeting, Victoria, B.C. Field Trip Guidebook, Trip 15, 46 p.

Eisbacher, G.H. and Clague, J.J. 1984. Destructive mass movements in high mountains: hazard and management. Geological Survey of Canada, Paper 84-16, 230 p.

Enos, P. 1977. Flow regimes in debris flows. Sedimentology, 24: 133-142.

Evans, S.G. 1984. The landslide response of tectonic assemblages in the southern Canadian Cordillera. Proceedings, IV International Symposium on Landslides, Toronto, 1984. Vol. 1: 495-502.

Evans, S.G. 1987a. A rock avalanche from the peak of Mount Meager, British Columbia. Current Research, Part A, Geological Survey of Canada, Paper 87-1A: 929-934.

Evans, S.G. 1987b. Surface displacement and massive toppling on the northeast ridge of Mount Currie, British Columbia. Current Research, Part A, Geological Survey of Canada, Paper 87-1A: 181-189.

Evans, S.G. 1990. Massive debris avalanches from volcanoes in the Garibaldi Volcanic Belt, British Columbia (abstract). Geological Association of Canada - Mineralogical Association of Canada, Annual Meeting, Vancouver, Program with Abstracts, 15: A38.

Evans, S.G. and Brooks, G.R. 1991. Prehistoric debris avalanches from Mount Cayley volcano, British Columbia. Canadian Journal of Earth Sciences, 28: 1365-1374.

Evans, S.G. and Lister, D.R. 1984. The geomorphic effects of the July 1983 rainstorms in the southern Cordillera and their impact on transportation facilities. Current Research, Part B, Geological Survey of Canada, Paper 84-1B: 223-235.

Evans, S.G., Clague, J.J., Woodsworth, G.J., and Hungr, O. 1989. The Pandemonium Creek rock avalanche, British Columbia. Canadian Geotechnical Journal, 26: 427-446.

Fairchild, L.H. 1985. Lahars at Mount St. Helens, Washington. Unpublished Ph.D. thesis, University of Washington, Seattle, 374 p.

Fannin, R.J. and Rollerson, T.P. 1993. Debris flows: some physical characteristics and behaviour. Canadian Geotechnical Journal, 30: 71-81.

Folk, R.L. 1966. A review of grain size parameters. Sedimentology, 6: 73-93.

Fread, D.L. 1991. The NWS DAMBRK model: theoretical background and user documentation. Revision 4, August 1991. U.S. Department of Commerce, National Weather Service, Silver Spring, Maryland.

Freeze, R.A. and Cherry, J.A. 1979. Groundwater. Prentice-Hall, New Jersey.

Gallino, G.L. and Pierson, T.C. 1985. Polallie Creek debris flow and subsequent dam-break flood of 1980, East Fork Hood River basin, Oregon. U.S. Geological Survey, Water Supply Paper 2273, 22 p.

Graf, W.H. 1971. Hydraulics of Sediment Transport. McGraw-Hill, New York, 513 p.

Green, N.L., Armstrong, R.L., Harakal, J., Souther, J.G., and Read, P.B. 1988. Eruptive history and K-Ar geochronology of the Garibaldi Volcanic Belt, southwestern British Columbia. Geological Society of America Bulletin, 100: 563-579.

Hart, J.S. 1979. Clastic sediment sources and suspended sediment yield in a Coast Mountains watershed, British Columbia. Unpublished M.A. thesis, Department of Geography, University of British Columbia.

Henderson, F.M. 1966. Open Channel Flow. Macmillan, New York, 522 p.

Hickin, E.J. and Sichingabula, H.M. 1987. The geomorphic impact of the catastrophic October 1984 flood on the planform of Squamish River, southwestern British Columbia. Canadian Journal of Earth Sciences, 25: 1078-1087.

Howes, D.E. and Kenk, E. 1988. Terrain classification system for British Columbia (revised edition) 1988. British Columbia, Ministry of Environment and Ministry of Crown Lands, MOE Manual 10, 90 p.

Hsu, K.J. 1975. Catastrophic debris streams (sturzstroms) generated by rockfalls. Geological Society of America Bulletin, 86: 129-140.

Hungr, O. 1981. Dynamics of rock avalanches and other types of slope movements. Unpublished Ph.D. thesis, University of Alberta.

Hungr, O. 1994. A model for the runout analysis of rapid flow slides. Paper submitted to Canadian Geotechnical Journal (in review).

Hungr, O. and McClung, D.M. 1987. An equation for calculating snow avalanche run-up against barriers. *In* Avalanche Formation, Movement, and Effects, Proceedings of the Davos Symposium, September 1986. International Association of Hydrological Sciences, Publication no. 162: 605-612.

Hungr, O., Morgan, G.C., and Kellerhals, R. 1984. Quantitative analysis of debris torrent hazards for design of remedial measures. Canadian Geotechnical Journal, 21: 663-677.

Hungr, O., Morgan, G.C., VanDine, D.F., and Lister, D.R. 1987. Debris flow defenses in British Columbia. *In* Debris Flows/Avalanches: Process, Recognition, and Mitigation. *Edited by* Costa, J.E. and Wieczorek, G.F. Geological Society of America, Reviews in Engineering Geology, VII: 201-222.

Hungr, O. and Morgenstern, N.R. 1984. Experiments on the flow behaviour of granular materials at high velocity in an open channel. Géotechnique, 34: 405-413.

Hutchinson, J.N. 1986. A sliding-consolidation model for flow slides. Canadian Geotechnical Journal, 23: 115-126.

Innes, J.L. 1983. Debris flows. Progress in Physical Geography, 7: 469-501.

Iverson,R.M. and Denlinger, R.P. 1987. The physics of debris flows - a conceptual assessment. International Association of Hydrological Sciences, Publication no. 165: 155-165.

Jackson, L.E. 1979. A catastrophic outburst flood (jokulhlaup) mechanism for debris flow generation at the Spiral Tunnels, Kicking Horse River basin, British Columbia. Canadian Geotechnical Journal, 16: 806-813.

Jackson, L.E. Jr., Hungr, O., Gardner, J.S., and MacKay, C. 1989. Cathedral Mountain debris flows, Canada. Bulletin of the International Association of Engineering Geology, 40: 35-54.

Janda, R.J., Scott, K.M., Nolan, K.M., and Martinson, H.A. 1981. Lahar movement, effects, and deposits. *In* The 1980 Eruptions of Mount St. Helens, Washington. *Edited by* Lipman, P.W. and Mullineaux, D.R. U.S. Geological Survey, Professional Paper 1250: 461-478.

Johnson, A.M 1970. Physical Processes in Geology. Freeman, Cooper & Co., San Francisco, 577 p.

Johnson, A.M. and Rodine, J.D. 1984. Debris flow. *In* Slope Instability. *Edited by* Brunsden, D. and Prior, D.B. J. Wiley & Sons, p. 257-361.

Jones, W.C. 1959. Cheekye River mudflows. British Columbia, Department of Mines, unpublished memorandum, 11 p.

Jordan, P. 1987a. Impacts of mass movement events on rivers in the southern Coast Mountains, British Columbia: summary report. Canada, Environment, Water Resources Branch, Inland Waters Directorate, IWD-HQ-WRB-SS-87-3, 62 p.

Jordan, P. 1987b. Terrain hazards and river channel impacts in the Squamish and Lillooet watersheds, British Columbia. Unpublished report submitted to Geological Survey of Canada.

Jordan, P. and Slaymaker, O. 1991. Holocene sediment production in the Lillooet River basin, British Columbia: a sediment budget approach. Géographie physique et Quaternaire, 45: 45-57.

Kellerhals, R. and Bray, D.I. 1971. Sampling procedures for coarse fluvial sediments. Journal of the Hydraulics Division, Proceedings, American Society of Civil Engineers, 97: 1165-1180.

Lambe, T.W. 1951. Soil Testing for Engineers. Wiley, New York, 165 p.

Leopold, L.B., Wolman, M.G., and Miller, J.P. 1964. Fluvial Processes in Geomorphology. W.H. Freeman, San Francisco.

Li Jian, Yuan Jianmo, Bi Cheng, and Luo Defu. 1983. The main features of the mudflow in Jiang-Jia Ravine. Zeitschrift für Geomorphologie, 27: 325-341.

Lowe, D.R. 1976. Grain flow and grain flow deposits. Journal of Sedimentary Petrology, 46: 188-199.

Major, J.J. 1984. Geologic and rheologic characteristics of the May 18, 1980 southwest flank lahars at Mount St. Helens, Washington. Unpublished M.Sc. thesis, Pennsylvania State University.

Major, J.J. and Iverson, R.M. 1993. Is the dynamic behaviour of a debris flow recorded by its deposit? (abstract). EOS, vol. 74, no. 43 (supplement): 315.

Major, J.J. and Pierson, T.C. 1990. Rheological analysis of fine-grained natural debris-flow material. *In* Hydraulics and Hydrology of Arid Lands. Proceedings of International Symposium, Hydraulics and Irrigation Division, American Society of Civil Engineers, San Diego, p. 225-231.

Major, J.J. and Voight, B. 1986. Sedimentology and clast orientation of the 18 May 1980 southwest-flank lahars, Mount St. Helens, Washington. Journal of Sedimentary Petrology, 56: 691-705.

Massey, B.S. 1970. Mechanics of Fluids (2nd ed.). Van Nostrand Reinhold, London, 508 p.

Mathews, W.H. 1958. Geology of the Mount Garibaldi map-area, southwestern British Columbia, Canada. Part II: Geomorphology and Quaternary volcanic rocks. Geological Society of America Bulletin, 69: 179-198.

Mayer, P.G. 1959. Roll waves and slug flows in open channels. Journal of the Hydraulics Division, Proceedings, American Society of Civil Engineers, 85: 99-141.

Middleton, G.V. and Hampton, M.A. 1976. Subaqueous sediment transport and deposition by sediment gravity flows. *In* Marine Sediment Transport and Environmental Management. *Edited by* Stanley, D.J. and Swift, J.P. Wiley, New York, p. 197-218.

Miles, M. and Kellerhals, R. 1981. Some engineering aspects of debris torrents. Canadian Society of Civil Engineers, 5th Canadian Hydrotechnical Conference, Fredericton, N.B., May, 1981, Proceedings, p. 395-420.

Mitchell, R.J. and Markell, A.R. 1974. Flowsliding in sensitive soils. Canadian Geotechnical Journal, 11: 11-31.

Mokievsky-Zubok, O. 1977. Glacier-caused slide near Pylon Peak, British Columbia. Canadian Journal of Earth Sciences, 14: 2657-2662.

Moore, D.P. and Mathews, W.H. 1978. The Rubble Creek landslide, southwestern British Columbia. Canadian Journal of Earth Sciences, 15: 1039-1052.

Morton, D.M. and Campbell, R.H. 1974. Spring mudflows at Wrightwood, southern California. Quarterly Journal of Engineering Geology, 7: 377-384.

Nasmith, H.W. and Mercer, A.G. 1979. Design of dykes to protect against debris flows at Port Alice, British Columbia. Canadian Geotechnical Journal, 16: 748-757.

Nesbitt-Porter, H.H. 1985. Pemberton valley flood protection, 1985 study. British Columbia, Ministry of Environment, Water Management Branch. Victoria, 76 p.

Niyazov, B.S. and Degovets, A.S. 1975. Estimation of the parameters of catastrophic mudflows in the basins of the lesser and greater Almatinka Rivers. Soviet Hydrology, 2: 75-80.

O'Brien, J.S. and Julien, P.Y. 1988. Laboratory analysis of mudflow properties. Journal of Hydraulic Engineering, 114: 877-887.

O'Loughlin, C.L. 1972. A preliminary study of landslides in the Coast Mountains of southwestern British Columbia. *In* Mountain Geomorphology. *Edited by* Slaymaker, H.O. and McPherson, H.J. Tantalus Research Ltd., Vancouver, p. 101-111.

Okuda, S., Suwa, H., Okunishi, K., Yokoyama, K., and Nakano, M. 1980. Observations on the motion of a debris flow and its geomorphological effects. Zeitschrift für Geomorphologie, Suppl. 35: 142-163.

Owens, I.F. 1972. Morphological characteristics of alpine mudflows in the Nigel Pass area. *In* Mountain Geomorphology. *Edited by* Slaymaker, H.O. and McPherson, H.J. Tantalus Research Ltd., Vancouver, p. 93-100.

Owens, I.F. 1973. Alpine mudflows in the Nigel Pass area, Canadian Rocky Mountains. Unpublished Ph.D. thesis, University of Toronto, 214 p..

Paterson, W.S.B. 1981. The Physics of Glaciers (2nd ed.). Pergamon Press, Oxford, 380 p.

Patton, F.D. 1976. The Devastation Glacier slide, Pemberton, B.C. (abstract). Cordilleran Section, Geological Association of Canada, Programme and Abstracts, p. 26-27.

Phillips, C.J. and Davies, T.R.H. 1991. Determining rheological parameters of debris flow material. Geomorphology, 4: 101-110.

Pierson, T.C. 1980. Erosion and deposition by debris flows at Mt Thomas, North Canterbury, New Zealand. Earth Surface Processes, 5: 227-247.

Pierson, T.C. 1981. Dominant particle support mechanisms in debris flows at Mt Thomas, New Zealand, and implications for flow mobility. Sedimentology, 28, p.49-60.

Pierson, T.C. 1985. Initiation and flow behavior of the 1980 Pine Creek and Muddy River lahars, Mount St. Helens, Washington. Geological Society of America Bulletin, 96: 1056-1069.

Pierson, T.C. 1986. Flow behavior of channelized debris flows, Mount St. Helens, Washington. *In* Hillslope Processes. *Edited by* Abrahams, A.D. Allen & Unwin, Boston, p. 269-297.

Pierson, T.C. and Costa, J.E. 1987. A rheologic classification of subareal sediment-water flows. *In* Debris Flows/Avalanches: Process, Recognition, and Mitigation. *Edited by* Costa, J.E. and Wieczorek, G.F. Geological Society of America, Reviews in Engineering Geology, VII: 1-12.

Pierson, T.C. and Scott, K.M. 1985. Downstream dilution of a lahar: transition from debris flow to hyperconcentrated streamflow. Water Resources Research, 21: 1511-1524.

Pierson, T.C., Janda, R.J., Thouret, J.-C., and Borrero, C.A. 1990. Perturbation and melting of snow and ice by the 13 November 1985 eruption of Nevado del Ruiz, Colombia, and consequent mobilization, flow, and deposition of lahars. Journal of Volcanology and Geothermal Research, 41: 17-66.

Rapp, A. 1960. Recent development of mountain slopes in Karkevagge and surroundings, northern Scandinavia. Geografiska Annaler, 42A: 65-200.

Read, P.B. 1978. Geology, Meager Creek geothermal area, British Columbia. Geological Survey of Canada, Open File 603.

Read, P.B. 1990. Mount Meager complex, Garibaldi Belt, southwestern British Columbia. Geoscience Canada, 17: 167-170.

Richardson, D.R. 1968. Glacier outburst floods in the Pacific Northwest. *In* Geological Survey Research 1968. U.S. Geological Survey, Professional Paper 600-D: D79-D86.

Rodolfo, K.S., Arguden, A.T., Solidum, R.U., and Umbal, J.V. 1989. Anatomy and behaviour of a post-eruptive rain lahar triggered by a typhoon on Mayon Volcano, Philippines. Bulletin of the International Association of Engineering Geology, 40: 55-66.

Russell, S.O. 1972. Behaviour of steep creeks in a large flood. *In* Mountain Geomorphology. *Edited by* Slaymaker, H.O. and McPherson, H.J. Tantalus Research Ltd., Vancouver, p. 223-227.

Ryder, J.M. 1971. The stratigraphy and morphology of para-glacial alluvial fans in south-central British Columbia. Canadian Journal of Earth Sciences, 8: 279-298.

Ryder, J.M. 1976. Terrain inventory and Quaternary geology, Ashcroft, British Columbia. Geological Survey of Canada Paper 74-49, 17 p.

Savage, S.B. 1988. Flow of granular materials. *In* Theoretical and Applied Mechanics. *Edited by* Germain, P. Piau, M., and Caillerie, D. Proceedings of the XVII International Congress of Theoretical and Applied Mechanics, Grenoble, France, 21-27 Aug. 1988, p. 241-266.

Savigny, K.W. 1990. Engineering geology of large landslides in the lower Fraser River Valley area, southwestern Canadian Cordillera (abstract). Geological Association of Canada - Mineralogical Association of Canada, Annual Meeting, Vancouver, Program with Abstracts, 15: A117.

Schaerer, P.A. and Salway, A.A. 1980. Seismic and impact pressure monitoring of flowing avalanches. Journal of Glaciology, 26: 179-187.

Scott, K.M. 1988. Origins, behavior, and sedimentology of lahars and lahar-runout flows in the Toutle-Cowlitz River system. United States Geological Survey, Professional Paper 1447-A, 74 p.

Scott, K.M. 1989. Magnitude and frequency of lahars and lahar-runout flows in the Toutle-Cowlitz River system. United States Geological Survey, Professional Paper 1447-B, 33 p.

Scott, K.M., Pringle, P.T., and Vallance, J.W. 1992. Sedimentology, behaviour, and hazards of debris flows at Mount Rainier, Washington. United States Geological Survey, Open-file Report 90-385, 106 p.

Sharp, R.P. and Nobles, L.H. 1953. Mudflow of 1941 at Wrightwood, southern California. Geological Society of America Bulletin, 64: 547-560.

Slaymaker, O. 1988. The distinctive attributes of debris torrents. Hydrological Sciences Journal, 33: 567-573.

Souther, J.G. 1980. Geothermal reconnaisance in the central Garibaldi Belt, British Columbia. *In* Current Research, Part A, Geological Survey of Canada, Paper 80-1A: 1-11.

Stini, J. 1910. Die Muren. Verlag der Wagner'schen Universitätsbuchhandlung, Innsbruck. (In German; referred to by Eisbacher and Clague, 1984.)

Strahler, A.N. 1952. Dynamic basis of geomorphology. Geological Society of America Bulletin, 63: 923-938.

Straub, L.G., Silberman, E., and Nelson, H.C. 1958. Open-channel flow at small Reynolds numbers. Transactions, American Society of Civil Engineers, 123: 685-706.

Swanston, D.N. and Swanson, F.J. 1976. Timber harvesting, mass erosion, and steepland forest geomorphology in the Pacific Northwest. *In* Geomorphology and Engineering. *Edited by* Coates, D.R. Dowden, Hutchinson, and Ross, Stroudsburg, Penn., p. 199-221.

Synge, J.L. 1953. Flow of viscous liquid through pipes and channels. Proceedings, Symposium in Applied Mathematics, American Mathematical Society, 4: 141-165.

Takahashi, T. 1978. Mechanical characteristics of debris flows. Journal of the Hydraulics Division, American Society of Civil Engineers, 104, no. HY8: 1153-1169.

Takahashi, T. 1980. Debris flow on prismatic open channel. Jour. Hydraulics Div., Proceedings, American Society of Civil Engineers, 106, no. HY8: 381-396.

Takahashi, T. 1981. Debris flow. Annual Review of Fluid Mechanics, 13: 57-77.

Takahashi, T. 1991. Debris flow. International Association for Hydraulic Research, Monograph Series. A.A. Balkema, Rotterdam, 165 p.

Takahashi, T. and Yoshida, H. 1979. Study on the deposition of debris flows, Part 1 - Deposition due to abrupt change of bed slope. Annuals, Disaster Prevention Research Institute, Kyoto University, Japan, 22 B-2. (In Japanese; reviewed by Hungr et al, 1984.)

Terzaghi, K. 1943. Theoretical Soil Mechanics. John Wiley & Sons, New York, 510 p.

Thomas, J. and Stobbe, S. 1984. Heavy rainfall on Thanksgiving weekend, 1984. Canada, Atmospheric Environment Service, Pacific Region, Technical Note 84-014, Vancouver, 4 p.

Thurber Consultants Ltd. 1983. Debris torrent and flooding hazards, Highway 99, Howe Sound. Unpublished report to British Columbia Ministry of Transportation and Highways, Victoria.

Thurber Engineering Ltd. and Golder Associates Ltd. 1993. Cheekye River terrain hazard study. Unpublished report to the the British Columbia Ministry of Environment, Lands, and Parks, Victoria.

VanDine, D.F. 1985. Debris flows and debris torrents in the southern Canadian cordillera. Canadian Geotechnical Journal, 22: 44-68.

Van Wazer, J.R., Lyons, J.M., Kim, K.Y., and Colwell, R.E. 1963. Viscosity and Flow Measurement. Interscience, New York, 406 p.

Varnes, D.J. 1978. Slope movement types and processes. *In* Landslides, Analysis and Control. *Edited by* Schuster, R.L. and Krizek, R.J. Special Report 176, Transportation Research Board, National Research Council, National Acadademy of Sciences, Washington, p.11-33.

Voellmy, A. 1955. Uber die Zerstörungskraft von Lawinen. Schweizerische Bauzeitung, 73: 159-165, 212-217, 246-249, 280-285. (In German; reviewed by Hungr et al, 1984.)

Whipple, K.X. and Dunne, T. 1992. The influence of debris-flow rheology on fan morphology, Owens Valley, California. Geological Society of America Bulletin, 104: 887-900.

Wigmosta, M.S. 1983. Rheology and flow dynamics of the Toutle debris flows from Mt. St. Helens. Unpublished M.Sc. thesis, University of Washington, 184 p.

Wilford, D.J. and Schwab, J.W. 1981. Soil mass movements in the Rennel Sound area, Queen Charlotte Islands, British Columbia. Unpublished report, British Columbia Ministry of Forests, Victoria.

Winder, C.G. 1965. Alluvial cone construction by alpine mudflow in a humid temperate region. Canadian Journal of Earth Sciences, 2: 270-277.

Personal Communication

Decker, J. C.R.B. Logging Ltd., Pemberton, B.C.